EVALUATE FRETTING FATIGUE DAMAGE IN SIMPLE AND COMPLEX GEOMETRIES LIKE DIESEL ENGINE HEAD GASKET

A Thesis Submitted

for the Degree of

Doctor of Philosophy

by

Amit Prakash Ozarde

Department of Mechanical Engineering

Indian Institute of Technology Guwahati, Guwahati, India

April 10 2023

भारतीय प्रौद्योगिकी संस्थान गुवाहाटी
Indian Institute of Technology Guwahati

DECLARATION

I hereby declare that the information presented in the thesis titled “Evaluate Fretting Fatigue Damage in Simple and Complex Geometries like Diesel Engine Head Gasket” is entirely my account of the research under the joint supervision of Dr. Sachin Singh Gautam and Dr. Gene H. McNay. No part of this work has been submitted for the award of any degree, diploma, associateship, fellowship, or its equivalent to any University or Institution. I have not violated any copyright and plagiarism law. In keeping with the general practice of reporting scientific observations, due acknowledgments have been made wherever the work described is based on the findings of other researchers.

September 2022 Amit P. Ozarde

भारतीय प्रौद्योगिकी संस्थान गुवाहाटी
Indian Institute of Technology Guwahati

CERTIFICATE

This is to certify that the thesis entitled "Evaluate Fretting Fatigue Damage in Simple and Complex Geometries like Diesel Engine Head Gasket" submitted by Amit P. Ozarde, Roll No. 176103013, to the Indian Institute of Technology Guwahati, for the award of the degree of Doctor of Philosophy in Mechanical Engineering, has been carried out by him under our joint supervision. The results contained in this thesis have not been submitted in part or full to any other University or Institute for the award of any degree.

Dr. Sachin Singh Gautam

Associate Professor
Department of Mechanical Engineering
Indian Institute of Technology Guwahati
Guwahati, India.

Dr. Gene H. McNay

Sr. Tech Advisor
Power Systems Business Unit
Cummins Inc.
Seymour, USA.

भारतीय प्रौद्योगिकी संस्थान गुवाहाटी
Indian Institute of Technology Guwahati

ACKNOWLEDGEMENTS

While reaching to this important milestone in my personal and professional journey, I would like to express my sincere gratitude to all those people whose direct/indirect support was involved towards the doctoral thesis work. Firstly, I would like to thank my PhD supervisors Dr. Sachin Singh Gautam (Department of Mechanical Engineering, IIT Guwahati) and Dr. Gene H. McNay (Power Systems Business Unit, Cummins Inc, USA) for their continuous support and guidance for my PhD study and related research. Their guidance, continuous support and motivation helped me significantly in this journey. I would also like to thank my Doctoral Committee members, Professor Uday S. Dixit (Department of Mechanical Engineering), Dr. Nelson Muthu (Department of Mechanical Engineering) and Professor Hemant B. Kaushik (Department of Civil Engineering). Their valuable suggestions proved to be of great help at the different stages of this research work.

I am also thankful to the leadership team of Cummins Technology India Ltd. for providing this opportunity to pursue the doctoral study and research work. I would like to specially thank Iain Revill (Power Systems Analysis Led Design & Validation Director, Cummins Inc. England, UK) for his support and guidance.

Further, I am also grateful to my friends and colleagues from IIT Guwahati and Cummins like Jyotindra Narayan, Dipak Vasudev, Dnyaneshwar Sangle for their direct and indirect support, I received in this work. Specially, when I was miles away from Guwahati, I used to rely on Jyotindra Narayan and Dipak Vasudev, for their help towards fulfilling different administrative formalities and they never let me down.

Finally, I would like to thank my parents and my family for their unspoken strong support. Specially my wife Sonali, who carried out all the family responsibilities well, when I was away from my home. The way, my wife and my kids, Piyusha and Chinmay, enjoyed and cherished my small, small achievements in this journey, really gave me the kind of courage and inner strength to complete this tough journey. I owe them beyond words for their support and sacrifices in these five years.

भारतीय प्रौद्योगिकी संस्थान गुवाहाटी
Indian Institute of Technology Guwahati

ABSTRACT

Fretting is a surface damage phenomenon and is observed at the contact interfaces like bolted, gasketed joints etc. Fretting related failures are observed in multiple components of an internal combustion engine. Such failures can cause partial/complete break-down of the engine and can result in a significant warranty cost. In this work, fretting fatigue evaluation is carried out for a simple geometry of a flat-flat, complete contact pair and a complex geometry of actual head gasket joint. Since the head gasket is a type of flat-flat, complete contact pair, equivalent analogy is assumed between the two problems. A new approach based on deviatoric strain amplitude-based parameter combined with Ding's parameter, D_{fret2} is proposed and explored through this work.

In the initial verification through Two-Dimensional (2D) FEA of a flat-flat contact pair, experimental correlation is carried out using the deviatoric strain amplitude-based method and traditional critical plane-based methods like Smith-Watson-Topper (SWT) and Fatemi-Socie (FS). Observing the high load-factor values, different non-linear material models like BKIN, MKIN and Chaboche are considered to evaluate the resultant fretting fatigue life results. Overall good experimental correlation, within a ± 3*N* scatter band, is observed for the considered flat-flat complete contact problem. The deviatoric strain amplitude-based parameter does not require critical plane-based calculations and hence, is computationally more efficient as compared to SWT and FS parameters. The effect of wear on fretting fatigue is explored through Archard's progressive wear model and Ding's parameter, D_{fret2}. Compared to the Archard's wear model, better correlation is observed with the Ding's parameter. Further, the effect of different parameters like varying Coefficient of friction (COF), frictional heat and fretting loads like normal, tangential and axial loads on the fretting fatigue damage are also explored through the current work.

Finally, the learnings from 2D FEA are considered in the fretting fatigue damage evaluation of actual head gasket using 3D FEA. Corresponding fretting damage results are compared with the traditional approach based on the Ruiz's parameter *F1*. To evaluate the consistency in the predicted results, correlation is carried out for three head gaskets of three different high horse-power engines. Further, alternative approach based on the 'Fretting limit line' is also proposed for simpler absolute and comparative fretting fatigue damage evaluation.

भारतीय प्रौद्योगिकी संस्थान गुवाहाटी
Indian Institute of Technology Guwahati

TABLE OF CONTENTS

LIST OF FIGURES

LIST OF TABLES

भारतीय प्रौद्योगिकी संस्थान गुवाहाटी
Indian Institute of Technology Guwahati

NOMENCLATURE

Latin Symbols

a	Half contact width of the complete flat contact pair
a'	Material constant in Chaboche damage model
A	Material dependent damage parameter of Lemaitre damage model
A_{II}	Amplitude of octahedral shear stress
A_{II}^{*}	Sines fatigue limit criterion
b	Fatigue strength exponent
b'	Fatigue strength exponent in torsion
b_2	Material constant in Chaboche damage model
c	Fatigue ductility exponent
c'	Fatigue ductility exponent in torsion
c_p	Specific heat
C	Material constant in Ding's parameter
$C_{1,2,3,4}$	Material constants in SSR parameter
d	Material grain size as per Hall-Petch relationship
D_{fret2}	Ding's fretting specific parameter
D_N	Damage after N cycles
D_α	Standard deviation
DP_{avg}	Averaged damage parameter
$\dot{D}$	Sliding velocity
E	Elastic modulus
$\sum E$	Dissipated frictional energy
E_t	Tangent modulus
$F1$	Ruiz's fretting damage parameter
$F2$	Ruiz's fretting intiation parameter
$FHTG$	Fraction of frictional dissipated energy converted into heat
$FWGT$	Weight factor for the distribution of heat between the contact and target surfaces
G	Shear modulus
H	Material hardness

$J_{2,a}$	Amplitude of second invariant of deviatoric stress tensor
$J_{2,m}$	Mean of second invariant of deviatoric stress tensor
k_2	Material constant in FS parameter
k_y	Material constants in Hall-Petch relationship
K	Archard's wear coefficient
K'	Ramberg-Osgood's strength coefficient
ΔK_{th}	Crack threshold stress intensity factor range
m	Material constant in SSR parameter
m'	Pressure exponent in Archard's wear equation
M_0	Material constant in Chaboche damage model
n	Material constant in Ding's parameter
n'	Power constant in Ramberg–Osgood equation
$n*$	Sliding velocity exponent
$n^{\wedge}$	Strain hardening exponent
N_{ei}	Analytical fatigue life (cycles)
N_f, N_{ti}	Experimental failure cycles
N_i	Fatigue initiation life
P	Normal load
P_m, P	Contact pressure
q	Frictional energy generated at the contact interface
q_c	Amount of frictional heat dissipated in contact surface
q_t	Amount of frictional heat dissipated in target surface
r	Radial distance (away from the center)
r_c	Critical dimension for stress-strain averaging
R_τ	Shear stress ratio i.e., τ_{min}/τ_{max}
R_ϑ	Triaxiality function of Lemaitre damage model
m'	Matake parameter coefficient
S'	Deviatoric stress tensor
ΔT	Net temperature change
V	Wear volume
V'	Sliding rate
W	ANSSY predicted wear depth

W_p	Plastic work
ΔW_I	Liu parameter1
ΔW_{II}	Liu parameter2
z	Power constant in Ramberg–Osgood equation

Greek Symbols

α	Dimensional wear coefficient as per Energy wear equation
α_i	Logarithm ratio between analytical life results and experimental test results
$\tilde{\alpha}$	Average of α_i
β	Material dependent damage parameter of Lemaitre damage model
β'	Material constant in Chaboche damage model
β_{int}	Taylor- Quinney coefficient
$\Delta\gamma$	Alternating shear strain range
γ_{dev}	Deviatoric strain
$\Delta\gamma_{max}$	Maximum alternating shear strain range
$\gamma_{xy,yz,xz}$	Shear strain on x-y, y-z and x-z planes
γ_θ	Shear strain on a plane with orientation as θ
γ_f'	Fatigue ductility coefficient in torsion
δ	Relative sliding distance
δ_{th}	Threshold limit value for the relative slip
ε_u	True strain corresponding to % elongation at UTS
$\varepsilon_{x,y,z}$	Normal strain in x, y and z directions
ε_{yt}	True strain corresponding to the strain at σ_{yt}
ε_f'	Fatigue ductility coefficient
ε_θ	Normal strain on a plane with orientation as θ
$\Delta\varepsilon, \Delta\varepsilon_n$	Alternating normal strain range
$\Delta\varepsilon_p$	Alternating plastic strain range
θ_{max}	Angle of critical plane
ρ	Material density
σ_{Bulk}	Axial bulk load
$\sigma_{eq,max}$	Maximum von Mises stress
$\sigma_{e,max}$	Maximum von Mises stress for Chaboche damage model

$\sigma_{eq,min}$	Minimum von Mises stress
σ_{f-1}	Fatigue limit in tension
$\sigma_{H,max}$	Maximum hydrostatic stress
σ_{max}	Maximum tensile stress
$\sigma_{n,a}$	Normal stress amplitude
σ_P	Contact pressure
σ_u, σ_{ut}	Ultimate tensile strength
$\sigma_{x,y,z}$	Normal stress in x, y and z directions
σ_y, σ_{yt}	Material yield strength
σ_0	Material constants in Hall-Petch relationship
σ_θ	Normal stress on a plane with orientation as θ
σ_n^{max}	Maximum normal stress
σ_f'	Fatigue strength coefficient
$\bar{\sigma}$	Mean stress during the loading cycle
$\Delta\sigma, \Delta\sigma_n$	Alternating normal stress range
τ	Frictional stress
$\tau_{a,max}$	Maximum shear stress amplitude
τ_{max}	Maximum shear stress
τ_{min}	Minimum shear stress
τ_{f-1}	Fatigue limit in torsion
$\tau_{xy,yz,xz}$	Shear stress on x-y, y-z and x-z planes
τ_θ	Shear stress on a plane with orientation as θ
τ_f'	Fatigue strength coefficient in shear
$\Delta\tau$	Alternating shear stress range
$\Delta\tau_{max}$	Maximum alternating shear stress range
ϑ	Poisson's ratio

ABBREVATIONS

2D	Two-Dimensional
3D	Three-Dimensional
APDL	ANSYS parametric design language
A	Assembly load condition
AT	Assembly loads + Maximum thermal load condition
APT	Assembly loads + Rated PCP (Peak Cylinder Pressure) + Maximum thermal load condition
AP	Assembly loads + Rated PCP condition
BKIN	Bi-linear kinematic hardening model
CXH	Chen, Xu and Huang criterion-based fatigue initiation parameter
COF	Coefficient of friction
CDM	Continuum damage mechanics
CFR	Critical function response
CL	Crossland parameter
DP	Damage parameter
DOE	Design of experiments
eI	Deviatoric strain amplitude-based fatigue initiation parameter
IDI	Direct injection
FS	Fatemi-Socie fatigue initiation parameter
FIP	Fatigue initiation parameter
FP	Findley fatigue initiation parameter
FEA	Finite element analysis
FDP	Fretting damage parameter
HCF	High cycle fatigue
DI	In-direct injection
IC	Internal combustion
LZ	Li and Zhang criterion-based fatigue initiation parameter
Liu1,2	Liu fatigue initiation parameter
LE	Lohr and Ellison criterion-based fatigue initiation parameter
LCF	Low cycle fatigue
MBC	Main bearing cap

MT	Matake criterion-based fatigue initiation parameter
MRFM	Material response fretting map
MD	McDiarmid fatigue initiation parameter
MSSR	Modified shear stress range fatigue initiation parameter
MKIN	Multilinear kinematic hardening model
NLCD	Non-linear continuous damage
PCP	Peak cylinder pressure
RSD	Relative sliding distance
RVE	Representative volume element
RT	Rolovic and Tipton fatigue initiation parameter
RCFM	Running condition fretting map
SSR	Shear stress range fatigue initiation parameter
SLTO	Slip tolerance
SWT	Smith-Watson-Topper fatigue initiation parameter
SN	Stress-life fatigue curve
TYC	Tresca yield criterion-based fatigue initiation parameter
UTS	Ultimate tensile strength

1. INTRODUCTION AND LITERATURE REVIEW

1.1. Introduction of Fretting Fatigue

Fretting is a special wear process that occurs at the contact area between two bodies held under the normal load while subjected to minute relative motion by the vibration or some other un-balanced force [1]. Fretting was first reported by Eden et al. in 1911 [2] who found brown oxide debris formed in the steel grips of the fatigue machine in contact with a steel specimen. Earlier, fretting failures were often termed as 'fretting corrosion' [2]. However, later based on the effect of environment, fretting corrosion is differentiated from fretting [3]. Since then, fretting failures have been studied extensively by various scientists and engineers.

Fretting damage is a complex interaction between different fields like material science, tribology, material fatigue, contact mechanics and is historically observed in bolted or mechanically fastened joints like - flanges, gaskets, bolts, washers, etc. [4]. Fretting damage usually stands differently compared to the reciprocating sliding damage as it is accepted that the transition from fretting damage to reciprocating sliding is in the range 300 μm regardless of the normal load. Further, based on the amount of the resultant slip at the contact junction, fretting damage can be classified into two categories as fretting wear and fretting fatigue [5]. Fretting fatigue results in crack initiation and propogation near the region of stress concentration in the sliding frictional contacts whereas fretting wear results in the loss of material near the region of stress concentration and often does not result in further crack propogation. Thus, fretting fatigue is a special case of fatigue damage under the fretting loads which cause the additional detrimental effect on the fatigue life results and is mainly because of the relative sliding distance, till a certain limit.

The economic implications due to fretting damage can be severe and could cause significant warranty cost if such failures are not timely detected, leading to the potential breakdown of the end application. For example, fretting fatigue causes about 17% of the

The contents of present chapter have been published in 'A. P. Ozarde, G. H. McNay and S. S. Gautam, "Fretting fatigue failures in internal combustion engine components: A review and future scope", SAE International Journal of Engines, vol. 14(2), 2021, doi:10.4271/03-14-02-0013'.

failures/downtime in aeronautical engines [6]. Also, as Brady et al. [7] mentioned, 8% of all wear failures are fretting induced. Fretting failures are observed in various applications like train wheel axles [8–9], steel cables [10], and orthopedic implants [11]. In case of fretting fatigue, often initially initiated cracks are hidden and very difficult to detect leading to serious consequences [12]. Such failures could be avoided if suitable fretting evaluation methodology is considered during the design stage of such components.

1.2. Fretting Fatigue Damage in Engine Components

Like other mechanical systems, historically fretting failures are also observed in 'Internal Combustion' (IC) engine components. Generally, such failures occur after an engine has run for considerable operating hours [13]. At that time, the cost to retrofit is highly unpredictable. In IC engines, crack initiation is mostly considered as the target design life of the component; therefore, suitable design methodology should be considered for fretting damage evaluation of such components.

A schematic diagram of a typical, single-cylinder IC engine is shown in Figure 1. It is a complex mechanical system of multiple components moving relative to each other. Even the simplest four-cylinder IC engine consists of more than 40 moving parts [14] and many of these parts are connected to each other through the bolted joints. Such a complex system is exposed to very high thermal, pressure, and dynamic loads, occurring simultaneously. Thus, as a combined effect of these loads, small relative displacement can occur between two contacting components held together using bolted joints. Further, if the resultant frictional energy, generated due to the contact stresses and relative displacement reaches the resultant limit value, fretting damage starts to initiate. Different fretting failures are observed in different engine components and are discussed in upcoming sections. These components are critical towards the reliable performance of any IC engine and failures in these components can stop the operation of the engine. Consequently, fretting fatigue failures of such critical components are discussed in the next sections.

1.2.1. Fretting Fatigue Failure of Main Bearing Cap in Gasoline Engine

'Main Bearing Cap' (MBC) supports the crankshaft bearings and is an important part of the crankshaft support structure of an engine block. This critical component is fastened

to the block through the required set of bolts and is subjected to the bearing loads due to engine operating conditions. Typical arrangement of the MBC with respect to the engine block, subjected to the engine loads is shown in Figure 2. Due to the engine loads, there occurs a small magnitude relative slip movement at the contact junction of MBC with the block. The joint's stiffness values varying in normal and lateral directions, contribute to such relative displacement. As a combined effect of the normal clamping load and the in-plane relative displacement, resultant fretting damage occurs at the surface of the MBC. Sato et al. [15] discussed the fretting failure observed in a MBC joint and mentioned that the combined effect of normal loads and relative sliding between the MBC and the block, primarily contributes to such failures.

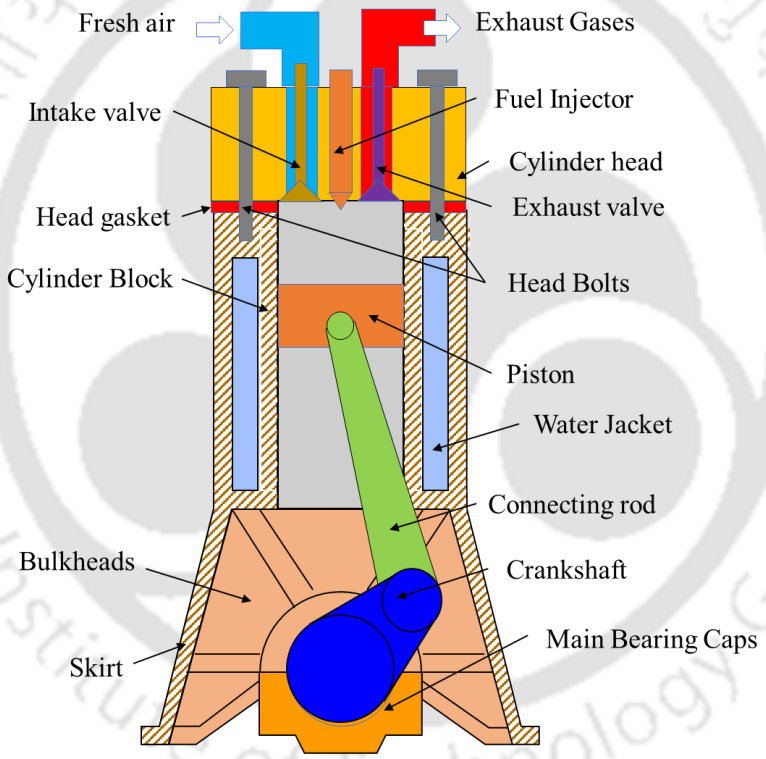

Figure 1: Schematic diagram of internal combustion diesel engine

Resultant crack due to the fretting damage can initiate at the contact surface of the MBC with respect to the engine block (see Figure 3). The combined effect of alternating stresses and relative slip magnitude can be considered to predict similar failures through 'Finite Element Analysis' (FEA), as shown in Figure 4. Doing so, combined effect of contact surface stresses and relative slip magnitude is considered towards the fretting fatigue

damage evaluation. Thus, this approach is similar to the historical approach of Ruiz's parameters [16].

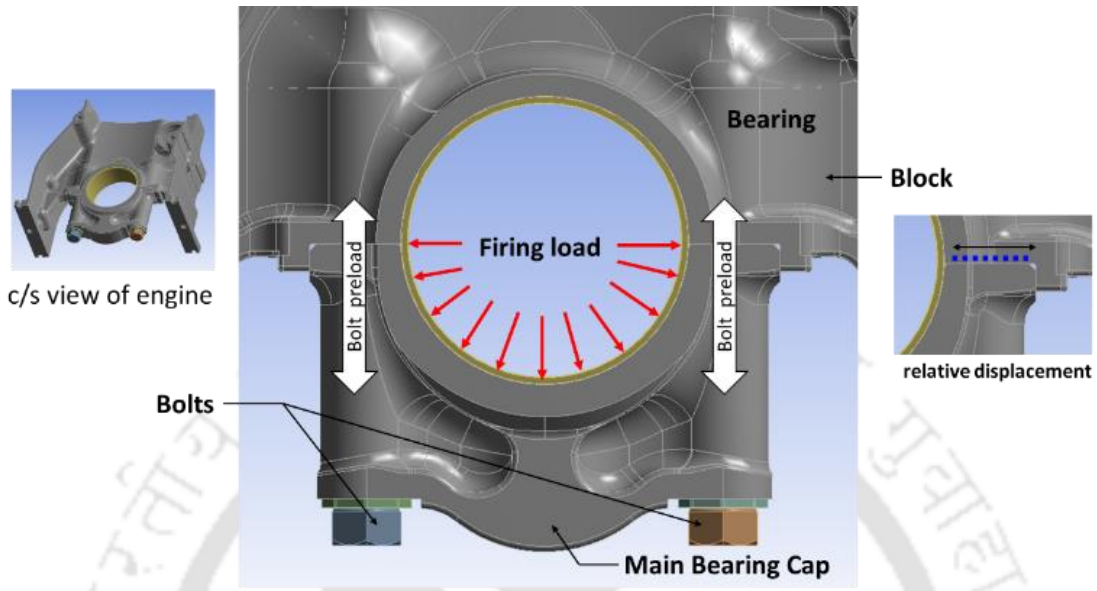

Figure 2: MBC joint subjected to normal and in-plane loads (Reprinted with permission from [18])

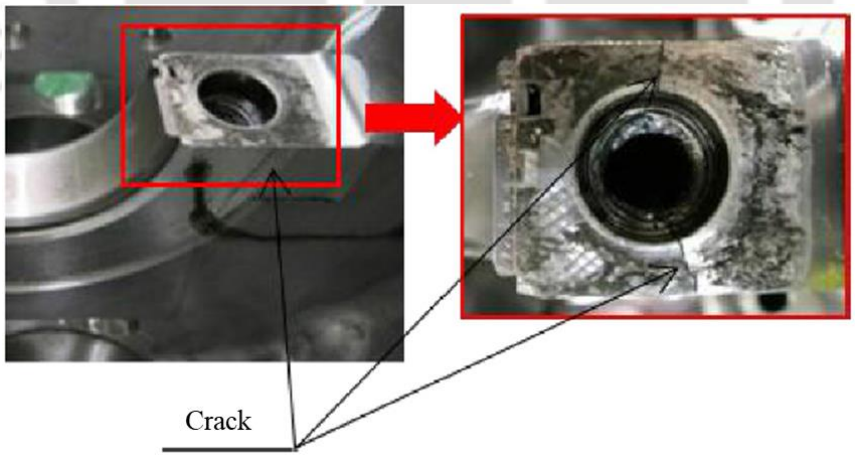

Figure 3: Fretting fatigue crack at MBC joint (Reprinted with permission from [15, 19])

In another study, Li et al. [17] also discussed a similar failure of the MBC, during which the Ruiz parameter; 'Fretting Damage Parameter' (FDP) [16] is considered towards the fretting damage evaluation. In this study, different engine parameters like bolt preload, bearing stiffness, contact surface shape, contact area, axial force and journal force are

identified as critical towards the resultant slip between MBC with respect to the block. Hence, these parameters are critical in the fretting damage evaluation in components like MBC [17].

1.2.2. Fretting Fatigue Failure of Engine Block

In automotive industry with the requirement of lightweight vehicles, there is an increasing trend of replacing heavy cast steel/iron engine block with lighter aluminum block, for the reasons like better fuel efficiency, better heat management and cleaner exhaust [20]. Subsequently with the increasing engine power density and lower material stiffness of aluminum, the resultant relative sliding at the block's mating surface also tends to increase. This further results in the increased risk of fretting fatigue failures, on the block's contact face with the bearing cap. Figure 5 shows such typical micro cracks generated on the block's contact face with the bearing cap. Due to the lower material strength as compared to the bearing cap, the fretting fatigue failures are observed on the block face rather than the MBC.

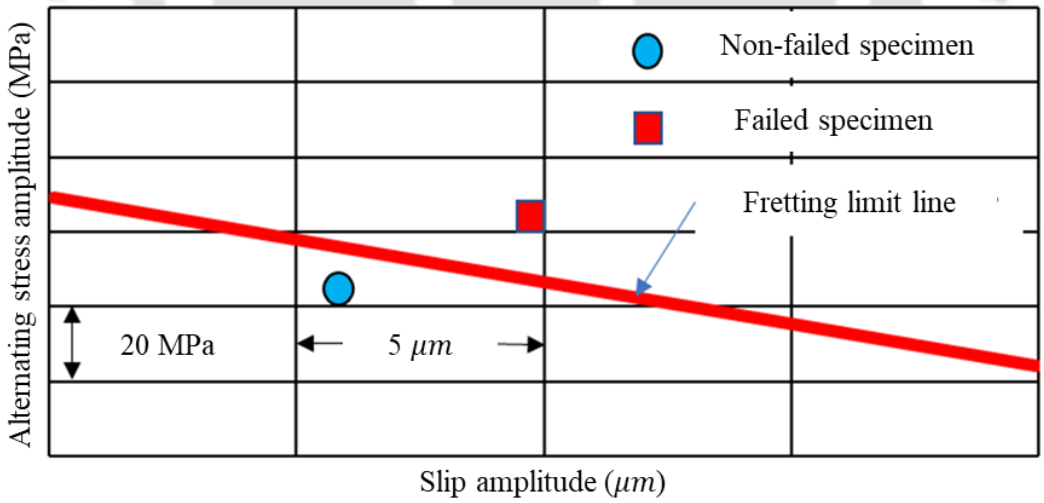

Figure 4: Fretting limit line with fracture probability of 10% (Reprinted with permission from [15, 19])

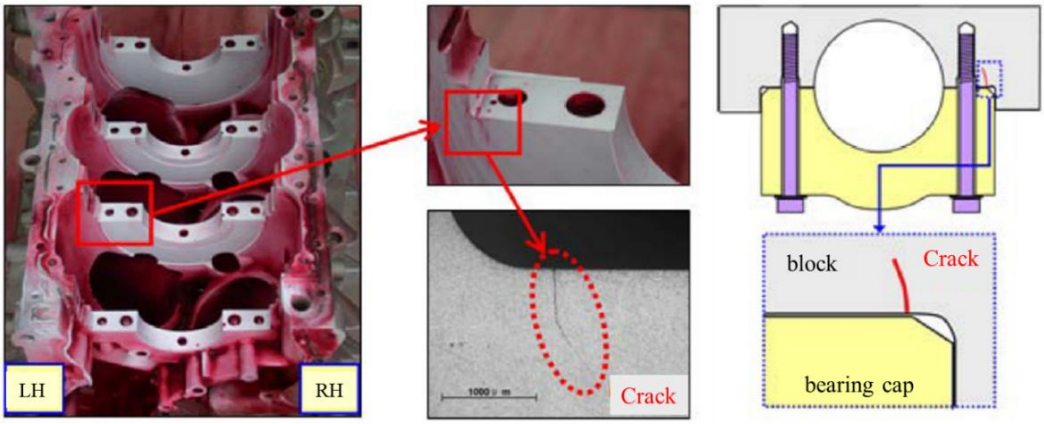

Figure 5: Fretting fatigue failures of the gasoline engine block (Reprinted with permission from [21])

Cha et al. [21] discussed and investigated such failures observed in the aluminum engine block. FEA is carried out considering the critical plane-based fatigue initiation methods like 'Smith-Watson-Topper' (SWT) [22] and 'Fatemi-Socie' (FS) [23]. Different critical engine parameters to be considered during the fretting damage evaluation of engine block are engine speed, bolt preload/contact pressure, design features like side-interference fit between the lock and bearing cap [21].

In another study, Hua et al. [24] mentioned that fretting crack in the engine block propagates in the direction perpendicular to the maximum principal stress at the fretting affected region, and the subsequent fatigue strength increases linearly with the contact pressure. Fretting fatigue failure observed in another critical engine component, i.e., connecting rod is discussed in the next section.

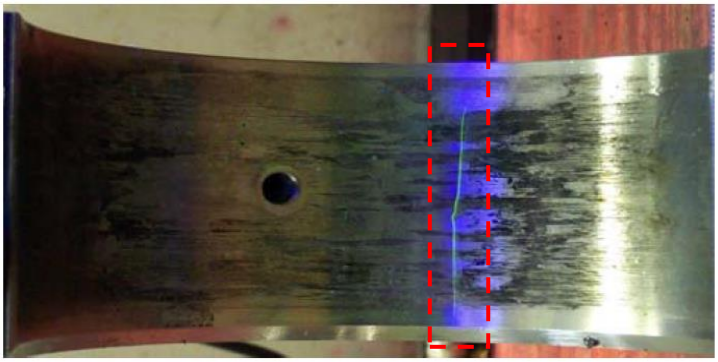

Figure 6: Connecting rod fracture due to fretting (Reprinted with permission from [25])

1.2.3. Fretting Fatigue Failure of Connecting Rod

As a result of complex dynamic loading, compared to other engine components, fretting fatigue is generally expected to occur more frequently in the connecting rod [13]. Connecting rod's design needs to meet various stringent design requirement like optimal bearing bore slip, bearing lubrication, bearing against the extreme engine operating loads like engine firing, engine inertia loads etc. Among such requirements, bearing bore slip primarily contributes to the possibility of fretting damage in the connecting rod. To accurately estimate the fretting damage, detailed transient analysis needs to be carried out by considering the contact pressure distribution obtained from an elasto-hydrodynamic bearing analysis. To obtain the reliable fretting damage prediction, both loads i.e., assembly loads and operating loads needs to be considered [26]. The combined effect of the relative slip between the connecting rod with the bearing and cyclic contact stresses, results in the fretting damage at the inner bore of the connecting rod. The resultant fretting damage can result in the micro-cracks which can further lead to the failure of the connecting rod, as shown in Figure 6. Ruiz parameters [16] are considered to evaluate fretting damage in the connecting rods [13, 25, 27]. Ruiz's criterion is comparatively simpler than other multiaxial-based fatigue prediction methods. Also, it considers the effect of parameters like contact pressure, coefficient of friction (COF) and relative slip motion. Thus, it is quite a popular technique for the comparative assessment of the fretting fatigue damage [13].

1.2.4. Fretting Fatigue Failure of Cylinder Head Gasket

Cylinder head gasket joint is one of the critical joints of any IC engine which is designed to provide necessary sealing forces against the in-cylinder pressurized hot combustion gases and also to avoid coolant/oil leakage out of the designed passages. The gasket is clamped between the cylinder head and block/liner/both. Considering the IC engine's extreme operating conditions, head gasket is a highly engineered product, design of which is finalized only after extensive design validation tests. Against the identified three possible failure modes of the head gaskets, as given below, analysis method for the fretting failure mode is comparatively less explored and developed [28];

1. Fluid/gas leakage due to low sealing pressure
2. Head gasket's bead cracking due to vertical load alteration

3. Gasket fretting failure

However, with the current design trend of increasing power density with the new engine designs, this failure mode is expected to occur more frequently [29]. Further, fretting damage of thin sheet components, similar to gaskets, is very less discussed in related research literatures. This is because most of the common fretting test methods are not well suited for thin structures [30]. As shown in Figure 7, fretting damage of the head gasket is a complex phenomenon with the interactions between different parts like cylinder block (with liner), cylinder head, head gasket, and head bolts. Thus, it needs to be investigated at the system level [31].

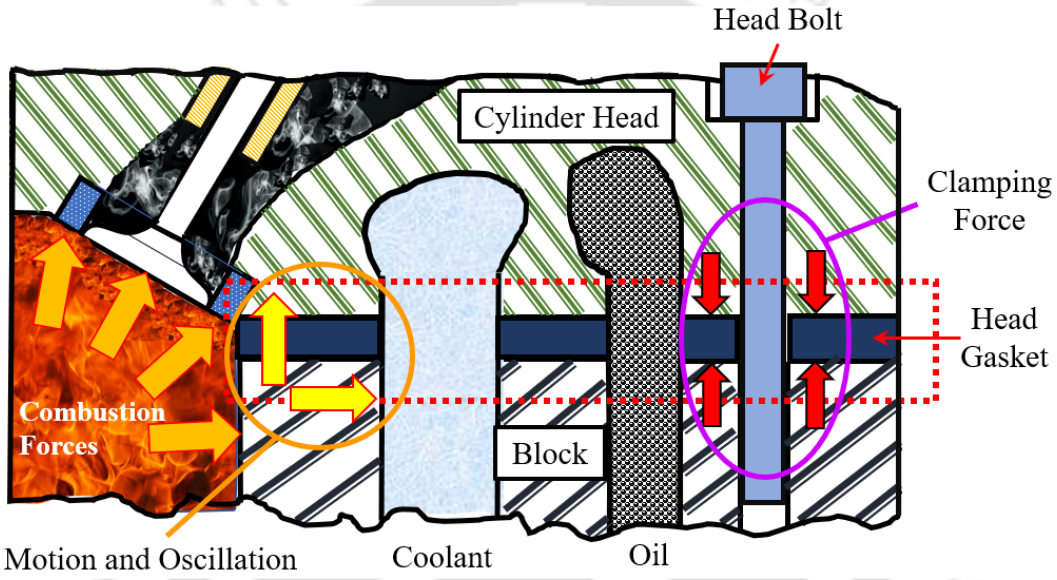

Figure 7: Head gasket fretting mechanism (Reprinted with permission from [33])

Figure 8 shows some of the observed fretting failures of the head gaskets. Different evaluation methods like Archard's wear equation [32] and Ruiz's parameter [16] have been individually considered for investigating the related problems. Brewer et al. [28] have considered the Archard's equation- based fretting wear parameter to correlate similar failures observed on the actual engine. The resultant wear parameter is based on parameters like contact pressure, relative sliding between the head and gasket, and the contact pair's wear coefficient and exponent. Similarly, in another head gasket fretting failure investigation [31], Ruiz's FDP parameter [16] is considered in the fretting fatigue failure prediction.

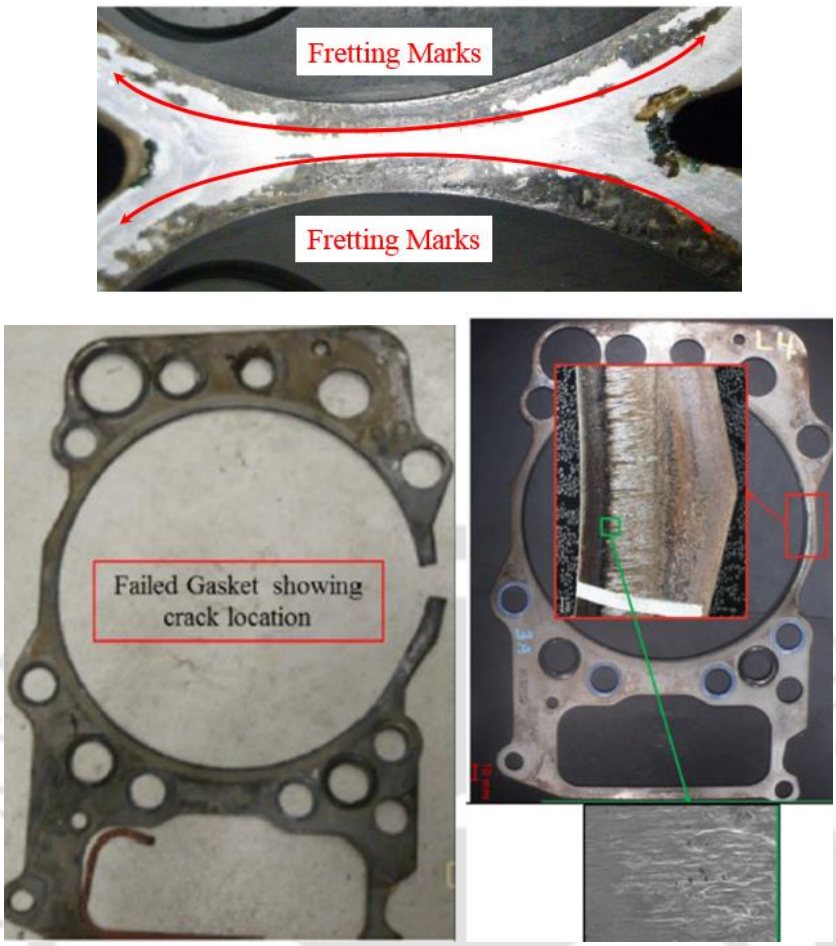

Figure 8: Fretting failures observed at the head gasket joint (Reprinted with permission from [28, 31])

Till now, fretting fatigue failures observed in different engine components like engine block, MBC, connecting rod, plain bearing and head gasket have been discussed in detail. Fretting damages are also observed in other engine parts like crankshaft balancing-weights [34] and diesel engine piston [35]. All these parts are critical to an IC engine, and subsequent failures can cause a partial/complete breakdown of the engine. Fretting fatigue can reduce the resultant fatigue life by 50-70% relative to plain fatigue theory [36]. Therefore, the development and validation of fretting fatigue analysis methodologies is justified to reduce the costs of failure in terms of warranty and downtime. Fretting fatigue is a surface degradation phenomenon with the combined interactions between different physical parameters involving tribology, contact mechanics, and material science. Consequently, different physical aspects of fretting fatigue need to be understood and are discussed in the next section.

1.3. Basics of Metal Fatigue Analysis

Fatigue failure results in a surface crack under the application of repetitive loads which would be else be too small to cause static failure of the same component. In most of the cases, fatigue damage initiates as shear cracks on the crystallographic slip planes. As shown in the Figure 9, during the fatigue failure, three stages are commonly observed as mentioned below:

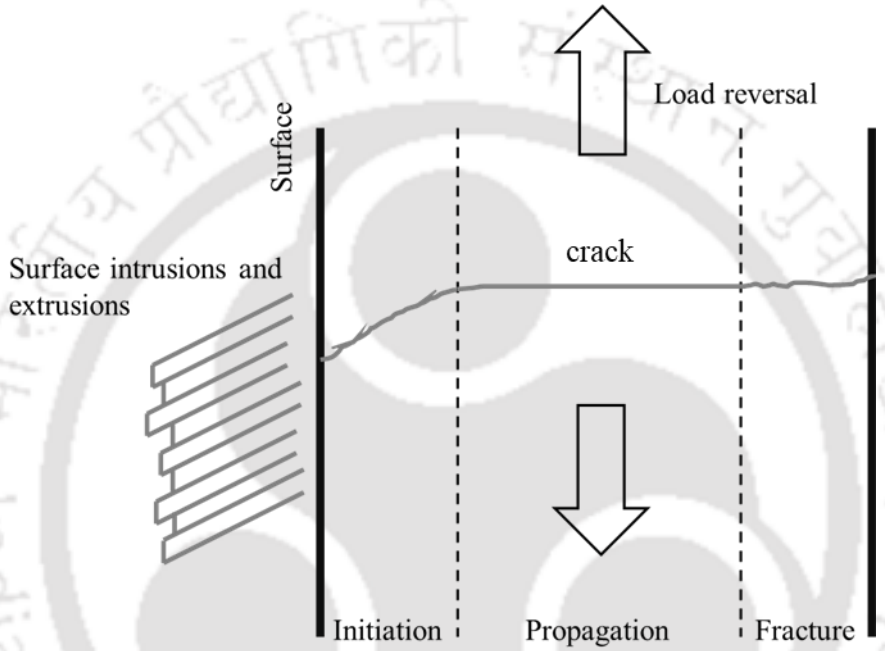

Figure 9: Three stages of fatigue failure

The three stages of fatigue failure are:

1. Crack initiation: In this stage, small micro length cracks are initiated under the influence of the local surface stress or strain. During this stage, the crack opening is typically like the mode II crack (as shown in Figure 10) i.e., the developed micro crack tends to grow along the plane experiencing maximum shear stress or strain amplitude.
2. Crack propagation: In this stage, the initially generated crack, grows further based on the stress state at the crack-tip. Typically observed as the mode I crack; the crack growth happens along the plane with maximum tensile stress amplitude.
3. Fracture: Once the crack is developed to significant depth, the component gets finally fractured.

For most of the internal combustion engine components, crack initiation is considered as the component design life. However, in the some of the industries like aerospace component's service life is considered as the combined life with crack initiation and crack propagation stages. Therefore, the choice of appropriate fatigue life estimation theory depends upon the end application and the corresponding market scenario (like warranty consideration etc.).

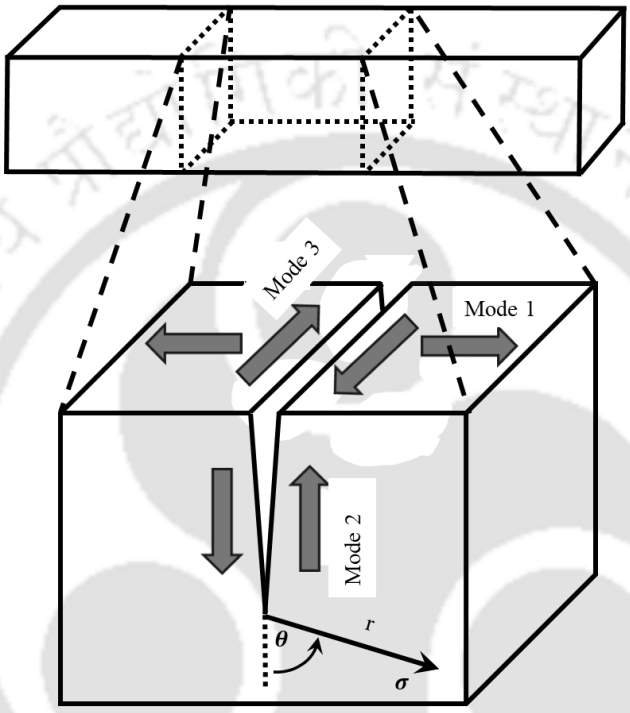

Figure 10: Three modes of loading of crack tip

1.3.1. Basic Fatigue Mechanism

Fluctuating operating load events (as shown in Figure 11) to which any structure is exposed to, is primarily responsible for fatigue failure of the structure. Thus, the resultant alternating stress due to the load reversal causes the fatigue failure of the component. Alternating stress magnitude combined with the resultant life, produces the endurance curve for the specific material or component. (Refer to Figure 12). The effect of mean stress on the fatigue life is also an important parameter and hence, needs to be considered. There are several theories which consider this effect. The corrected alternating stress, with appropriate mean stress correction is considered to estimate the resultant fatigue life of the structure. Several mean stress correction theories for SN curves have been proposed

by Goodman [37], Gerber [38], Soderberg [39] and Morrow [40]. Along with the mean stress effect, there are several other parameters which affect the endurance limit of the structure such as size factor, surface finish factor, environment, surface treatment etc.

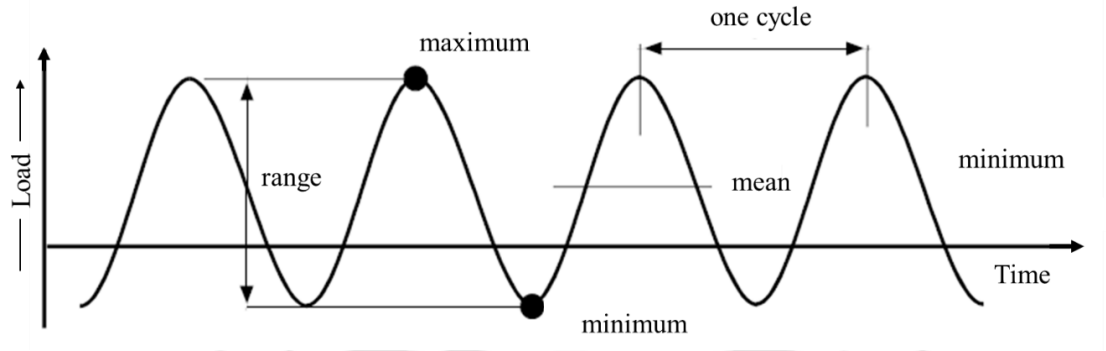

Figure 11: Load reversal with time

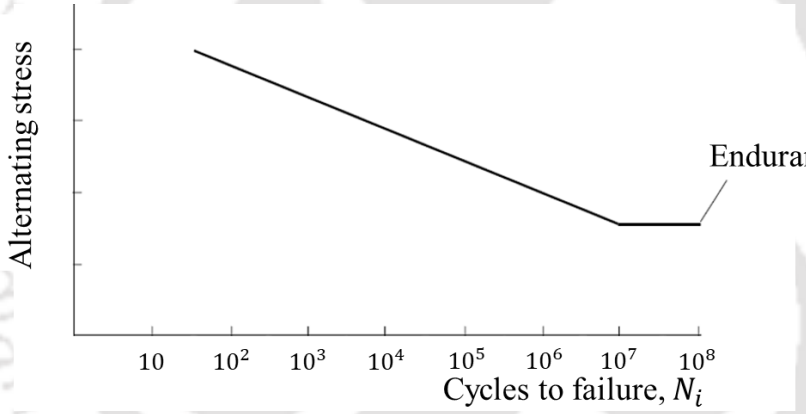

Figure 12: Typical endurance curve

1.3.2. Basic Classification of Fatigue Analysis: Stress Based and Strain Based Fatigue Analysis:

Based on consideration of either stress or strain values towards fatigue life estimation, fatigue analysis theories can be broadly classified into either stress-life approach or strain-life approach. The stress–life, linear relationship (Figure 13), firstly introduced by Basquin [41] is

$$\Delta\sigma/2 = \sigma_f'(2N_i)^b \quad (1)$$

where $\Delta\sigma$ is alternating stress range, σ_f' is fatigue strength coefficient, b is fatigue strength exponent and N_i is fatigue initiation life.

This stress-based fatigue life relationship is more appropriate in cases with low load levels where stresses and strains are linearly dependent. At high load levels i.e., in the low cycle fatigue regime, this relationship is observed to be conservative. In low cycle fatigue (LCF) regime, material behavior can be best modelled with strain-controlled conditions and the fatigue damage is dependent upon the resultant strain conditions [42]. Consequently, strain-based fatigue life relationship has been proposed later, especially for the LCF life calculation.

The plastic strain-life relationship proposed by Coffin [43] and Manson [44] is

$$\Delta\varepsilon_p/2 = \varepsilon_f'(2N_i)^c \tag{2}$$

Further, combining both elastic and plastic strains, finally the total strain-life relationship [45] (as shown in Figure 14) is

$$\Delta\varepsilon/2 = \left(\sigma_f'/E\right)(2N_i)^b + \varepsilon_f'(2N_i)^c \tag{3}$$

where $\Delta\varepsilon$ is alternating total strain range, $\Delta\varepsilon_p$ is alternating plastic strain range, ε_f' is fatigue ductility coefficient, c is fatigue ductility exponent, E is elastic modulus, N_i is fatigue initiation life, σ_f' is fatigue strength coefficient, b is fatigue strength exponent.

At large strain amplitudes, the strain-life curve coincides with the plastic line and at low strain amplitudes, the curve coincides with the elastic line. Thus, this relationship can be used for both LCF and high cycle fatigue (HCF) life calculations.

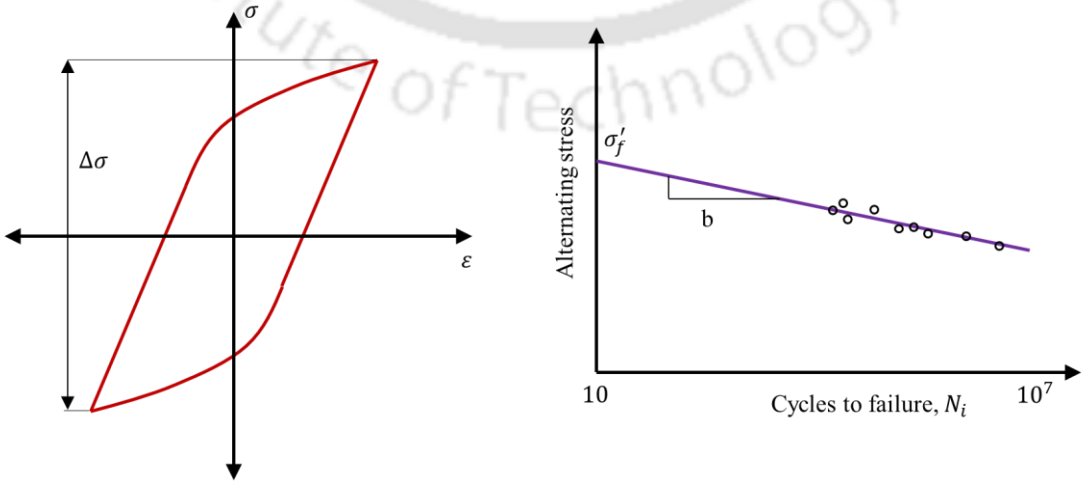

Figure 13: Stress-life relationship

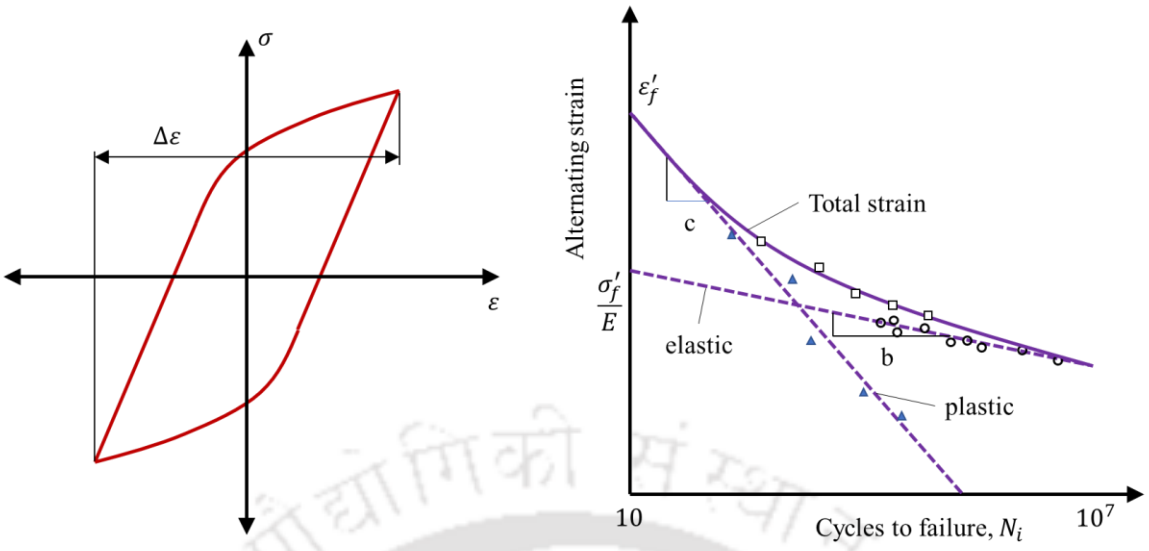

Figure 14: Total strain-life relationship

As compared to the stress-based life calculations, strain-based life calculations are observed to predict comparatively more accurate results, especially for low life results, where the component stresses are observed to be above or near yield limit. The above equations hold good for cases where the load cycle is fully reversible and needs to be modified in order to consider the mean stress effect. Fretting fatigue is a special fatigue damage phenomenon of the contacting bodies, as a result of cyclic stresses on the contacting bodies and reduces the fatigue life extensively compared with non-fretting fatigue.

1.4. Basics of Fretting

Most general definition of fretting is “damage at the junction of contacting bodies due to presence of oscillating force, which generates relative displacement between the contacting bodies”. Resultant loads during the fretting phenomenon produce a similar effect on the material as a sharp, dynamic loading notch [36]. It is observed that the predicted life correlation is improved by a factor of 2, after considering fretting fatigue corrections [46]. This observation signifies the effect of consideration of fretting related in contact problems.

Generally, the contact surface consists of two regions i.e.,

1. Stick region: is the region of the contact surface where relative displacement is zero/negligible.

2. Stick-slip region occurs near the edges of the contact, where comparatively higher relative displacement occurs. In the stick-slip region, relative displacement is observed between the contacting bodies, along with high contact stresses, causing the surface degradation i.e., fretting.

It is observed that the transition from fretting to reciprocating sliding is usually in the range till 300 μm, regardless of the normal load [5]. Further, based on the amount of the resultant slip at the contact junction, fretting damage is classified into two categories:

1. Fretting wear: It occurs in the gross-slip region of contact, typically when the slip amplitude is in the range of 20-300 μm . It results in the surface damage; however, the crack formation is very limited or absent.
2. Fretting fatigue: It occurs at low slip amplitude (generally below 20 μm) and the development of crack is dominant. Fretting fatigue is usually dominant at the mixed stick-slip region of the contact.

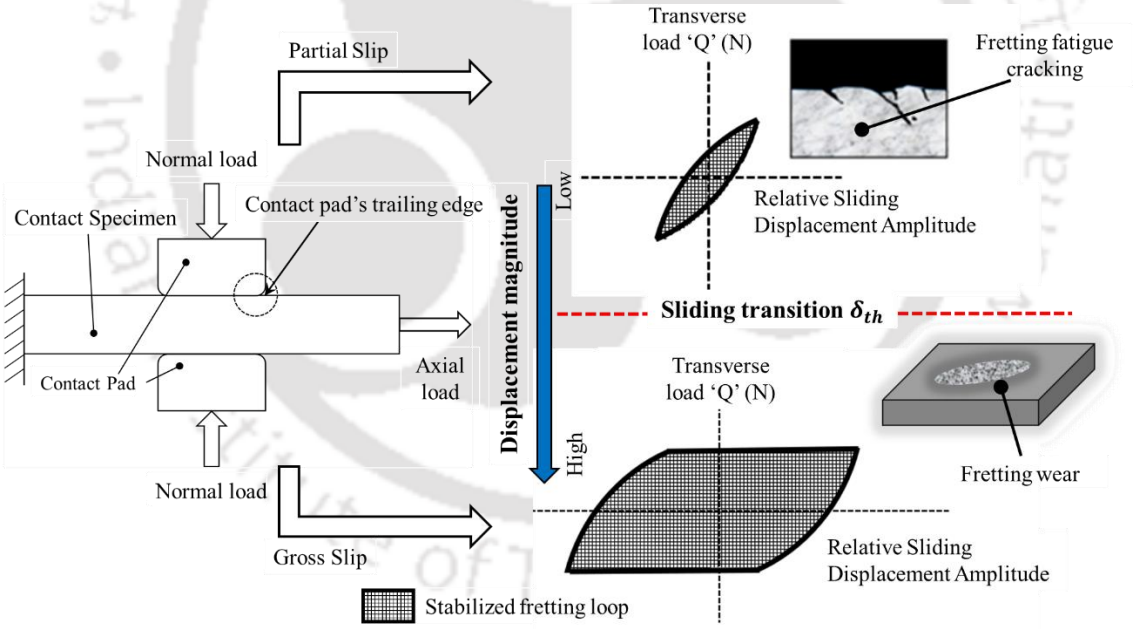

Figure 15: Illustration of fretting damage (Reproduced based on [52])

The combined effect of normal and bulk loads at the contact interface, causes the loss of mechanical energy in form of frictional energy due to friction and energy dissipation process. The area under the hysteresis curve between the transverse load (Q) and relative slip (δ), as shown in Figure 15, corresponds to the frictional energy generated during the resultant oscillatory movements at the contact surface. As the resultant frictional energy

exceeds the threshold strain energy limit, the dislocation of shear slip bands occurs, and crack starts to nucleate. Further, based on the relative slip magnitude, either fretting wear failure or fretting fatigue failure is observed at the contact surface.

As shown in Figure 16, it can be observed that fretting fatigue life decreases with increase in relative displacement value till certain threshold slip amplitude. Beyond this limit value, fretting fatigue life is observed to start increasing again. With the initial increase in relative slip displacement, the resultant surface traction also increases, resulting in the slip bands forming at the critical locations and thus forming the micro-cracks. However, with the higher relative displacement, the formed micro-cracks get shredded off and no further crack propagation can occur. Instead, the wear effect becomes more dominant beyond the critical value of the relative slip magnitude.

1.4.1. Fretting Fatigue

Under the influence of oscillating bulk forces, small amplitude oscillatory movement is observed at the contact interface and due to the applied normal contact load, cyclic stresses occur at the contact surface. Such cyclic stresses are mostly non-proportional and multiaxial in nature [49]. The cracks started to nucleate at the edge of the contact, where the tension induced due to the bulk loads is maximum. Initially the crack nucleation direction is approximately + 45° to the surface, like the mode II cracks [4].

Thus, the initial crack has two possible trajectories. In this early stage, the crack growth is dominated by the contact surface stresses. Later, as the crack grows beyond a certain critical length, the crack direction changes, and it becomes perpendicular to the contact surface. Thus becoming, mode I type crack. Now the contact growth is dominated not by the contact stresses but by the resultant stresses due to the bulk loading, like axial loads acting on the components etc. [49]. Schematic representation of the three modes of loading of the crack tip (Modes I, II, and III) is as shown in Figure 10. Commonly oblique crack length in the range of tens of microns till 3 mm is observed in various literature. [49].

Thus, to initiate a crack at the contact surface, alternating shear stresses are mentioned to cause a material dislocation in form of a slip band. Higher the amplitude of alternating stresses, higher is the probability of forming slip band. The amplitude of alternating shear stresses is directly proportional to the amplitude of relative slip magnitude at contact

surface: at low amplitude the fretting influence will be small whereas with increase in relative displacement up to threshold limit, it increases and again decreases at higher amplitudes. At higher amplitudes, the fretting wear effect gets more dominant. So, any embryonic crack which is developed gets ground away.

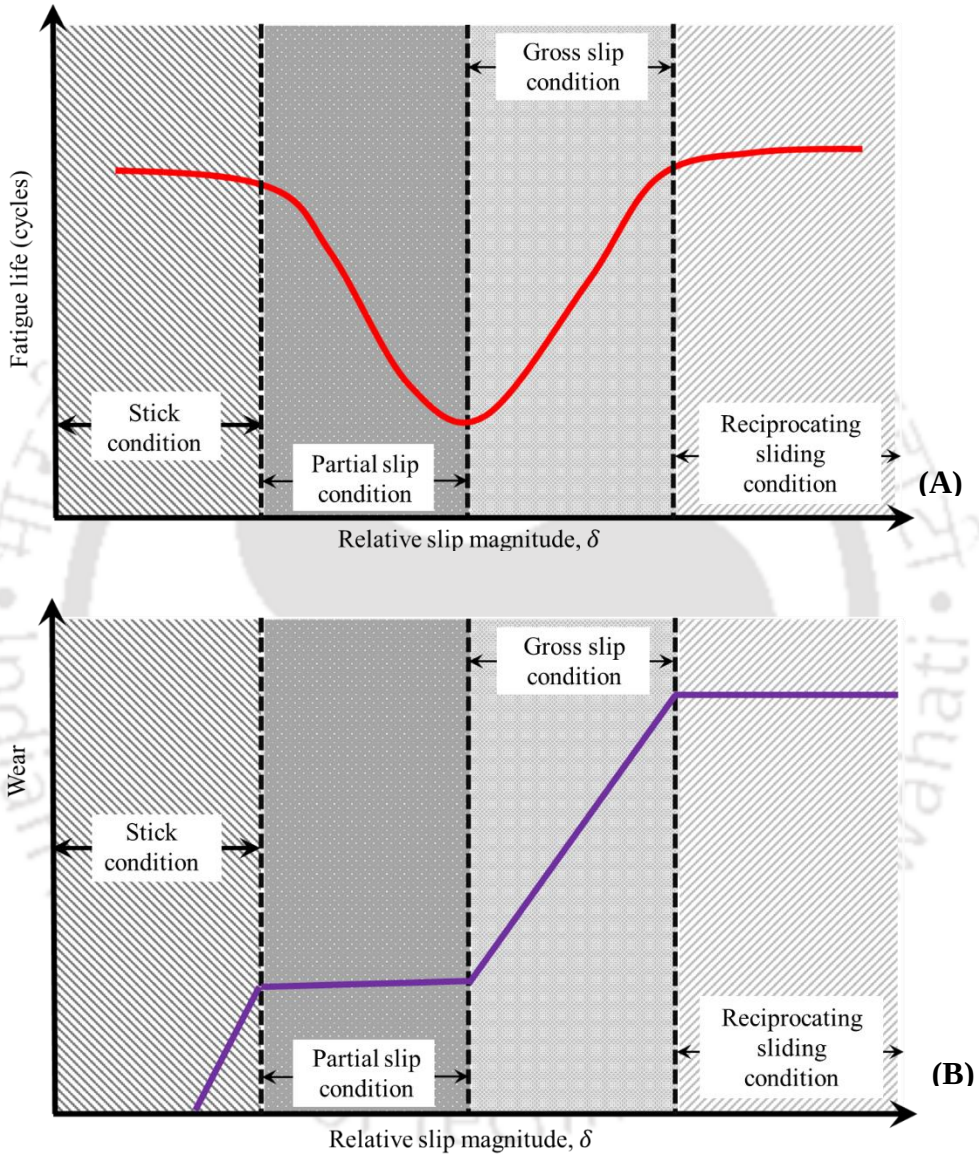

Figure 16 : Effect of slip amplitude on fretting fatigue life (A) and on fretting wear rate (B) (Reproduced based on [48])

Thus, it can be observed that contact stresses and relative sliding displacement between two contacting bodies, primarily drive the phenomenon of fretting fatigue initiation. Though it is mentioned that there are overall more than 50 parameters [50] which affect

the fretting fatigue, the above mentioned two parameters along with the coefficient of friction (COF) are the key parameters.

Using the resultant contact stress/strain conditions, fretting fatigue life can be appropriately estimated. In the next section, different crack initiation methods considered in various literatures towards the prediction of fretting fatigue failure are discussed.

1.5. Different Fretting Fatigue Crack Initiation Methods

According to Hills and Nowell [4], the focus of fretting fatigue should be on crack initiation, as most of the fretting fatigue life is involved in the crack formation rather than crack propagation. Further, as evident in several studies related to the fretting fatigue failures observed in IC engine components, good correlation is observed between the crack initiation life and the actual fatigue life results [51].

Different methods considered by various authors for evaluating fretting fatigue initiation life, can be broadly classified into four categories as given below [52]. Also, the overall summary of the different techniques is given in Figure 17.

1. Critical plane-based approach
2. Stress invariant approach
3. Continuum damage mechanics-based approach
4. Fretting-specific parameter-based approach

1.5.1. Critical Plane-Based Methods

In the real-world engineering problems, due to the nature of complex loadings, evaluation the critical plane with maximum fatigue damage is not always obvious. In the nonproportional loading cycle, the highest shear stress/strain and highest normal stress/strain often occurs at different time instances. Hence, the time history associated to the corresponding damage parameter should be considered during the evaluation of the critical plane and resultant initiation life [53]. In such cases, it is required to resolve the stress-strain components on number of planes and calculate the resultant fatigue damage on each plane. This methodology is termed as the critical plane method and has been considered as the most effective criteria in fatigue life evaluation [52]. The schematic representation of critical plane method in the fretting fatigue problem is shown in Figure

18. This concept was first introduced by Findley et al. [54]. Different critical plane-based methods considered so-far in the fretting fatigue damage evaluation are discussed further in the upcoming sections.

1.5.1.1. Stress-Based Critical Plane Methods

In the stress-based methods, alternating stress values are considered for the resultant fatigue damage and life evaluation. Generally, these parameters are more suitable for shear mode failures [52]. Being dependent only on stress values, these parameters do not include plastic terms in the fatigue life estimation and so, they are most suitable for HCF life calculations only.

- Findley parameter (FP): Introduced by Findley [54], this parameter is derived as

$$FP = \Delta\tau_{max}/2 + k_1\sigma_n^{max} \tag{4}$$

where $\Delta\tau_{max}$ is maximum alternating shear stress range and σ_n^{max} is maximum normal stress in the perpendicular direction to the critical plane with maximum shear stress range observed.

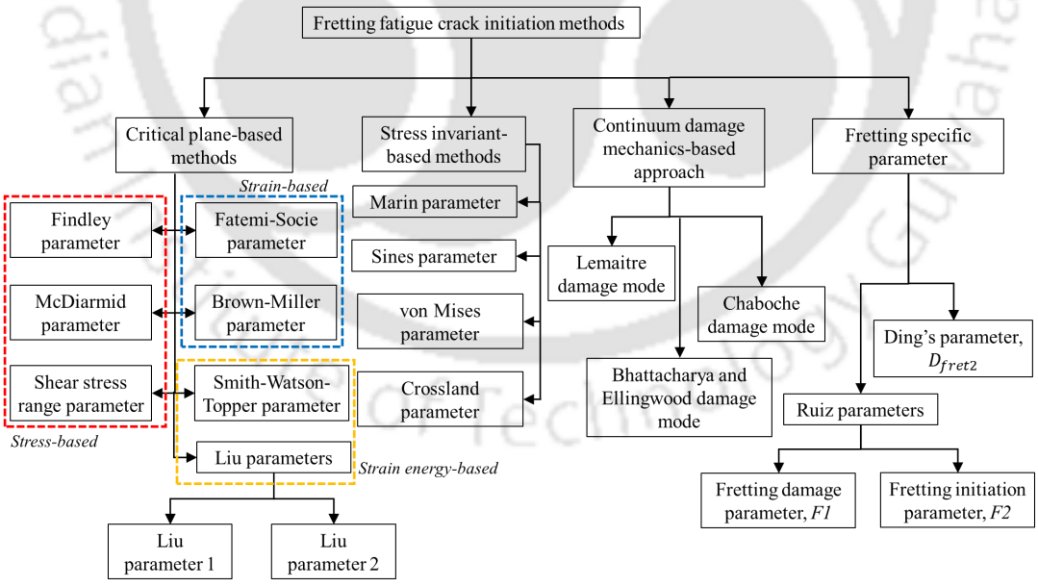

Figure 17: Generalized classification of fretting fatigue crack initiation criteria (Reproduced based on [52])

Material specific parameter, k_1 in the Equation 4 is evaluated as

$$\sigma_{f-1}/\tau_{f-1} = 2/(1 + (k_1/\sqrt{1 + (k_1)^2})) \tag{5}$$

where σ_{f-1} is fatigue limit in tension and τ_{f-1} is the fatigue limit in torsion.

The fatigue life corresponding to FP parameter is evaluated as

$$FP = \tau_f'(2N_i^{b'}) \tag{6}$$

where τ_f' is fatigue strength coefficient in shear, b' is fatigue strength exponent in torsion, N_i is the cycle to crack initiation.

Findley parameter (FP) is expected to be more suitable where the crack initiation and propagation directions are the same and failure is dominated by shear and normal stresses [45]. Lee et al. [55] and Murthy et al. [56], have observed that fretting fatigue life estimation based on FP parameter is within $\pm$ 3N scatter band with respect to the experimental fatigue life results. Like Findley parameter, there are several other stress-based, critical plane methods also like McDiarmid parameter (MD) and shear stress range parameter (SSR), Matake criterion (MT) and are discussed below.

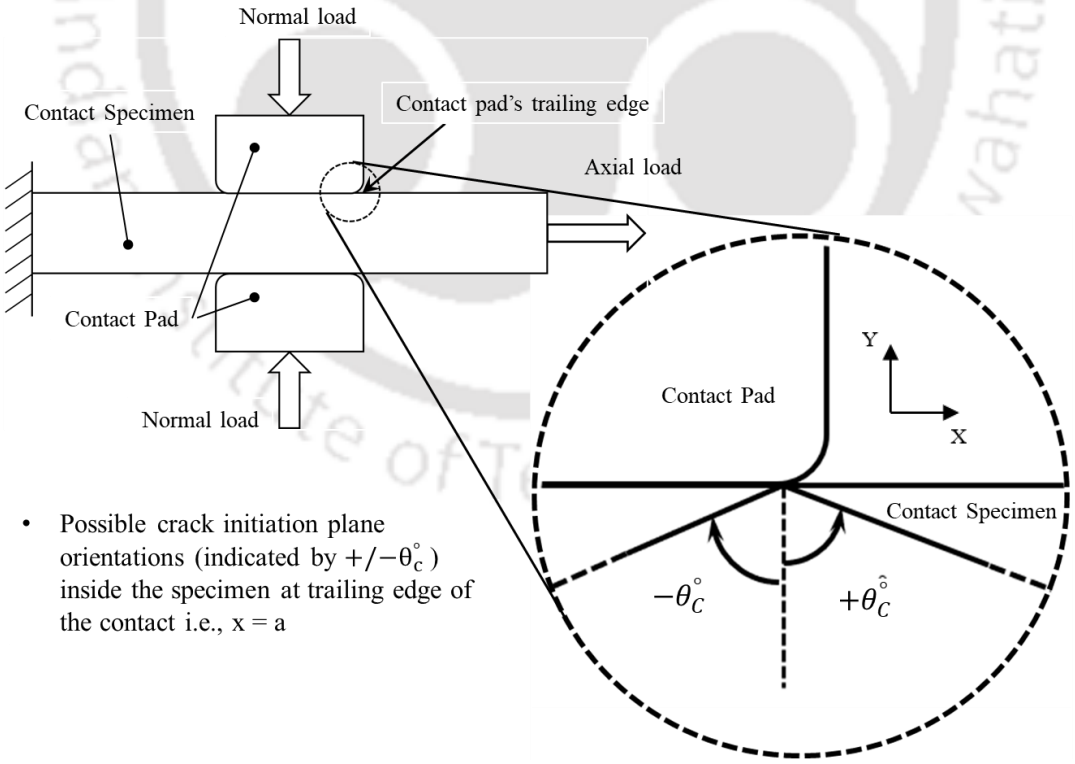

Figure 18: Critical plane consideration in fretting fatigue evaluation (Reproduced based on [52])

- McDiarmid parameter (MD): This parameter derived by McDiarmid et al. [57] can be applied to the situations in which the crack grows either parallel to the surface or into the surface. It is generally useful for HCF multiaxial loading. This parameter is derived as

$$MD = \Delta\tau_{max}/2 + (\tau_{f-1}/2\sigma_u)\,\sigma_n^{max} \tag{7}$$

and corresponding fatigue life is calculated as

$$MD = 0.5\left(1 + \left(\tau_{f-1}/2\sigma_u\right)\right)\sigma_f'(2N_i)^{b'} \tag{8}$$

where $\Delta\tau_{max}$ is alternating shear stress range, τ_{f-1} is the fatigue limit in torsion, σ_u is ultimate tensile strength, σ_n^{max} is maximum normal stress in perpendicular direction to the critical plane with maximum shear stress range, σ_f' is fatigue strength coefficient, N_i is the cycles to crack initiation and b' is fatigue strength exponent in torsion.

This parameter is observed to predict fretting fatigue initiation life results within $\pm$ 3N scatter band as compared to the experimental test results [58–60]

- Shear stress range parameter (SSR): This parameter introduced by Lykins et al. [61] is derived as

$$SSR = \tau_{max}\left(1 - R_\tau\right)^m = C_1 N_i^{C_2} + C_3 N_i^{C_4} \tag{9}$$

where τ_{max} is maximum shear stress, R_τ is the shear stress ratio i.e., τ_{min}/τ_{max}, m, C_1, C_2, C_3, C_4 are material parameters obtained through experimental test results and are required to be calibrated each time as they generally vary based on geometry, material or loading conditions and N_i is the cycle to crack initiation.

This parameter can be applied to the situations in which the fatigue crack initiation is governed by the maximum shear stress. To evaluate the effect of normal stresses on fretting fatigue life, Jin et al. [62] combined the SSR parameter with the maximum normal stress on the critical plane i.e., $\sigma_{n,max}$ to propose the modified SSR (MSSR) parameter as

$$MSSR = A(SSR^B) + C(\sigma_{n,max}^D) \tag{10}$$

Here, parameters *A-D* are determined by curve fitting of experimental fretting fatigue data. Shear stress range-based investigation for fretting problems is observed within $\pm$ 3N

scatter band with respect to the experimental fatigue life results [61–62]. In addition to the above-mentioned stress-based parameters, several other parameters like Matake (MT) criterion [63] is also considered towards the fretting fatigue life evaluation.

- Matake criterion (MT): This parameter proposed by Matake et al. [63] assumes that the fatigue damage is due to the maximum shear stress amplitude, $\tau_{a,max}$ along with the normal stress amplitude, $\sigma_{n,a}$ corresponding to the plane of maximum shear stress amplitude and is derived as

$$MT = \tau_{a,max} + m'\sigma_{n,a} \tag{11}$$

The coefficient m' is derived from the uniaxial fatigue tests as

$$m' = 2\frac{\tau_{f-1}}{\sigma_{f-1}} - 1$$

where $\tau_{a,max}$ is maximum shear stress amplitude, $\sigma_{n,a}$ is normal stress amplitude, τ_{f-1} is the fatigue limit in torsion, σ_{f-1} is fatigue limit in tension.

Fretting fatigue initiation life using MT parameter is observed within $\pm$ 3N scatter band with respect to the experimental life results [64]. Above discussed stress-based parameters are generally suitable for high cycle life fatigue situations, where strains are mainly elastic. Cases, in which, there is significant plastic deformation, strain-based approaches are more suitable. Some of the strain-based parameters, considered in the fretting fatigue life evaluation are discussed in the next section.

1.5.1.2. Strain-based Critical Plane-Based Parameters

Strain-based crack initiation parameters consider the total strain values. At large strain amplitudes, the strain-life curve coincides with the plastic line and at low strain amplitudes, the curve coincides with the elastic line. Thus, this relationship can be used for both LCF and high cycle fatigue (HCF) life calculations. Henceforward, in cases where yielding is expected, these parameters generally predict better correlation than the stress-based methods, However, during the non-proportional loading, when the maxima of shear strain and normal strain occurs at different time instances during the loading cycle, care needs to be taken.

- Fatemi-Socie parameter (FS): This strain-based parameter is the further modification of the Brown-Miller parameter [65] and is proposed by Fatemi and Socie [23, 66]. This parameter considers that fatigue failure is a function of the maximum shear strain amplitude i.e., $\Delta\gamma_{max}/2$ and the maximum tensile stress on the critical plane, σ_n^{max} and is derived as

$$FS = (\Delta\gamma_{max}/2)\left(1 + k_2(\sigma_n^{max}/\sigma_{yt})\right) = \tau_f'/G(2N_i)^{b'} + \gamma_f'(2N_i)^{c'} \quad (12)$$

where $\Delta\gamma_{max}$ is the alternating shear strain range, k_2 is ratio of σ_{yt}/σ_f', σ_{yt} is material yield strength, σ_f' is fatigue strength coefficient, σ_n^{max} is the maximum normal stress on the critical plane, τ_f' is fatigue strength coefficient in shear, G is shear modulus, N_i is the cycle to crack initiation, b' is fatigue strength exponent in torsion, c' is fatigue ductility exponent in torsion, γ_f' is shear fatigue ductility coefficient.

The schematic representation for this parameter is shown in Figure 19. This parameter considers the non-proportional loading effect and is given by the Equation 12.

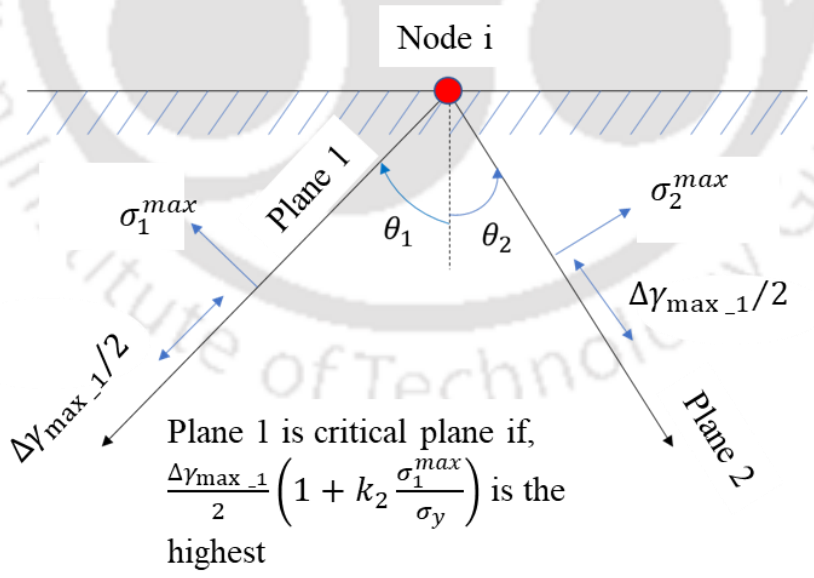

Figure 19: Schematic representation of FS parameter (Reproduced based on [36])

Szolwinski et al. [67] considered FS parameter to predict fretting fatigue crack initiation lifetime and was able to predict the fatigue life within $\pm$ 2N scatter band. Other strain-

based parameters considered for the fretting life evaluation are 'Tresca Yield Criterion (TYC)' [68], 'Lohr and Ellison (LE) criterion' [69], 'Li and Zhang criterion (LZ) [70].

- Tresca Yield Criterion (TYC): Tresca Yield Criterion [68] assumes that fatigue damage depends upon the maximum shear strain amplitude, $\Delta\gamma_{max}/2$ and the crack will initiate along the plane with maximum shear strain amplitude. This parameter is derived as

$$TYC = \frac{\Delta\gamma_{max}}{2} = 1.3\frac{\sigma_f'}{E}(2N_i)^b + 1.5\varepsilon_f'(2N_i)^c \quad (13)$$

where $\Delta\gamma_{max}$ is the alternating shear strain range, σ_f' is fatigue strength coefficient, E is elastic modulus, N_i is the cycle to crack initiation, b is fatigue strength exponent in tension, c is fatigue ductility exponent in tension and ε_f' is fatigue ductility coefficient.

Fretting fatigue initiation life using TYC parameter is observed within $\pm$ 2N scatter band with reference to the experimental fatigue life results [64].

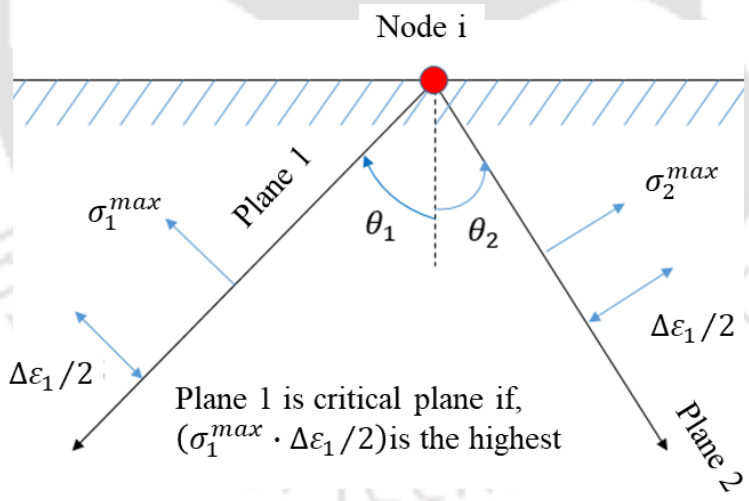

Figure 20: Schematic representation of SWT parameter (Reproduced based on [36])

1.5.1.3. Strain Energy-Based Parameters

In comparison to the stress-based and strain-based parameters, strain energy-based parameters generally produce more realistic results for fretting fatigue conditions where stress gradient is very high and material cyclic plasticity play an important role in the life estimation. The strain energy-based parameters depict path dependence of fatigue

properties more precisely than either of stress or strain-based approaches. Also, they can produce more realistic results for small pad radii and flat contact cases. However, the strain energy-based parameters like Smith-Watson-Topper (SWT) parameters produce good comparison with respect to fatigue initiation life and crack location but it has certain limitations towards predicting crack initiation orientation correctly [52].

- Smith-Watson-Topper parameter (SWT): This parameter proposed by Smith, Watson and Topper [22, 71] considers that the fatigue life is a function of the product of maximum normal stress, σ_n^{max} and normal strain amplitude, $\Delta\varepsilon_n/2$ i.e., the strain energy. Schematic representation of the SWT parameter is given in Figure 20. The SWT parameter is derived as

$$SWT = \sigma_n^{max}(\Delta\varepsilon_n/2) = \sigma_f'^2(2N_i)^{2b} + \sigma_f'\varepsilon_f'(2N_i)^{b+c} \quad (14)$$

where σ_n^{max} is the maximum normal stress on the critical plane, $\Delta\varepsilon_n$ is normal strain range on the critical plane, σ_f' is fatigue strength coefficient, N_i is the cycle to crack initiation, b is fatigue strength exponent in tension, c is fatigue ductility exponent in tension and ε_f' is fatigue ductility coefficient.

This parameter is mostly useful in cased in which expected fatigue failure is in mode I manner (Figure 10). Also, it is applicable to both LCF and HCF failures. This parameter considers the tensile stress as a main contributor to the fatigue damage accumulation process and initiation location is mainly dependent on it. This parameter has been extensively used by several researchers for fretting fatigue life evaluation [49, 72–77] etc. with the resultant experimental correlation obtained within $\pm$ 3N scatter band.

- Liu Parameters: Liu et al. [78] proposed two models based on mode I or mode II behavior of cracks (Figure 10). The first parameter which is based on mode I behavioral crack, is driven by the range of principal stresses ($\Delta\sigma_n$) and principal strains ($\Delta\varepsilon_n$) and is derived as

$$\begin{aligned}\Delta W_I &= (\Delta\sigma_n\Delta\varepsilon_n)_{\theta_{max}} + (\Delta\tau\Delta\gamma) \\ &= 4\sigma_f'^2/E\,(2N_i)^{2b} + 4\sigma_f'\varepsilon_f'(2N_i)^{b+c}\end{aligned} \quad (15)$$

where ΔW_I corresponds to total, elastic and plastic, work for mode I failure, $\Delta\sigma_n$ is the normal stress range on the critical plane, $\Delta\varepsilon_n$ is the normal strain range on the critical plane, θ_{max} is the critical plane with maximum value of $\Delta\sigma_n\Delta\varepsilon_n$, $\Delta\tau$ is the shear stress range on the critical plane, $\Delta\gamma$ is the shear strain range on the critical plane, σ_f' is the fatigue strength coefficient, N_i is the cycle to crack initiation, b is the fatigue strength exponent in tension, c is the fatigue ductility exponent in tension, ε_f' is the fatigue ductility coefficient, E is the elastic modulus.

The second parameter, based on mode II behavior of crack, is driven by the amplitude of shear stresses ($\Delta\tau$) and shear strains ($\Delta\gamma$) as

$$\begin{aligned}\Delta W_{II} &= (\Delta\tau\Delta\gamma)_{\theta_{max}} + (\Delta\sigma_n\Delta\varepsilon_n)\\ &= 4\tau_f'^2/G\,(2N_i)^{2b'} + 4\tau_f'\gamma_f'(2N_i)^{b'+c'}\end{aligned} \tag{16}$$

where ΔW_{II} corresponds to total, elastic and plastic, work for mode II failure, θ_{max} is the critical plane with maximum value of $\Delta\tau\Delta\gamma$.

Predicted fretting fatigue life results using these parameters are within $\pm$ 3N scatter band [52]. Like above parameters, there are several other strain-energy based parameters considered towards fretting fatigue life evaluation like 'Rolovic and Tipton (RT)' criterion [79], Chen, Xu and Huang (CXH) criterion [80]. However, results predicted using these methods do not correlate well with the experimental results [63]. Critical plane methods calculate the resultant fatigue damage values of above discussed 'Fatigue Initiation Parameters' (FIP's) over different planes passing through each node of the considered FEA domain. In order to obtain corresponding FIP values over different planes, stress-strain transformation on such planes needs to be carried out. Subsequent details are discussed in the next section.

1.5.1.4. Stress-Strain Transformations

Through critical plane-based method, maximum value of the corresponding FIP is obtained to predict the resultant minimum fatigue life results. To obtain these results, above mentioned FIP's are combined with critical plane-based method. In critical plane

method, using the transformation equations [81–82], the nodal stress and strain values are transformed on different planes as

$$\sigma_\theta = (\sigma_x + \sigma_y)/2 + \big((\sigma_x - \sigma_y)/2\big)cos2\theta + \tau_{xy}sin2\theta \quad (17)$$

$$\tau_\theta = \big((\sigma_x - \sigma_y)/2\big)sin2\theta - \tau_{xy}cos2\theta \quad (18)$$

$$\varepsilon_\theta = (\varepsilon_x + \varepsilon_y)/2 + \big((\varepsilon_x - \varepsilon_y)/2\big)cos2\theta + (\gamma_{xy}/2)sin2\theta \quad (19)$$

$$\gamma_\theta = -((\varepsilon_x - \varepsilon_y)/2)sin2\theta + (\gamma_{xy}/2)cos2\theta \quad (20)$$

where σ_θ is the normal stress on a plane with orientation as θ, ε_θ is the normal strain on a plane with orientation as θ, σ_x is the normal stress in x direction, σ_y is the normal stress in y direction, ε_x is the normal strain in x direction, ε_y is the normal strain in x direction, γ_{xy} is the shear strain on x-y plane, τ_θ is the shear stress on a plane with orientation as θ, γ_θ is the shear strain on a plane with orientation as θ.

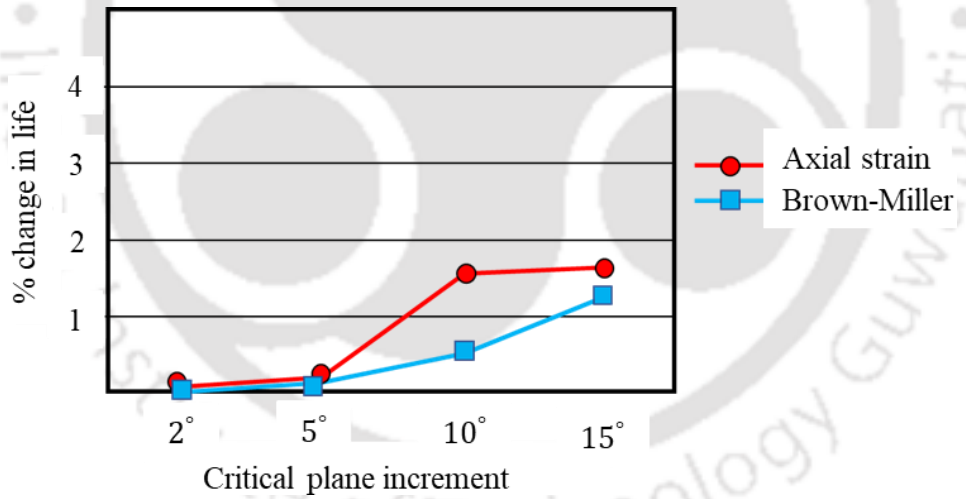

Figure 21: Percentage change in life results with critical plane angle increment (Reproduced based on [45])

Using the transformed stress-strain values, FIP value is calculated for each plane passing through each point in the considered FEA domain. These planes are selected often in 10° increment. Figure 21 shows the effect of change in fatigue life by varying this increment. It is observed that the increment of 10° with less than 2% change in fatigue life results, achieves the right balance between the accuracy and required solution time.

1.5.2. Stress Invariant-Based Approach

Looking from the aspect of computational efficiency, stress invariant-based techniques can be possibly considered as the most promising for the fatigue life estimation. This approach is generally suitable for medium/high cycle fatigue regime Among the various approaches available like Marin [83], Sines [84], von Mises [85] etc. Crosland parameter is mostly considered to analyse the fretting fatigue issues [60, 86–87] and discussed in the next section.

- Crossland Parameter (CL): Unlike critical plane-based methods, Crossland parameter [88] does not require the damage values to be calculated along the critical planes but it is based on the stress invariant values and produces scalar results in bulk material. The corresponding fatigue life relationship is derived as

$$CL = \sqrt{J_{2a}} + \sigma_{H,max}\left(3\tau_{f-1}/\sigma_{f-1} - \sqrt{3}\right) \tag{21}$$

where $J_{2,a}$ is the amplitude of the second deviatoric stress tensor, $\sigma_{H,max}$ is the maximum hydrostatic stress tensor, σ_x is the normal stress in x direction, σ_y is the normal stress in Y direction, τ_{f-1} is the fatigue limit in torsion, σ_{f-1} is fatigue limit in tension.

The failure happens as the value of CL parameter exceeds the torsional fatigue limit of the material i.e., τ_{f-1} . Further, it can also be combined with Basquin's equation [41] to assess the resultant fatigue life [60] as

$$CL\left(\frac{\sigma_{f-1}}{\tau_{f-1}}\right) = \sigma_f'(2N_i)^b \tag{22}$$

where σ_f' is the fatigue strength coefficient, N_i is the cycle to crack initiation, b is the fatigue strength exponent in tension.

Compared to the critical plane-based approaches, this parameter has the advantage of shorter computational time because in this approach damage is calculated in bulk material and not on any critical plane. However, simultaneously it has the disadvantage that it

cannot predict the crack initiation orientation. Also, it is observed to have relatively high fatigue index error of 15%-45% [52].

1.5.3. Continuum Damage Mechanics-Based Approach

'Continuum Damage Mechanics'-based (CDM) approach, originally introduced by Kachanov [89] (shown in Figure 22) is another popular approach, evolved recently in the fretting fatigue damage evaluation. It calculates the damage variable; D inside a 'Representative Volume Element' (RVE) of a damage body. This damage variable is then combined with the effective stress to calculate the corresponding damage. The crack is expected to initiate as the calculated damage variable reaches the material's threshold limit value. The CDM approach has been further extended by many researchers for failure modes like LCF [90] and HCF [91]. Among the various CDM approach-based models available, only those models which have been applied to the fretting fatigue problems, are discussed here.

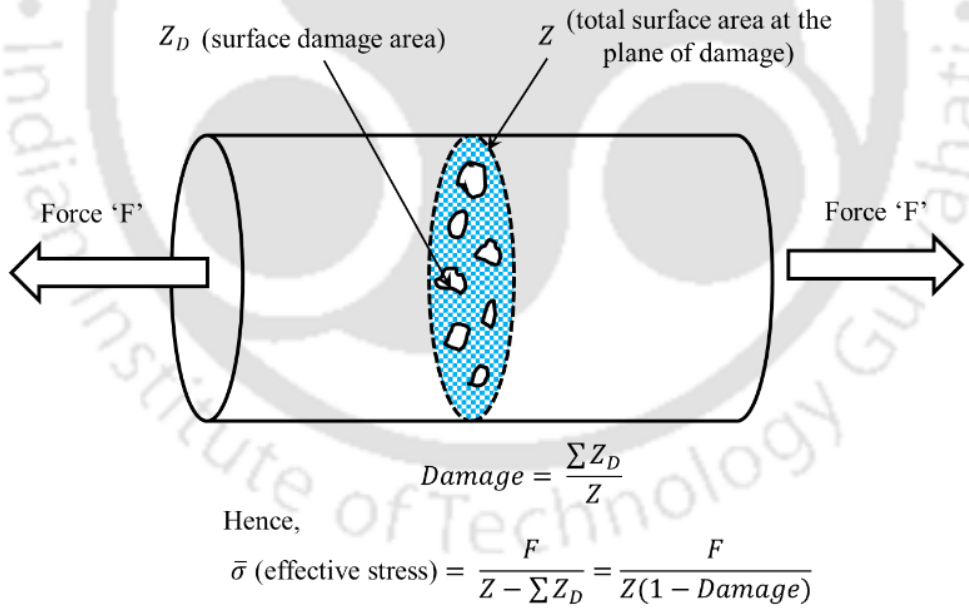

Figure 22: Concept of CDM approach with representative volume element of a damaged body (Reproduced based on [52])

- Lemaitre damage model: A damage model initially proposed by Lemaitre et al. [92] is further extended by Talemi and Wahab, for both elastic [93] and elastic-plastic conditions [94]. Corresponding fatigue life equation for elastic condition is

$$N_i = (1/A(\beta+3))\,(\sigma_{eq,max}^{\beta+2} - \sigma_{eq,min}^{\beta+2})^{-1} R_\vartheta^{-((\beta/2)-1)} \quad (23)$$

and for elasto-plastic condition is

$$N_i = \frac{(\sigma_{eq\,max}^{-(m+2\beta} - \sigma_{eq\,min}^{-(m+2\beta})R_\vartheta^{-\beta}}{A(z+2\beta+2)} \quad (24)$$

where $\sigma_{eq,max}$ is the maximum equivalent von Mises stress, $\sigma_{eq,min}$ is the minimum equivalent von Mises stress, A is the material dependent damage parameter, β is the material dependent damage parameter, z is the power constant in Ramberg–Osgood equation [95], R_ϑ is the triaxiality function [94] and N_i is the cycle to crack initiation.

Here, parameters A and β need to be obtained experimentally.

- Bhattacharya and Ellingwood model: Bhattacharya et al. [96] considered the thermodynamic framework towards damage calculations. This approach was further extended by Quraishi et al [97] to propose the subsurface shear stress-based fretting fatigue life results. In this work, it is assumed that the crack due to fretting fatigue initiates just below the surface. Thus, subsequent material degradation occurs inside the surface. This assumption helped to overcome the drawback of CDM approach that it predicts only volume wide degradation and surface damage modes like wear and fretting, cannot be modeled using CDM. Also, compared to other CDM approaches, this parameter avoids using empirical relationships which are generally obtained through experimental testing. Rather, it uses bulk material properties to predict crack initiation.

  As per this approach, fretting fatigue damage at the end of N cycles i.e., D_N is derived as

$$D_N = 1 - (1 - D_{N-1}) \prod_{i=1}^{N} F \quad (25)$$

where parameter F considers the loading conditions and different required material properties and D_{N-1} is the accumulated damage at *N-1* cycles. In this approach crack propogation phase is neglected.

- Chaboche damage model: Chaboche et al. [98] proposed a 'Nonlinear Continuous Damage' (NLCD) fatigue damage model. Zhang et al. [99] extended this work and validated it for plain fatigue and fretting fatigue. By integrating the damage evolution, $\dot{D}$, between two material states i.e., initial virgin material condition, *D=0* to material condition with micro-initiation cracks (10-200 μm) i.e., *D=1*, they proposed the number of cycles to failure against the multiaxial loadings as

$$N_i = \frac{1}{1+\beta'} \frac{1}{a' \, M_0^{-\beta'}} \frac{\langle \sigma_u - \sigma_{e,max} \rangle}{\langle A_{II} - A_{II}^* \rangle} \left[\frac{A_{II}}{1 - 3b_2 \bar{\sigma}} \right]^{-\beta'} \tag{26}$$

where A_{II} is the amplitude of octahedral shear stress, A_{II}^* is the Sines fatigue limit criterion, β, a, M_0, b_2 are the required material constants, to be obtained from fatigue tests or *SN* curve, σ_u is the ultimate tensile strength, $\sigma_{e,max}$ is the maximum equivalent stress during the loading cycle, $\bar{\sigma}$ is the mean stress during the loading cycle, N_i is the cycle to crack initiation.

The predicted fatigue results using this approach are found to be within $\pm$ 3*N* scatter band [52]. With respect to the experimental results, CDM approaches show good correlation in terms of the crack location and also overall, the predicted life is in the range of $\pm$ *2N* scatter band [52]. Also, compared to the critical plane-based approaches, CDM approach shows lower deviation. The proportion of initiation life with respect to total life predicted by CDM approach has been maximum i.e., 55%[52]. This method has been used in various literatures [100–101] and is observed to be effective in terms of predicting the fretting fatigue life results in and crack location. Similar to the stress invariant approach, CDM approach is also computationally less expensive as compared to the critical plane methods, but it produces results in terms of scalar and does not provide any information in terms of crack orientation. In addition, it requires extensive material testing to obtain the required material parameters.

1.5.4. Fretting Specific Parameter

Fretting fatigue being mainly a surface degradation phenomenon, damage parameters like Ruiz parameters [16], Ding's Fretting damage parameter (D_{fret2}) [102], involving contact

surface slip and contact stresses, are some of the useful techniques to evaluate the resultant fretting fatigue damage and are discussed here.

- Ruiz Parameters (*F1* and *F2*): During their study, Ruiz et al. [16] considered a dovetail joint between the blade and the disc of a gas turbine on a biaxial fatigue machine. They proposed that the reduction in the fatigue life for contact problems can be primarily attributed to the fretting damage in terms of relative slip and contact peak stresses. Based on the experimental observations, they proposed two parameters i.e., *F1* and *F2*, combining the effect of slip amplitude and contact stress components. The first parameter *F1*, also known as damager or wear parameter, is the product of contact frictional stress τ and relative sliding distance δ. It can be interpreted as the resultant frictional energy created due to contact forces. It is observed that for most of the cases, the maximum value of *F1* closely correlates with the experimental maximum fretting wear location [52]. *F1* parameter is derived as

$$F1 = \tau\delta \tag{27}$$

The second parameter *F2*, also known as the initiation parameter, is a product of contact frictional stress τ, relative slip amplitude δ and maximum tensile stress, σ_{max} and is derived as

$$F2 = \tau\delta\sigma_{max} \tag{28}$$

Between the two parameters, *F2*, is observed to be more effective to match the crack initiation location [25, 74]. Though being simple and fast to evaluate, some of the main disadvantages is of Ruiz parameters are mentioned below:

- These parameters cannot predict fretting fatigue initiation life.
- Also, there is no material dependent critical limit defined towards crack initiation.
- These parameters do not show any insight towards crack initiation orientation.
- Mainly, being stress-dependent parameters, these parameters have limitations towards the cases with metal-plasticity.

However, as mentioned earlier, being simple and fast to evaluate Ruiz's parameters are quite popular for the comparative assessment of fretting fatigue damage [13] and is

considered for comparative fretting fatigue damage evaluation in different IC engine components [13, 17, 25, 27, 31].

- Fretting Damage Parameter (D_{fre2}): This parameter proposed by Ding et al. [102], combines multiaxial FIP and the estimated surface damage due to fretting, in order to calculate subsequent crack initiation life. The key advantage of this parameter is that it includes the effect of frictional work i.e., $\tau\delta$, as considered in Ruiz's parameters [16]. In this way, the detrimental effect of fretting wear/relative sliding on fatigue life results can be considered which are generally neglected in fatigue life estimation, using just plain FIP's [52].

  In this parameter, the effect of wear on fretting fatigue is considered through the threshold slip magnitude. As explained earlier in 'Section 1.4', fretting fatigue life initially decreases with the increase in slip magnitude until a certain threshold limit. Beyond this limit value, slip magnitude does not have any detrimental effect on fretting fatigue. Ding's D_{fre2} parameter [102], accounts for the detrimental effect of the increasing sliding distance on fretting fatigue life as

$$D_{fret2} = (1 + C\tau\delta)\left\langle 1 - \frac{\delta}{(\delta)_{th}}\right\rangle^{n} \tag{29}$$

  where C, n are the material constants, δ is the relative sliding distance, τ is the contact frictional stress, δ_{th} is the threshold limit value for the relative slip beyond which fretting wear mode becomes more dominant over the fretting fatigue mode.

  Ding's parameter, D_{fre2} is applicable till the relative sliding reaches the corresponding threshold sliding limit value. It should be noted here that in this approach beyond the threshold limit value, fatigue life results are decoupled from the effect of slip magnitude.

  The constants like C, n and δ_{th} constants are obtained from fretting wear and fretting test data and are material constants and independent of geometry and loading conditions. This correction factor can then be applied to the corresponding FIP values to obtain the resultant fretting fatigue life results. Ding has mentioned that this parameter is valid only for the condition $\delta \leq \delta_{th}$. For cases in which $\delta > \delta_{th}$, conventional FIP parameter equation can be considered, and, in that case, this correction factor is not considered to calculate fretting fatigue life results.

The key advantage of this approach is that it computes fretting fatigue life accurately without considering the incremental wear calculations, which will need additional computational efforts. By considering this parameter, the effect of wear towards life estimation is considered which is generally neglected using plain FIP's. Thus, it captures the change in fatigue life results with subsequent changes in the relative slip magnitude in the partial slip regime, as shown in Figure 16. Compared to earlier discussed methods, this approach is relatively new and has been earlier evaluated only with the SWT parameter [102]. The fatigue life estimation using the modified SWT parameter is

$$\sigma_n^{max}(\Delta\varepsilon_n/2)D_{fret2} = ((\sigma_f')^2/E)(2N_i)^{2b} + \sigma_f'\varepsilon_f'(2N_i)^{b+c} \quad (30)$$

However, it can be also applied to any other multiaxial fatigue criterion, for different materials and loading modes.

So far, along with observed fretting fatigue failures in different engine components and different crack initiation methods, physics behind fretting fatigue are discussed. Some of these methods like Ruiz parameters, critical plane-based methods like SWT and FS parameters are already considered towards identifying the crack initiation location/s due to fretting fatigue in IC engine components. Further, different parameters, physical and analytical, critical towards fretting fatigue need to be explored. Like contact stresses and relative slip amplitude, 50+ different physical and analytical parameters are important towards the accurate estimation of fretting fatigue failure [50]. Hence, in the next section, several physical and analytical parameters, critical towards fretting fatigue damage of the IC engine components are discussed.

1.6. Important Parameters in Fretting Fatigue Evaluation

It is mentioned that there are more than 50 parameters- both physical and analytical in nature- which affect the resultant fretting damage [50]. Some of these factors are as shown in Figure 23. Among these parameters three critical parameters which affect the fretting fatigue are normal load, relative displacement and coefficient of friction. All other parameters are secondary and affect fretting through these three primary variables [1]. Below are presented the relevant parameters to be considered towards fretting fatigue damage in internal combustion engine components.

1.6.1. Operating Loads, Phase Difference and Frequency

Bolted joints in IC engine undergo extreme dynamic loads, varying in both, amplitude and frequency. For example, as shown in Figure 24, head bolt preload value changes during engine operating conditions and experiences further stretch/relaxation based on the nature of normal forces.

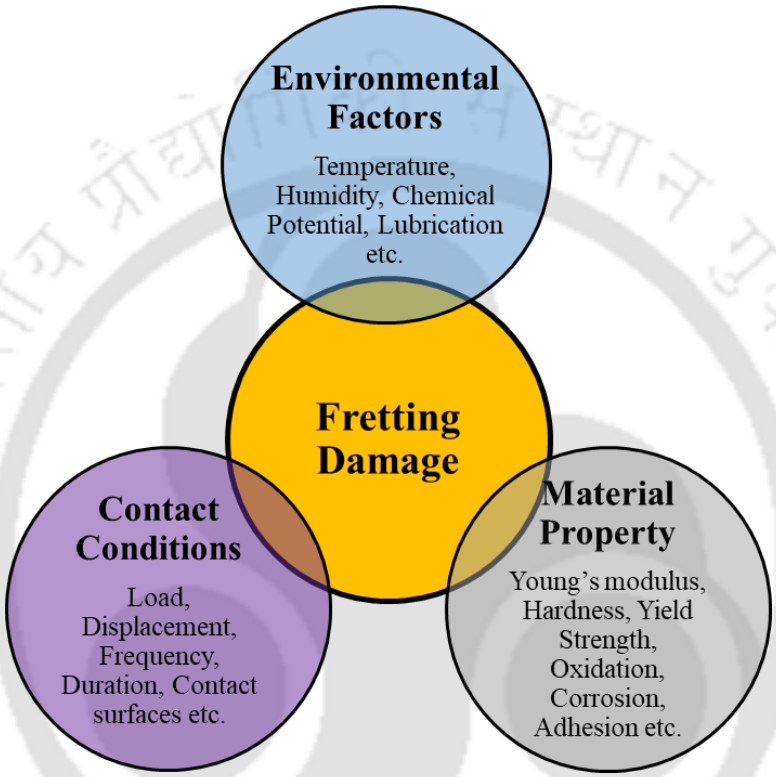

Figure 23: Different factors affecting fretting (Reproduced based on [103])

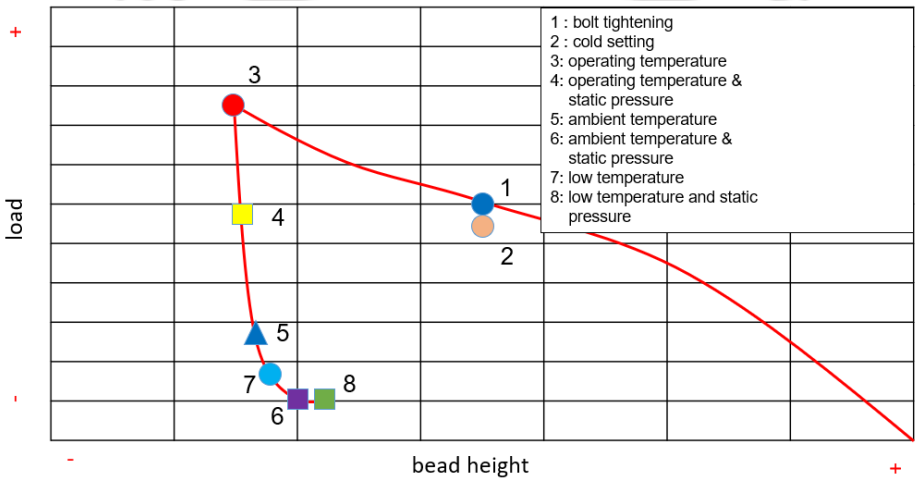

Figure 24: Bolt preload variation for engine operating condition (Reprinted with permission from [33])

These load variations occur at different frequencies. For example, cylinder head bolt load variation due to engine firing forces occur more frequently than the load variation due to corresponding thermal loads. Also, the different engine loads do not necessarily occur at the same time instance and will have some phase difference with each other. Thus, there will always be a complex dynamic loading pattern onto bolted joints in internal combustion engine.

1.6.1.1. Phase Difference

The normal, tangential and axial bulk load acting onto a typical fretting test set-up, as shown in Figure 25, resemble the resultant loads acting onto a bolted joint of an IC engine. The normal load resembles the bolt preload acting onto a typical gasket joint, the axial bulk load resembles the resultant load primarily due to the engine firing and the tangential force resembles the force due to the relative thermal expansion between the gasket and head/block/both. In the experimental fretting fatigue evaluation, it is observed that the phase difference between the transverse load 'Q' and axial load σ_{bulk} affects both the damage initiation location and fatigue life [53, 100–101, 105].

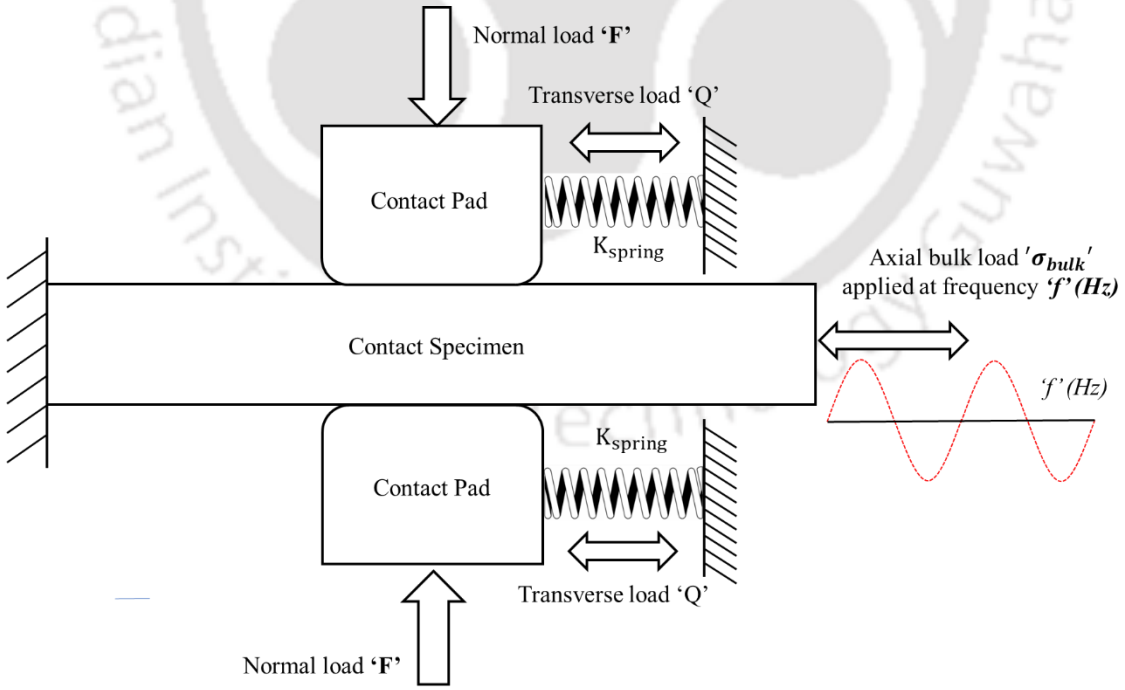

Figure 25: Schematic representation of fretting fatigue experimental set-up (Reproduced based on [104])

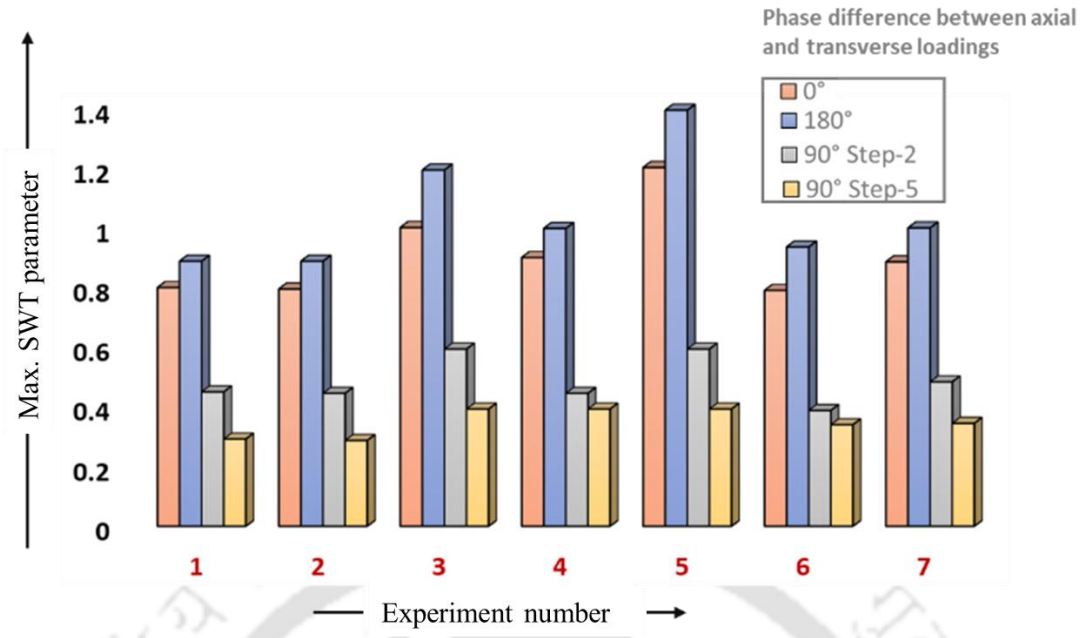

Figure 26: Effect of phase difference between loadings on fretting damage (Reproduced based on [105])

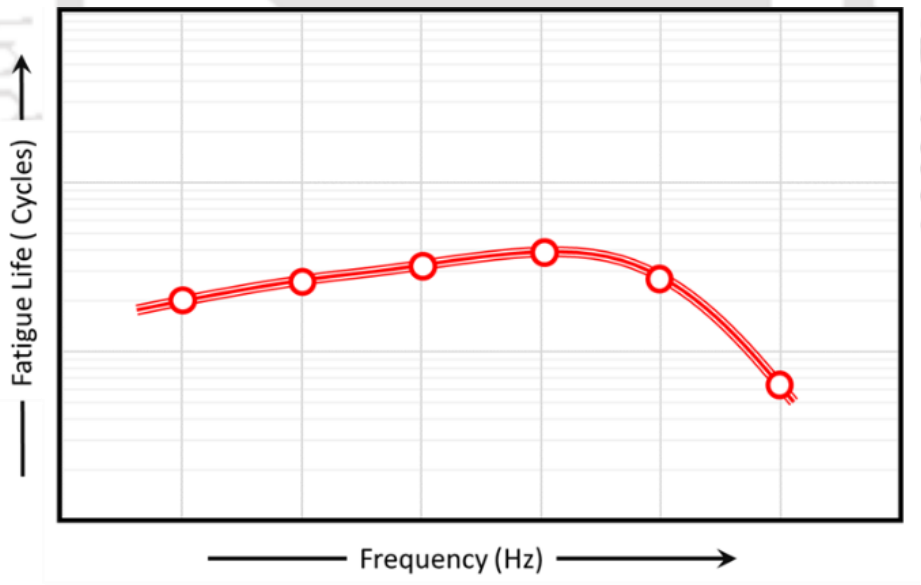

Figure 27: Variation of fretting fatigue life vs frequency damage (Reproduced based on [48])

As shown in Figure 26, compared to the in-phase loading, with phase difference of 90° and 180°, crack initiation life increases and decreases respectively. Also, it is observed that phase difference of 90° results in higher number of shearing planes for crack

initiation, compared to in-phase loading. Orientation of the critical planes also get affected by the phase difference between tangential and axial bulk loads. For example, compared to in-phase loading, for phase difference of 180°, orientation of critical plane is exactly opposite [53]. With these observations, possible phase difference between different engine operating loads is important and should be considered through appropriate duty cycle towards predicting reliable fretting fatigue damage and subsequent life results.

1.6.1.2. Operating Load Magnitude

Along with the phase difference, subsequent load magnitudes also significantly affect the fretting fatigue damage. For example, if the transverse and axial loads are kept constant, with increase in normal load, critical stress value for crack initiation initially decreases and for very high normal load, it again increases due to resultant stick conditions [48]. However, in another investigation, Lykins et al. [106] observed that at higher bulk stress amplitude, fretting fatigue life decreases monotonically, with increasing pressure.

For general bolted joint assembly, fretting fatigue life is observed to decrease with increase in tightening torque, which corresponds to the increase in the normal force [107]. In IC engine components also, fretting fatigue results are observed to be affected by bolt preload values. For example, as observed in plain bearing fitted in connecting rod, change in bolt preload value contributes significantly towards the resultant fretting fatigue damage and decrease in contact pressure between bearing and connecting rod, corresponds to increase in fretting damage [26, 51]. There is always certain scatter in the engine operating loads. Hence, during the design stage, appropriate load levels need to be considered to evaluate the worst possible fretting fatigue damage for the corresponding bolted joint in the IC engine.

1.6.1.3. Operating Load Frequency

Next important parameter which affects the fretting fatigue life is the operating load frequency. Figure 27 shows the reduction in fretting fatigue life at higher frequency. This observation can be attributed to the corresponding increase in the surface crack nucleation rate and its growth, due to increase in the interfacial strain rate. Iyer et al. [108] have reported that the effect of normal force value on fretting fatigue life varies with different

cyclic frequencies. They observed that at lower normal forces, with the increase in frequency value from 1 Hz to 200 Hz, drop in fretting fatigue life results is observed.

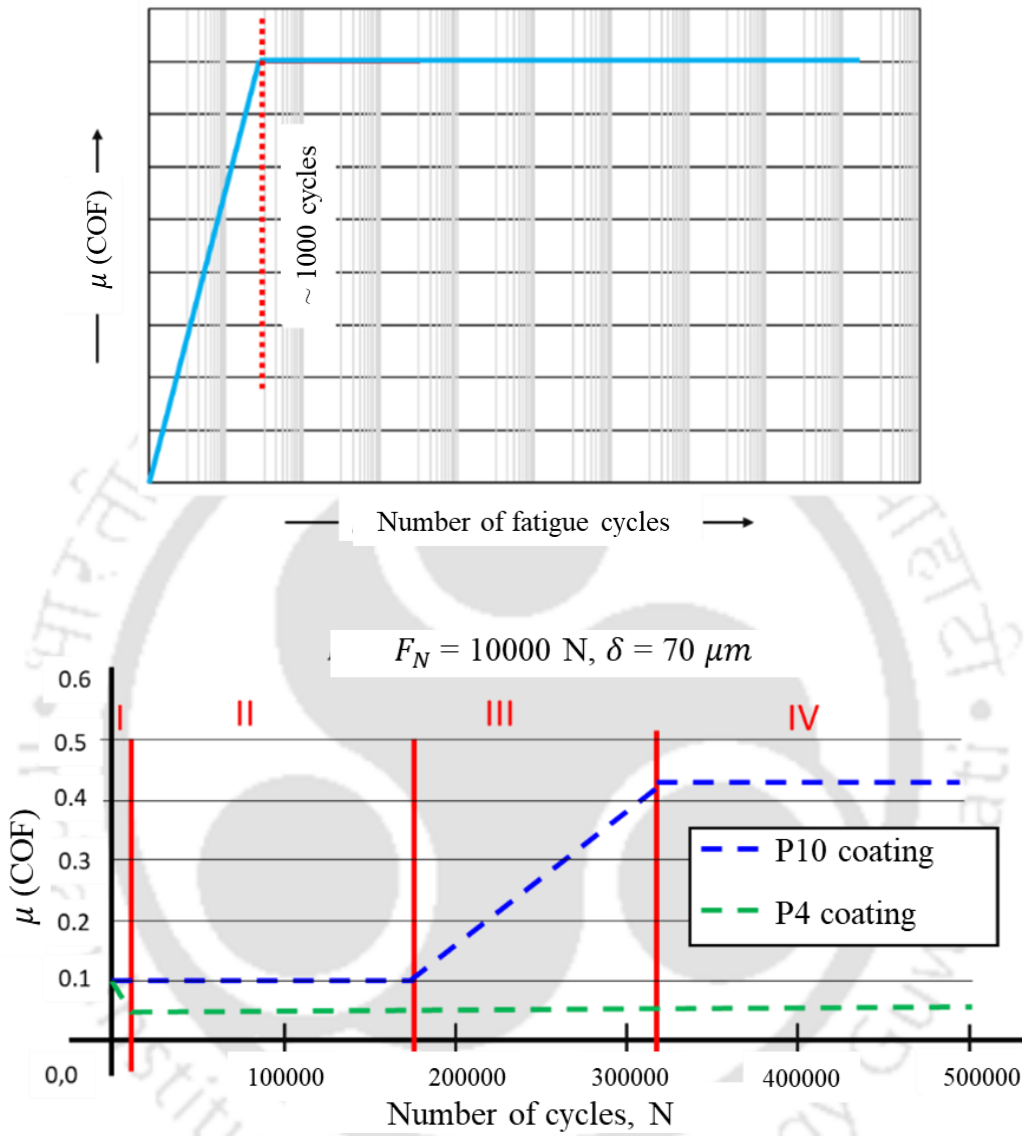

Figure 28: Stabilization of COF value over cycles damage (Reproduced based on [36, 109])

However higher contact forces does not have any effect on fretting fatigue life results at 200 Hz. Thus, along with considering the appropriate load level, effect of corresponding operating load frequency should also be explored in the fretting fatigue evaluation.

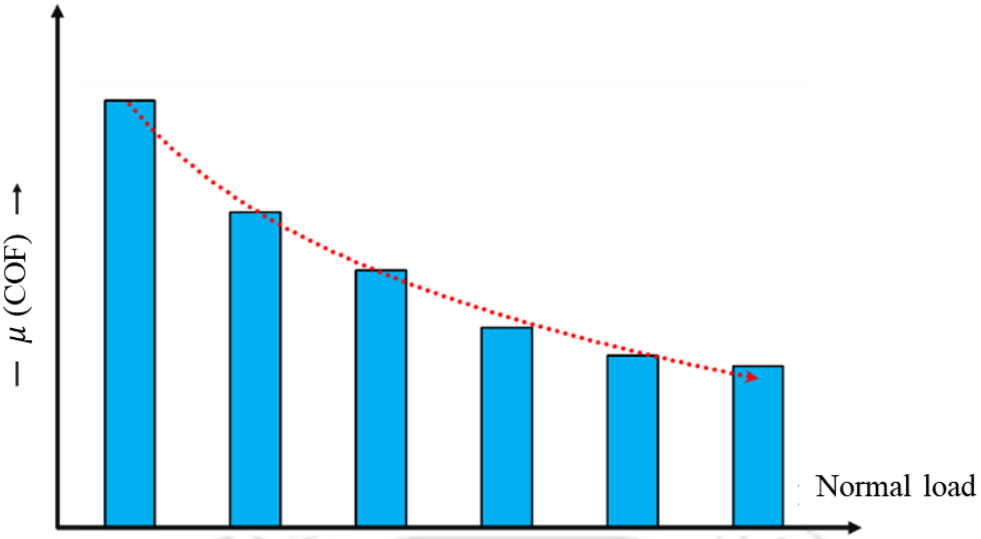

Figure 29: Variation in COF with change in normal load damage (Reproduced based on [103])

1.6.2. Coefficient of Friction (COF)

Surface finish at contact is another critical parameter towards the fretting fatigue results. At higher coefficient of friction, it results in the increased surface stresses and consequently, number of fatigue cycles reduces with increase in COF [49]. During earlier research works it is observed that the COF value initially increases for few thousands of cycles and thereafter it remains constant. This evolution of COF during fretting process consists of three stages relating to the initial protection due to surface coating, it's gradual removal and finally achieving the balance between generation and ejection of debris [109]. Also, a low and stable friction behavior is generally observed till certain number cycles beyond which, sharp increase in COF is observed due to the removal of surface coating and hence, resulting in metal-to-metal interactions [110].

Figure 28, shows different COF stabilization patterns observed in several literatures [36], [109]. Along with COF stabilization over cycles, it also changes with respect to the operating loads like normal load, sliding distance values etc. Figure 29 shows that for a given displacement amplitude COF decreases with increase in normal load. This is because at small normal loads, asperities of rough contact surface get interlocked, leading to high COF. With increase in normal load, plastic deformation of asperities occurs, which leads to lesser interlocking and subsequently in lower COF [111]. COF value also varies with the sliding distance.

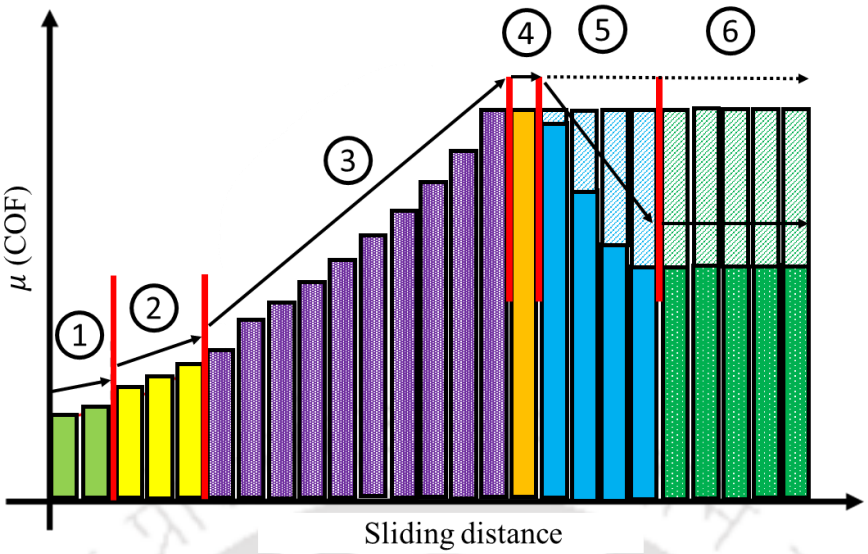

Figure 30: Variation in COF with sliding distance damage (Reproduced based on [113])

As shown in Figure 30, it varies in six stages. Initial increase in COF value is mainly due to formation of slip band at contact surface, thereafter it remains constant for certain range of sliding distance value and the decreases again. The drop in COF value at higher sliding distances, can be contributed to subsequent change in contact surface condition. Thus, with these different observations, it can be concluded that variation in COF value is quite a complex process and careful attention needs to be given to select the appropriate value. In general, in several fretting fatigue investigations, compared to the lubricated joint, higher value of COF ~ 0.65 - 0.8 is considered, for example [58, 60, 100, 112] etc.

1.6.3. Contact Geometry

Contact geometry is also observed as a critical parameter towards fretting fatigue life. As shown in Figure 31, variation in fretting fatigue life is observed with respect to change in contact size. As the contact size increases, subsequent drop in fatigue life results is also observed [105]. This is possible because, for small contacts the stress gradient is more rapid, compared to the larger contacts. Hence, the crack propagation will be more favorable with larger contacts than the smaller assuming the surface stress state is same in both the cases.

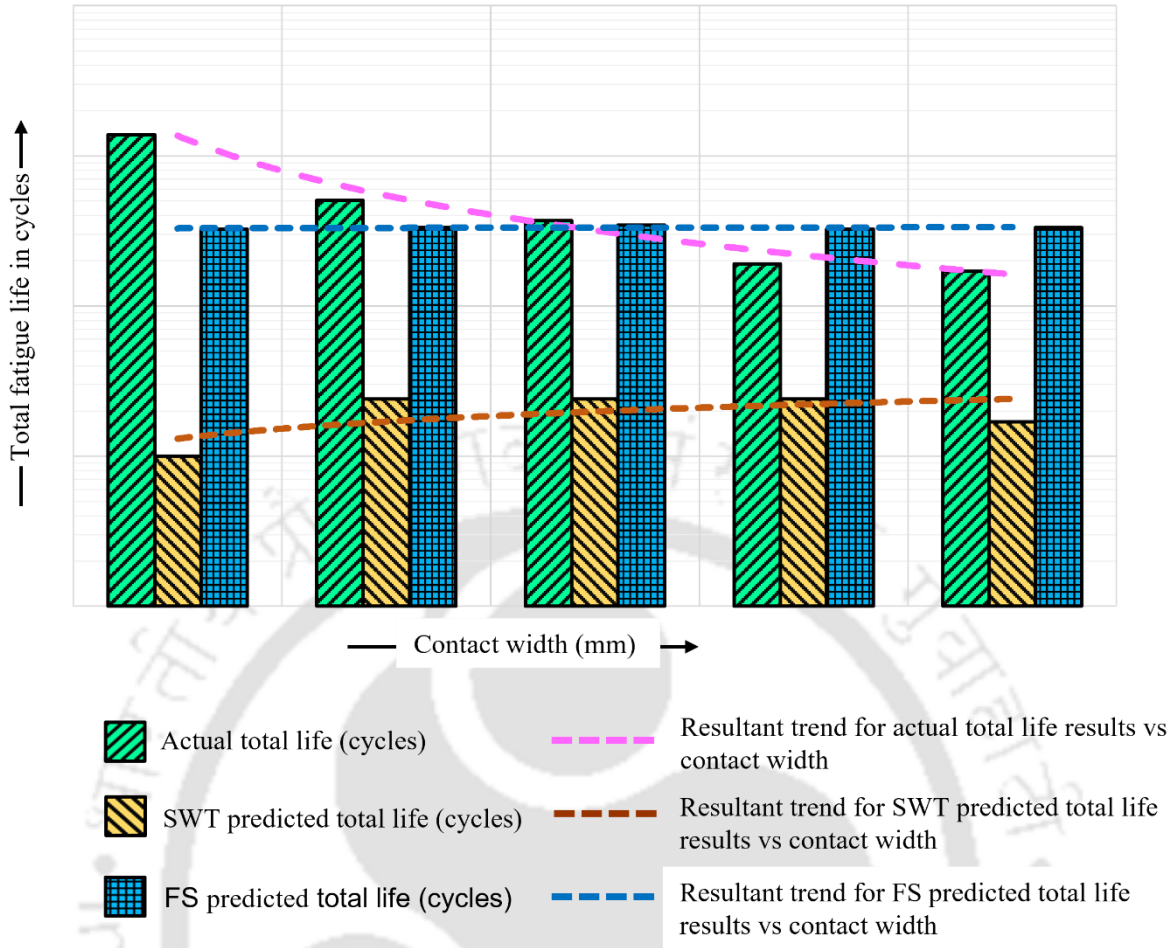

Figure 31: Variation of fatigue life across range of contact sizes damage (Reproduced based on [112])

1.6.4. Effect of Slip and Wear

Fretting contact differs from the sliding contact as in fretting, applied tangential force causes only local micro-scale relative motion and does not cause global relative motion of the contact surface [47]. As per the 'material response fretting map (MRFM)' shown in Figure 32, there exists a certain relationship between the normal force and relative slip amplitude towards the associated surface damage. The area inside the hysteresis loop is the energy dissipated during the relative displacement between the contacting bodies. Higher wear rate occurs in 'gross slip regime' due to the corresponding high dissipated energy. As the relative slip magnitude decreases, the energy dissipation rate decreases as well. Subsequently the wear rate decreases, and cracking becomes the dominant damage mechanism. It is observed that relative sliding displacement values of 7-26 μm can cause significant reductions in fatigue strength [114]. So, the effect of slip magnitude towards

fretting fatigue damage is always an important parameter and it can be considered by considering two different methods i.e., with incremental wear modeling and alternatively by considering the threshold slip magnitude.

1.6.4.1. Incremental Wear Modeling

When two surfaces are in contact and sliding with respect to each other, particle detachment i.e., 'wear', can be observed at one or both the surfaces. This phenomenon is progressive in nature and causes continuous surface degradation. Subsequent changes in the contact surface shape and profile can be evaluated using following two methods: 'Archard's wear equation' and 'Energy Wear equation'.

- Archard's Wear Equation: The classical Archard's wear equation for the sliding wear [32] relates the resultant wear to the normal load as

$$V/\delta = K\,P/H \tag{31}$$

where V is the wear volume, δ is the relative sliding distance, K is the dimensionless wear coefficient (material pair dependent) related to the probability of each contacting asperity leading to the loss of material through wear, P is the normal load, H is the material hardness.

The ratio *P/H* signifies the real area of contact considering fully plastic asperities [115]. Thus, the material loss through wear is proportional to the product of sliding distance and normal load. Material's severity towards wear can be described by the quantity *K/H*, which is referred as Archard's wear coefficient or dimensional wear coefficient (k). It is dependent on the load and stroke [5].

- Energy Wear Equation: Another wear prediction method known as the 'energy wear' method, considers that the frictional energy is related to the resultant surface wear [116] and corresponding dissipated energy is related to wear as

$$V = \alpha \sum E \tag{32}$$

where V is the wear volume, α is the dimensional wear coefficient, $\sum E$ is the accumulated dissipated frictional energy.

Accumulated dissipated energy during the complete wear process is the summation of frictional work occurring in each wear cycle. Further, through experiments linear relationship is observed between the wear volume V and the accumulated dissipated energy, $\sum E$ [119]. It is also mentioned that there exists certain threshold of dissipated energy E_{th}, before the fretting wear starts. The main advantage of this model over Archard's equation is that evolution of COF gets explicitly considered in the wear volume calculations [103]. In gross slip regime, the two approaches are same in predicting wear results. However, in the partial slip /stick-slip regime, two approaches will predict different results [5].

1.6.4.2. Threshold Slip Magnitude

In the wear modeling techniques as mentioned above, effect of wear on material loss needs to be predicted using incremental/progressive wear modeling. Thus, the gradual evolving contact surface profile during the wear needs to be considered, by considering appropriate subroutines while solving such problem in FEA.

In order to study the effect of wear onto fretting fatigue, this can be a computationally expensive way and may not be always feasible option in case of large, complex FEA problems. There is also another way to consider the effect of wear onto fretting fatigue i.e., by considering the threshold slip magnitude.

As discussed earlier, fretting fatigue life initially decreases with the increase in slip magnitude till certain threshold limit. Post this value, slip magnitude does not have detrimental effect onto fretting fatigue. Accordingly, the effect of slip magnitude onto fretting fatigue results can be considered as shown in the Figure 33. Only here it should be noted that beyond threshold limit value, fatigue life results are decoupled from the effect of slip magnitude. This approach has been proposed by Ding et. al [102]. This approach is computationally more efficient than the incremental wear modeling, as in Ding's approach the change in contact surface shape and profile does not need to be modelled.

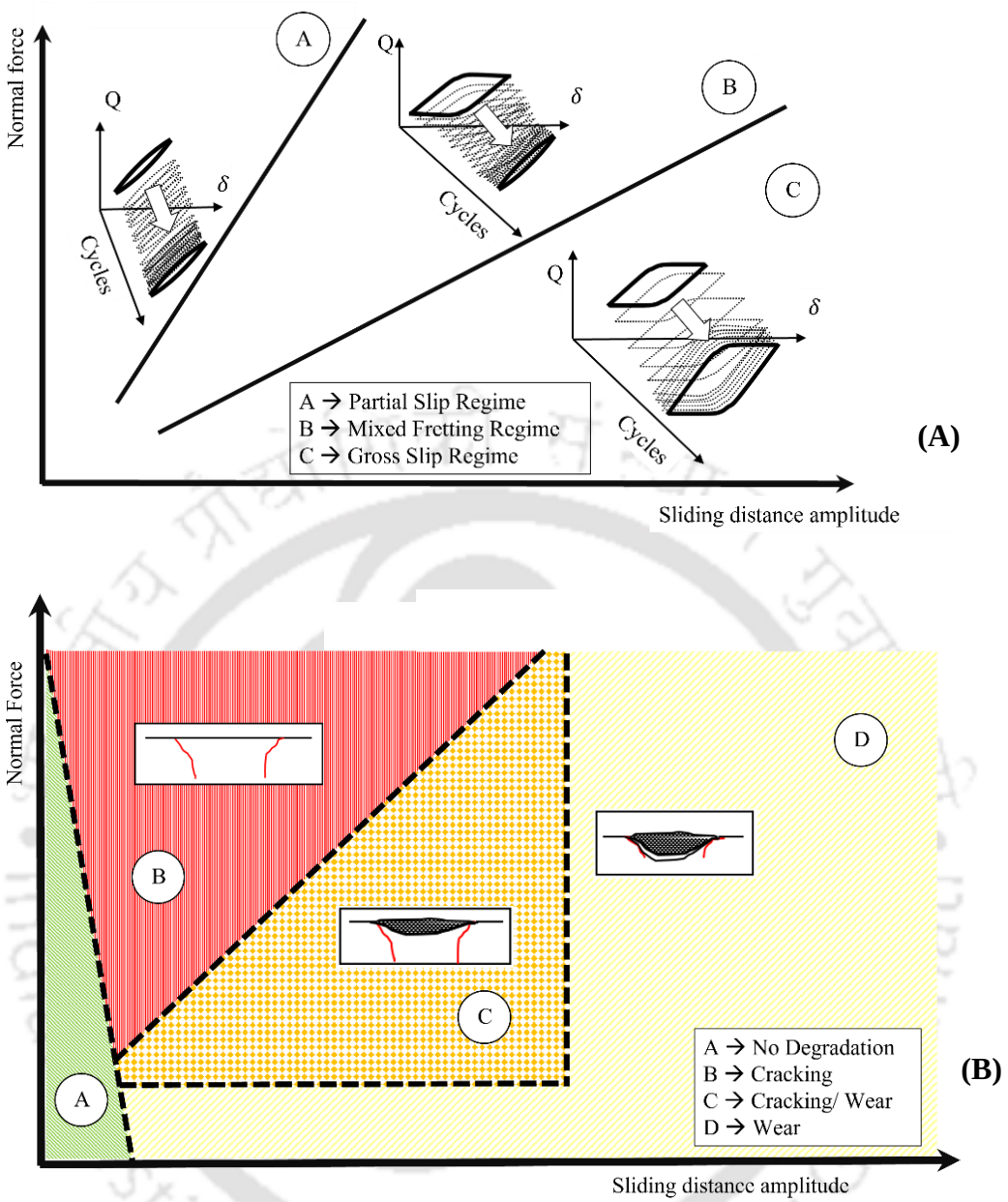

Figure 32: Running Condition Fretting Map (RCFM) (A) and Material Response Fretting Map (MRFM) (B) damage (Reproduced based on [117–118])

1.6.5. Stress-Strain Averaging Methods

At the contact surface, susceptible to fretting fatigue there is always a high stress gradient. The further growth of the initial micro surface cracks further depends upon the stress-strain condition below the surface. Multiaxial fatigue initiation parameters do not explicitly account for the effect of such stress-strain gradient towards the predicted fatigue life results. By averaging the multiaxial FIP's over a critical dimension, realistic fatigue life estimation can be obtained.

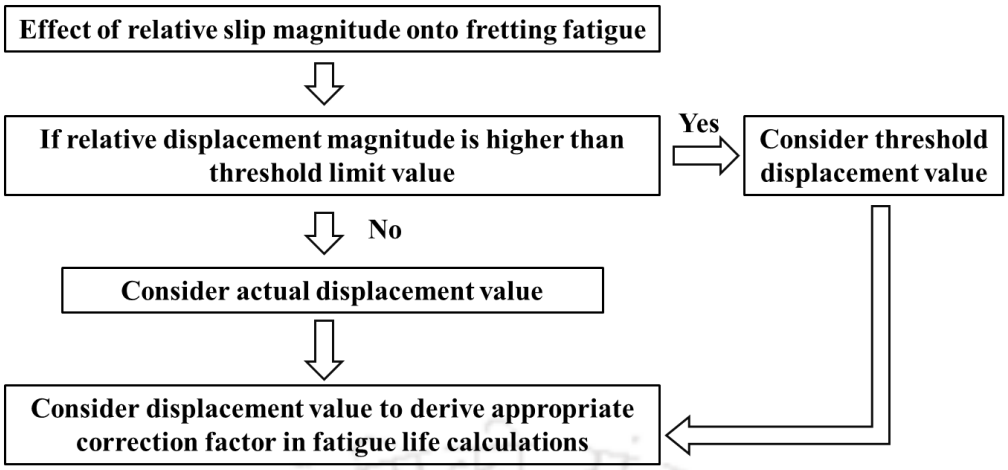

Figure 33: Flowchart towards capturing effect of slip magnitude on fretting fatigue results

To capture the resultant stress gradient, there are different stress averaging methods considered in the literature [59–60, 75–77, 100–101, 112]. Using these methods, the stress averaging can be carried out around the contact surface nodes, over the certain critical dimension. By considering such averaged stress-strain values in the fretting fatigue initiation criteria, more realistic damage value can be obtained to get better experimental correlation. Figure 34 shows the schematic representation of different averaging methods.

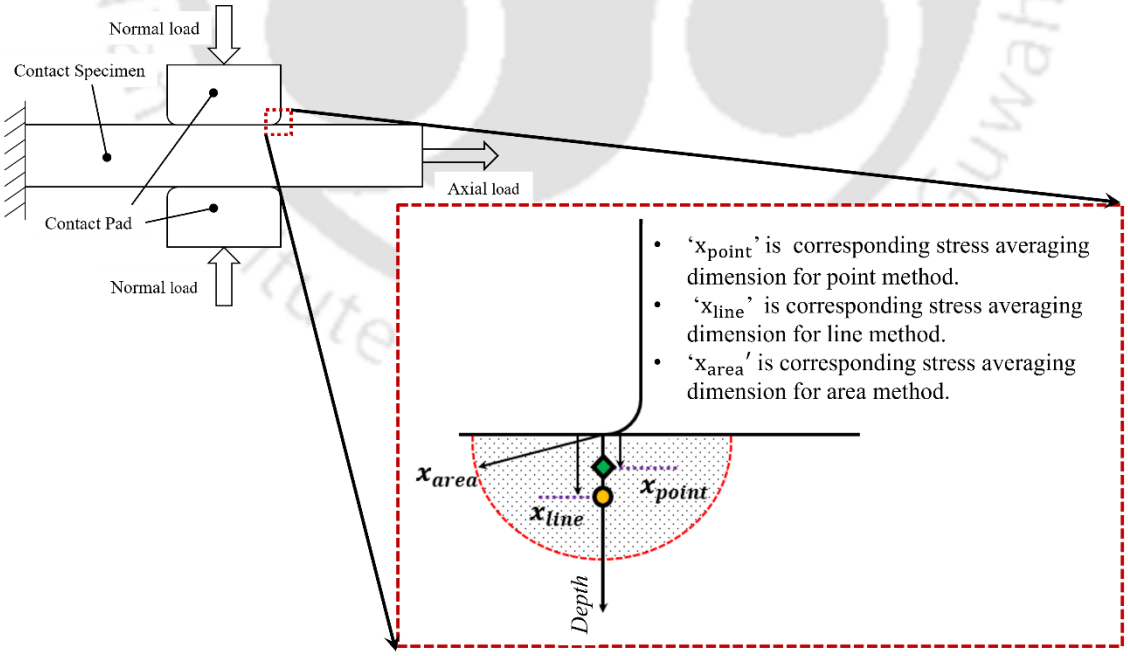

Figure 34: Schematic representation of different stress-strain averaging methods damage (Reproduced based on [59])

Based on the corresponding domain considered for averaging, these averaging methods can be further classified into four methods, as given below.

- Surface method: This method considers the contact nodal stress values only. Often the results predicted with this method are highly conservative.
- Point method: In this method, stress-strain state at a point located at a certain distance inside the material along the critical plane is considered in the fretting fatigue life evaluation. Schematic representation of this method is similar to that of line method, as shown in Figure 35. Compared to the line method, here the averaging along the critical plane is not carried out.
- Line method: As shown in Figure 35, line method averages the damage parameter data (DP) for the nodes along the critical plane till critical dimension. The averaged damage parameter (DP_{avg}) data is then considered to predict crack initiation life. This method can be considered as the simplest and most intuitive averaging method among the mentioned stress averaging methods [52].
- Volume/Area method: Volume/Area method is similar to the line method except here instead of line, the averaging of damage parameter is done over the selected volume/area. The radius of the averaging volume/area can be evaluated in the same way as the critical dimension for line method is evaluated. Figure 36 shows the schematic representation of this method.

The critical dimension, r_c [101], needed for stress-strain averaging is derived as

$$r_c = (1/\pi)[\Delta K_{th}/\sigma_{f-1}]^2 \tag{33}$$

where r_c is the critical dimension for stress-strain averaging, ΔK_{th} is the crack threshold stress intensity factor range, σ_{f-1} is fatigue limit in tension.

Often it is observed that this critical dimension is generally of the similar order of the magnitude as the material's grain size [112].

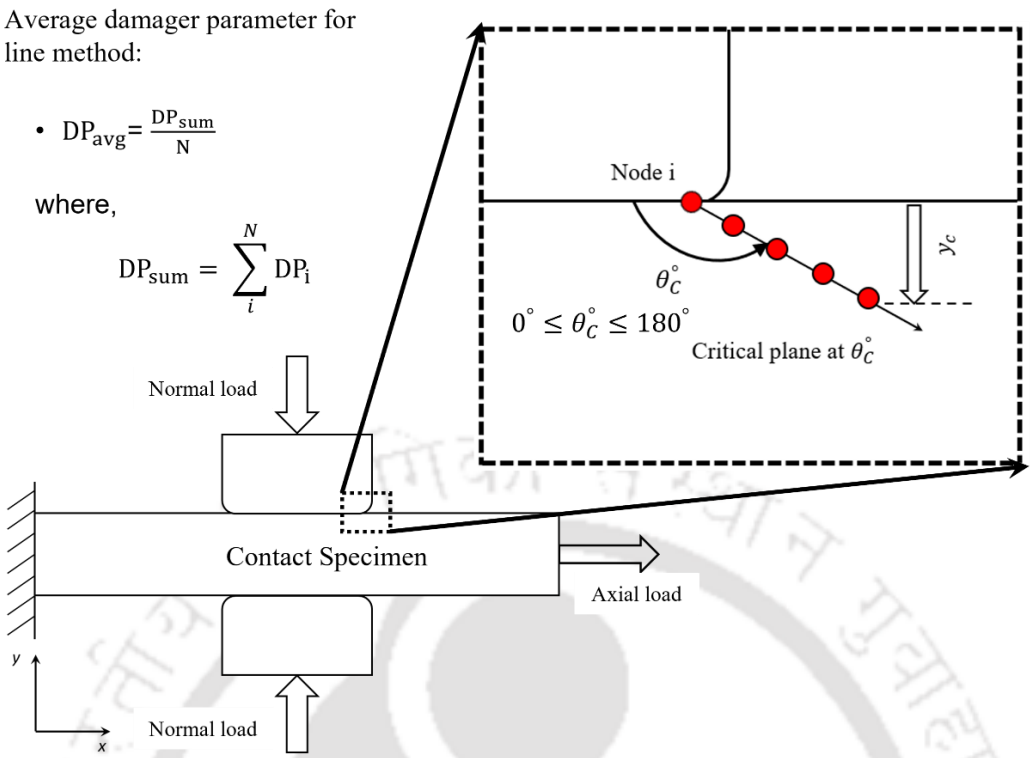

Figure 35: Line averaging method damage (Reproduced based on [52])

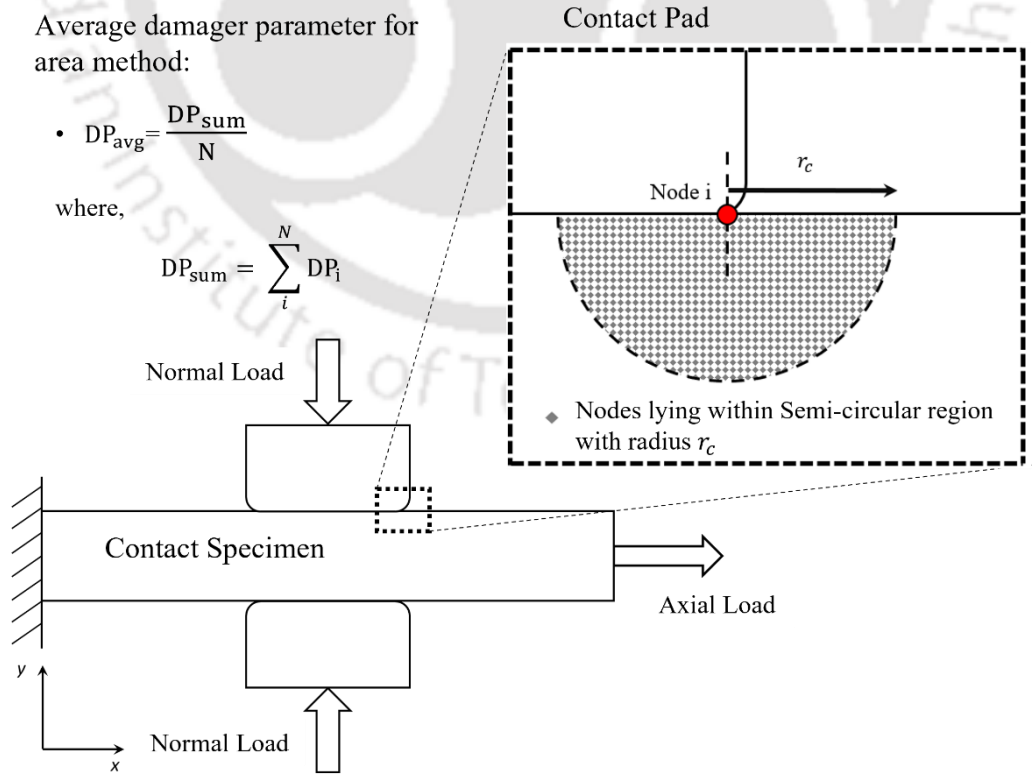

Figure 36: Volume/area averaging method damage (Reproduced based on [52])

Table 1: Experimentally observed relationship between critical dimension and failure cycles (r_c is the critical dimension for stress averaging, N_i is the cycle to crack initiation) [121]

Sr. No.	Material	Relationship
1	Al/4%Cu	$r_c = 15.2N_i^{-0.312}$
2	Al2024-T351	$r_c = 12.6N_i^{-0.231}$
3	Al7075-T6	$r_c = 21.7N_i^{-0.347}$
4	Ti-6Al-4 V,	$r_c = 0.42N_i^{-0.135}$

Table 2: Statistic results considering the ratio of estimated cycles and actual cycles [59]

r_c	Surface method	Point method	Line method	Area/ Volume method	Variable initiation length method
Mean					
1 mm	0.027	1.102	1.133	1.067	0.913
0.5 mm	0.153	1.088	1.120	1.066	
0.2 mm	0.428	1.053	1.080	1.038	
Standard Deviation					
1 mm	0.0087	0.395	0.371	0.364	0.286
0.5 mm	0.054	0.363	0.349	0.341	
0.2 mm	0.151	0.326	0.323	0.309	

Resultant value of the critical dimension r_c, from Equation 33, can be used in the point method (i.e., considering the stress at a point located at distance of $r_c/2$ from critical stress point), line method (i.e., averaging stress evaluated over a distance $2r_c$) or

volume/area method (i.e., averaging stress semi-circular area / half sphere of radius r_c) [120].

In another method for stress-strain averaging i.e., the variable length method, the critical dimension is not constant but is observed to be function of number of failure cycles. The resultant experimental relationship between the critical dimension for point method and the number of failure cycles is given in the Table 1, for various materials [121]. From Table 1, it is observed that the critical dimension decreases as the number of fatigue cycles increases and vice-versa. It is based on the theory of critical distance [122] considered in in the form of point method [123]. The observed relationship is thus a fatigue property of individual material and is based on the assumption that linear elastic constitutive law can be used to predict mechanical behavior for most of the engineering materials. Hence, the change in size of plastic zone near the notch tip with change in cyclic loadings depends upon the magnitude of cyclic loading. With the corresponding critical dimension, stress values are obtained using critical plane method and considered to evaluate resultant fatigue life. The predicted fatigue results found to be within the scatter band of $\pm$ 3N.

Navarro et al. [59] have mentioned that with the above averaging methods, estimated fatigue life correlates better with the experimental life as observed through the corresponding mean and standard deviation values of the ratio of estimated fatigue life and experimental fatigue life. As per his study, volume method results are close to line method results. Also compared to the results obtained using variable initiation length method, they are on conservative sign, which is good from design perspective. Also, comparatively lesser dependence on averaging dimension is observed for the volume/area method. Thus, it indicates the averaging stress/strains over a critical dimension can contribute towards the better prediction of crack initiation life, especially in cases where high stress-gradients are present. Table 2 shows the comparative assessment of results obtained using different stress averaging methods.

1.6.6. Humidity, Temperature and Material Properties

Environmental factors like humidity, temperature and material properties are also important towards fretting fatigue. During the experimental testing with AZ61 magnesium alloy, effect of low humidity on fretting fatigue strength is observed to be

very significant, whereas high humidity does not have that much significant influence [124]. Goto et al. [125] have observed that, pure materials like aluminum, iron, copper, titanium, chromium and nickel showed maximum fretting damage at specific relative humidity levels RH_{max}. This specific relative humidity level is observed to be independent on mechanical test conditions like contact load, fretting amplitude, and the frequency range.

Table 3: Design trend in automotive diesel engines [129]

	Past	Current	Future
Cylinder Block Material	Cast Iron	Cast Iron	Aluminum with Liners
Cylinder Block Configuration	Closed-Deck	Closed-Deck	Open-Deck
Cylinder Head Material	Cast Iron	Aluminum	Aluminum
Number of Valves	2	2/4	4
Bolts per Cylinder	6	4	4
Peak Firing Pressure	12 MPa	15-17 MPa	17-20 MPa
Total Bolt Preload to Firing Load Ratio	4-6.5	3.5-4.5	~ 3.7
Injection System	IDI	DI, Common Rail	Common Rail

Next important parameter is the operating temperature. It is observed that as compared to room temperature, at elevated temperature of 600°C, fretting fatigue results of nickel-base superalloy IN100 are improved. Such anomalous behavior is mentioned due to initially increased yield and the tensile strength values of these alloys, with increase in temperature [126]. Also, Ownby [127] observed that, elevated temperature has effect on the crack initiation as well as crack propogation life. In another at elevated temperature study of Al7076-T6 alloy, fretting fatigue life decreases significantly at elevated

temperatures, especially for the LCF regime, approximately by 30-46% at 200°C. In LCF regime, temperature effect is more dominant on crack initiation lifetime whereas in HCF regime, temperature effect is more dominant on crack propogation lifetime [128]. Thus, temperature is an important factor need to be considered during elevated temperature fretting fatigue evaluation and appropriate temperature dependent properties like yield, tensile strength and fatigue properties need to be considered.

1.7. Motivation and Objective of The Thesis

Until now, different fretting failure mechanisms observed in internal combustions engines are discussed along with exploring the physics and engineering aspects behind the fretting fatigue and its evaluation. Components like cylinder block, connecting rod, head gasket, MBC are critical components of any IC engine, and any related failures can cause complete or partial breakdown of the engine. Further, fretting damages generally occur after a considerable engine running hours [13]. At this time, cost to retrofit is very unpredictable. Often fretting fatigue-initiated cracks are hidden and very difficult to be detected before just failure, leading to the serious consequences [12].

Table 4: Summary of approaches considered in the fretting fatigue evaluation of IC engine components

IC engine component	Considered approach for fretting damage evaluation	Limitations observed in the considered fretting damage evaluation approach
Main bearing cap	Fretting limit line [15, 19]	- More suitable for HCF evaluation as stress-based limit is considered. However, on similar basis an approach can be proposed for LCF evaluation.
	Ruiz's parameter [17]	- Only suitable for comparative fretting damage assessment and not suitable as the absolute 'Pass/Fail' criterion. - Resultant fretting damage results cannot be converted further into resultant fatigue life values.

		- Also being stress-based, restricted application to the cases in which material yielding is expected.
Engine block	SWT and FS [21]	- Though considered approach is suitable for both LCF and HCF, no fretting fatigue life estimation has been carried. - Also, resultant fatigue damage results are not corrected for the relative sliding.
Connecting rod	Ruiz's parameter [13, 25, 27].	- Only suitable for comparative fretting damage assessment and not suitable as the absolute 'Pass/Fail' criterion. - Resultant fretting damage results cannot be converted further into resultant fatigue life values. - Also being stress-based, restricted application to the cases in which material yielding is expected.
Cylinder head gasket	Archard's wear [28]	- Only suitable for comparative fretting damage assessment and not suitable for absolute 'Pass/Fail' criterion. - With its limitations, Archard's wear is primarily suitable for gross slip condition. - Being progressive wear modeling approach, require additional equilibrium iterations which can increase the solution time.
	Ruiz's parameter	- Only suitable for comparative fretting damage assessment and not suitable as the absolute 'Pass/Fail' criterion. - Resultant fretting damage results cannot be converted further into resultant fatigue life values.

		- Also being stress-based, restricted application to the cases in which material yielding is expected.
Crankshaft balancing weight	Archard's wear and Findley Parameter [34]	- With its limitations, Archard's wear is mainly suitable for gross slip condition. - Findley parameter is suitable primarily for HCF evaluation. - No fretting fatigue life estimation has been carried.
Piston	Archard's wear and SWT Parameter [35]	- With its limitations, Archard's wear is mainly suitable for gross slip condition. - Though considered SWT parameter is suitable for LCF and HCF, no fretting fatigue life estimation has been carried.

With the continuous expectations of increasing power density and lean designs, resultant loads on IC engine components are expected to increase in proportion. For example, considering the latest design trends observed in automobile diesel engines (see Table 3), with the reduction in 'Total Bolt Preload to Firing Load Ratio' and with increasing use of aluminum material for head and blocks, relative sliding between the mating parts is expected to increase. Such an increase in the relative sliding further combined with high contact stresses will cause higher possibility of the fretting fatigue damage in near future. Hence, economic implications of subsequent failures can be severe and significant warranty cost could be saved if the wear and fretting fatigue life of components is improved [5]. So, after considering the significant warranty cost and observing reduction in the fatigue strength by 50-70% relative to the conventional fatigue [36], more focus should be given towards identifying and developing more reliable and accurate fretting fatigue analysis methodology for actual complex IC engine components and assemblies.

Different approaches considered so-far for the fretting damage assessment of different engine components, with the corresponding limitations are summarized in Table 4. Also, different fatigue initiation methods are effectively considered towards the fretting fatigue life evaluation of basic, simple geometries. If considered appropriately, these methods can be also effective in the fretting fatigue damage evaluation of actual engine

components. The summary of these different crack initiation methods is presented in Table 5. Different crack-initiation methods have significant advantage over the traditional Ruiz's parameter-based approach, in terms of their capability towards crack initiation life evaluation in fretting fatigue.

Table 5: Comparative assessment of different fretting fatigue crack initiation criterion considered for fretting fatigue life evaluation of basic, simple geometries

Category	Fatigue initiation parameter	Scatter band / Fatigue index error	Observed limitations in the approach
Stress-based critical plane method	FP	$\pm 3N$ [55–56]	- Dependent only on stress values. Consequently, these parameters are suitable for HCF life calculations only. - Being critical planed based methods, need stress-strain transformations along different planes. Hence, need more computational efforts.
	MD	$\pm 3N$ [58–60]	
	SSR, MSSR	$\pm 3N$ [61–62]	
	MT	$\pm 3N$ [64]	
Strain-based critical plane method	FS	$\pm 2N$ [67]	- Though useful for LCF and HCF fatigue life calculations, need stress-strain transformations over different planes passing through the nodes of considered FEA domain. Hence, need more computational efforts.
	TYC	$\pm 2N$ [64]	
Strain-energy based critical plane method	SWT	$\pm 3N$ [49, 72–77]	- Though useful for LCF and HCF fatigue life calculations, need stress-strain transformations over different planes passing through the nodes of considered FEA domain. Hence, need more computational efforts.
	Liu1, Liu2	$\pm 3N$ [52]	

Stress invariant	CL	15 % -45% [52]	- Though does not need critical plane-based calculations, have high fatigue index error. - Also being stress based, suitable for HCF fatigue only. - Also does not predict crack initiation orientation.
Continuum damage mechanics-based method	Lemaitre	$\pm 2N$ [93–94], [100]	- Though computationally more efficient than critical plane methods, need extensive testing to obtain corresponding material constants. - Does not predict crack initiation orientation.
	Bhattacharya and Ellingwood	NA	
	Chaboche	$\pm 3N$ [99]	
Fretting specific parameter	Ruiz's parameter, Ding's parameter	N.A.	Ruiz parameter: - Not possible to be converted into resultant fretting fatigue life results. Therefore, useful for comparative assessment only. - Compared to the Ding's parameter, cannot combine with any FIP. - Compared to Ding's parameter, does not consider the dependency of fretting fatigue/wear on the relative sliding distance value. Ding's parameter: - Need to be combined with the corresponding FIP to obtain resultant fretting fatigue life results.
		N.A.	

Further, some of these methods like CDM based methods, stress-invariant based methods are computationally more efficient than the traditional critical plane-based methods, as these methods do not require the calculation of resultant fatigue damage across different planes passing through each node but instead these methods calculate the associated damage in terms of scalar damage results per node.

Further, based on the possible localized yielding around the fretting affected zone(s), strain-based methods should be considered to predict more reliable results, as compared to the stress-based methods. Hence, based on the comparative assessment between different approaches considered for IC engine components (as shown in Table 4) and different crack initiation methods (as presented in Table 5), there is a possible potential scope to identify the most suitable approach in order to efficiently obtain the realistic fretting fatigue damage and resultant crack initiation life for different engine components. Further, the approach should be suitable for both LCF and HCF conditions.

While evaluating for the most suitable crack initiation method, different critical physical and analytical parameters towards the fretting fatigue initiation should be also considered in the fretting fatigue damage evaluation of actual engine component/s. Among such 50+ identified parameters [50], normal load, relative displacement and coefficient of friction are mentioned to be primary parameters whereas others are mentioned as secondary and affect the fretting results through these three primary variables [1]. Moreover, to capture the high stress gradient present at the fretting affected zone(s), suitable stress averaging technique should be considered in the fretting fatigue life evaluation.

Also, the effect of wear on fretting fatigue is an important parameter and should be considered while evaluating the fretting damage and resultant fatigue life results. Compared to the progressive wear modeling-based approaches like Archard's wear [32] and energy wear method [116], alternative approach of Ding's parameter i.e., D_{fre2}, can be more efficient approach. The Ding's parameter is based on the 'Threshold Slip Magnitude' and the effect of resultant wear can be considered without actually modeling the incremental progressive wear. Thus, such an approach can be more computationally efficient approach while evaluating fretting fatigue damage in actual IC engine components.

By considering the most effective crack initiation technique and the critical parameters, more realistic fretting damage results for the engine components can be predicted. Such

an approach can be considered in the early design stage to identify the possible fretting fatigue risk and to suggest appropriate design modifications. So, through this thesis work, it is aimed to identify the most suitable crack-initiation method and identify critical physical, analytical factors towards fretting fatigue damage and life evaluation of actual engine component. Head gasket joint is one of the critical joints of an IC engine which is exposed to extreme critical engine operating loads. Thus, the fretting damage of a head gasket is a complex phenomenon with simultaneous system-level interactions between different engine parts like cylinder block (with liner), cylinder head, head gasket and head bolts. Thus, it is considered as a case-study for this thesis work. The comparative assessment between the traditional approach of Ruiz's parameters and the proposed approach will be carried out for the identified case-study of the head gasket.

1.8. Structure of The Thesis

In-line with the earlier discussions, development of a systematic analysis approach for fretting fatigue evaluation for actual engine components, is planned within the scope of this work. Head gasket joint is identified as the case-study, considering the complex physics it is exposed during the engine operating condition. The rest of the thesis work is organized into four chapters, followed by the appendices and references.

Chapter 2-Fretting fatigue life evaluation of flat contact pair using 2-dimensional (2D) FEA

Cylinder head-gasket joint will be similar to a flat contact pair. Hence, initially 2D FEA of a flat contact pair is carried out. Compared to the spherical and cylindrical contact pad geometries (i.e., Hertzian contacts), resultant contact pressure distribution and resultant stress-distribution will be significantly different in flat contact pair [4]. Here, a suitable case-study with a flat contact pair problem is identified and solved using ANSYS software to obtain corresponding fatigue initiation life results. The learnings from the considered flat contact pair problem are further considered in the complex 3D analysis with actual engine components and associated loads. With such approach, considerable time can be saved which would otherwise be required during complex 3D FEA with actual head gasket to obtain suitable crack initiation method and other critical physical and analytical parameters.

In Chapter 2, fretting fatigue life evaluation of the 2D flat contact pair is carried out, considering different crack initiation methods like critical plane-based methods (SWT, FS), stress invariant based-method (CL) and deviatoric strain amplitude-based method (eI). Similar to the stress invariant-based methods, recently deviatoric strain amplitude-based method [130] is proposed for fatigue life evaluation. Through this work, effectiveness of this method will be studied for the first-time for the fretting fatigue life evaluation.

Chapter 3- Identify critical parameters towards fretting fatigue damage of flat contact pair through 2D FEA

As mentioned earlier, there are almost more than 50 identified parameters, critical towards fretting fatigue. In this chapter, different critical parameters towards fretting fatigue results are evaluated, based on the 2D FEA of the considered flat contact pair. Considered parameters within the scope of current work, are based on their relevance to the actual head-gasket joint.

Chapter 4- Fretting fatigue analysis of actual head gasket joint through 3-dimensional (3D) FEA

The learnings from the Chapters 2 and 3, are considered towards the fretting fatigue evaluation of the actual head gasket joint through 3D FEA. As mentioned earlier, since fretting damage of the head gasket is a complex phenomenon with simultaneous interactions between different engine parts, system level 3D FEA is carried out with actual engine operating loads. Subsequent fretting fatigue damage and life results of actual head gasket are evaluated and discussed here. To check for the effectiveness of the identified method and associated parameters, correlation is carried out between actual head gasket failures and FEA predicted results. Further correlation will be carried out with respect to the current industry-standard approach based on Ruiz's parameter. To check for the consistency in results trend, three different engine platforms are considered as the case-studies for this correlation work. Here, the aim is to identify the most effective approach for fretting fatigue damage and life evaluation of a head gasket.

Chapter 5- Conclusion

In this chapter, summary of the results based on the work completed so-far is presented, followed by the conclusions and learnings. Also, based on these learnings, the scope of future work is identified and discussed subsequently.

2. FRETTING FATIGUE LIFE EVALUATION USING 2D FEA

As mentioned earlier, development of the systematic analysis approach for fretting fatigue damage evaluation for critical engine components, by considering both i.e., intricate details captured from the simple geometry's FEA analysis and complex, actual engine operating loads, is planned within the scope of current work. Head gasket joint is identified as the case-study, considering the complex physics it is exposed to during the engine operating conditions. As a part of overall scope of work, initially fretting fatigue life evaluation of a flat contact pair is carried out by considering 2-Dimensional (2D) FEA. For this task, different crack initiation methods, as mentioned below are considered.

- Critical plane-based methods like
  1. Smith Watson Topper (SWT) parameter [22, 71]
  2. Fatemi-Socie (FS) parameter [23, 66]
- Stress invariant -based method like
  3. Crossland (CL) parameter [88]
- Strain invariant -based method like
  4. Deviatoric strain amplitude-based parameter (eI) [130]

Among these, methods like SWT and FS have been extensively considered in multiple cases of fretting fatigue life evaluations and are considered as the effective and reliable methods for fretting fatigue life evaluation. Whereas the approach of CL parameter is comparatively less explored in fretting fatigue life evaluation [60, 87, 131] and the deviatoric strain amplitude-based method [130] (eI) is considered for the first-time for fretting fatigue life evaluation. Hence, corresponding results obtained using these lesser explored methods will be compared with the results obtained using SWT and FS parameters. To consider the resultant stress-gradient present beneath the contact surface, different stress-averaging methods like point, line and area methods are combined with the above-mentioned FIP's and subsequent experimental is carried out.

To carry out the first step i.e., 'fretting fatigue life evaluation of flat contact pair using 2D FEA', appropriate reference test case [58] is considered, based on its relevance to the identified case-study of head-gasket joint. Since both contacts are flat-flat, complete contact type, equivalent analogy can be applied between both the problems as shown in

Figure 37. Hence, initial experimental correlation is carried out by considering this identified test case. Different technical details like material properties, loading conditions, test results, required for 2D FEA and further experimental test results, are considered from the same test-case. In the scope of current carried-out work, FEA model is built and solved using ANSYS (v.19.1). Subsequent FEA results like stress and strains are post-processed using 'ANSYS Parametric Design Language' (APDL) based macros to evaluate the resultant fretting fatigue life against the different crack initiation methods and by considering area stress averaging technique. Corresponding details are discussed in the subsequent sections.

2.1. Details of Experimental Setup

Fretting fatigue is observed at the partial slip regime between two contacting bodies [4]. Hence, subsequent fretting fatigue tests need to be carried out to create such conditions in the experimental set-up. Based on the type of contact, fretting test configurations are broadly classified in two groups: incomplete contact and complete contact [4]. There are two further configurations of the fretting fatigue experimental set-up: First type is bridge type [4], which consists of two separate contact pads connected in the form of a bridge (as shown in Figure 38) and another configuration with the single contact pad, as shown in Figure 39. Bridge type configuration, despite being easy to manufacture, has certain disadvantages like having difficulty in determining accurate contact pressure evaluation due to possible tilting of the contact pads. Also, due to difficulty in achieving consistent level of surface finish and cleanliness at all four pads, it may be possible to have adhesion at one pair of contact pads, whereas total relative displacement at the other pair of contact pads. Some of these disadvantages can be avoided using configuration of single contacting pad. Also, this configuration is expected to generate sufficient slip at contact pair to cause fretting condition. In the considered reference work [58], fretting fatigue tests are carried out using a square ended indenter creating the partial slip regime at the contact junction.

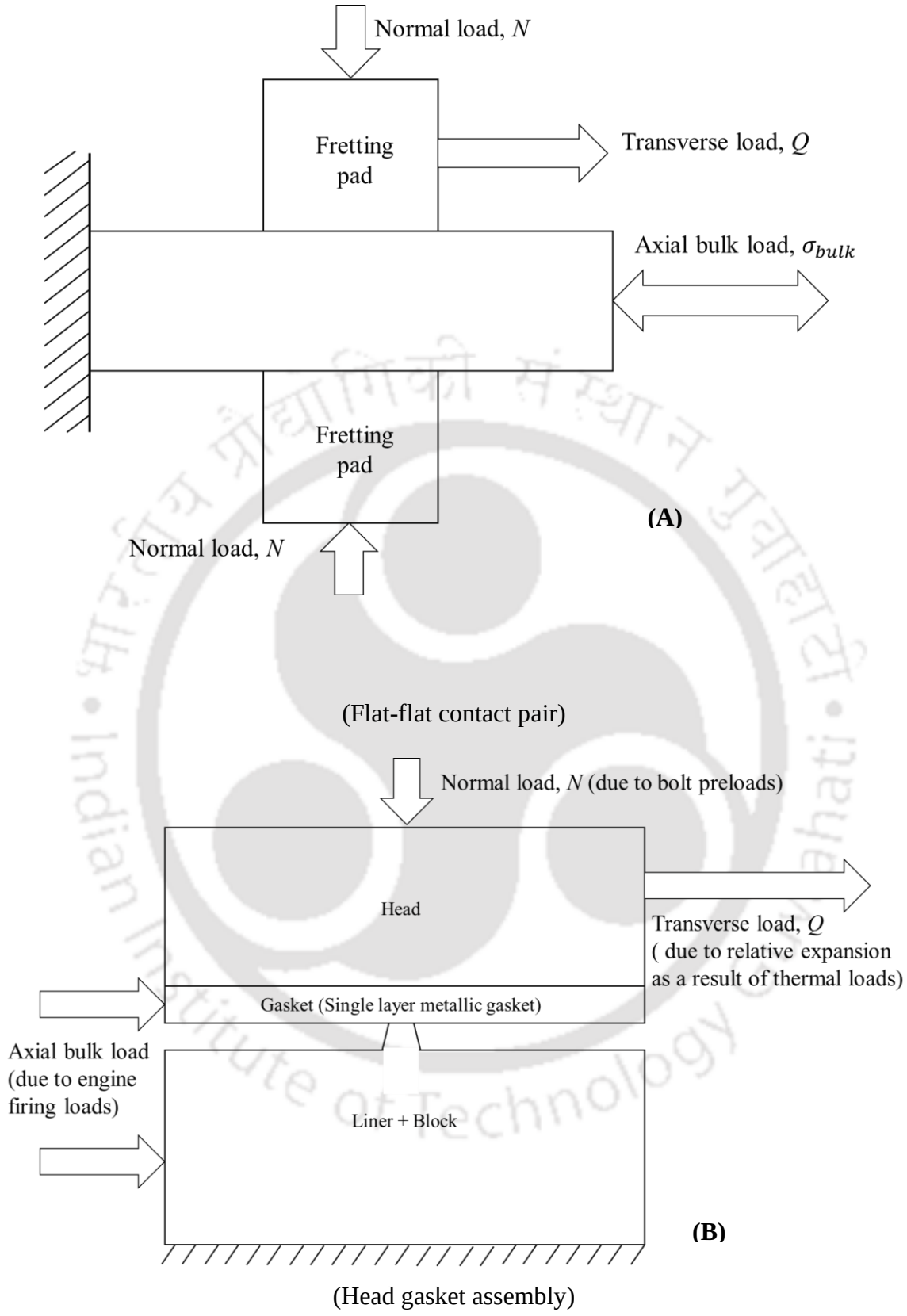

Figure 37: Schematic representation of (A) flat contact pair fretting problem set-up and (B) head gasket assembly

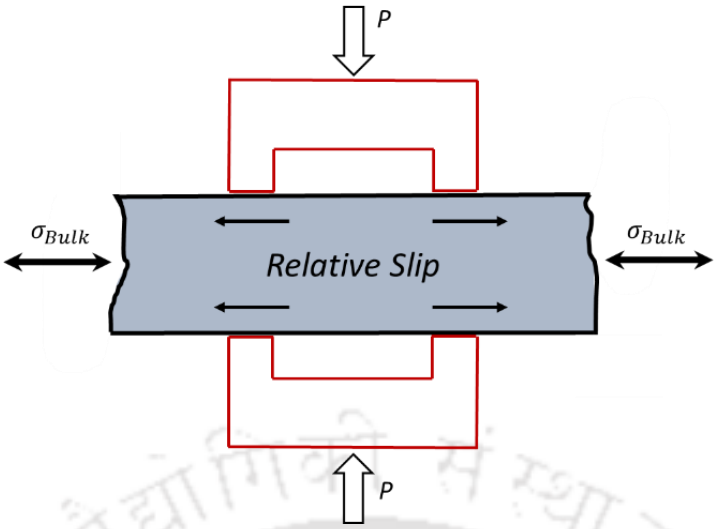

Figure 38: Schematic representation of fretting fatigue bridge type test damage (Reproduced based on [58])

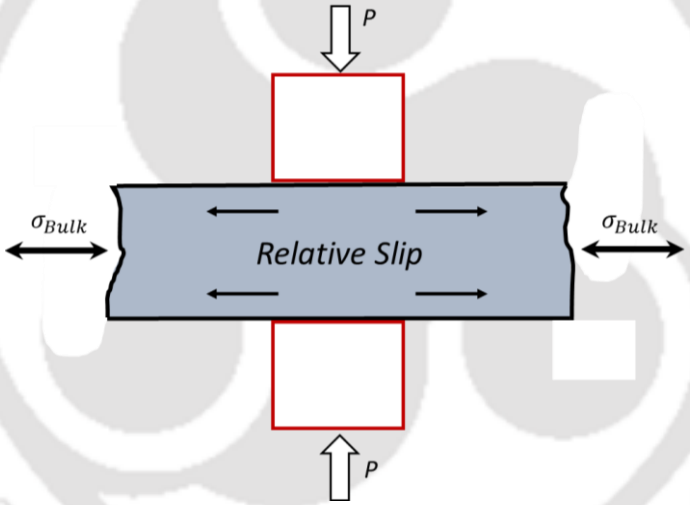

Figure 39: Schematic representation of fretting fatigue flat-ended pad (Reproduced based on [58])

During the experimental tests in the reference problem, a uniaxial servo-hydraulic fatigue test machine with a load capacity of $\pm$ 100 kN is considered to carry out the required fretting fatigue tests. Normal pressure loads onto contact pads are achieved using an assembly rig, with the maximum load capacity of 10 kN with an accuracy of $\pm$ 0.025 kN. All the tests are carried out in the ambient conditions.

Bulk loading is performed in a cyclic manner, with the constant amplitude stress ratio of R = –1 and frequency of 15 Hz. Total 15 experimental load cases, varying in both normal

and bulk loads are carried out (see Table 6). The contact pressure, σ_P, is calculated as $\sigma_P = P/2at$, where $2a$ is the contact width and t is the thickness of the specimen (as shown in Figure 40). The initial surface roughness of the contact surface is kept at R_a= 0.1 μm in the transverse direction using the grinding operation. Considered load sequence is shown in Figure 41.

For both the contact pad and the specimen, same material i.e., AL7075-T6 is used. This material is used in several engineering applications like aircraft fittings, gears and shafts, fuse parts, meter shafts and gears, missile parts, regulating valve parts, worm gears, keys, aircraft, aerospace and defense applications: bike frames, all-terrain vehicle (ATV) sprockets, etc. [132]. Corresponding material properties of ALA7075-T6 are mentioned in Table 7.

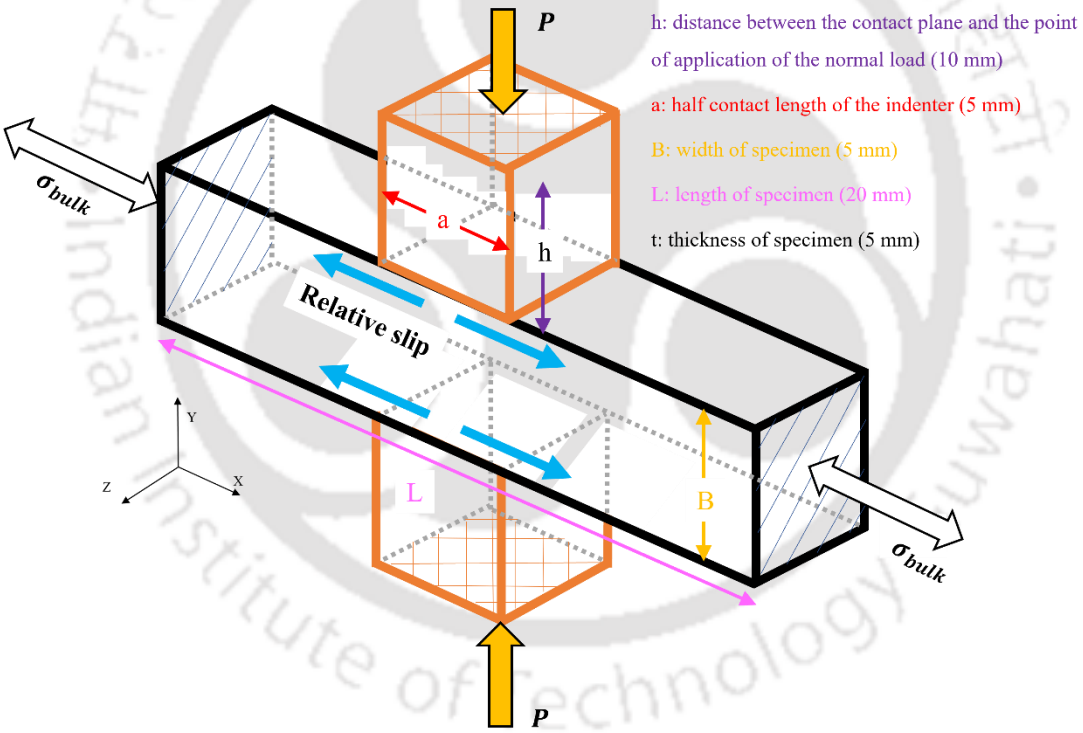

Figure 40: Geometry and applied load details (Reproduced based on [58])

2.2. Details of FEA Problem Setup in ANSYS

Compared to the reference problem solved using ABAQUS software, in the current work, the same problem is solved using ANSYS (version 19.1). Due to the problem symmetry, only 1/4th of the FEA model is considered (see Figure 40). 2D FEA plane strain approach

is considered using four noded, plane strain quadrilateral elements with thickness option i.e., Plane 182 elements [133]. Assuming the stabilized condition, similar to reference problem, constant value of COF as 0.8 is considered initially. Contact algorithm is considered as 'Augmented Lagrange' (symmetric option). Based on the mesh convergence study considering the contact pressure results (as shown in Figure 42), a mesh size of 15 μm is considered near the right end of the contact zone. The corresponding FEA mesh details are shown in Figure 43.

Table 6: Applied loads and experimentally obtained number of cycles to failure for the reference problem (P is the normal load, σ_P is the contact pressure, σ_{Bulk} is the axial bulk load, N_f is the experimental failure cycles) [58]

Test Number	P(kN)	σ_P(MPa)	σ_{Bulk}(MPa)	N_f(cycles)
1	2	40	110	105,958
2	4	80	110	92,259
3	8	160	110	82,549
4	2	40	130	64,764
5	4	80	130	47,714
6	8	160	130	43,567
7	2	40	150	35,181
8	4	80	150	32,905
9	8	160	150	25,872
10	2	40	170	24,306
11	4	80	170	27,391
12	8	160	170	23,046
13	2	40	190	12,509
14	4	80	190	9,590
15	8	160	190	8,760

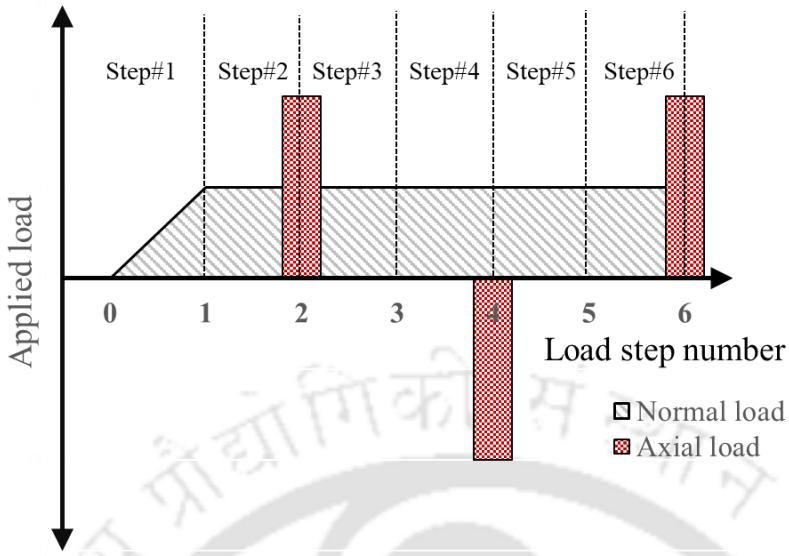

Figure 41: Loading sequence considered in FEA

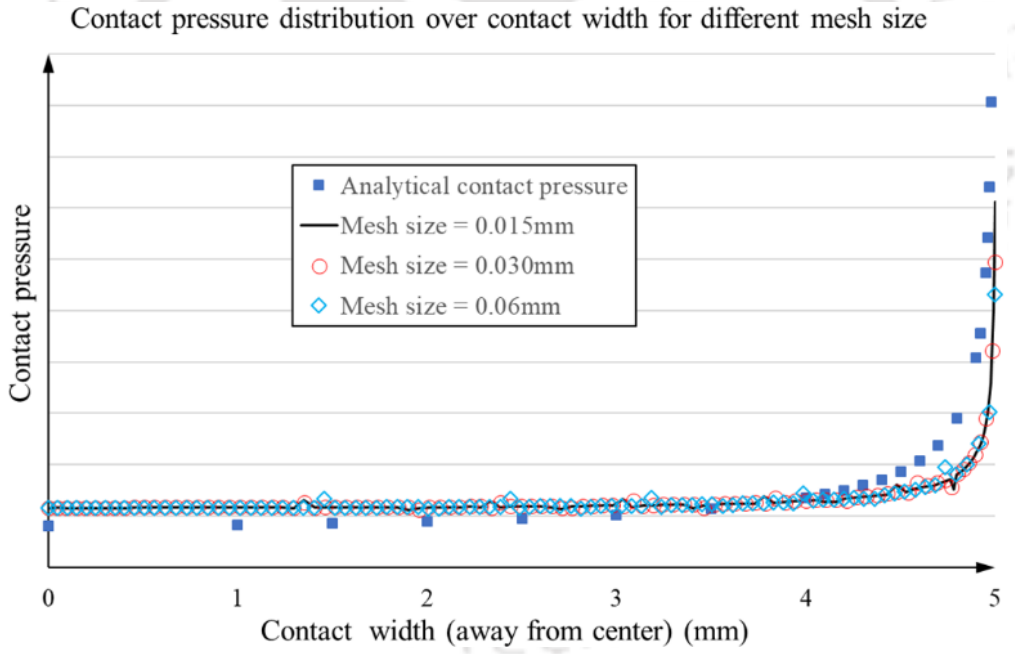

Figure 42: Mesh convergence study results

The contact pressure distribution for a flat contact pair [134] is derived as

$$P_m \, \alpha \, -0.5/\sqrt{1-(r/a)^2} \tag{34}$$

where P_m is the resultant contact pressure, r is the radial distance (away from the center), a is half contact width of the complete flat contact pair.

The minimum contact pressure is obtained at the center and mathematically approaches to infinity at the contact edge. As compared to the reference model solved in ABAQUS using 5 μm element size, comparatively higher mesh size are kept in the current work, in ANSYS. Comparison between ANSYS and ABAQUS results [135], for the same mesh setting, is shown in Figure 44. It shows that in comparison to ABAQUS, higher stresses are observed in ANSYS for the same mesh size. Thus, it is observed that different mesh settings can be required in different numerical software's.

Similar to the reference problem, initially, the FEA model is solved with linear elastic material properties, for one test condition i.e., test number 15. It is observed that the equivalent stresses near the corner, are above the material yield limit over the region with the radius of ~ 0.2 mm (as shown in Figure 45). Subsequent fatigue life results calculated using such stress-strain values can produce erroneous results. Therefore, appropriate material non-linearity needs to be considered to get more realistic results.

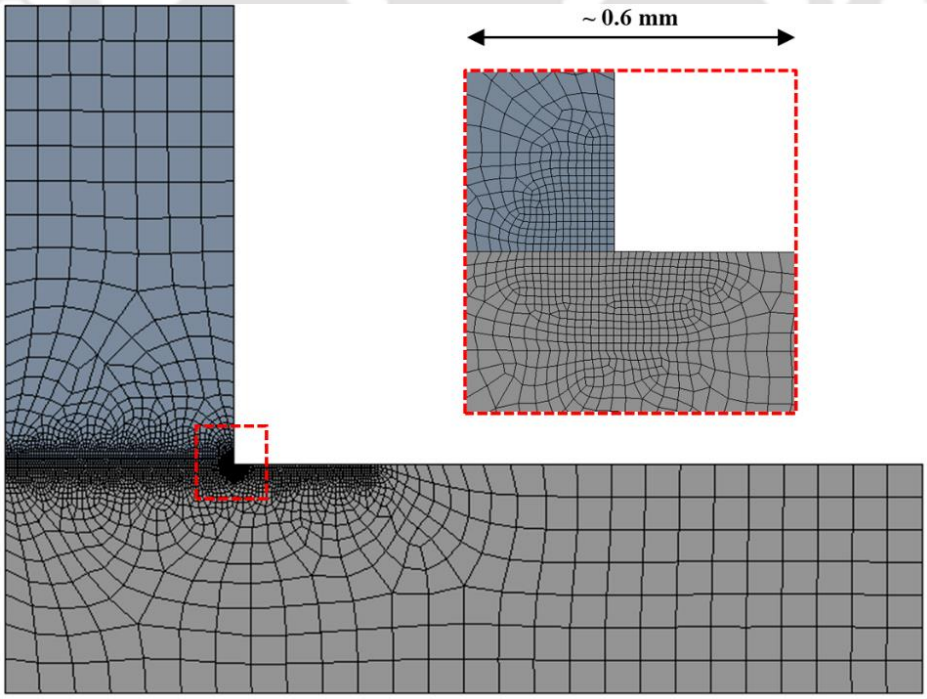

Figure 43: 2D FEA model details (1/4th Symmetric model)

Table 7: Material properties of AL7075-T6

Material Parameter	Value (Unit)	Reference
E (Elastic modulus)	72000 (MPa)	[58]
ϑ (Poisson's ratio)	0.33	
σ_{yt} (Yield strength)	503 (MPa)	
σ_{ut} (Ultimate strength)	572 (MPa)	
Ramberg-Osgood's strength coefficient, K'	787 (MPa)	[136]
Ramberg-Osgood's strain hardening exponent, $n^{\wedge}$	0.07	
Chaboche material constants	C1= 4318.3 Y1= 36.89 C2= 4318.3 Y2= 29.72	-
Elongation at break	11%	[132]
Fatigue strength coefficient, σ_f' (MPa)	1485.6 (MPa)	[58]
Fatigue ductility coefficient, ε_f'	0.262	[137]
Shear fatigue ductility coefficient, γ_f'	0.453	
Fatigue strength coefficient in shear, τ_f'	846 (MPa)	
Fatigue strength exponent in tension, b	-0.1445	[58]
Fatigue strength exponent in torsion, b' (assumed identical to b)		-
Fatigue ductility exponent in tension, c	-0.619	[137]
Fatigue ductility exponent in torsion, c' (assumed identical to c)		-
ΔK_{th}	2.2 (MPa $\sqrt{\text{m}}$)	[138]
σ_{f-1}	169 (MPa)	
K	10^{-04}	[139]
H	168 (MPa) ($\sigma_{yt}/3$)	[140]

C	14.45 ($MPa^{-1}mm^{-1}$)	[102]
n	2.655	
δ_{th}	30 (μm)	[141]

Initially 'Bi-linear kinematic hardening (BKIN)' non-linear model is considered to capture the post-yielding stress-strain behavior. Subsequently considered material properties for BKIN material model are given in Table 7. Considering the possible path dependency because of non-linear FEA model, FEA run should be carried for sufficient number of duty block repetitions to obtain the stabilized stress-strain condition [142]. Hence, FEA is carried out for 20 duty cycle blocks, with the corresponding load history as shown in Figure 46. One duty cycle block corresponds to one complete load reversal cycle. Thus, 20 duty cycle blocks correspond to 20 such load reversals. Resultant stress-strain stabilization of maximum stress and strain values is shown in Figure 47. It is observed that after 20 duty cycle blocks, resultant stress-strain results are stabilized. These stabilized stress-strain results can be considered for the further FIP and resultant fretting fatigue life calculations by considering different crack initiation methods.

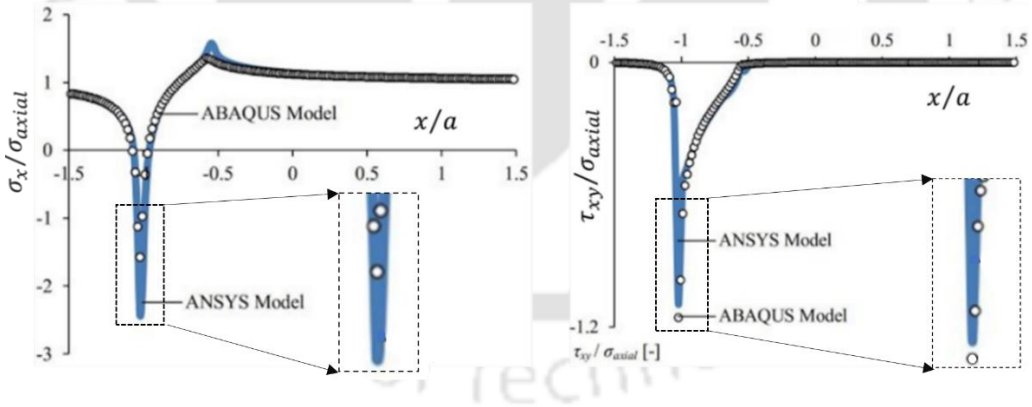

Figure 44: Comparison of normalized stress distribution (normal and tangential shear) over contact interface between ANSYS and ABAQUS FEA models (Reprinted with permission from [135])

2.3. Critical Plane Based Fatigue Life Evaluation

Since the resultant stress-strain condition at the contact surface between the contacting bodies is complex and non-proportional in nature, critical plane-based fatigue analysis has often proved to be a valid option to determine resultant fatigue life due to fretting

fatigue loads [143]. As mentioned earlier, critical plane-based fatigue crack initiation methods are classified into three groups, (i) stress-based, (ii) strain-based, and (iii) strain energy-based fatigue initiation parameters i.e., FIP's. Among such FIP's, following critical plane-based methods are considered during the scope of current work.

- Strain-based method of Fatemi-Socie (FS) [23]
- Strain-energy based method of Smith-Watson-Topper (SWT) [22]

As the material yielding is predicted through FEA results (see Figure 45), stress-based critical plane methods are not considered here. In the critical plane-based methods, stresses and strains need to be resolved along different planes passing through the individual nodes and then overall maximum FIP value and resultant fatigue life is evaluated. Corresponding details are discussed in the next section.

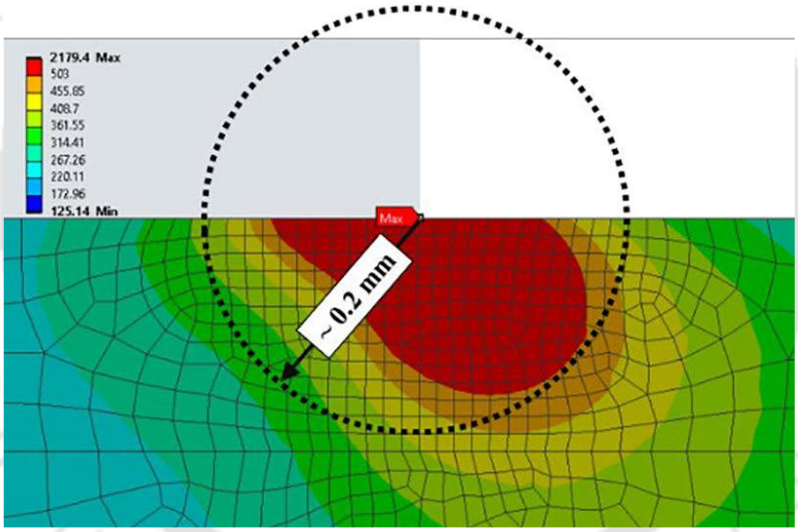

Figure 45: Equivalent stress plot with linear material properties (for test#15) (unit: MPa)

2.3.1. Stress-Strain Transformation Along Critical Plane

Stress-strain values in different planes are calculated using the transformation equations as mentioned earlier (Equation 17-20). Once the FEA model is solved for all 15 test conditions with 20 duty cycle blocks for each test load conditions, fatigue life evaluation is carried out using SWT and FS critical plane-based methods. For critical plane-based methods, nodal stress and strains are resolved at each plane passing through each node.

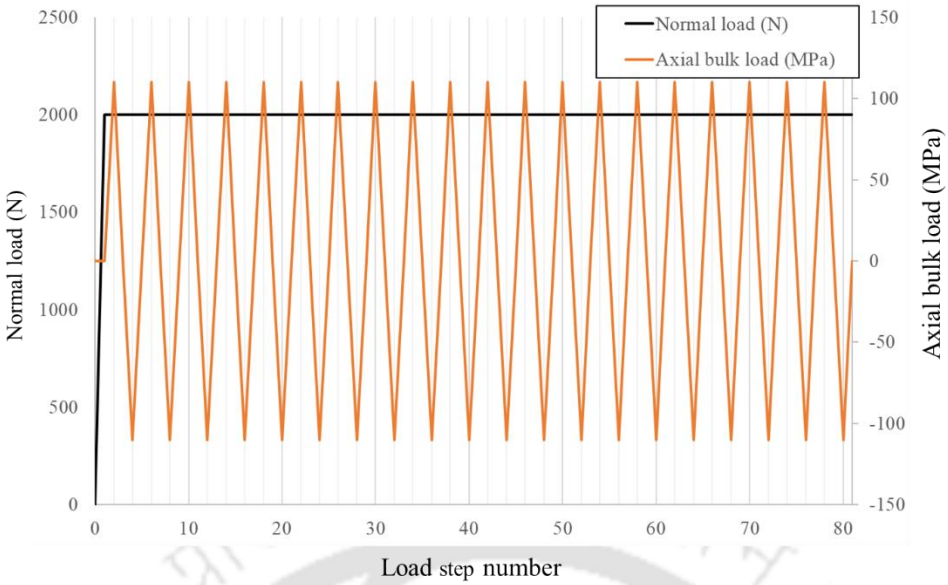

Figure 46: Load history considered in the ANSYS model

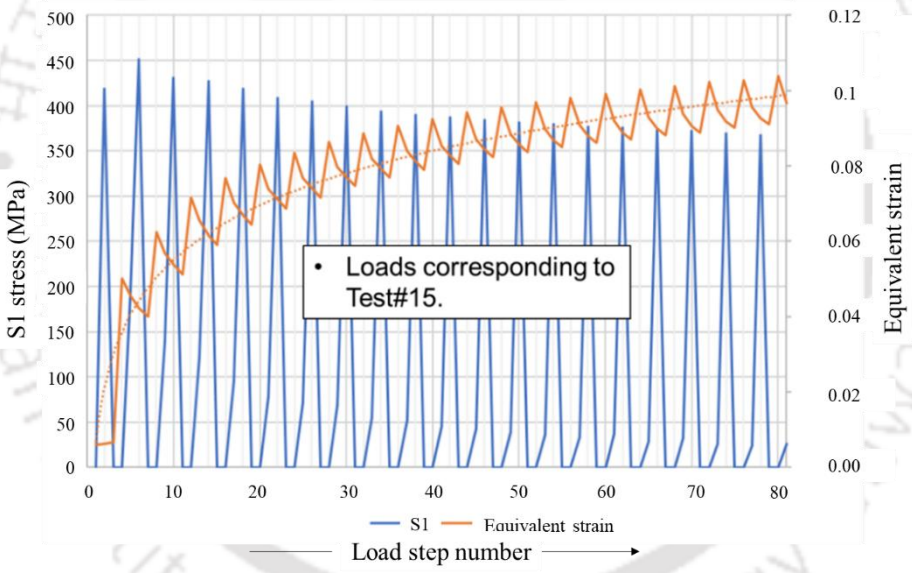

Figure 47: Stress-strain stabilization results (for test#15)

As shown earlier in Figure 21 , a critical plane increment of 10° achieves the right balance between the accuracy and subsequent computational time. Once the stress-strain values are resolved, resultant fatigue damage parameter is calculated at each plane and the plane with the maximum damage value is considered as the critical plane and corresponding damage value is considered to evaluate the resultant fatigue initiation life. Corresponding details are discussed in the following sections.

2.3.2. SWT Parameter-Based Fatigue Life Evaluation

SWT parameter, which is an energy based FIP, was proposed by Smith, Watson and Topper [22]. It considers that the fatigue crack initiation life is a function of product of maximum normal stress and maximum normal strain amplitude as shown in Figure 48. APDL based macros are developed for carrying out the required stress-strain transformations (as per the Equations 17-20), and for SWT damage and resultant minimum fatigue life evaluation (see Equation 14). The schematic representation for the SWT parameter is shown earlier in Figure 20, and the corresponding flow-chart for SWT parameter and resultant fatigue life evaluation is shown in Figure 50. To validate the results of APDL macro, initial correlation is done considering a benchmark problem of plain fatigue loadings, by comparing the results obtained using APDL macro with experimental results of the benchmark problem. The results are given in the Section 2.6.

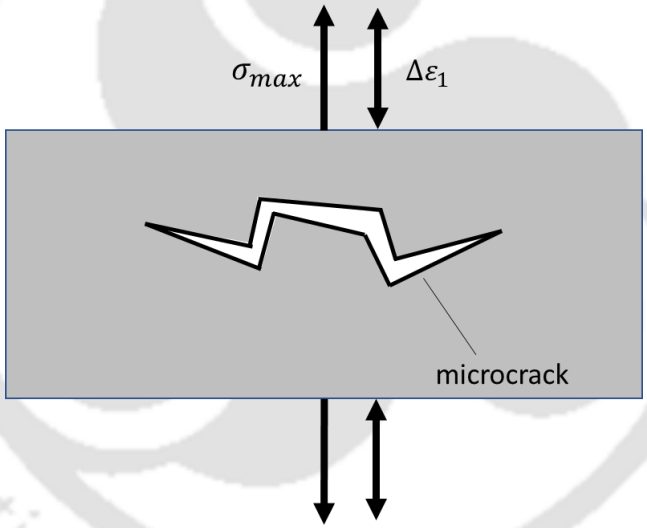

Figure 48: Critical parameters for SWT multiaxial model (Reproduced based on [144])

2.3.3. FS Parameter-Based Fatigue Life Evaluation

FS parameter, which is a strain based FIP, is proposed by Fatemi and Socie [23, 71]. It considers that the fatigue crack initiation life is a function of product of maximum normal stress and maximum shear strain amplitude (see Figure 49). Similar to SWT, for FS parameter also, APDL based macros are written for carrying out the subsequent stress-strain transformations, damage calculation and minimum fatigue life evaluation, as per the Equation 12. The corresponding schematic representation of FS parameter calculation is shown earlier in Figure 19 and the flow-chart for resultant fatigue life evaluation for

this parameter is shown in Figure 51. It is similar to the flow-chart considered for SWT parameter, except for the considerations of appropriate stress/strain types.

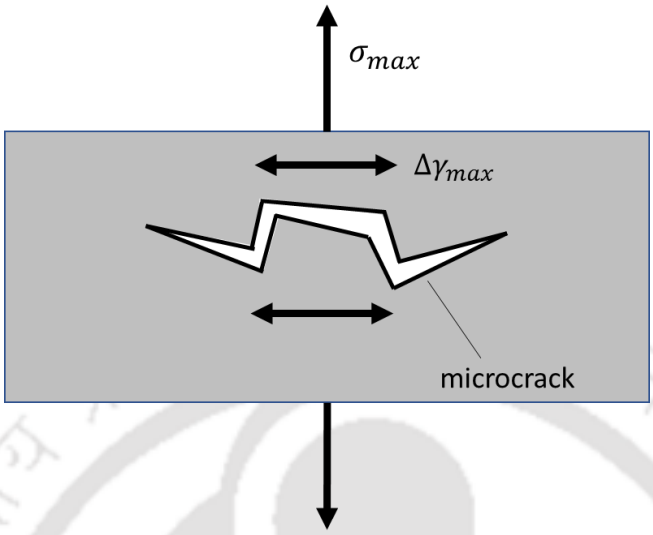

Figure 49: Critical parameters for FS multiaxial model (Reproduced based on [144])

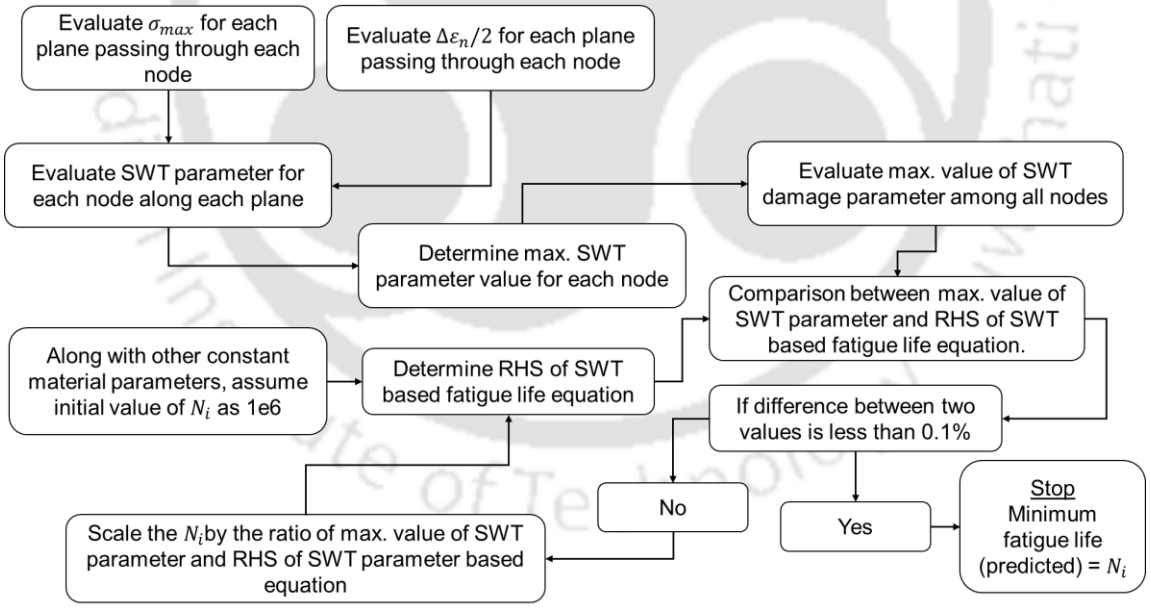

Figure 50: Flow-chart for SWT parameter calculation

2.4. Stress Invariant-Based Fatigue Life Evaluation:

Among the various stress invariant-based approaches like Marin, Sines, von Mises [85] etc., Crossland parameter [88] is mostly considered to analyze the fretting fatigue

problems [52]. Hence, in the current work, it is considered for the comparative assessment with other methods. APDL based macros are written for carrying out corresponding fatigue damage calculation and minimum life evaluation (see Equation 21). The flow-chart is shown in the Figure 52. Here, unlike earlier discussed methods of SWT and FS, the fatigue damage value is a scalar parameter calculated at each node and does not require the stress-strain transformations along different planes passing through each node of the considered FEA domain.

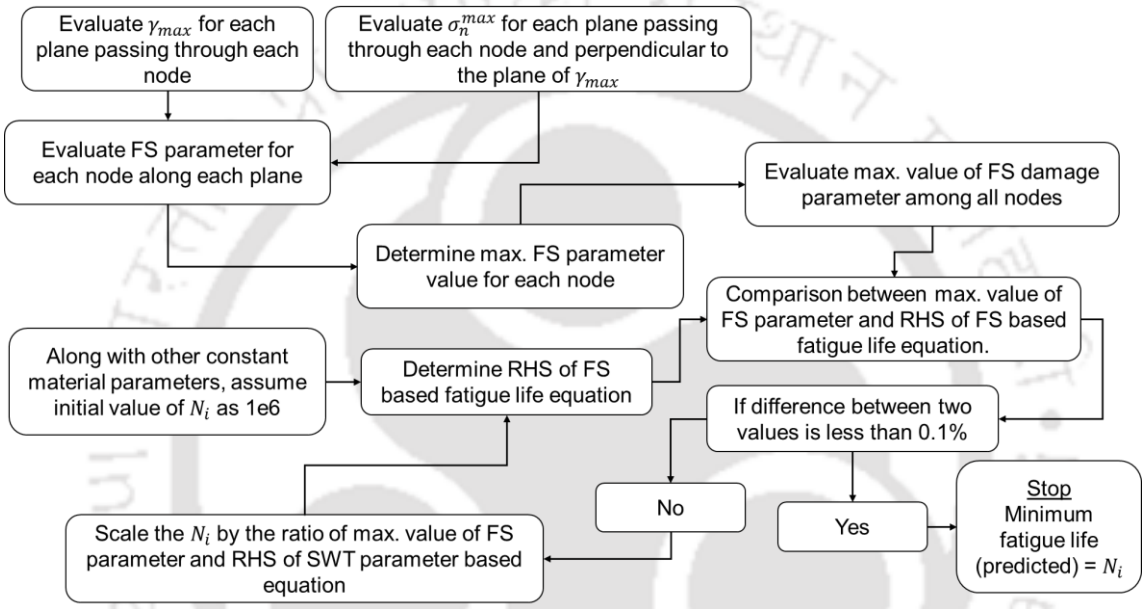

Figure 51: Flow-chart for FS parameter calculation

2.5. Deviotoric Strain Amplitude-Based Method (eI) for Fatigue Life evaluation

Recently a new approach based on deviatoric strain amplitude is proposed for finite fatigue life evaluation [130]. In this approach, along with the deviatoric strain amplitude, mean normal stress effect is considered through hydrostatic stress term and mean shear stresses effect is considered through the mean value of the second invariant of the deviatoric stress tensor. The combined effect thus incorporates the effect of non-proportional loading on the fatigue life. During the assessment with total 211 strain-controlled axial-torsional loading conditions, as applied on three steels (SAE 1045 HR, S460N and stainless steel 304) and two aluminum alloys (7075-T651 and 6061-T6), this parameter is observed to predict fatigue life within $\pm$ 2N scatter band [130].

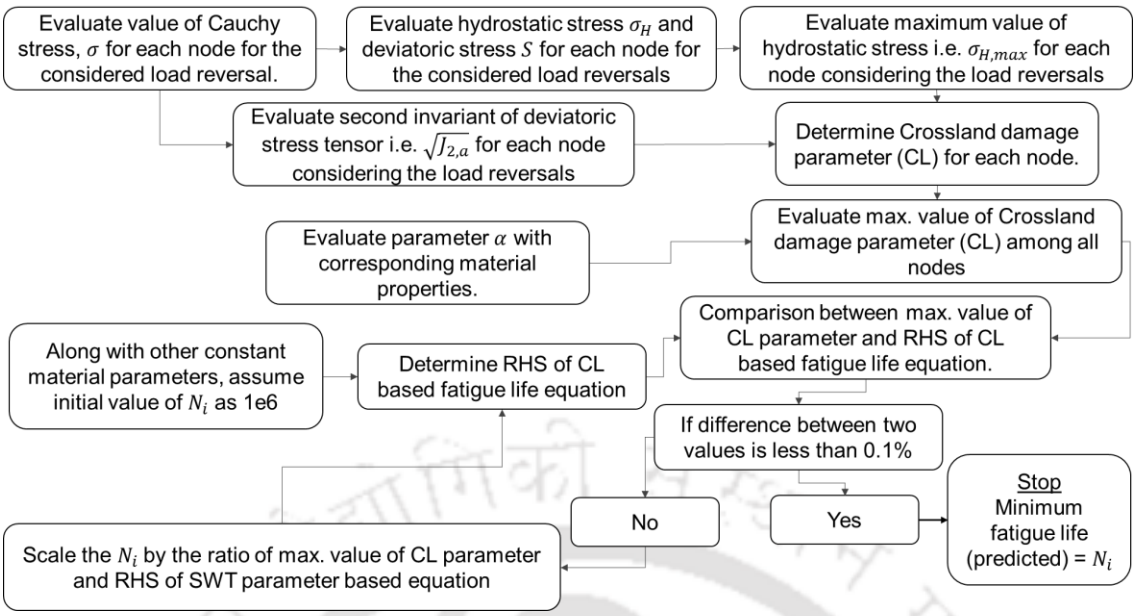

Figure 52: Flow-chart for CL parameter calculation

According to this parameter, fatigue degradation is a result of combination of loading modes in mutually orthogonal directions in the deviatoric strain space. Effectiveness of this parameter towards predicting fretting fatigue life is not yet studied. Being strain based parameter, it can be considered in both LCF and HCF regime. Therefore, this parameter is considered during the scope of this work. Resultant fatigue life relationship using this parameter is

$$\gamma_{dev} + \frac{k}{G}\,\sigma_{H,max} = \frac{\tau_f' - \sqrt{J_{2m}}}{G}(2N_i)^b + \gamma_f'(2N_i)^c \tag{35}$$

The parameters considered in above equation are calculated as given below:

$$\gamma_{dev} = \max_{\theta}\left(2\sum_{i=1}^{5} a_i^2(\theta)\right)^{\frac{1}{2}}$$

$$a_i = \frac{1}{2}\left(\max_t e_i(t) - \min_t e_i(t)\right), \quad i = 1, \ldots, 5$$

$$e_1 = \frac{1}{\sqrt{6}}\left(2\varepsilon_x - \varepsilon_y - \varepsilon_z\right), e_2 = \frac{1}{\sqrt{2}}\left(\quad_y - \varepsilon_z\right),$$

$$e_3 = \frac{1}{\sqrt{2}}\gamma_{xy}, e_4 = \frac{1}{\sqrt{2}}\gamma_{xz}, e_5 = \frac{1}{\sqrt{2}}\gamma_{yz}$$

$$\sqrt{J_{2m}} = \frac{1}{2}\max_{t_0 \in T}\left\{\max_{t \in T}\left[\frac{1}{2}\left(S'(t) + S'(t_0) : \left(S'(t) + S'(t_0)\right)\right)\right]^{1/2}\right\}$$

$$k = G\frac{\left[\frac{\tau_f'}{G}(2N_i)^{b'} + \gamma_f'(2N_i)^{c'}\right] - \sqrt{3}\left[\frac{2}{3}(1+\vartheta)\frac{\sigma_f'}{E}(2N_i)^{b} + \varepsilon_f'(2N_i)^{c}\right]}{\frac{1}{3}\sigma_f'(2N_i)^{b}}$$

where γ_{dev} is the resultant deviatoric strain, $\sigma_{H,max}$ is the maximum hydrostatic stress, G is the shear modulus of material, τ_f' is the fatigue strength coefficient in shear, J_{2m} is the mean value of second invariant of deviatoric stress, N_i is the cycles to crack initiation, γ_f' is the shear fatigue ductility coefficient, b is the fatigue strength exponent, c is the fatigue ductility exponent, ε_x is the normal strain in x direction, ε_y is the normal strain in y direction, ε_z is the normal strain in z direction, γ_{xy} is the shear strain in x-y plane, γ_{yz} is the shear strain in y-z plane, γ_{xz} is the shear strain in x-z plane, S' is the deviatoric stress tensor.

Similar to the stress-invariant based parameters like Crossland parameter (CL) [88], this parameter also produces scalar results at each node and does not require the critical plane calculations. APDL macros are written for carrying out resultant stress-strain transformations, damage calculation and minimum life evaluation. The corresponding flow-chart is shown in the Figure 53.

2.6. Initial Verification With Plain Fatigue Benchmark Problem

APDL based post-processing macros are developed to evaluate the resultant FIP values for each node of the considered FEA domain. Further, the maximum FIP value is obtained, and corresponding crack initiation life is calculated for this node. For the critical plane-based parameters like SWT and FS, additional information in terms of possible crack initiation angle can also be obtained. As shown in Figure 50–53, minimum fatigue life is calculated for all the considered FIP's, by using the iterative approach and considering allowed convergence error as 0.1%.

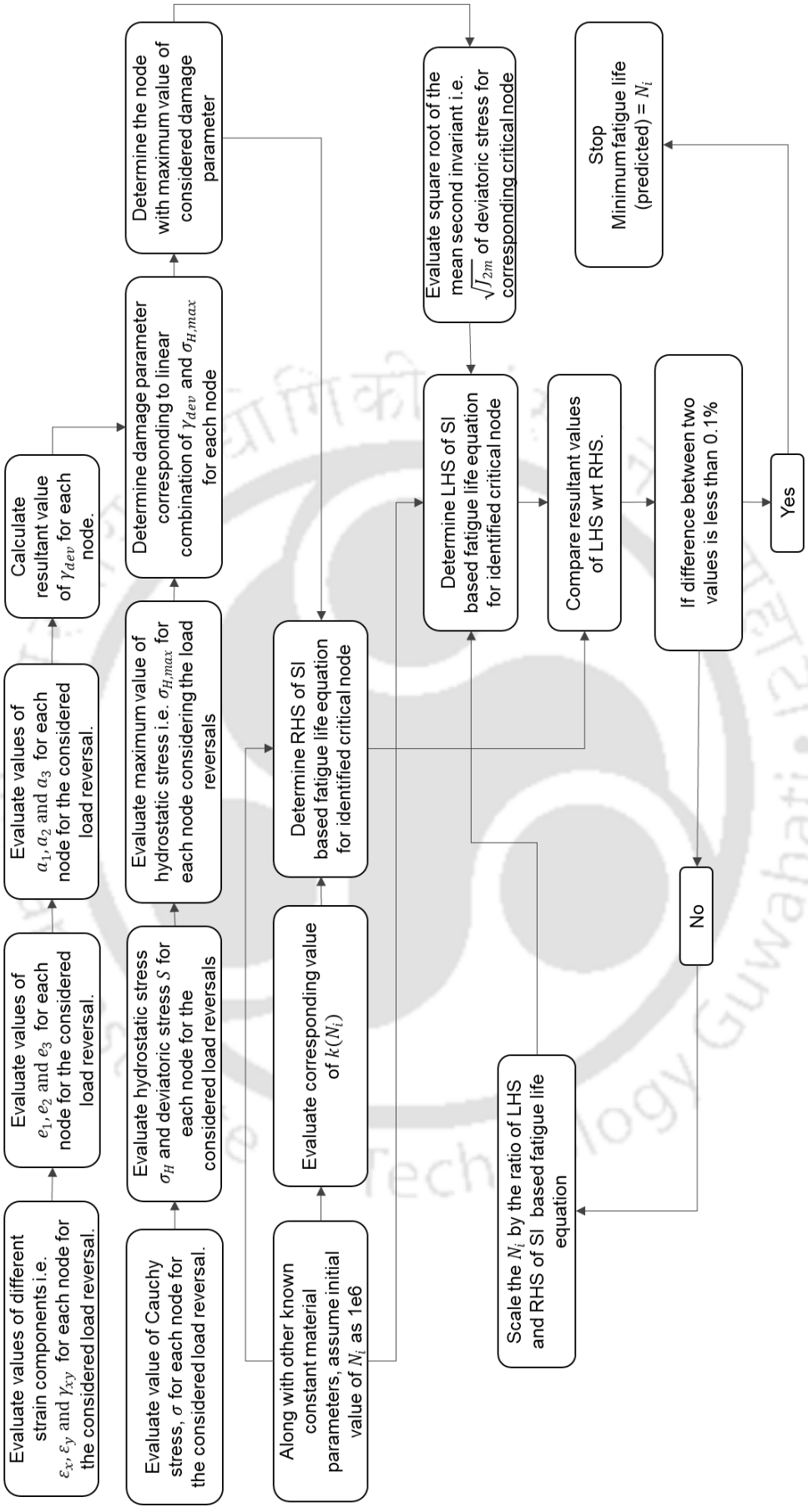

Figure 53: Flow-chart for eI parameter calculation

To verify the correct functionality of these macros, initial verification is carried out by considering the benchmark problem of 'SAE Keyhole Test Program' [145]. Since this problem is of a plain fatigue case, the high stress gradients usually observed at the contact surface/s in the case of fretting fatigue are absent. Thus, if good correlation is achieved for this initial verification step, the developed macros can be considered to be suitable towards further fretting fatigue life evaluation. Subsequent details of the loads and boundary conditions applied in the benchmark problem of "SAE keyhole test program" along with the corresponding FEA model details, are given in the Figure 54. FEA mesh discretization is kept identical to the benchmark problem. Related material properties are given in Table 8.

Table 8: Material Properties of Bethlehem Steel RQC-100 [145]

Material Property (Unit)	Value
Elastic Modulus, E (GPa)	203
Yield Strength σ_{yt} (MPa)	565
Ultimate Strength, σ_{ut} (MPa)	820
Fatigue Strength Coefficient, σ_f' (MPa)	1160
b/b'	-0.075
ε_f'	1.06
c/c'	-0.75

FEA model is prepared and solved for the considered loads and BC's and fatigue life evaluation is carried out for different FIP's using the APDL macros. Further the predicted fatigue life results are compared with the experimental life values and corresponding correlation results are given in Figure 55. As can be seen, the experimental correlation is observed within $\pm$ 2N scatter band for most of the FIP results, except CL parameter for which one result point lie well outside the $\pm$ 2N scatter band. Thus, it is observed that the developed APDL macros are able to correlate the experimental results well within $\pm$ 2N scatter band for plain fatigue condition and therefore, can be further considered for the fretting fatigue life evaluation of the reference fretting fatigue problem [58].

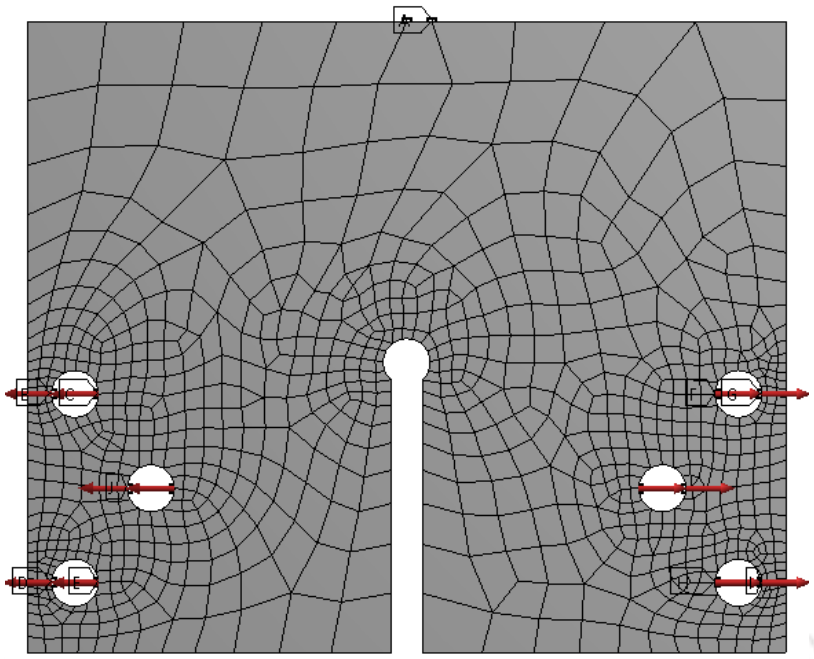

Figure 54: FEA model details of plain fatigue benchmark problem

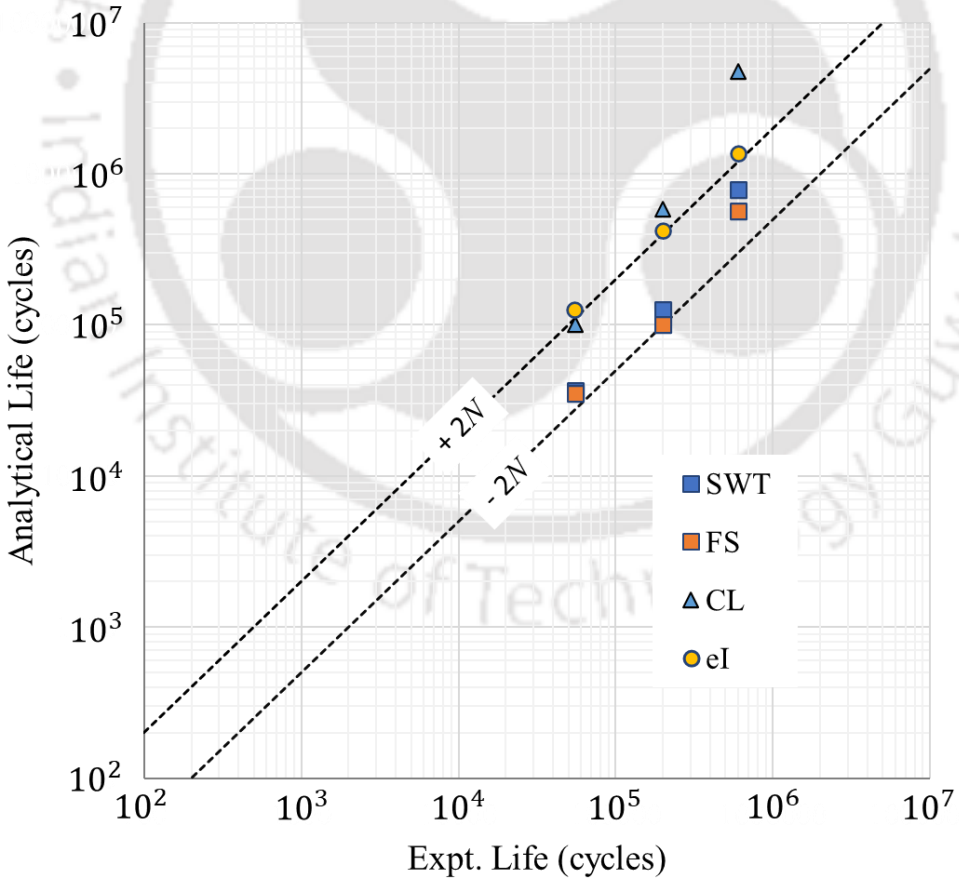

Figure 55: Experimental correlation results for plain fatigue benchmark problem

2.7. Consideration of Stress Averaging Methods to Capture Resultant Stress Gradient

In fretting fatigue problems, the stress gradient at the contact surface is very high. To capture the resultant stress gradient at the contact surface, there are different stress averaging methods already discussed in Section 1.6.5. These methods carry out the stress-strain averaging around the contact surface nodes, over the critical dimension. This critical dimension is a material dependent property. Considering such averaged stress-strain values in the fretting fatigue initiation criteria, more realistic FIP value and more comparable fatigue life results can be obtained.

In the case of fretting fatigue, by considering the area/volume averaging method at the location with maximum fatigue damage, better experimental correlation is observed for the various slip ranges [102]. Also, comparatively lesser dependence on averaging dimension is observed for the area method [59]. Therefore, in this work, area-based stress averaging method is considered in conjunction with different fatigue initiation methods discussed earlier. Considering the Equation 33 and corresponding material parameter values, as given in Table 7, resultant value for the critical dimension i.e., r_c is obtained.

2.8. Fretting Fatigue Life Results for Different Considered Crack Initiation Methods

After observing the initial verification through the identified benchmark problem of plain fatigue case [145], now experimental correlation is carried out for the considered reference fretting fatigue problem. Earlier used FIP's are considered for this correlation study in conjunction with the area stress averaging method. Resultant fatigue life results are compared with the experimental fatigue life results. The critical dimension i.e., r_c, needed for stress-strain averaging is evaluated using the Equation 33. Corresponding material parameter values for ΔK_{th} and σ_{f-1}, for AL7075-T6 are given in Table 7. Resultant value of r_c of 55 μm, is in reasonable agreement with the grain size of 35 μm for AL7075-T6 material [138]. This critical dimension is generally of the similar order of the magnitude as the material's grain size [112]. The resultant value of r_c is considered in the area stress-strain averaging method to calculate the resultant damage value for different considered FIP's.

For all the experimental correlation work, FEA results of the 20th duty block, as shown in Table 9, are considered. Based on the localized yielding, material nonlinearity in terms

of the BKIN material model is considered. Material data required for BKIN is considered based on the material properties like % elongation at break, elastic modulus, tensile strength (UTS) and yield strength. The elongation at UTS (%), is assumed as 50% of the elongation at break. Using these data, the tangent modulus, E_t, is calculated as

$$E_t = (\sigma_{ut} - \sigma_{yt})/(\varepsilon_u - \varepsilon_{yt}) \tag{36}$$

where σ_{ut} is the material UTS, σ_{yt} is the yield strength of the material, ε_u is the true strain corresponding to % elongation at UTS, ε_{yt} is the true strain corresponding to the strain at σ_{yt}.

It is then used as an input parameter towards BKIN material model in ANSYS. Since this material model considers the Bauschinger effect [146], it is suitable for the load situations with repetitive loading and unloading.

Figure 56, shows the resultant experimental correlation obtained using the FS parameter and subsequent tabular summary is given in the Table 10. In this work, for experimental correlation, statistical parameters proposed by Navarro et al. [60] are considered. Against all 15 test cases, logarithm ratio i.e., α_i is determined between the analytical life results N_{ei} and the experimental test results N_{ti} as

$$\alpha_i = \log\left(\frac{N_{ei}}{N_{ti}}\right) \tag{37}$$

Further average value $\tilde{\alpha}$, along with the standard deviation D_α are calculated as

$$\tilde{\alpha} = \frac{1}{N}\sum_{i=1}^{N} \alpha_i \tag{38}$$

$$D_\alpha = \sqrt{\frac{1}{N-1}\sum_{i=1}^{N} (\alpha_i - \tilde{\alpha})^2} \tag{39}$$

Finally, results used for experimental correlation are the antilogarithms of these values as

$$\tilde{x} = 10^{\bar{\alpha}}$$
$$D_x = 10^{D_\alpha} \quad (40)$$

For the perfect correlation, both the above values should be equal to 1 i.e., $\tilde{x} = 1$ and $D_x = 1$ [60].

Similarly, experimental correlation is carried out by considering the SWT parameter and subsequent results are shown in the Figure 57 and resultant tabular summary is given in the Table 11 . Experimental correlation considering CL parameter is shown in in the Figure 58 and corresponding tabular summary is given in the Table 12. Here it should be noted that CL parameter is based on the stress values only. Hence, with the consideration of material nonlinearity, evaluating the fatigue life results based on stress values only, is physically not correct, though the resultant experimental correlation appears to be comparable. So, with the CL parameter, effect of area-based stress averaging technique is not studied further.

Table 9: Considered duty cycle loading

<table>
<tr><td rowspan="2"></td><td colspan="5">Duty Cycle block Number →</td><td rowspan="2">Normal Load (2/4/8 kN)</td><td rowspan="2">Axial Load (110,130,150,170,190 MPa)</td></tr>
<tr><td>1</td><td>2</td><td>3</td><td>4</td><td>5</td></tr>
<tr><td rowspan="5">Load Step Number ↓</td><td>1</td><td></td><td></td><td></td><td></td><td rowspan="10">Applied</td><td>0</td></tr>
<tr><td>2</td><td>6</td><td>10</td><td>14</td><td>18</td><td>+ve</td></tr>
<tr><td>3</td><td>7</td><td>11</td><td>15</td><td>19</td><td>0</td></tr>
<tr><td>4</td><td>8</td><td>12</td><td>16</td><td>20</td><td>-ve</td></tr>
<tr><td>5</td><td>9</td><td>13</td><td>17</td><td>21</td><td>0</td></tr>
<tr><td rowspan="2"></td><td colspan="5">Duty Cycle block Number →</td><td rowspan="2">Axial Load</td></tr>
<tr><td>6</td><td>7</td><td>8</td><td>9</td><td>10</td></tr>
<tr><td rowspan="5">Load Step Number ↓</td><td>22</td><td>26</td><td>30</td><td>34</td><td>38</td><td>+ve</td></tr>
<tr><td>23</td><td>27</td><td>31</td><td>35</td><td>39</td><td>0</td></tr>
<tr><td>24</td><td>28</td><td>32</td><td>36</td><td>40</td><td>-ve</td></tr>
<tr><td>25</td><td>29</td><td>33</td><td>37</td><td>41</td><td>0</td></tr>
</table>

	Duty Cycle block Number →					Applied	Axial Load
	11	12	13	14	15		
Load Step Number ↓	42	46	50	54	58		+ve
	43	47	51	55	59		0
	44	48	52	56	60		-ve
	45	49	53	57	61		0
	Duty Cycle block Number →						Axial Load
	16	17	18	19	20		
Load Step Number ↓	62	66	70	74	78		+ve
	63	67	71	75	79		0
	64	68	72	76	80		-ve
	65	69	73	77	81		0

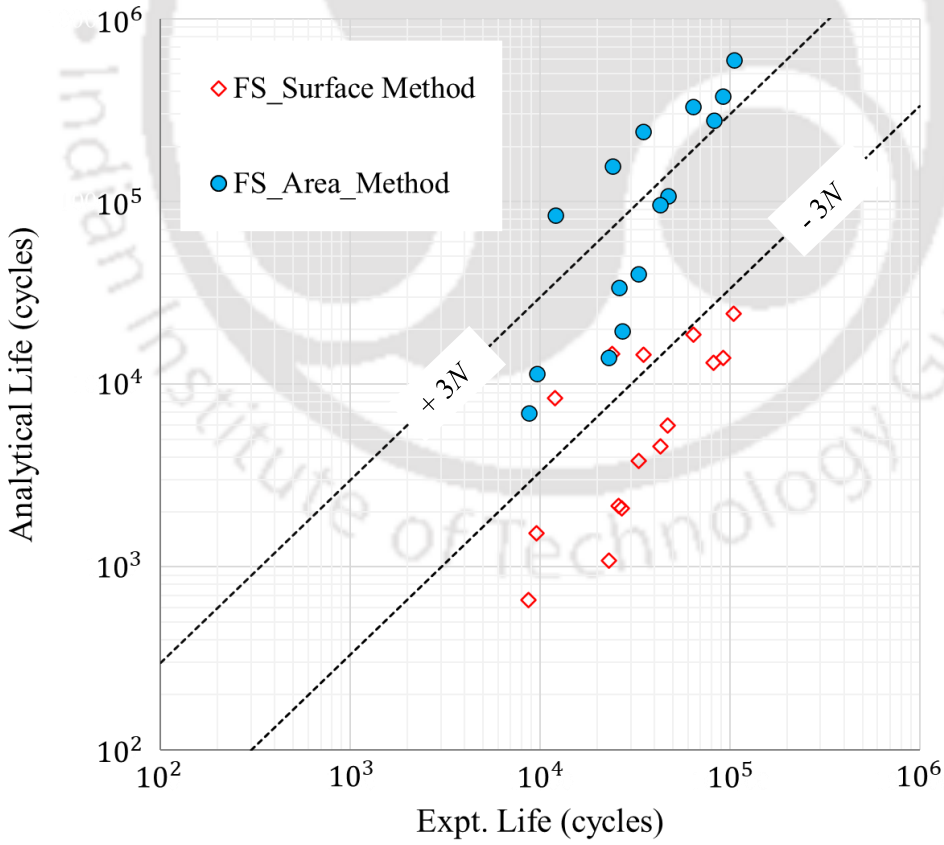

Figure 56: Experimental correlation obtained for reference fretting fatigue problem with FS parameter with surface averaging and area averaging methods

Experimental correlation considering the deviatoric strain amplitude-based parameter (eI) is shown in in the Figure 59 and the subsequent tabular summary is given in the Table 13. Deviatoric strain amplitude-based parameter, similar to the CL parameter, is a scalar parameter, calculated over the different nodes of the FEA model. It does not provide any information over the critical plane orientation.

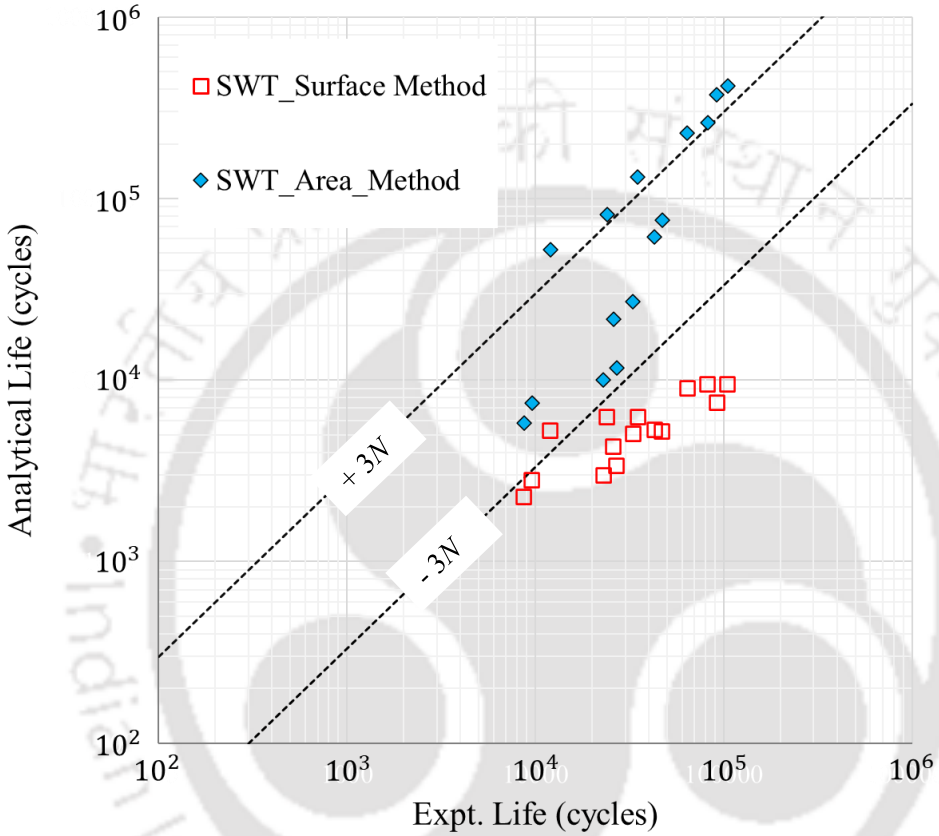

Figure 57: Experimental correlation obtained for reference fretting fatigue problem with SWT parameter with surface averaging and area averaging methods

As observed with different set of results resultant experimental correlation is improved after considering the area-based averaging method. The surface method provides much lower estimations than the experimental life results. Hence, it is less accurate and should not be considered for estimating the fretting fatigue life results. Overall experimental correlation obtained using area-based averaging method for different FIP's is shown in the Table 14. Thus, the overall experimental correlation is observed within $\pm$ 3N scatter band, for most of the considered test cases, using above different FIP's like FS, SWT and eI with area stress-strain averaging method.

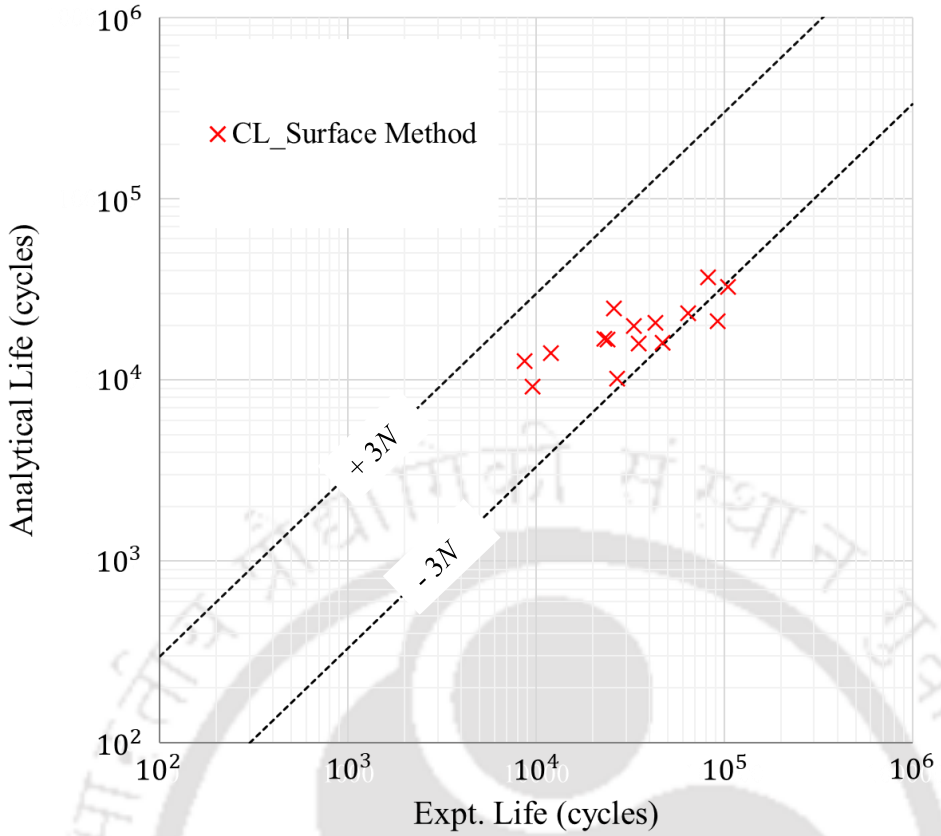

Figure 58: Experimental correlation obtained for reference fretting fatigue problem with CL parameter with surface averaging

Table 10: Experimental correlation results obtained using FS parameter

Fatigue Initiation Parameter	Stress Averaging Method	Average	Deviation
FS	Surface	0.16	2.20
	Area	2.37	2.41

Table 11: Experimental correlation results obtained using SWT parameter

Fatigue Initiation Parameter	Stress Averaging Method	Average	Deviation
SWT	Surface	0.16	1.59
	Area	1.63	2.40

Table 12: Experimental correlation results obtained using CL parameter

Fatigue Initiation Parameter	Stress Averaging Method	Average	Deviation
CL	Surface	0.56	1.71

Table 13: Experimental correlation results obtained using eI parameter

Fatigue Initiation Parameter	Stress Averaging Method	Average	Deviation
eI	Surface	0.18	2.19
	Area	1.87	2.19

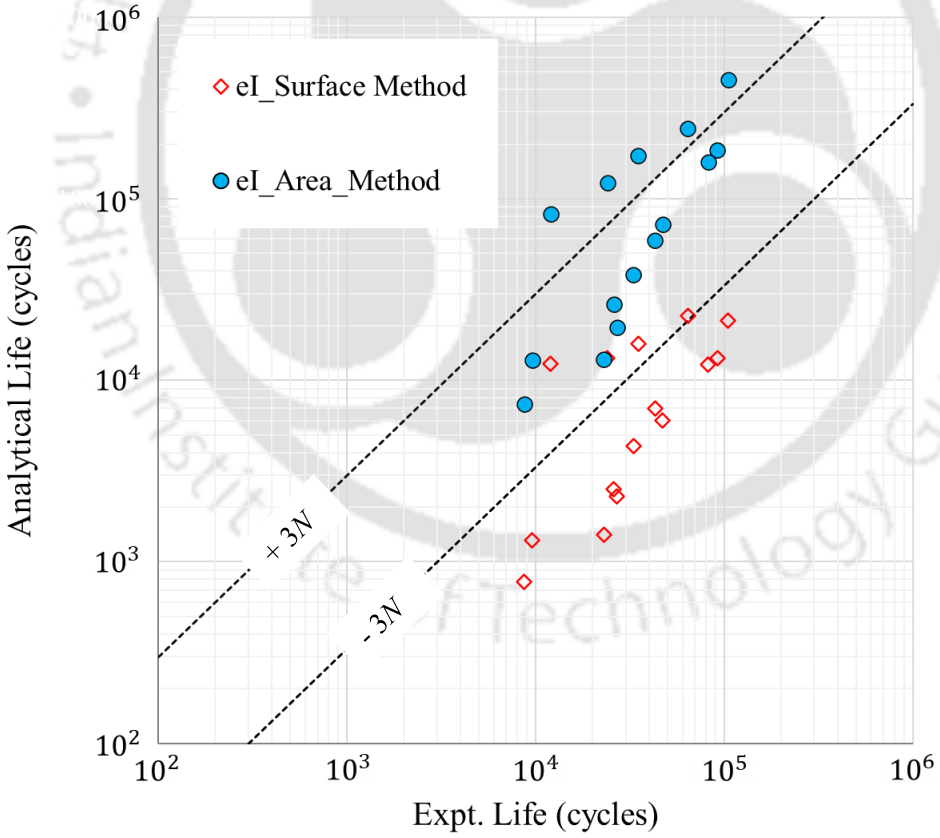

Figure 59: Experimental correlation obtained for reference fretting fatigue problem with eI parameter with surface averaging and area averaging methods

Table 14: Overall experimental correlation with area-based stress averaging results

Fatigue Initiation Parameter	Stress Averaging Method	Average	Deviation
FS	Area	2.37	2.41
SWT		1.63	2.40
eI		1.87	2.19

As compared to the surface-based results, with the area averaging method, resultant average values are improved for the considered FIP's like SWT, FS and eI. Also, the resultant deviation value is quite similar for different FIP's. Comparatively better experimental correlation is observed with normal stress-strain-based parameter, i.e., SWT parameter. In the case of complete flat-flat contact, fretting fatigue failure is generally dominated by a high normal stress-strain range at the contact edge, leading to mode I type of cracks [147]. Next, eI parameter results show better correlation. Through this work, the eI parameter is considered for the first-time for any fretting fatigue damage and life evaluation.

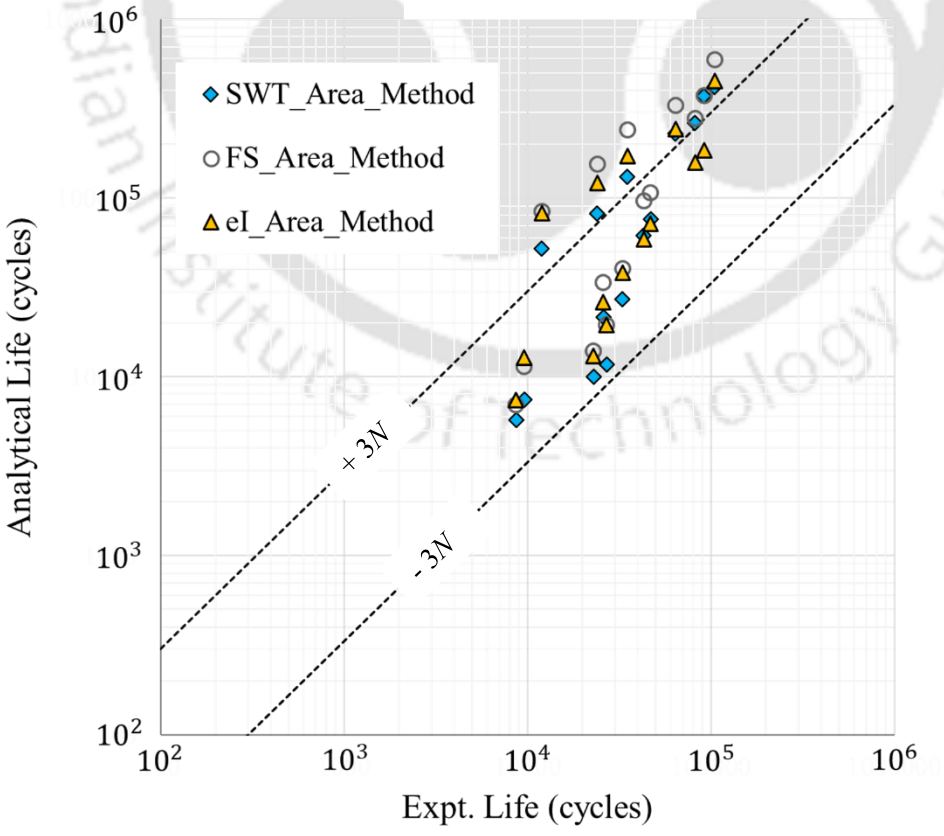

Figure 60: Comparison between SWT, FS and eI results with area-based averaging

Though the results with CL parameter, without any averaging, shows correlation within +/- 3*N* scatter band with the experimental life, as it is based on stress results only, it does not consider the actual post yielding strain results. So, for the cases in which the fatigue life results are based on the combined effect of total stress-strain results, CL parameter fails to consider this effect. So, though lesser spread is observed in the results with CL parameter, it is mainly due to the consideration of stress values only and neglecting the elasto-plastic strains in the fatigue damage calculations.

As shown in Figure 60, among 15 test-cases, for most of the cases, experimental correlation is observed with $\pm$ 3*N* scatter band. For few cases i.e., Test#1, 4, 7, 10 and 13, the analytical life results are above the + 3*N* limit line. These tests, as shown in Table 6, are with the minimum applied normal load i.e., with 2 kN. With minimum normal load applied, relative sliding distance values will be higher and can possibly cause higher damage due to resultant fretting wear. Currently, the obtained fatigue life results are without considering any wear correction/modeling. Hence, this wear correction effect is studied further in the next chapter, along with other critical parameters like varying COF, resultant stress-strain stabilization due to different material non-linear models etc. Corresponding details are discussed in the next chapter.

भारतीय प्रौद्योगिकी संस्थान गुवाहाटी
Indian Institute of Technology Guwahati

3. CRITICAL PARAMETERS TOWARDS FRETTING FATIGUE DAMAGE OF FLAT CONTACT PAIR

In continuation to the study of different crack initiation parameters combined with the area stress-strain average technique, there are certain additional parameters which needs to be considered for the reliable fretting fatigue evaluation. As mentioned earlier, there are more than 50 such parameters- physical and analytical in nature- which affect the fretting fatigue [50]. As shown earlier in Figure 23, these parameters can be broadly classified into three categories i.e., environmental factors, contact conditions and material properties. The parameters considered within the scope of current work are as given below. They are considered primarily based on their significance to the considered case-study of the head gasket.

- Material nonlinearity
- Varying coefficient of friction
- Wear due to relative sliding distance
- Frictional heat
- Variation in normal axial and tangential loads

The corresponding results obtained with the above-mentioned parameters are discussed in this chapter.

3.1. Effect of Material Nonlinearity on Fretting Fatigue Life Results

Till now, it is observed that the resultant stresses in the fretting specimen are above the yield limit of AL7075-T6 over a small-localized region. Since the resultant fretting fatigue life is evaluated considering the contact surface stress and strains, appropriate material nonlinear model needs to be selected. Elleuch et al. [148] mentioned that based

The contents of present chapter have been published in 'A. P. Ozarde, G. H. McNay and S. S. Gautam, " Comparative fretting fatigue life evaluation between critical plane based and deviatoric strain amplitude based methods corrected for surface wear damage", SAE International Journal of Materials and Manufacturing, vol. 15(2), 2022, doi: 10.4271/05-15-02-0009'

on the coefficient of friction and the 'load factor', fretting specimens which are elasto-plastic in nature, usually responds to the cyclic loadings in three different ways, as shown in Figure 61.

Therefore, the 'load factor' results are obtained for the considered 2D FEA model for all the 15 test-cases, using linear material properties. The corresponding results are given in Table 15. The 'load factor' is the ratio of maximum contact pressure, estimated using linear material properties and the material's yield strength.

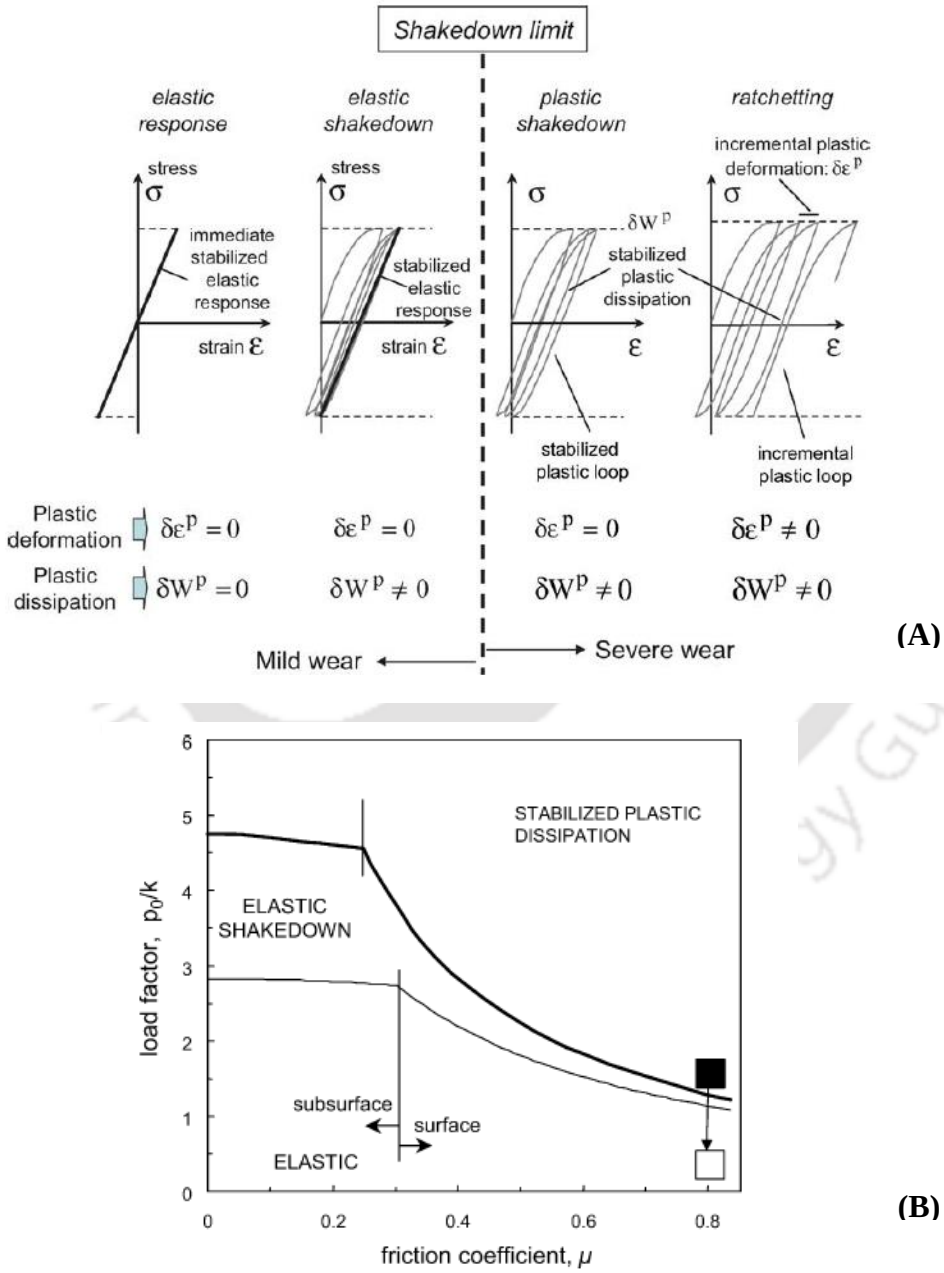

Figure 61: Response of elastoplastic structure to cyclic loading (A) and shakedown chart under repeated sliding condition (B) (Reprinted with permission from [148])

Thus, it indicates that the different elasto-plastic regimes are the combined function of the load factor and the COF. The resultant high load factor values (as shown in Table 15) indicate that the resultant stress-strain condition at the critical location is of the kind of 'stabilized plastic dissipation' for all the test cases. Therefore, to evaluate the suitable material non-linear model, 2D FEA model is solved with three different material non-linear models available in ANSYS and subsequent results are discussed in the next section.

Table 15: Load factor results for 15 test cases (using elastic material properties)

Test Number	Normal Load 'P' (kN)	Axial force in terms of bulk stress 'σ_{Bulk}' (MPa)	Maximum Contact Pressure (MPa)	Yield Strength of Al7075-T6 (MPa)	Load Factor
1	2	110	842.2		1.67
2	4	110	1828.5		3.64
3	8	110	1749.5		3.48
4	2	130	1031.1		2.05
5	4	130	1941.6		3.86
6	8	130	2734.4		5.44
7	2	150	1025.7		2.04
8	4	150	2046.7	503	4.07
9	8	150	3000.2		5.96
10	2	170	1006.6		2.00
11	4	170	2161.5		4.30
12	8	170	3184.1		6.33
13	2	190	974.5		1.94
14	4	190	1616.3		3.21
15	8	190	3344.6		6.54

3.1.1. Resultant Stress-Strain Stabilization with Different Non-Linear Material Models

To check the stress-strain stabilization for the considered problem, the following three material models from ANSYS are explored within the scope of current work.

- Bilinear kinematic hardening model (BKIN) [149]: The salient features of this model are as below.
  - Linear kinematic hardening model i.e., yield surface translates as a rigid body during plastic flow, as shown in Figure 62.
  - Bauschinger effect is considered.
  - Can be considered for cyclic loading condition. However, it is recommended for the situations with the relatively low true strain levels (< 5-10%).
  - As it considers only one plastic slope, it cannot be considered in cases with strain hardening (most of the metals).

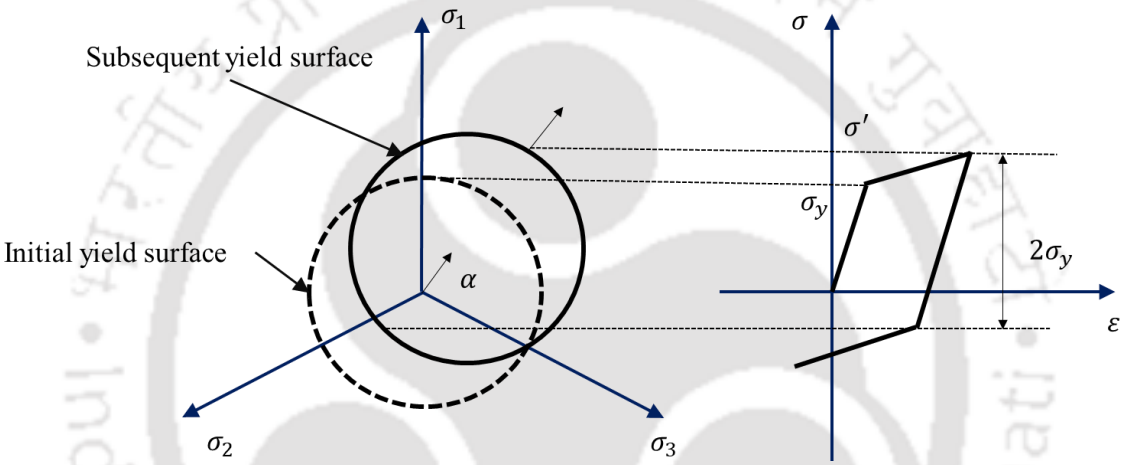

Figure 62: Bilinear Kinematic Hardening model (BKIN)

- Multilinear kinematic hardening model (MKIN) [149]: The salient features of this model are as below.
  - Multilinear kinematic hardening model differs primarily with respect to the BKIN model, as it characterizes multilinear behavior of elasto-perfectly plastic 'sub-volumes', each of which yields at different points.

- Nonlinear kinematic hardening model of Chaboche [149]: The salient features of this model are as below.
  - Nonlinear kinematic hardening model is similar to the multilinear kinematic hardening except for the fact that it does not have the linear relationship between hardening and plastic strain.

- Also, unlike linear kinematic hardening, it has the limiting yield surface and the translation of the yield surface in principal stress space is limited within a specific region (see Figure 63).
- Considers the 'Bauschinger effect' and hence, is suitable for cyclic loading. Also suitable for the large strain (i.e., true strain > 10%)
- Can model ratchetting and shakedown phenomenon (refer to Figure 61). Under ratchetting phenomenon, there is progressive increase in strain per each cycle whereas under shakedown phenomenon, there is progressive stabilization of strain per cycle.

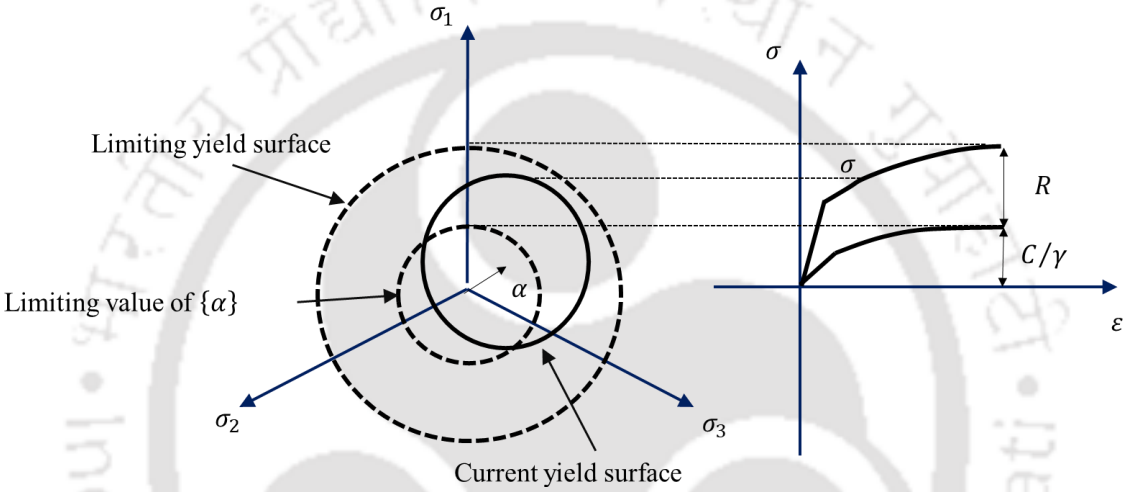

Figure 63: Nonlinear Kinematic Hardening model

In the present work, the 2D FEA model, is solved for the BKIN, MKIN and Chaboche material models. Corresponding material properties are earlier given in Table 7. In order to obtain the stabilized stress-strain condition, FEA is carried out for 80 load steps, which correspond to repetition on 20 duty cycle blocks, as shown in Table 9. Resultant normal stress, strain values for the critical node, as obtained for the test#10, 11 and 12, at the end of duty block#1,10 and 20 are given in the Figure 64 . The results for the remaining tests look similar to these results and hence, are not given here. As seen in Figure 64, for the test#10, comparable stress-strain results are observed for all three material models i.e., BKIN, MKIN and Chaboche. Also, the stress-strain condition does not vary significantly between the duty block# 10 and 20 i.e., stress-strain stabilization is achieved quite early during the duty cycle. However, for test#11 and 12, as the applied reversible axial load value is increased, the three material models predict different stress-strain values. Also, the resultant strain results keep changing as the FEA is progressed from the duty block#10

to duty block#20. The observed stress-strain condition in test#11 and 12, appears to be similar to the shakedown condition, as it shows gradual strain stabilization across the duty cycles. In addition, the normal strain values are around 12-14% for which the Chaboche material model appears to be the more suitable material model than BKIN and MKIN. To further validate this observation from the fretting fatigue results perspective, fatigue life results are predicted using the resultant stress-strain values obtained using BKIN, MKIN and Chaboche material models. To carry out the comparative assessment, between these three material models, fatigue life results are evaluated for duty block#1 (i.e., reversal between load step#2 and load step#4), duty block#10 (i.e., reversal between load step#38 and load step#40) and duty block#20 (i.e., reversal between load step#78 and load step#80) using the SWT (surface) method and subsequent results are given in Figure 65. As the objective here, is to obtain the resultant number of load repetitions to be considered while solving FEA for all the 15 test-cases for the considered three non-linear material models, SWT (surface) method is considered for this comparative study. Resultant average and deviation values obtained for different set of results are given in Table 16 with the same details as shown in Figure 65. As observed from this study, for the three material models, the resultant deviation and average values tend to get stabilized after the 20^{th} duty block and almost similar levels of deviation and average values are observed for BKIN, MKIN and Chaboche material models.

Considering this observation, fretting fatigue life results are obtained for the 20^{th} duty block, between the load step#78 and load step#80, for SWT, FS and eI parameters using the area stress-strain averaging method. The obtained fretting fatigue life results are shown in Figure 66–68 and the corresponding results are summarized in Table 17. As observed, similar results are observed for three considered material models. It can be seen from the Figure 64 that at the end of 20^{th} duty block, alternating normal strain range and associated normal stress values are almost similar for the three different material models. Consequently, the calculated fatigue life results are also observed to be comparable with the considered three material non-linear models.

3.2. Effect of Coefficient of Friction (COF) on Fretting Fatigue Life Results

The COF which represents the surface condition at the contact surfaces, is another critical parameter towards the fretting fatigue results. At higher coefficient of friction, surface

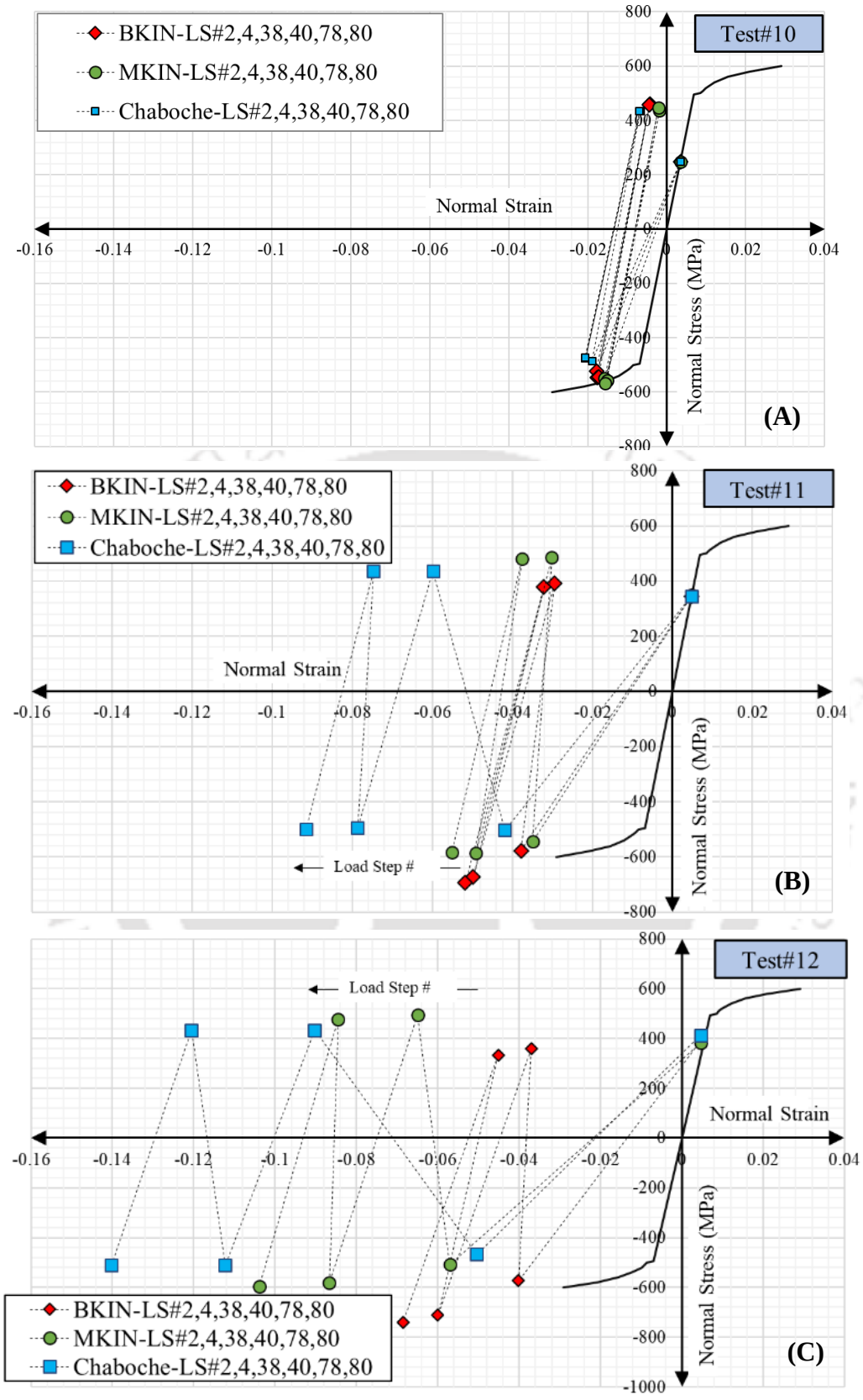

Figure 64: Resultant normal stress (σ_x) - normal strain (ε_x) results at the critical node using BKIN, MKIN and Chaboche material models for Test#10 (A), Test#11 (B) and Test#12 (C)

stress singularity tends to increase. Hence, number of fatigue cycles will reduce with the higher COF. The value of COF keeps on evolving based on the subsequent contact surface condition [29]. In FEA, effect of varying COF with respect to temperature, time, normal pressure and sliding distance/sliding relative velocity can be considered [150]. Earlier a constant value of COF of 0.8 is considered, assuming the stabilized contact condition [58]. In the current work, in order to verify the effect of varying COF onto the fretting fatigue life results, COF's variation with respect to the sliding distance is considered, and corresponding results are discussed in this section.

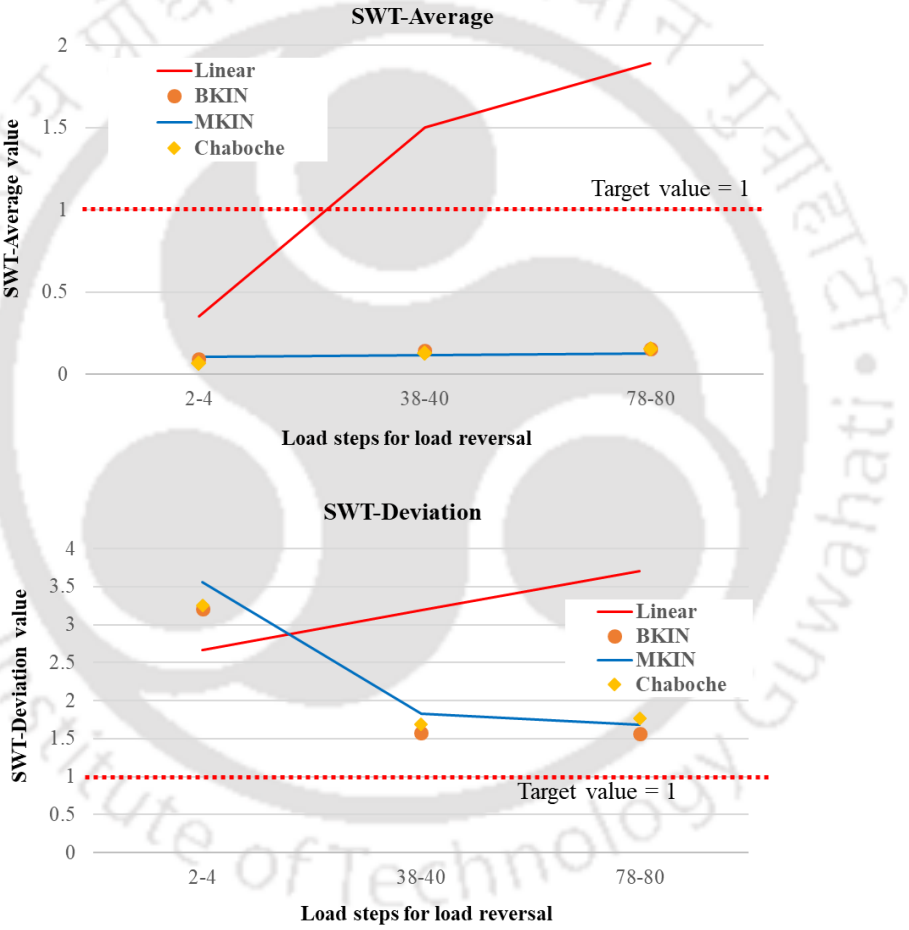

Figure 65: Resultant average and deviation results with SWT parameter for the considered material models

Resultant COF's variation with respect to the sliding distance amplitude is as shown in Figure 69. Here, the experimentally obtained data for AL357 [148] is considered to predict the similar data for AL7075-T6, by parallelly off-setting the data-line of AL357 to go through the maximum COF data-point of 0.8 for AL7075-T6. Ideally, similar to the

AL357, COF data needs to be experimentally obtained for AL7075-T6. However, in absence of the experimental data, similar contact surface evolution is assumed between the two aluminum alloys i.e., AL357 and AL7075-T6.

Table 16: Resultant average and deviation results obtained using BKIN, MKIN and Chaboche material models for the considered load reversals with SWT (surface) method

Material Model	Load reversal between					
	LS#2-4		LS#38-40		LS#78-40	
	Average	Deviation	Average	Deviation	Average	Deviation
Linear	0.35	2.67	1.5	3.19	1.89	3.71
BKIN	0.093	3.21	0.14	1.58	**0.15**	**1.57**
MKIN	0.11	3.56	0.12	1.82	**0.16**	**1.67**
Chaboche	0.07	3.25	0.13	1.68	**0.16**	**1.76**

Table 17: Resultant average and deviation results obtained using BKIN, MKIN and Chaboche material models for SWT, FS and eI FIP's with area stress averaging

Fatigue Initiation Parameter	Stress Averaging Method	BKIN		MKIN		Chaboche	
		Average	Deviation	Average	Deviation	Average	Deviation
FS	Area	2.37	2.41	2.56	2.36	2.35	2.15
SWT		1.63	2.40	1.76	2.51	1.53	2.29
eI		1.87	2.19	1.95	2.21	2.00	1.99

Next, the effect of varying COF with respect to the sliding distance is considered in ANSYS using the APDL commands. Next, FEA is carried out for the considered 15 test-cases. The corresponding fatigue life results obtained for the 15 test cases with constant COF and varying COF are shown in Figure 70–72 for three different material models. As observed, except for Test#1, Test#4, Test#7, Test#10 and Test#13, for the remaining test cases, almost no difference is observed in the fretting fatigue life results with the constant COF value of 0.8 and with the varying COF.

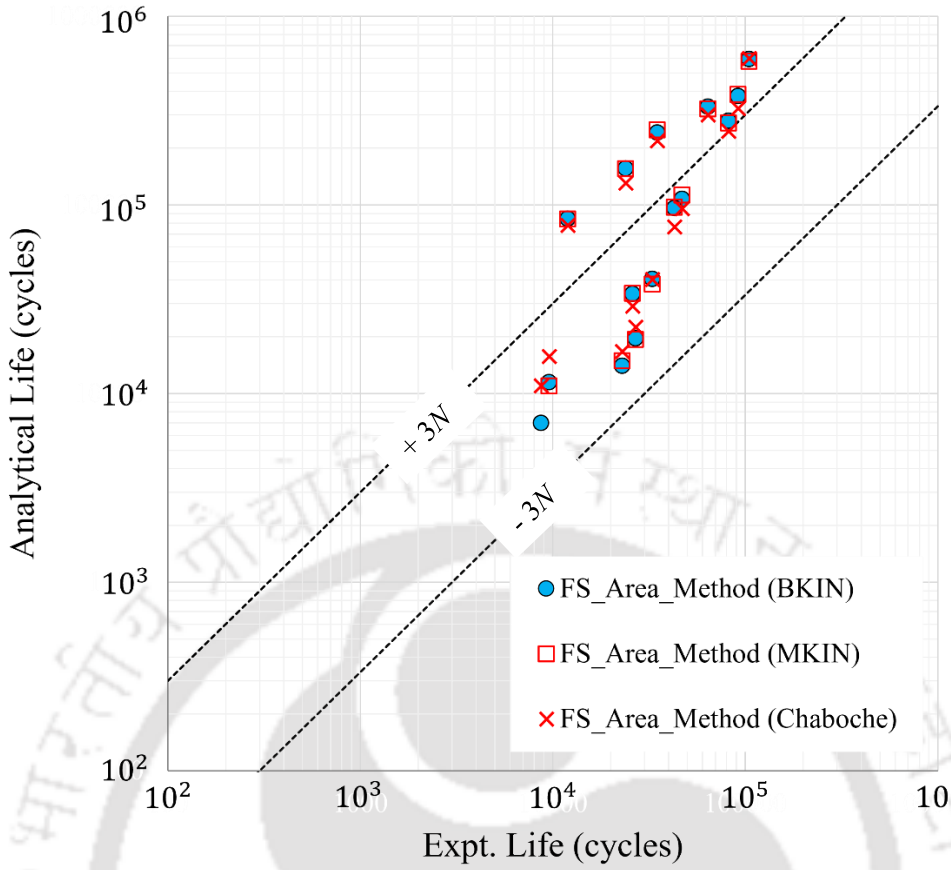

Figure 66: Experimental correlation for reference fretting fatigue problem using FS (area) method for three different material models with constant COF

It is primarily because, comparatively higher sliding distance is observed for test#1, 4, 7, 10 and 13, as shown in the Figure 73. For these four test cases i.e., test#1, 4, 7, 10 and 13, the normal contact force value is minimum i.e., 2kN (see Table 6). Thus, with the increasing axial force, relative sliding between the contact specimens also increases which will result in reduced COF and the subsequent decrease in the surface stress singularity. Consequently, resultant increase in the fretting fatigue life results is observed with varying COF for these test cases. Corresponding experimental correlation for the fretting fatigue life results obtained with the varying COF is shown in Figure 74 for three different material models and subsequent tabular summary is given in Table 18. These results are with area stress averaging method.

Though, after consideration of varying COF, the experiment correlation is marginally reduced as compared to the constant COF, the effect of the variation of the sliding distance on the resultant fretting fatigue life results can be captured. Hence, this observation indicates that it is critical to consider the possible variations in COF based on

the applied loads and should be considered during the scope of fretting fatigue life evaluation. Further, different relative sliding distance values can possibly cause different fretting wear damage to the associated geometries. Hence, in the following section, effect of resultant wear on the fretting fatigue life results is discussed.

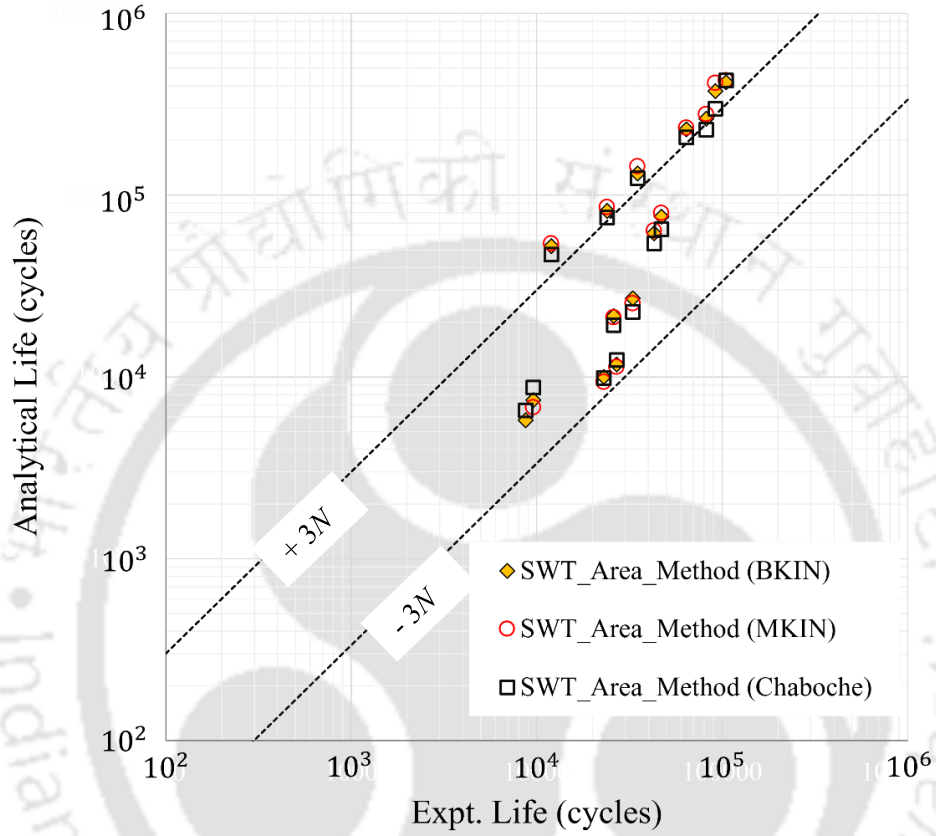

Figure 67: Experimental correlation for reference fretting fatigue problem using SWT (area) method for three different material models with constant COF

3.3. Effect of Wear Due to Relative Sliding

So far, the critical evaluation of the stress-strain history towards the crack initiation life prediction is carried out. Along with this, another important parameter which affects the growth of the initial embryonic crack, is the magnitude of relative sliding displacement between the two contacting bodies. Fretting contact differs from the sliding contact; as in fretting, the applied tangential forces cause only local microscale relative motion and not the global relative motion of the contact surface [47]. According to the fretting map (as shown in Figure 16), fatigue life initially decreases till certain threshold relative sliding displacement value, and it again increases. With an initial increase in the subsurface shear

stresses corresponding to the increasing relative sliding displacement, small embryonic cracks start initiating. When the relative sliding displacement value reaches the threshold limit value, the generated embryonic crack/s get/s ground away and hence, do not propagate further.

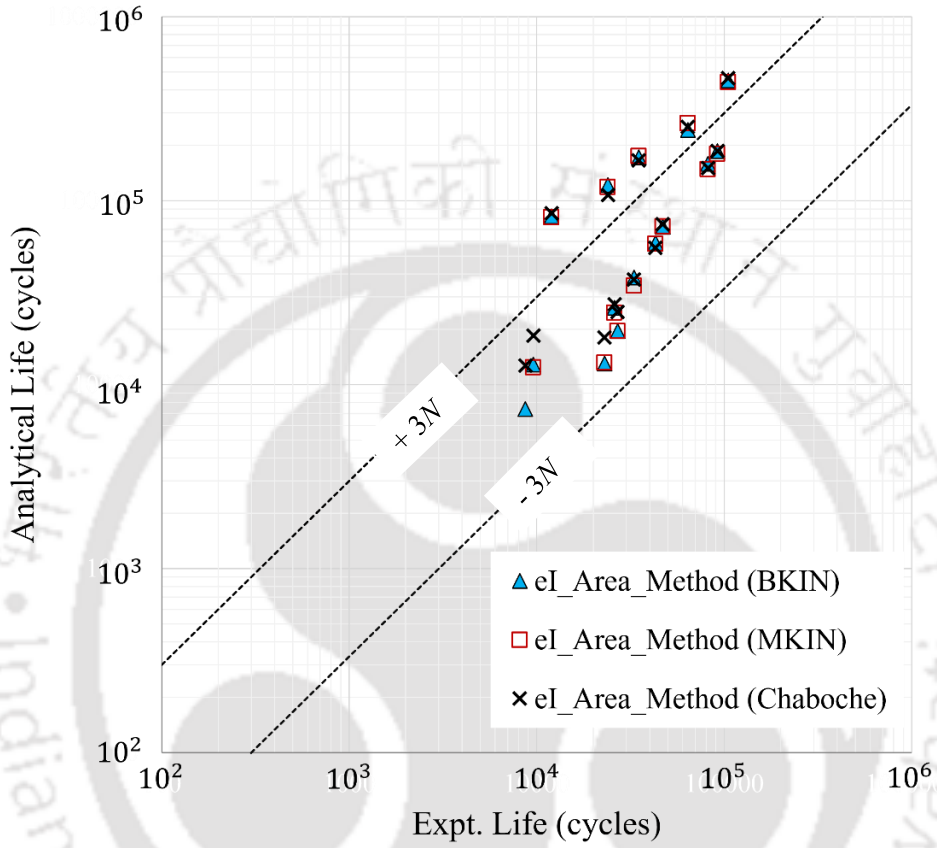

Figure 68: Experimental correlation for reference fretting fatigue problem using eI (area) method for three different material models with constant COF

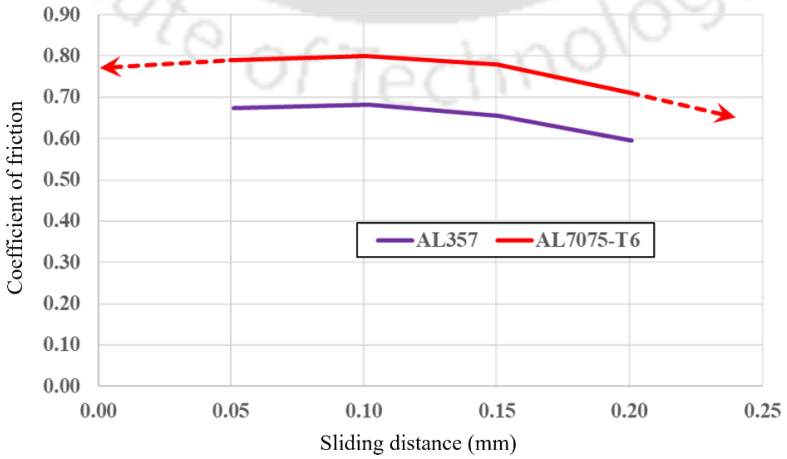

Figure 69: Extrapolated COF data for AL7075-T6

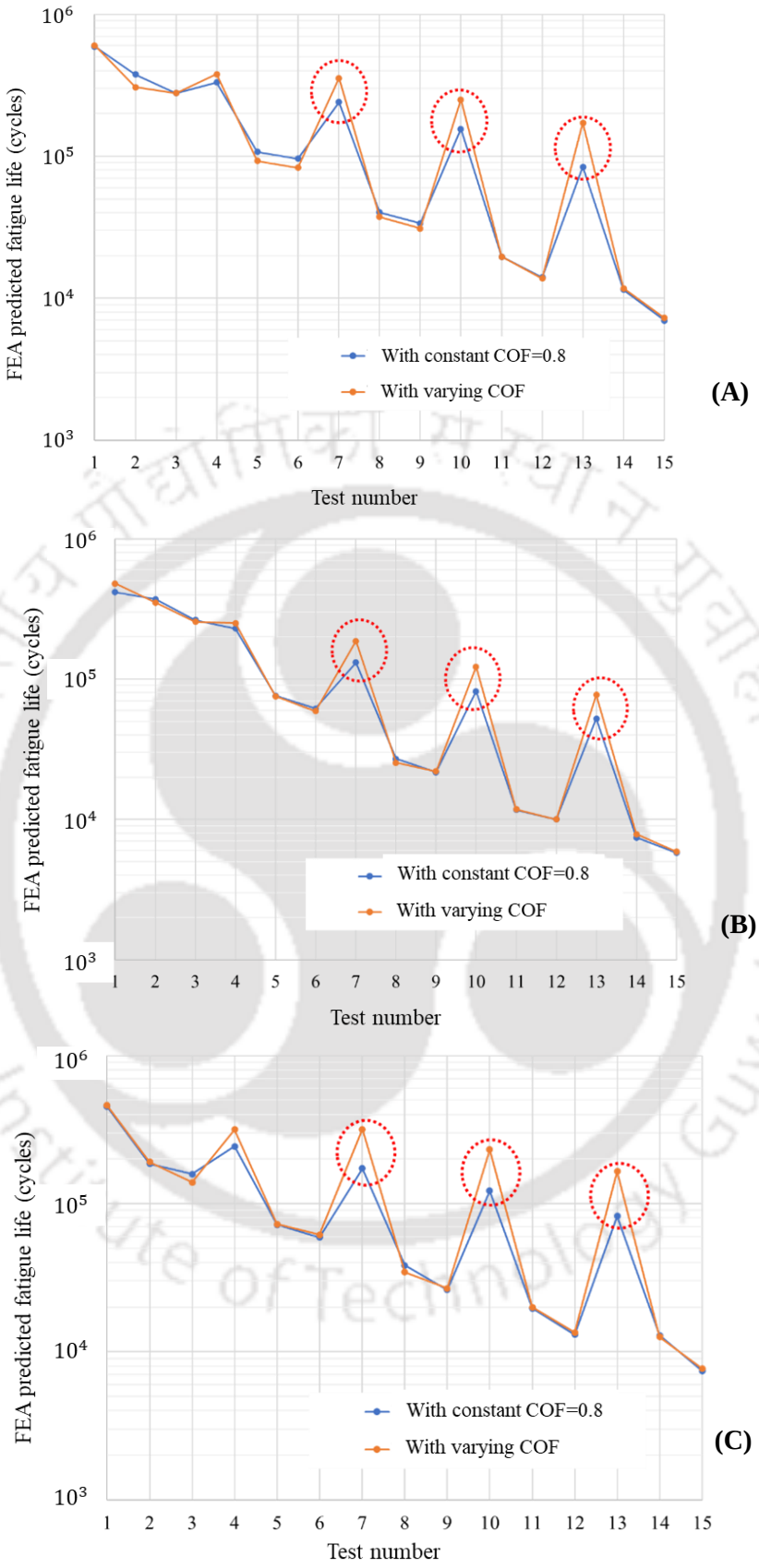

Figure 70: Effect of varying COF on fretting fatigue life results with FS (area) method (A), SWT (area) method (B) and eI (area) method (C) for BKIN material model

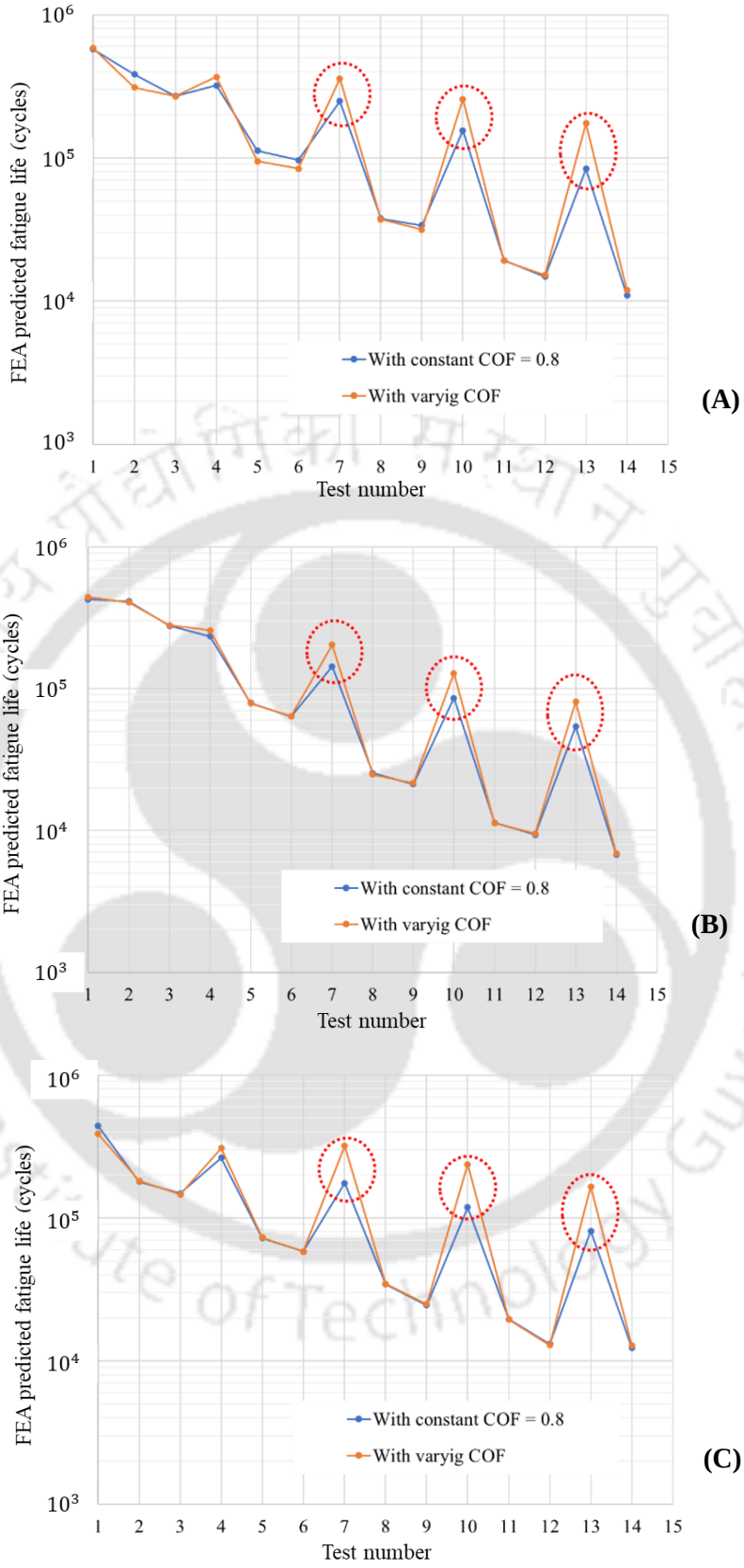

Figure 71: Effect of varying COF on fretting fatigue life results with FS (area) method (A), SWT (area) method (B) and eI (area) method (C) for MKIN material model

Beyond the threshold sliding displacement value, the fretting wear becomes the more dominant damaging mode. Hence, the effect of relative slip magnitude on the fretting fatigue is an important parameter and needs to be studied. To evaluate the effect of relative sliding displacement on fretting fatigue, Archard's wear model [32] and Ding's D_{fret2} parameter-based approach [102] are considered during the scope of current work. Archard's model is based on the actual 'incremental wear modeling' during the FEA solution whereas Ding et. al. [102] proposed a correction factor equivalent to the resultant frictional energy which is further applied to the fatigue initiation parameter (FIP) and then resultant crack initiation life is evaluated. Different constants in Ding's D_{fret2} parameter need to be obtained through the fretting wear and fretting test data and are material constants and thus, independent of geometry and loading conditions [52].

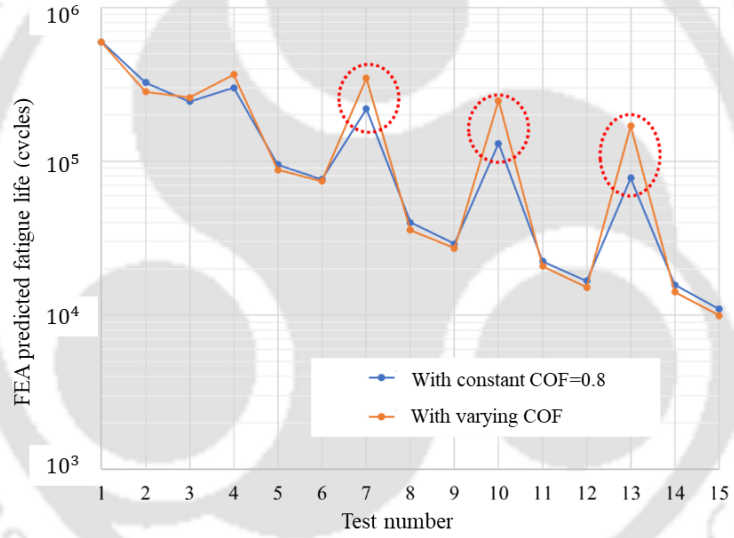

(A)

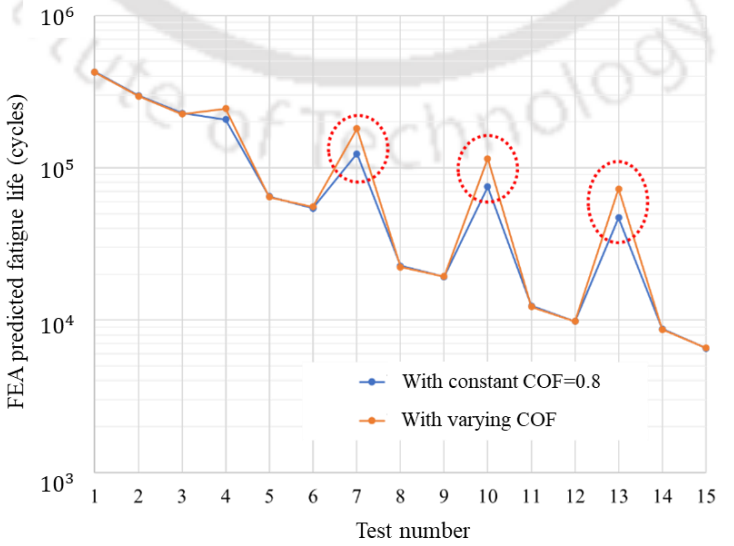

(B)

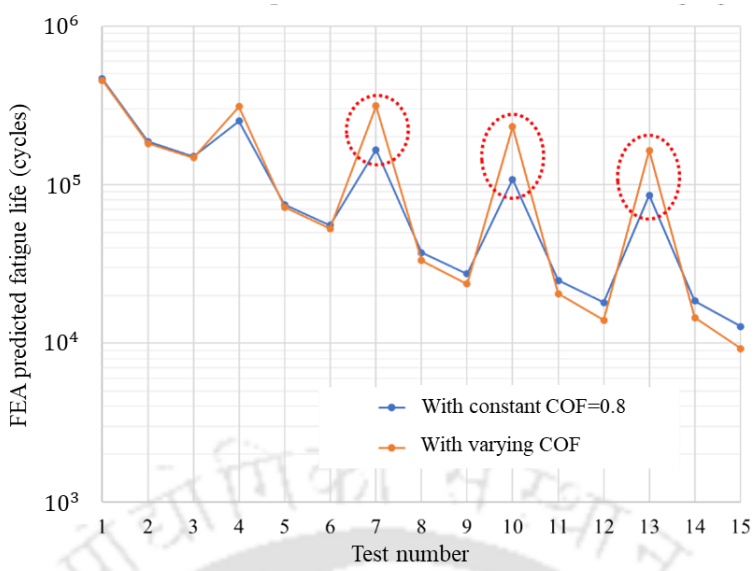

Figure 72: Effect of varying COF on fretting fatigue life results with FS (area) method (A), SWT (area) method (B) and eI (area) method (C) for Chaboche material model

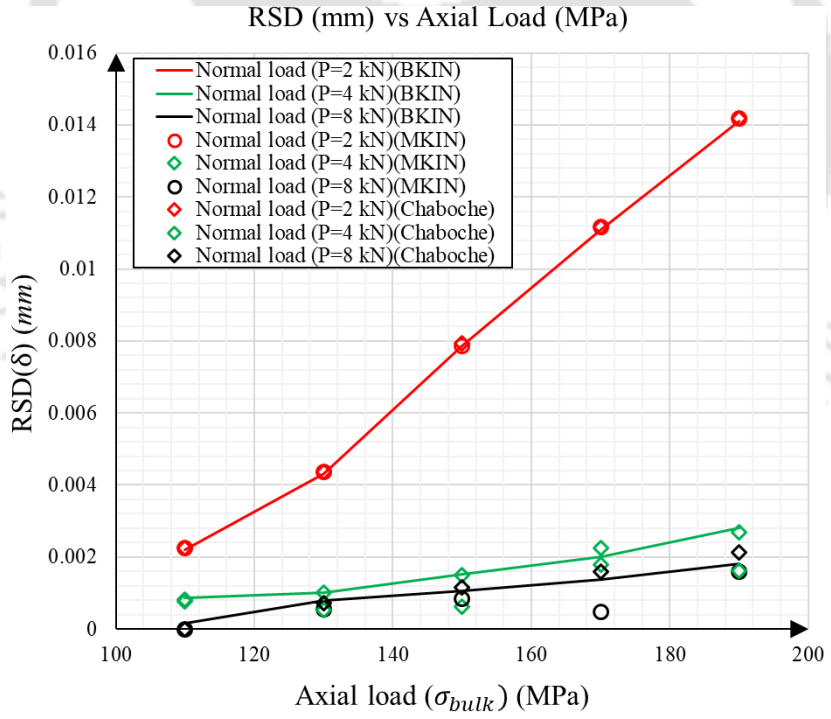

Figure 73: Sliding distance vs Axial load

Compared to the progressive wear modeling approach like Archard's wear model, Ding's approach is computationally more efficient, as it does not require to model the progressive wear while solving the FEA model.

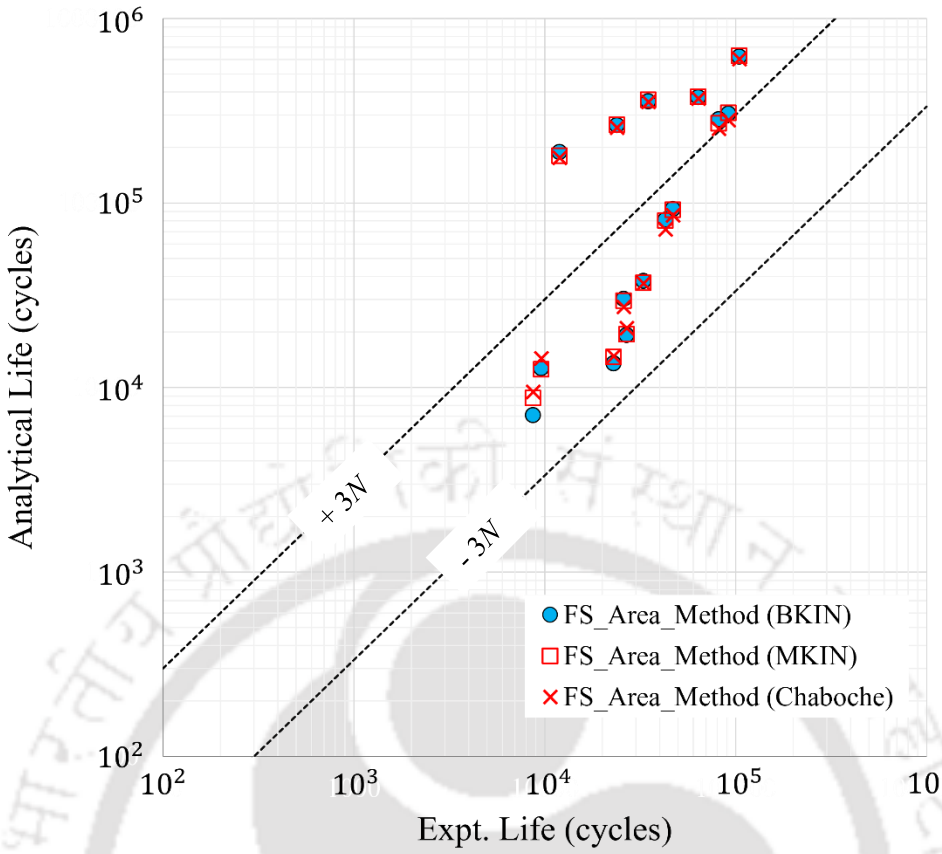
Analytical Life (cycles)
Expt. Life (cycles)
+ 3N
- 3N
FS_Area_Method (BKIN)
FS_Area_Method (MKIN)
FS_Area_Method (Chaboche)

(A)

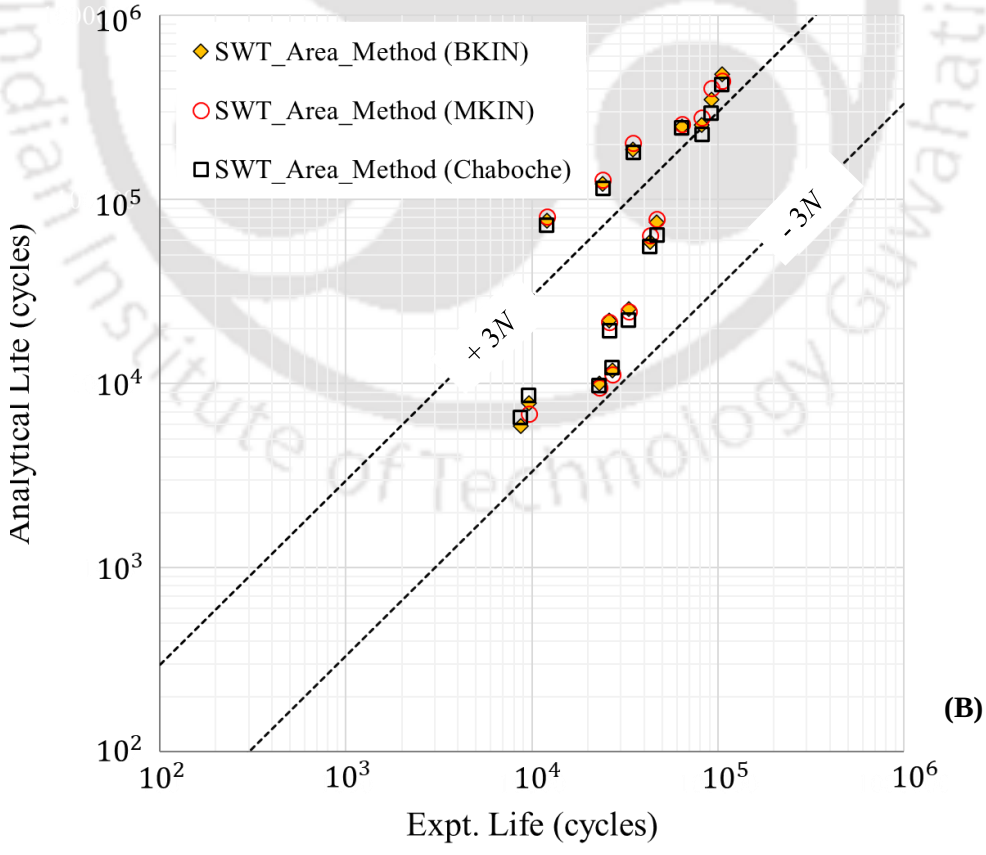
Analytical Lite (cycles)
Expt. Life (cycles)
+ 3N
- 3N
SWT_Area_Method (BKIN)
SWT_Area_Method (MKIN)
SWT_Area_Method (Chaboche)

(B)

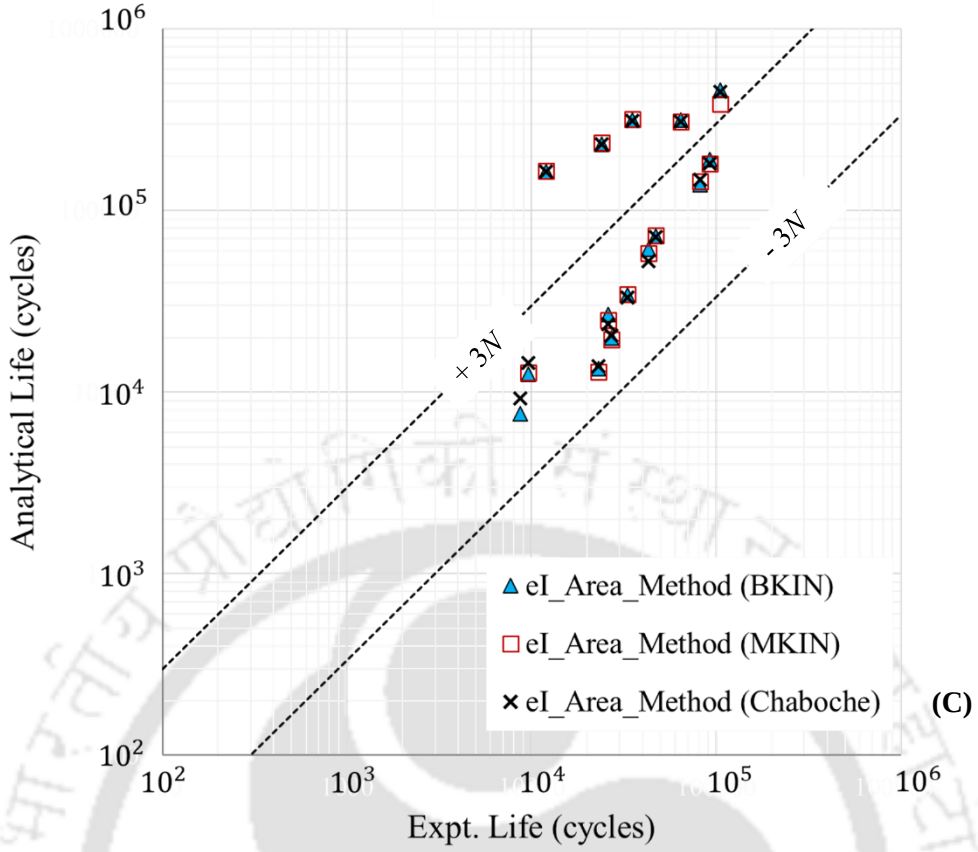

Figure 74: Experimental correlation for BKIN (A), MKIN (B) and Chaboche (C) with area stress-averaging technique with varying COF

Table 18: Resultant correlation results obtained using varying COF for BKIN, MKIN and Chaboche material models with SWT, FS and eI FIP's with area stress averaging

Fatigue Initiation Parameter	Stress Averaging Method	BKIN		MKIN		Chaboche	
		Average	Deviation	Average	Deviation	Average	Deviation
FS	Area	2.56	2.84	2.80	2.78	2.58	2.73
SWT		1.78	2.64	1.93	2.80	1.68	2.56
eI		2.17	2.74	2.26	2.84	2.17	2.71

3.3.1. Effect of Wear using Archard's Model

When two surfaces are in contact and sliding with respect to each other, particle detachment i.e., 'wear', can be observed at one or both the surfaces. This phenomenon is incremental in nature and causes continuous surface degradation. The classical Archard's

wear equation [32], is basically based on the theory of asperity contact [151] and is given as

$$\frac{V}{\delta} = K\frac{N}{H} \tag{41}$$

where V is the wear volume, δ is the sliding distance, K is the dimensionless wear coefficient, which is generally obtained experimentally and is dependent upon the specific metal pair, N is the normal applied load, H is the hardness of the softer material in the contact pair.

Here, the quantity *K/H* i.e., dimensional wear coefficient, is dependent upon the load and stroke [152]. Archard's wear model equation is available in ANSYS through a subroutine [153] and it predicts the resultant wear rate as

$$\frac{dW}{dt} = K\frac{P^{m'}\dot{D}^{n^*}}{H} \tag{42}$$

where W is the wear depth, P is the contact pressure, $\dot{D}$ is the sliding velocity, H is the hardness of the softer material in the contact pair, m' is the contact pressure exponent, n^* is the sliding velocity exponent.

In the present work, rate of wear is assumed to be linearly proportional to the contact pressure and contact sliding distances. Considered values for parameters like K, H are shown in Table 7. FEA solution process involves progressive wear depth calculation, and it continues till the equilibrium conditions are met. The contact nodes are moved corresponding to the predicted wear increment after each substep, and the process continues till all the substeps get converged (see Figure 75). This simulation process is computationally more expensive, because in addition to the equilibrium iterations required for force and displacement convergence, additional equilibrium iterations are required to predict the wear increment per substep. Also, per substep, mesh refinement happens to account for the corresponding geometry change in contacting bodies.

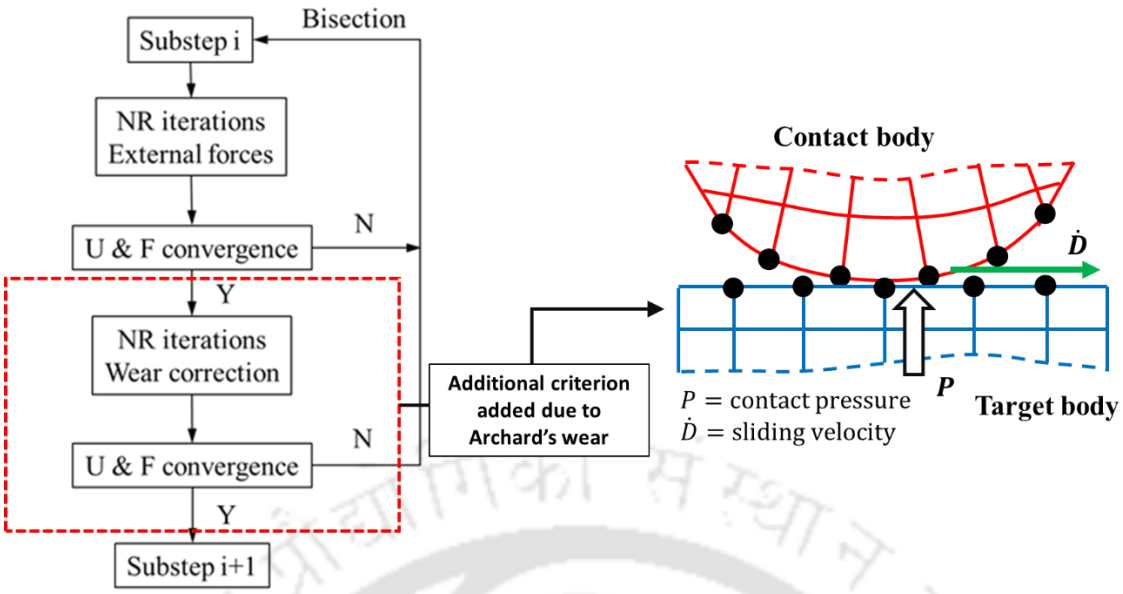

Figure 75: ANSYS solver process considered in Archard's progressive wear calculation (Reproduced based on [153])

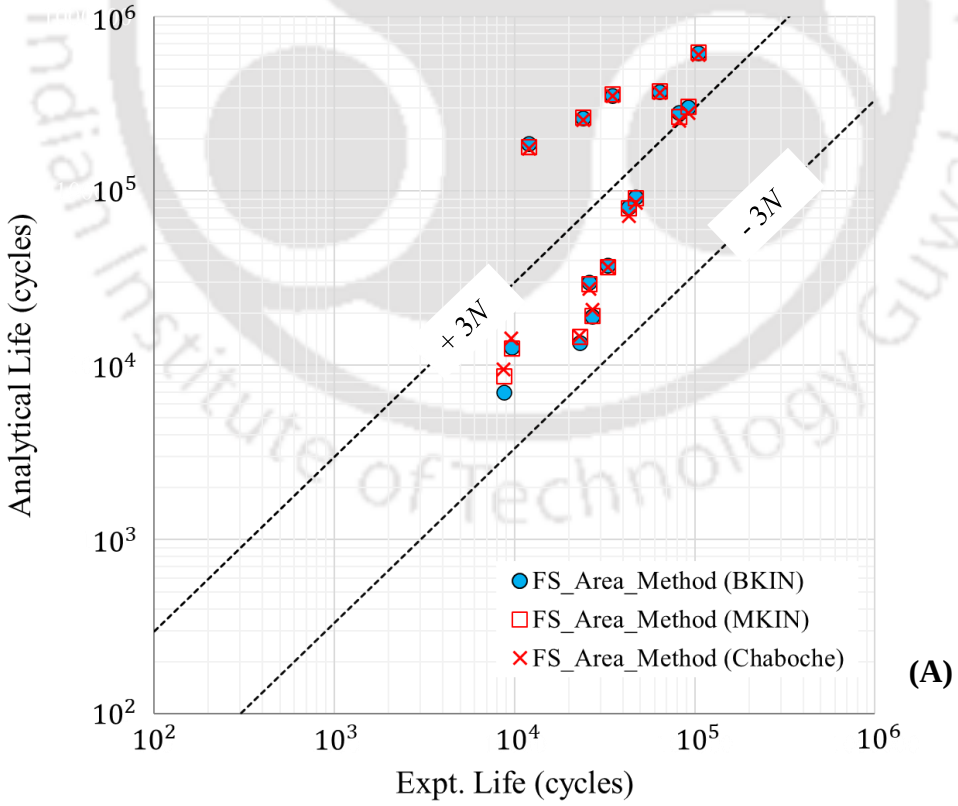

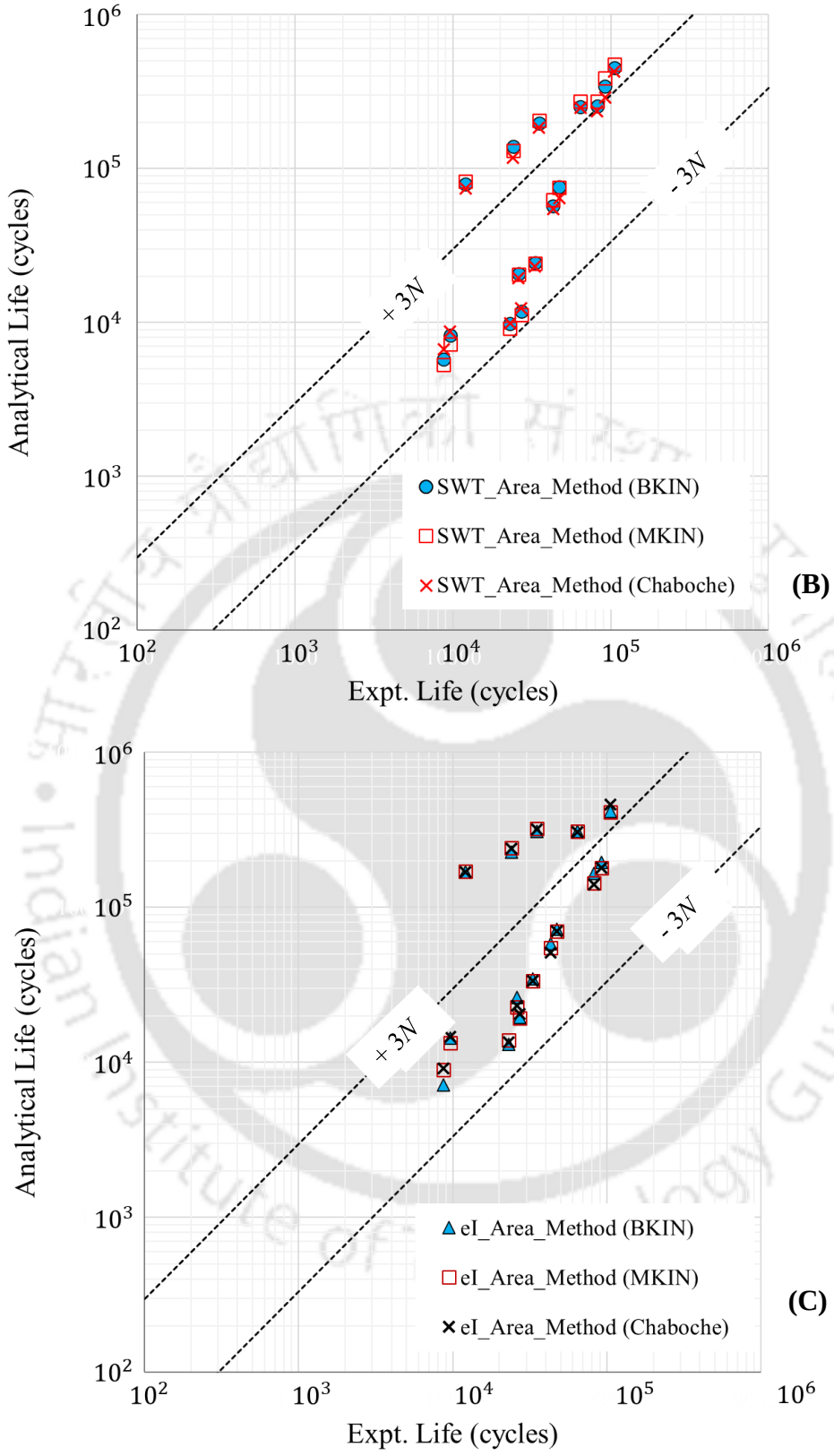

Figure 76: Experimental correlation for BKIN (A), MKIN (B) and Chaboche (C) with area stress averaging technique, with varying COF and with Archard's wear correction

Consequently, as a result, the solution time increases with such progressive wear modeling approach.

In the present work the FEA model is solved considering the Archard's subroutine. Resultant stress-strain results are post-processed for SWT, FS and SI methods. The resultant experimental correlation results obtained with Archard's wear correction are given in Figure 76. The fretting fatigue life results obtained using the Archard's wear model are observed to be quite identical to the fatigue life results obtained without considering any wear correction. Hence, the Archard's wear model does not contribute towards any improvement in the experimental correlation. Further it is mentioned that Archard's wear model is generally suitable to predict the wear calculation in the gross slip regime [5].

Table 19: Contact regime at corner node for 15 test cases

Test #	Frictional Stress (MPa) (Q)	Contact Pressure (MPa) (P)	Limiting Frictional Stress limit (μP)	Resultant contact regime
1	486.94	618.30	494.64	Partial slip
2	430.13	550.38	440.32	Partial slip
3	546.13	1324.71	1059.77	Partial slip
4	761.10	956.40	765.13	Partial slip
5	453.88	578.56	462.85	Partial slip
6	606.86	841.21	672.97	Partial slip
7	629.89	791.09	632.87	Partial slip
8	474.16	601.83	481.47	Partial slip
9	724.48	931.40	745.12	Partial slip
10	556.43	709.38	567.50	Partial slip
11	493.65	624.14	499.36	Partial slip
12	781.46	1003.26	802.60	Partial slip
13	488.59	650.29	520.23	Partial slip
14	937.49	1205.09	964.07	Partial slip
15	831.84	1066.24	852.99	Partial slip

As given in Table 19, for all 15 test-cases, corresponding frictional stress at the critical node is lesser than the limiting frictional stress limit and hence, the resultant contact regime is of the 'Partial slip/stick-slip' type. In the partial slip regime, with low dynamic COF, Archard's wear model generally leads towards predicting very small wear [154]. Further, it is also mentioned that in the partial slip regime, with the single coefficient K for different load-stroke combinations, Archard's model has limitations towards wear predictions and for different slip regimes, different K values should be considered [152].

Thus, with these above-mentioned limitations against Archard's model, predicted fretting fatigue life results do not change much compared to without Archard's model consideration. Further, as see in Figure 77, for test#15, predicted wear depth with Archard's wear model, is very low i.e., 0.0035 μm, indicating no significant loss of material and corresponding negligible effect onto the fretting fatigue life results also. Further, with the Archard's wear model, additional equilibrium iterations are also required. Hence, with no noticeable difference observed in predicted fretting fatigue life results by considering Archard's wear model (as seen in Figure 76 and Table 18), next approach to be investigated is the Ding's D_{fret2} parameter.

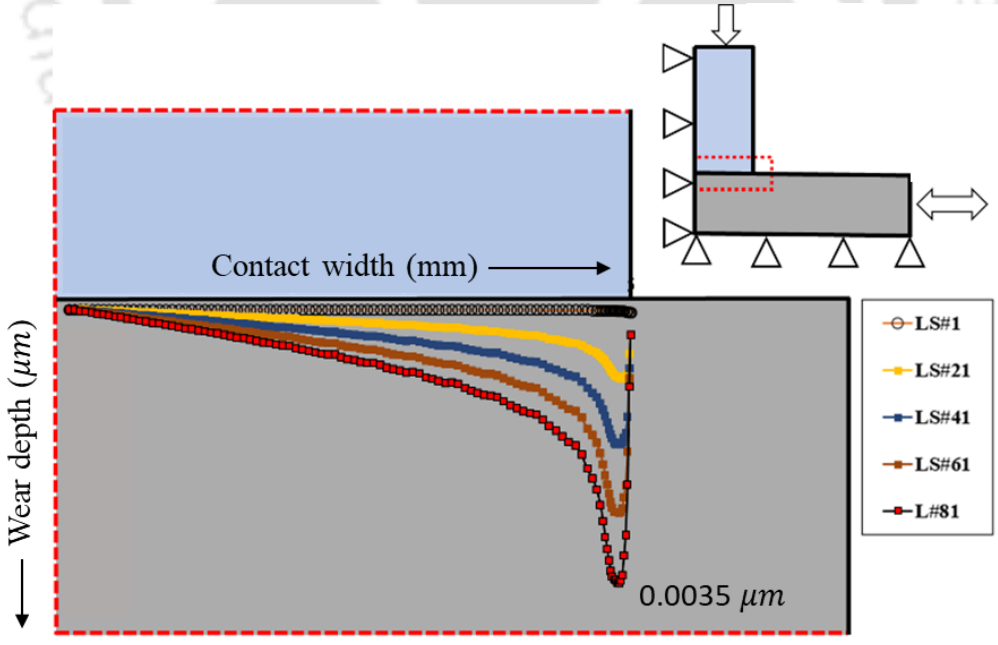

Figure 77: Predicted wear depth for test#15 with Archard's wear model

Table 20: Resultant correlation results using varying COF and with Archard's wear model for BKIN, MKIN and Chaboche material models with area stress averaging

Fatigue Initiation Parameter	Stress Averaging Method	BKIN		MKIN		Chaboche	
		Average	Deviation	Average	Deviation	Average	Deviation
FS	Area	2.58	2.90	2.79	2.84	2.57	2.76
SWT		1.78	2.69	1.79	2.81	1.70	2.56
eI		2.17	2.74	2.14	2.76	2.16	2.75

3.3.2. Effect of Slip using Fretting Specific Parameter of Ding's Parameter (D_{fret2})

In the Archard's wear modeling technique, effect of wear is predicted using the incremental/progressive wear modeling technique. The appropriate subroutines for the gradual evolution of the contact surface profile is considered while solving such problem in ANSYS. However, due to the additional equilibrium iterations required to account for the incremental wear calculations during each solution sub-step, this approach can be computationally expensive approach. Another method to consider the effect of wear on the fretting fatigue is by considering the threshold slip magnitude. Fretting fatigue life initially decreases with the increase in slip magnitude till certain threshold limit. Beyond this limit value, slip magnitude does not have any detrimental effect onto fretting fatigue. Accordingly, the effect of slip magnitude onto fretting fatigue results can be considered, as shown earlier in the Figure 33. It should be noted here that beyond the threshold limit value, fatigue life calculations are decoupled from the effect of slip magnitude. This approach has been proposed by Ding et. al [102]. This approach is computationally more efficient than the incremental wear modelling approach like Archard's method, because in this approach the change in contact surface shape profile is not modelled and additional equilibrium iterations and additional imposed solution convergence criterion are not required here.

Ding's D_{fret2} parameter [102], as given in the Equation 29, accounts for the detrimental effect of increasing sliding distance on fretting fatigue life, till the relative sliding reaches the threshold sliding limit value. Ding et al. [102] have mentioned that this parameter is valid only for the condition $\delta \leq \delta_{th}$. For $\delta > \delta_{th}$, fretting wear becomes more dominant

mode than the fretting fatigue and in that case, this correction factor is not considered in the fretting fatigue life calculations. Ding has applied this correction factor to SWT parameter as

$$\sigma_n^{max}(\Delta\varepsilon_n/2)D_{fret2} = \sigma_f'^2(2N_i)^{2b} + \sigma_f'\varepsilon_f'(2N_i)^{b+c} \quad (43)$$

The factor, D_{fret2} , provides the corrected fatigue life results accounted for the relative slip magnitude, especially till the threshold sliding value, as shown in Figure 78. The values for the parameters like C, n and δ_{th}, are given in Table 7. These constants are obtained for another aluminum alloy (with similar % of aluminum) and are considered here assuming the similar behavior for AL7075-T6. In the similar approach of applying to the SWT parameter, corresponding corrections are applied to FS and eI parameters as

For FS FIP:

$$\Delta\gamma_{max}/2\left(1 + k_2\left(\sigma_n^{max}/\sigma_y\right)\right)D_{fret2} = \tau_f'/G\,(2N_i)^{b'} + \gamma_f'(2N_i)^{c'} \quad (44)$$

For eI FIP:

$$\left(\gamma_{dev} + \frac{k}{G}\,\sigma_{H,max}\right)D_{fret2} = \frac{\tau_f' - \sqrt{J_{2m}}}{G}(2N_i)^b + \gamma_f'(2N_i)^c \quad (45)$$

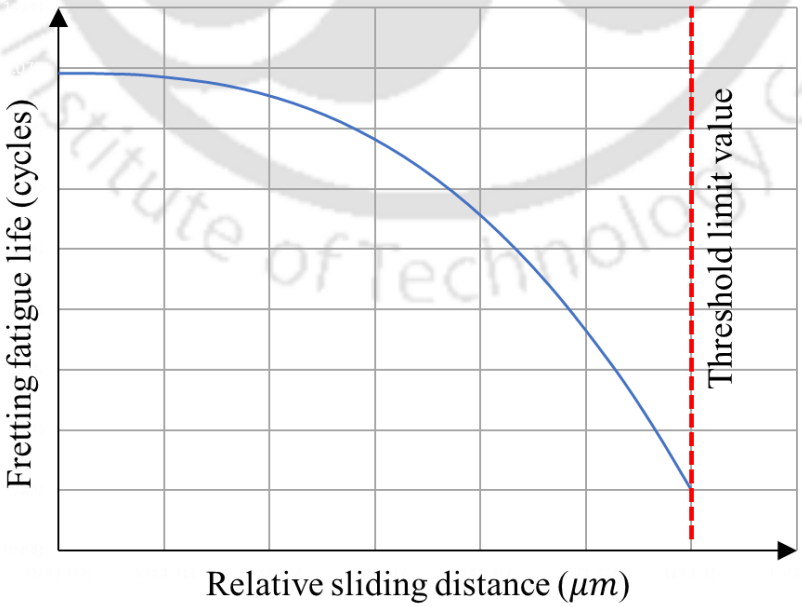

Figure 78: Effect of relative sliding distance till threshold limit value on fretting fatigue life

As mentioned earlier, the parameter, D_{fret2}, is valid only for the condition $\delta \leq \delta_{th}$. For $\delta > \delta_{th}$, fretting wear becomes more dominant mode than the fretting fatigue and in that case, the unmodified FIP parameter equations are considered. The maximum frictional stress and relative sliding distance values between the load cases 78 and 80 are extracted for the most critical node and further resultant values for D_{fret2} parameter are obtained using the Equation 29 for BKIN, MKIN and Chaboche material models.

Table 21: Resultant D_{fret2}values for 15 test cases

Test#	Frictional Stress (MPa)	RSD (μm)	D_{fret2}		
			BKIN	MKIN	Chaboche
1	557.83	2.25	1.09	1.09	1.08
2	1022.29	0.76	1.05	1.06	1.06
3	1008.53	0.00	1.00	1.01	1.00
4	684.40	4.35	1.20	1.2	1.19
5	1021.47	1.02	1.07	1.07	1.04
6	1185.21	0.55	1.05	1.06	1.06
7	576.55	7.87	1.28	1.27	1.25
8	1056.77	0.61	1.05	1.11	1.10
9	1242.55	0.84	1.07	1.08	1.09
10	543.84	11.17	1.32	1.27	1.24
11	1041.44	1.79	1.13	1.14	1.14
12	1284.66	0.48	1.04	1.11	1.12
13	454.66	14.19	1.25	1.24	1.19
14	1005.89	2.68	1.18	1.19	1.09
15	1324.90	1.59	1.15	1.14	1.16

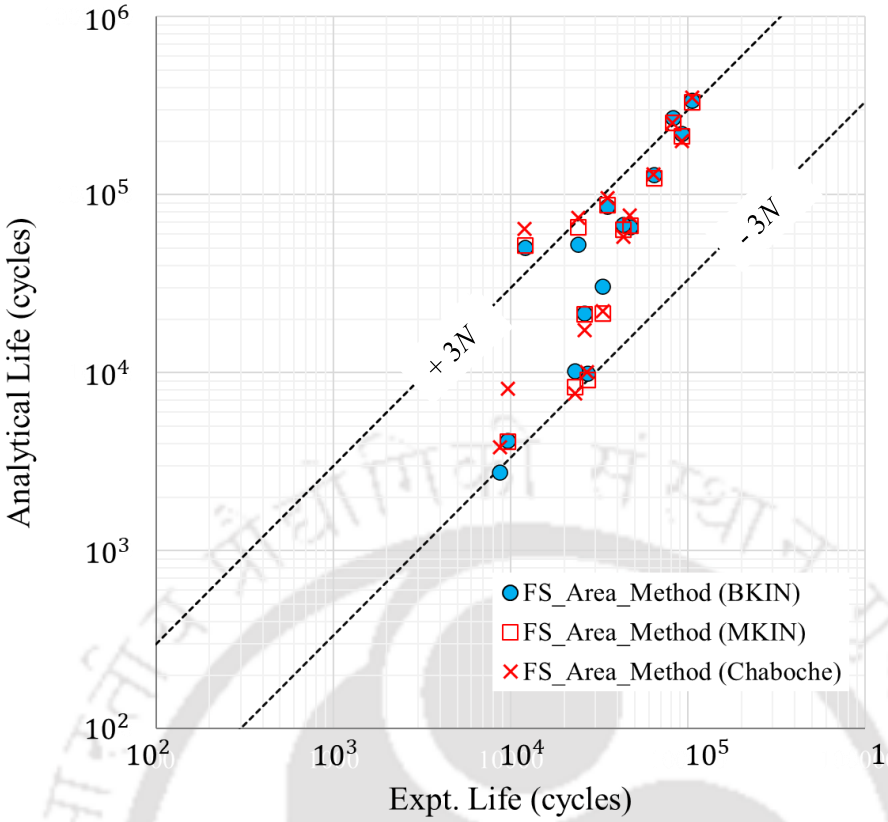
Analytical Life (cycles)
Expt. Life (cycles)
+ 3N
- 3N
FS_Area_Method (BKIN)
FS_Area_Method (MKIN)
FS_Area_Method (Chaboche)

(A)

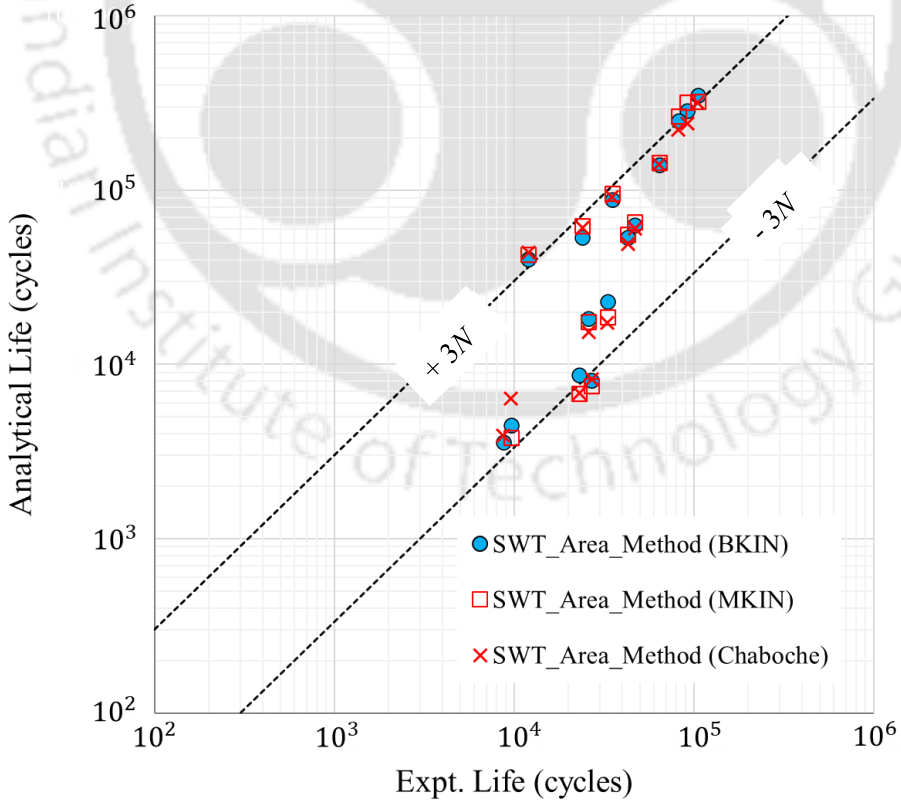
Analytical Life (cycles)
Expt. Life (cycles)
+ 3N
- 3N
SWT_Area_Method (BKIN)
SWT_Area_Method (MKIN)
SWT_Area_Method (Chaboche)

(B)

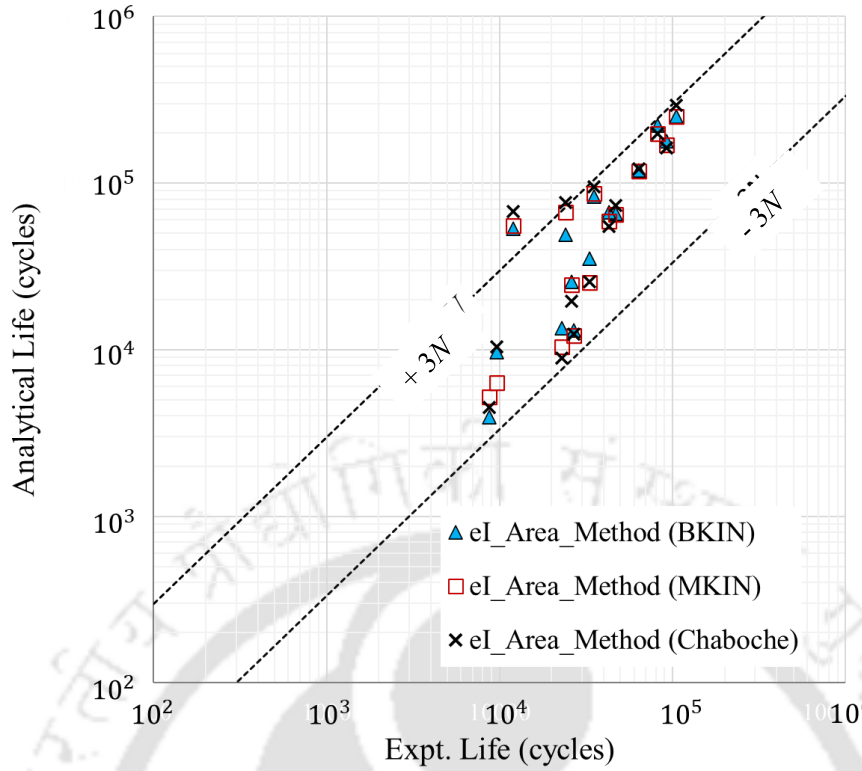

(C)

Figure 79: Experimental correlation for BKIN (A) MKIN (B) and Chaboche (C) with area stress averaging technique and with Ding's parameter

Further, fretting fatigue life results are corrected for the resultant Ding's D_{fret2} parameter values and corresponding experimental correlation is given in the Figure 79. As compared to the earlier fretting fatigue life estimation, better experimental correlation is observed for test#1, 4, 7, 10 and 13 after considering the Ding's D_{fret2} parameter. Thus, overall correlation is observed within $\pm$ 3N scatter band. The improved resultant average and deviation values with Ding's D_{fret2} parameter are given in Table 22 . As mentioned earlier, test#1, 4, 7, 10 and 13 correspond to higher sliding displacement values, which result in the subsequent higher values of D_{fret2} parameter for these tests only and comparatively lower values are observed for the remaining tests. Thus, after considering the Ding's D_{fret2} parameter, overall correlation gets improved.

The next parameter investigated is the increase in contact surface's temperature due to the frictional heat generated at the interface. Corresponding details are mentioned in the next section.

Table 22: Resultant correlation results using varying COF and with Ding's parameter for BKIN, MKIN and Chaboche material models with area stress averaging

FIP	Material Non-linear Model	Average $\tilde{x}$	Deviation D_x
SWT	BKIN	1.24	2.43
	MKIN	1.31	2.61
	Chaboche	1.19	2.45
FS	BKIN	1.29	2.39
	MKIN	1.37	2.39
	Chaboche	1.36	2.44
eI	BKIN	1.39	1.94
	MKIN	1.33	2.05
	Chaboche	1.38	2.20

3.4. Effect of Frictional Heat

In order to model the possible heat generation due to the frictional dissipated energy at the contact junction, coupled thermal-structural analysis is carried out. To carry out such coupled analysis within the ANSYS Workbench, both structural and thermal DOF's of the contact elements (CONTA172) are activated.

The rate of frictional energy dissipation at the contact interface [155] is derived as

$$q = (FHTG)(\tau)(V') \tag{46}$$

where τ is the maximum frictional stress, *V'* is the sliding rate, *FHTG* is the fraction of frictional dissipated energy converted into heat.

In this work, default value of 1 against *FHTG* is considered i.e., it is assumed that the resultant frictional heat is equal to the product of τ i.e., maximum frictional stress and *V* i.e., sliding rate for transient analysis (and sliding distance for static analysis). This will be the worst-case scenario towards the maximum frictional heat generation at the contact interface. Further, the amount of dissipated frictional heat is split between the contact and target surfaces. The distribution of dissipated frictional heat into the contact surface is

$$q_c = (FWGT)(FHTG)(\tau)(V) \quad (47)$$

and into the target surface is

$$q_T = (1 - FWGT)(FWGT)(FHTG)(\tau)(V) \quad (48)$$

where $FWGT$ is the weight factor for the distribution of heat between the contact and target surfaces.

Here, the conservative assumed value of 0.8 is considered i.e., 80% of the frictional dissipated energy is transferred to the contact body i.e., fretting specimen and remaining 20% is transferred to the target body i.e., fretting pad. FEA is carried out for all 15 test cases with the initial ambient temperature considered as 22 °C. Further, in order to consider the possible conversion of the fraction of plastic work into the thermal energy, Taylor- Quinney coefficient [156], is considered through the ALDL commands as

$$\beta_{int} \int dW_p = \rho c_p \Delta T \quad (49)$$

where β_{int} is the Taylor- Quinney coefficient (fraction of the plastic strain energy density converted into heat), $\int dW_p$ is the resultant plastic work, ρ is the material density, c_p is the specific heat capacity, ΔT is the resultant temperature rise.

For AL7075-T6 aluminum alloy, Taylor- Quinney coefficient varies from 0.3 to 0.96 [157]. Corresponding value for Taylor- Quinney coefficient is assumed as 0.9, as the conservative approach, thus allowing most of the plastic work getting converted into the thermal energy. Related material property details are given in Table 7. In order to convert the frictional heat and plastic work into resultant thermal energy, coupled field analysis needs to be carried out. Accordingly, 2D 4-Node coupled-field element, Plane222 [158], is considered here, with the plane strain behavior. As the FEA is carried out for all the 15 test cases, corresponding result towards the resultant maximum surface temperature are given in Table 23.

Table 23: Maximum temperature observed for contact pad

Test #	Contact Pad's Maximum Temperature (°C)
1	30.87
2	30.23
3	45.56
4	30.87
5	30.23
6	45.56
7	30.87
8	30.24
9	45.56
10	30.87
11	30.24
12	45.56
13	30.87
14	30.24
15	45.56

FEA is carried out for two duty cycle blocks. Based on the obtained FEA results for all 15 test cases, it is observed that frictional dissipated energy contributes to minimum increased surface temperature of 30.87 °C and maximum increased surface temperature of 45.6 °C for the fretting specimen. Though compared to the initial ambient temperature this temperature rise appears significant, material properties of AL7075-T6 will not change significantly with this temperature increase and hence, the effect of frictional dissipated energy onto fretting fatigue life results is not explored further.

3.5. Effect of Normal, Axial and Tangential Loads using 2D Axi-Symmetric Liner-Gasket-Block FEA Model

The parameters investigated so far are mainly physical parameters and effect of those is expected to be similar across different set of geometries. Next set of investigated parameters are actual applied-load related parameters like normal, axial and tangential loads, effect of which is expected to differ across the different set of geometries. Thus,

effect of these parameters is studied using a different set of geometry, which represents the actual head gasket joint, which is the final planned case study in this work.

Further, as shown earlier in Figure 37 , considering the equivalent analogy between the flat-flat contact pair and the actual head-gasket geometry, equivalent resemblance can be established between the two sets of geometries and applied loads on a flat-flat contact pair i.e., normal, axial and tangential loads and actual operational loads on a typical head gasket joint. Required details of the typical head gasket joint of the high horsepower diesel engine are given in the next section.

3.5.1. Typical Head Gasket Joint of High Horse-Power Diesel Engine

The schematic representation of a typical head gasket joint using single layer steel gasket is shown in Figure 80. Using a set of head bolts, the head gasket is clamped between the head and the liner which is mostly press-fitted in the engine block. This joint is mainly exposed to the engine operating loads like peak cylinder pressure and thermal loads. As the combined result of these loads, micro relative sliding occurs at the gasket's interfaces. This micro sliding combined with high contact stresses, causes the fretting damage of the gasket. In such head- gasket joints, the assembly load due to bolt preloads is distributed in-proportion between the liner and the block.

The liner protrusion over the block's machined top face has much influence on the resultant load split between the liner and block. The load transferred to the liner gets further distributed over the contacting surface of the liner with the gasket, due to the design feature provided on the liner termed as 'bite ring /bead'. The bite ring geometry is designed to distribute the loads across the sealing region at gasket-liner interface as per the sealing requirement. In addition to the sealing force distribution, the bite- ring also serves the purpose of localized yielding of the gasket and therefore creating a localized but high-pressure sealing region to prevent the leakage of hot combustion gases. Thus, the bite ring geometry is a critical design feature towards the required combustion sealing function of the head gasket.

3.5.2. 2D Axisymmetric FEA of Head-Gasket-Joint

In this step, 3D geometry, as shown in Figure 81 (A) is suitably represented using 2D

axisymmetric geometry set-up as shown in Figure 81 (B). Here, except the dummy head, for remaining parts, actual axisymmetric portion of the corresponding geometry is considered. A close view of the liner bite ring geometry is given in Figure 82. The schematic representation of the load transfer across the different regions of liner bite ring geometry and also between liner and block is shown in Figure 83.

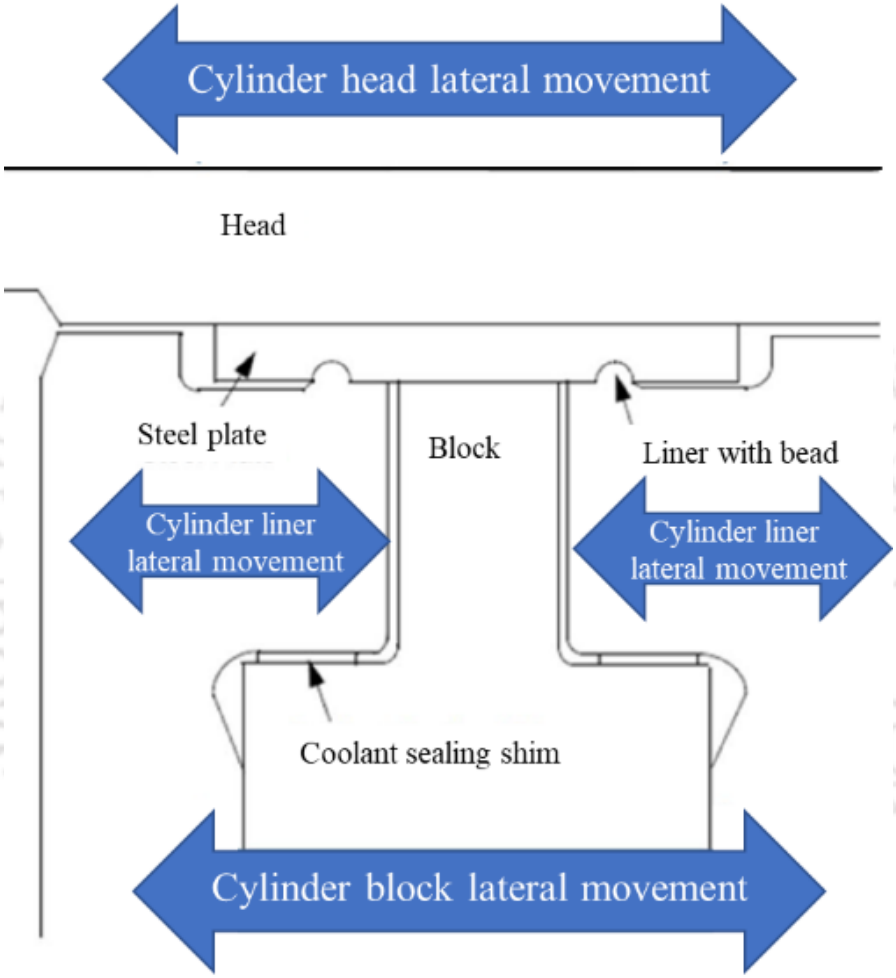

Figure 80: Schematic representation of the gasket joint with single layer steel gasket (Reprinted with permission from [31])

For meshing, second order quad elements; Plane183 [133] are considered. Based on the contact pressure convergence test performed by varying the mesh size of the bite ring width portion, mesh size of 10 μm is considered for meshing the bite ring geometry as shown in 8Figure 84. Suitable mesh size is kept elsewhere. The resultant 2D FEA meshed model is shown in Figure 85. Material properties considered for different engine parts are

given in Table 24. For the gasket, MKIN material model is considered based on the non-linear stress-strain curve as shown in Figure 86.

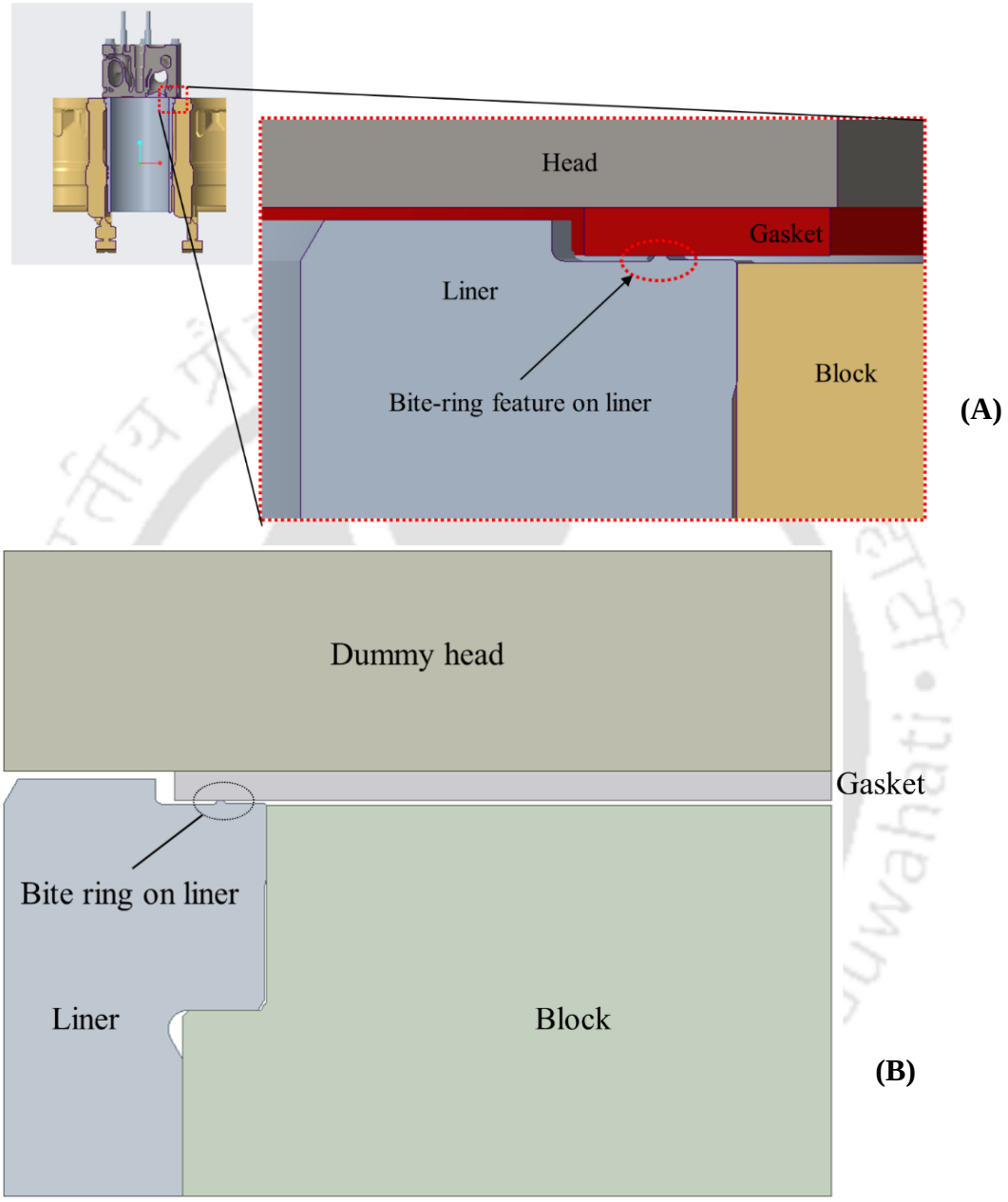

Figure 81: Sectional view of actual 3D geometry (A) and axisymmetric geometry considered in the 2D axisymmetric FEA model (B)

Considered loads and boundary conditions are shown in Figure 87, with supporting details mentioned in Table 25. Here, the downward pressure '***X1***' corresponds to the resultant load on the head due to be applied bolt preloads. Pressure '***X3***' applied onto head and liner region till 'Top Ring Reversal' (TRR), corresponds to the peak cylinder pressure

of the engine during the engine firing at rated power condition. Transverse load '***X2***' applied on the right vertical edge of dummy head corresponds to the frictional resistance force at the head gasket's contact surface with the head and is primarily associated to the relative thermal sliding displacement of head with respect to the gasket.

Frictional type contact, with 'Augmented Lagrange' option is considered at the contact interfaces of 'gasket with head' and 'gasket with block and liner' and based on the current industry standards, constant friction coefficient value of 0.4 is applied. Once the finite element model is prepared, it is solved for the load sequence mentioned in the Table 25. Corresponding values against the parameters ***X1***, ***X2*** and ***X3*** for different load cases are considered from the actual 3D FEA model [31] and considered values are given in Table 26.

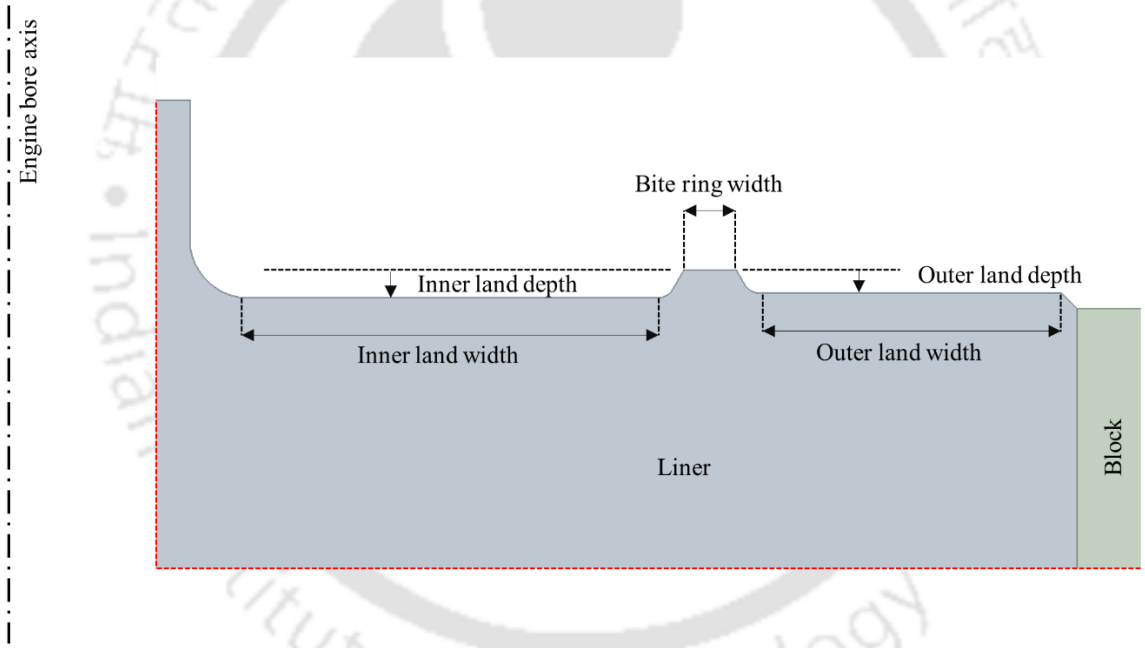

Figure 82: Liner bite ring geometry and associated design parameters

These load values represents the actual variations in the corresponding loads in the 3D FEA. Due to the considered non-linearities like material, contact and geometric, it makes the FEA model path-dependent and hence, 5 duty cycle blocks are considered to obtain the stabilized stress-strain condition and the results of the 5th duty block are considered for the fretting fatigue life evaluation after observing the equivalent strain convergence at the end of 5th duty cycles (see Figure 88).

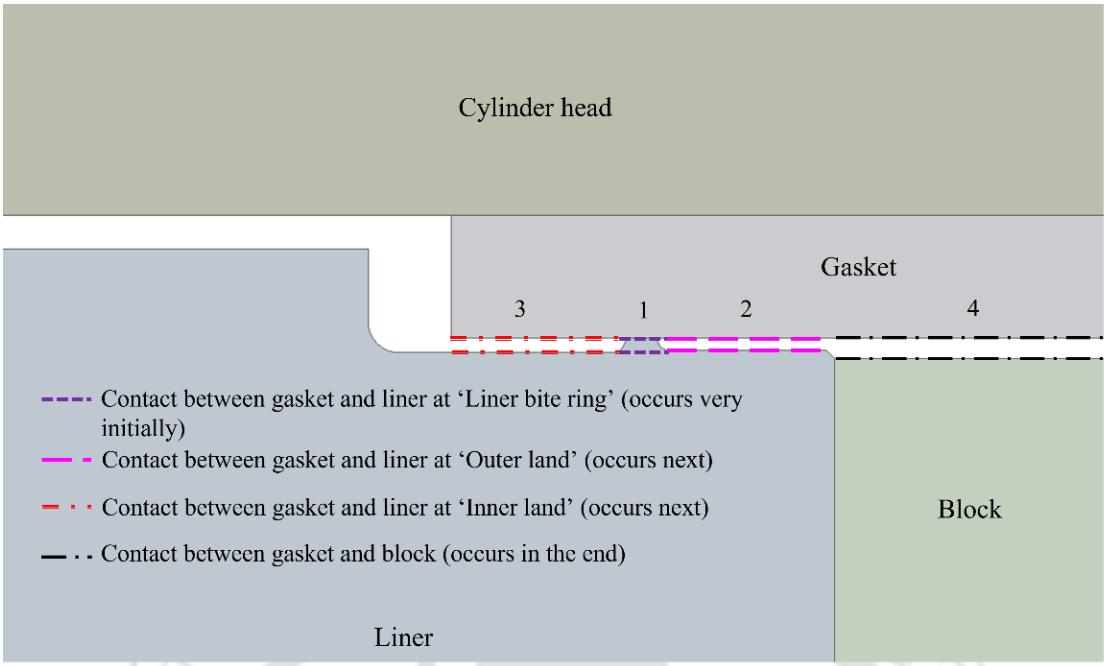

Figure 83: Schematic representation of load transfer across liner and block

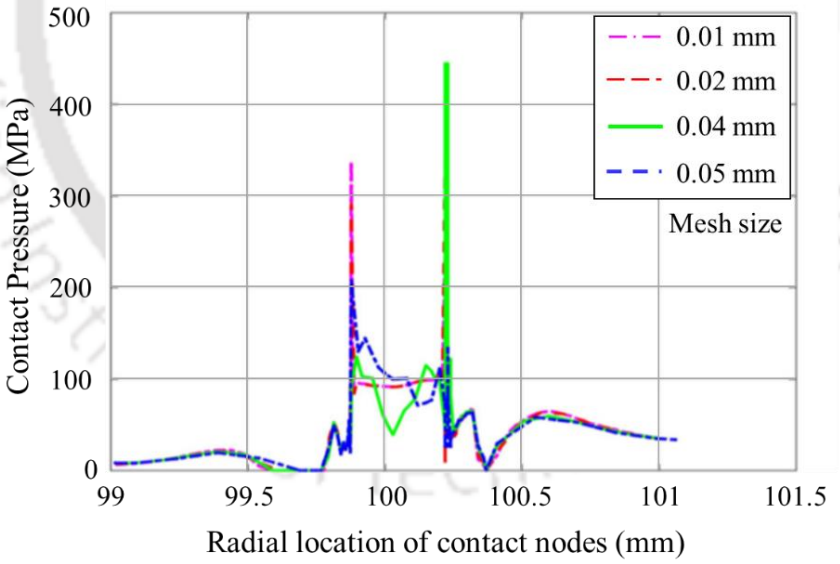

8Figure 84: Mesh convergence test considering contact pressure

Carrying out 2D axi-symmetric analysis based on the actual corresponding load values considered from the 3D FEA, is expected to be a time-effective approach and primarily suitable for the comparative assessment between different parameters/geometric changes rather than the absolute damage evaluation [160]. Further, the effectiveness of such 2D

axi-symmetric analysis approach is verified by carrying out the comparative assessment between the Ruiz's parameter *F1* results obtained using 2D axi-symmetric analysis and 3D FEA results obtained using 3D FEA with actual geometries and engine loads, as shown in Figure 89. Please refer to the Appendix A for the details over the related carried work.

3.5.3. Effect of Normal Load

As mentioned earlier, normal load '***X1***' corresponds to the vertical displacement applied onto the top face of the dummy head and represents the applied displacement during the assembly due to bolt tightening. Every bolt tightening method has the inherent scatter. Consequently, bolt preload values can vary within the allowed scatter. For the considered head bolts, with the bolt tightening method as 'Torque Plus Angle in the Plastic Range' [159], the scatter is expected within $\pm$ 10% [18]. Hence, the normal load applied through vertical displacement '***X1***' is also varied by $\pm$ 10%. While varying normal load, other loads i.e., axial load and tangential load values are retained at the nominal values. The considered load values are given in Table 26. Corresponding nominal load values are considered from the 3D FEA model [31] and then $\pm$ 10% variation is applied to the nominal normal load value.

3.5.4. Effect of Axial Load

Further, the axial load '***X3***' corresponds to the peak cylinder pressure. Generally, the peak cylinder pressure is an important design parameter of each engine family and has certain scatter in terms of the maximum value. Thus, the axial load applied i.e., '***X3***' is also varied by $\pm$ 10%. While varying axial load, other loads i.e., normal load and tangential load values are retained at the nominal values. Corresponding considered values are given in Table 26. Nominal load values are considered from the 3D FEA model [31] and considered $\pm$ 10% variation is applied to the nominal axial load value.

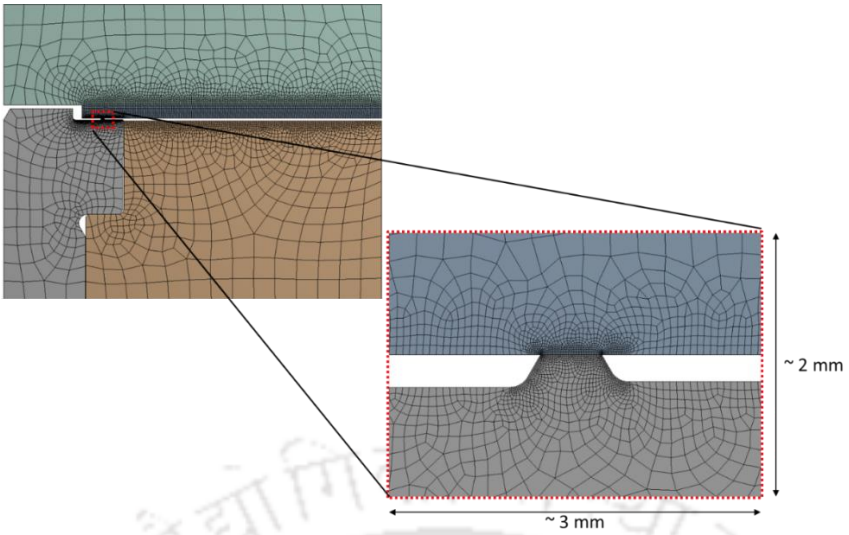

Figure 85: 2D FEA meshed model

Table 24: Material properties for 2D axi-symmetric FEA model

Component	Material	Material Properties	Reference
Liner	Cast Iron	$E = 110$ GPa, $\vartheta = 0.26$	[18]
Head	Cast Iron	$E = 110$ GPa, $\vartheta = 0.25$	[18]
Block	Cast Iron		
Gasket	Steel	$E = 200$ GPa, $\vartheta = 0.3$ (non-linear material properties defined in terms of stress-strain curve as shown in Figure 86.)	[18]

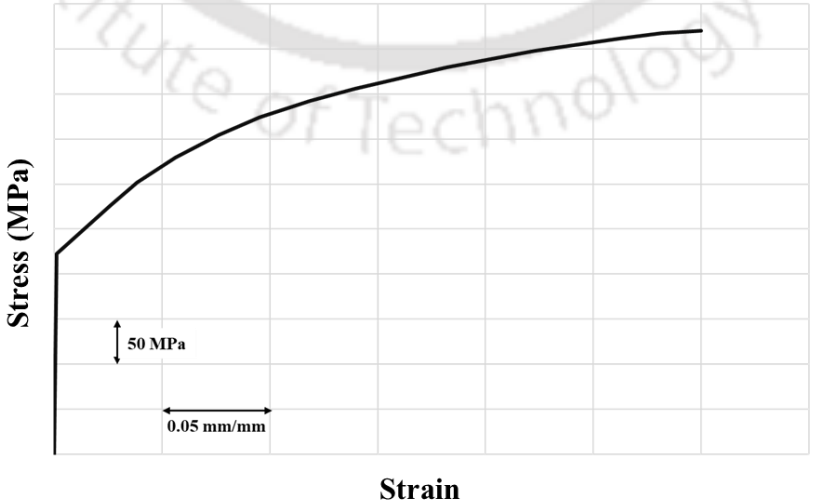

Figure 86: Stress strain curve for gasket material

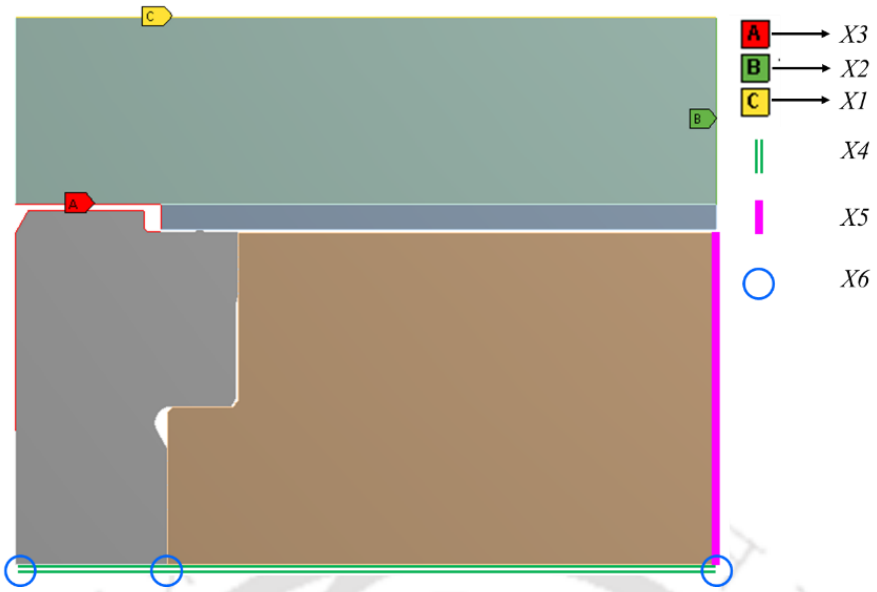

X1: Normal pressure in down direction onto top edge of head (value to be obtained from 3D FEA model),

X2: Normal force in horizontal direction towards right (value to be obtained from 3D FEA model),

X3: Engine peak cylinder pressure,

X4: Normal constraints onto bottom edges of liner and block,

X5: Normal constraints onto right edge of the block,

X6: Fixed support at three selected points.

Figure 87: Loads and boundary conditions considered in 2D axisymmetric FEA model of head gasket joint

3.5.5. Effect of Tangential Load

Tangential load '***X2***' corresponds to the relative thermal sliding of head with respect to the gasket's contact surface. Along with the other considered loads, this force component is critical towards the gasket's contact stresses. Engine head being one of the hottest components of a diesel engine, is cooled with the coolant flowing through the water jackets casted in the head geometry. The pressurized engine coolant is circulated inside the head and block using the water-pump. Hence, the cooling of head and block, is dependent upon the rate of coolant getting circulated inside the system. Considering the possible scatter in the pump's operating efficiency, $\pm$ 10% variation is assumed towards the tangential load value, while retaining other loads i.e., normal and axial loads at the nominal levels. Corresponding considered values are shown in Table 26.

Table 25: Load sequence in 2D Axi-symmetric FEA

(A: Assembly load, AP: Assembly + Rated PCP, APT: Assembly + Rated PCP + Maximum thermal condition AT: Assembly + Maximum thermal condition)

	Duty Cycle block Number →					***X1***	***X2***	***X3***	Remarks
	1	2	3	4	5				
Load Step Number ↓	1-6					Initial adjustments			
	7	12	17	22	**27**	Applied	NA	NA	A
	8	13	18	23	28		NA	Applied	AP
	9	14	19	24	**29**		Applied	Applied	APT
	10	15	20	25	30		Applied	NA	AT
	11	16	21	26	31		NA	NA	AP

Resultant fretting fatigue life results, against these considered variations, are obtained using the deviatoric strain amplitude-based parameter i.e., eI, for the load reversal 'A-APT'. This load reversal corresponds to the two extreme engine operating load conditions. The stress-strain values from the 5th duty cycle block are considered to obtain subsequent fatigue life results. The fretting fatigue life results, against the considered load variations are shown in Figure 90. Here, it should be noted that the primary expectation is to understand the critical parameters towards the resultant fretting fatigue damage. The corresponding results are without any stress-averaging methods and without considering any surface wear damage. Also, unsymmetric nature of the considered loads cannot be captured through the 2D axi-symmetric FEA. Therefore, these results should be considered only to identify the critical parameters and not for the absolute fretting fatigue damage evaluation. For the absolute assessment, 3D FEA needs to be carried out.

However, these results can still be effective to identify the most critical parameter among axial, lateral and transverse loads and can be considered to minimize the number of computationally expensive 3D FEA else required. Based on the results shown in Figure 90, it is observed that the peak cylinder pressure (PCP) is observed to be most the significant parameter in order to cause possible change in the gasket's fretting fatigue life.

Table 26: Considered load details in 2D Axi-symmetric FEA

Run#	Normal Load (MPa)	PCP (MPa)	Transverse Load (N)	Note
1	62 (Nominal)	18.62 (Nominal)	3.20E+05 (Nominal)	Nominal load condition
2	55.8 (-10%)	18.62 (Nominal)	3.20E+05 (Nominal)	Normal load (***X1***) with - 10% variation
3	68.2 (+10%)	18.62 (Nominal)	3.20E+05 (Nominal)	Normal load (***X1***) with + 10% variation
4	62 (Nominal)	16.758 (-10%)	3.20E+05 (Nominal)	PCP (***X3***) with - 10% variation
5	62 (Nominal)	20.482 (+10%)	3.20E+05 (Nominal)	PCP (***X3***) with + 10% variation
6	62 (Nominal)	18.62 (Nominal)	2.88E+05 (-10%)	Transverse load (***X2***) with - 10% variation
7	62 (Nominal)	18.62 (Nominal)	3.52E+05 (+10%)	Transverse load (***X2***) with + 10% variation

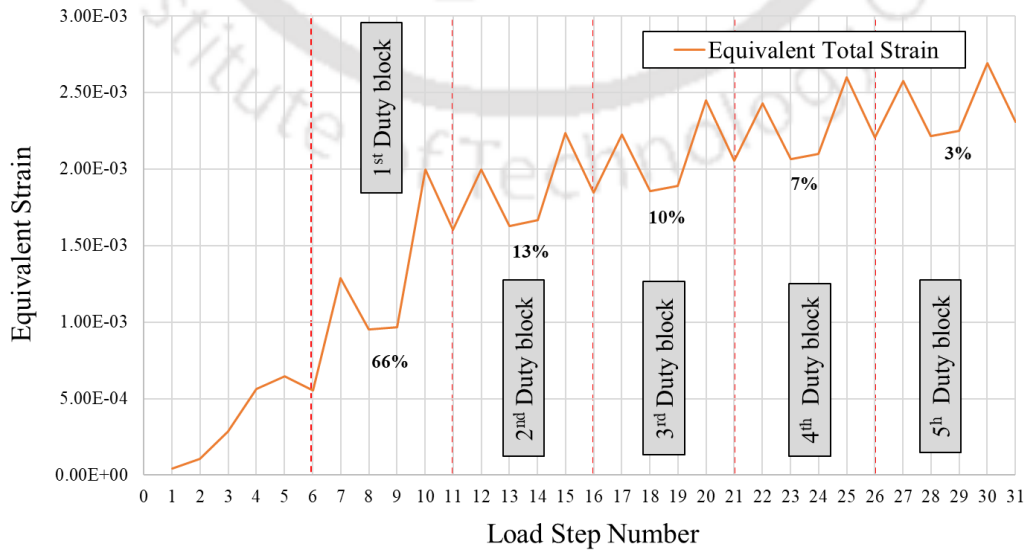

Figure 88: Equivalent total strain convergence

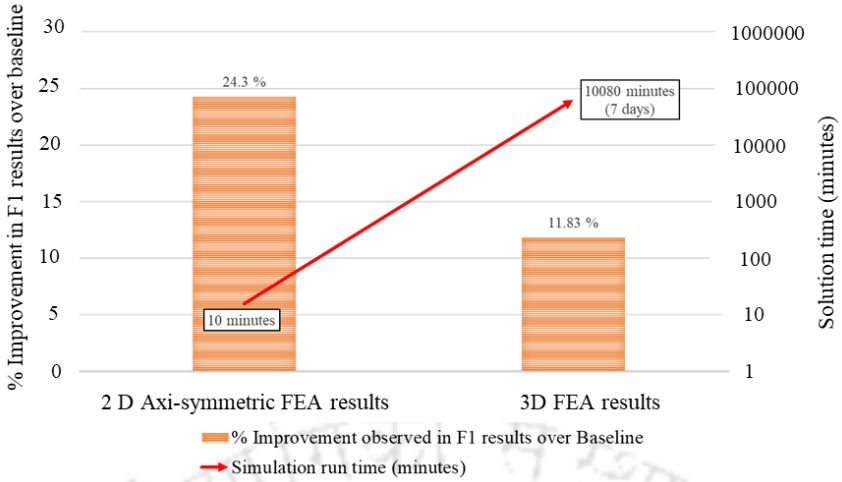

Figure 89: Comparison between 2D axi-symmetric FEA and 3D FEA results for head gasket

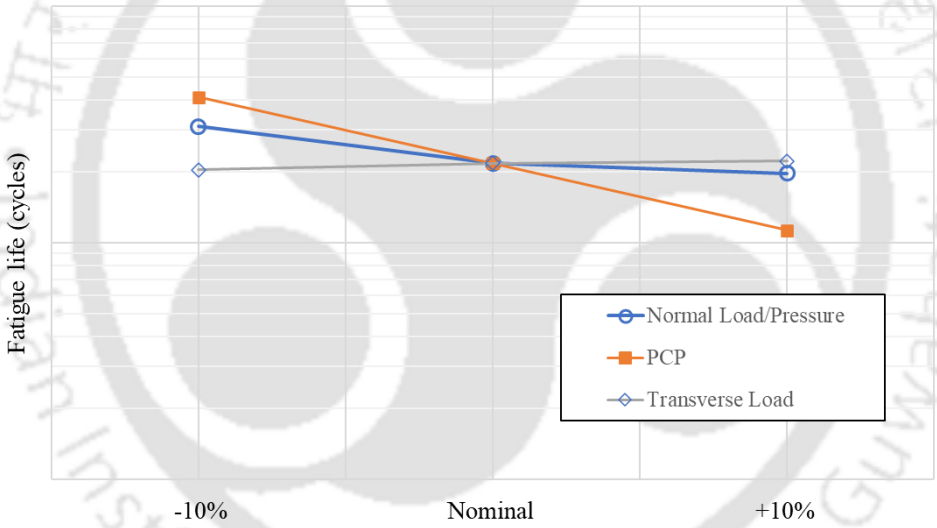

Figure 90: Variation in fretting fatigue life results for considered load variations in 2D axisymmetric FEA of head gasket

As seen in Figure 90, an increase in the PCP load value causes the reduction in the fretting fatigue life results as the resultant stress-strain reversal is expected to increase. The normal load variation is the next critical parameter in terms of affecting the fretting fatigue life result of the head gasket. Here, also with an increase in the normal load fretting fatigue life results are observed to reduce. Comparatively the transverse load is not observed to cause much change in the resultant fretting fatigue life results.

Thus, the 2D axi-symmetric analysis approach enabled efficient identification of the critical parameters in terms of the corresponding contribution towards the fretting fatigue life results. Similar to the Figure 89, carrying out initial 2D axi-symmetric FEA, is a good practice to limit the scope of complex 3D FEA to obtain the corresponding minimum fretting fatigue life for the head gasket [160]. Thus, it will save a significant amount of computational time and resources else would be required.

भारतीय प्रौद्योगिकी संस्थान गुवाहाटी
Indian Institute of Technology Guwahati

4. FRETTING FATIGUE ANALYSIS OF ACTUAL HEAD GASKET JOINT

The learnings from the work completed so far, are considered for the fretting fatigue damage and life evaluation of the actual head-gasket joint. Earlier, Ruiz's parameter, FDP has been considered for fretting damage evaluation of the head gasket [31]. However, as mentioned earlier, resultant damage values predicted using this parameter cannot be converted to the corresponding fretting fatigue life results. Further, since Ruiz's parameter is based on stress values only, it cannot be considered in cases where material yielding is expected, and where resultant damage should consider strain values also. Hence, Ruiz's parameters are suitable towards the comparative assessment only and therefore, have limited correlation with the actual field results. Earlier, in Chapter 3 it is observed that combined consideration of eI parameter and Ding's parameter D_{fret2} is effective towards the experimental correlation within $\pm$ 3N scatter band. So, during the scope of current work, fretting fatigue life results for the head gasket are evaluated considering both these parameters. Resultant fretting fatigue life results corrected for the surface wear, are compared with the earlier results obtained using the traditional industry approach of Ruiz's parameter. Further, in order to check for the results consistency, correlation study is carried out considering three different engine platforms which vary in geometry and operating loads. The high-level summary of the overall scope of completed work, is as shown in Figure 91.

4.1. Fretting Fatigue Failure of Cylinder Head Gasket of High Horsepower Engine

Internal combustion engine is a complex mechanical assembly of multiple components. Cylinder head gasket joint is one of the critical joints in any IC engine, designed to seal hot combustion gases in the power cylinder and prevent coolant/oil leakage out of the designed passages. The head gasket is clamped between cylinder head and block/liner/both. Among the three possible failure modes for head gasket, mentioned as

The contents of present chapter have been accepted as a journal article 'A. P. Ozarde, G. H. McNay and S. S. Gautam, " Fretting fatigue damage and life evaluation of cylinder head gasket using deviotoric strain amplitude-based parameter corrected for surface wear damage"' in SAE International Journal of Engines on 29 July 2022.

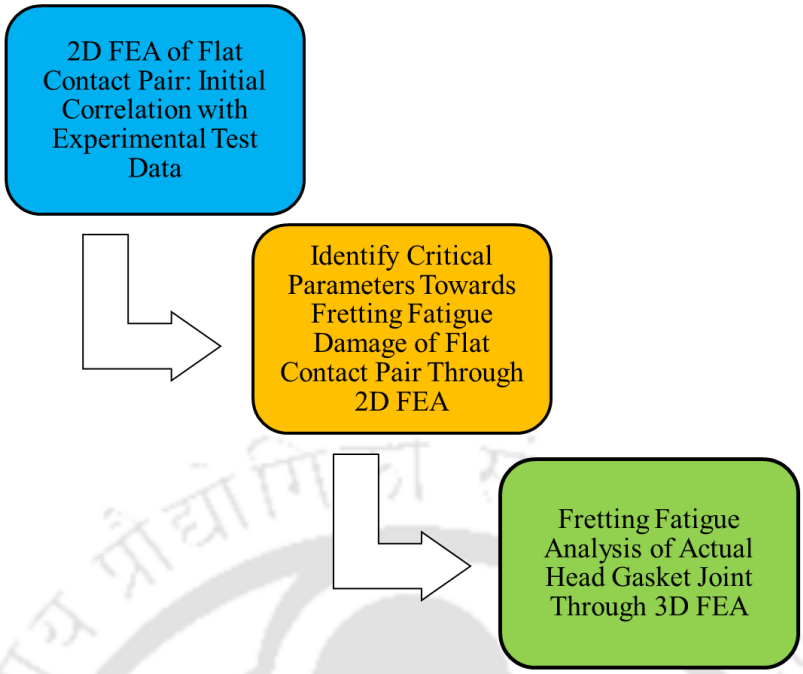

Figure 91: High-level summary of the overall scope of completed work

sealing, fatigue and fretting, analysis methodology for the fretting failure mode is comparatively less explored and developed [28].

Fretting damage of head gasket being a complex phenomenon with simultaneous interactions between different parts like cylinder block (with liner), cylinder head, head gasket and head bolts, it needs to be investigated at the system level rather than only component level. Different evaluation methods like Archard's wear model [32] and Ruiz's parameter [16] have been respectively considered towards specific problems with close correlation in terms of critical location/s predictions [28, 35]. However, these methods have critical limitations of not able to predict the corresponding fretting fatigue life and are effective towards comparative assessment only. Also, by considering progressive wear technique like Archard's wear model [32], FEA model turns to be computationally more expensive due to the additional equilibrium iterations needed for progressive wear calculation [161]. Further, being only stress-based methods, these methods have limited applications in the cases where material yielding is expected.

Typically, a high horsepower engine with unit heads has single steel plate gasket with integral elastomer sealing beads. Along with its primary function to seal combustion gases, coolant and oil, head gasket also serves the secondary function of accommodating the surface irregularities and part variation at the mating interfaces. Gasket's

scrubbing/fretting occurs primarily due to engine firing pressure and corresponding engine thermal response during the engine operation. Engine operating conditions change corresponding to the end applications. Hence, the resultant fretting fatigue damage of the head gasket will also change for different engine platforms based on the individual field applications.

In this work, three different engine platforms are considered towards the comparative fretting damage assessment of the corresponding head gaskets. Single layer steel gasket is considered during the scope of current work. It is mostly used in high horsepower engines (engine capacity > 19 liter). High horsepower engines are typically fitted with a top-stop replaceable liner [162]. The top of the liner has a design feature called a bite-ring that locally yields the steel plate head gasket [35]. Fretting damage in such head gaskets occurs at the contact surface with head/liner, mainly due to the resultant micro-slip movement at the gasket interface with the cylinder head (as shown in Figure 8 (B)). Fretting damage is primarily driven by the normal load and lateral relative movement in the joint. Figure 80 shows the schematic of cylinder head gasket structure and shows lateral direction of head and block. For fretting damage evaluation of the head gasket, different factors to be considered in the system-level investigation include variation in the joint loads, relative slip magnitude, coefficient of friction etc. Corresponding details related to head gasket fretting analysis procedure are given in the following section.

4.2. Head Gasket Fretting Fatigue Analysis Procedure

In the cylinder head gasket joint, occurrences of gasket's lateral movements due to thermal deformation is low and thus, associated gasket fretting failure due to thermal deformation are considered as "low cycle fretting" failure. On the contrary, the frequency of head gasket's lateral movement due to the peak cylinder firing pressure is very high and hence, subsequent gasket fretting damage due to firing pressure can be considered as a "high cycle" failure. Gasket body's fretting damage can finally result in the fluid or gas leakage. To carry out the fretting analysis of the head gasket, associated engine operating load sequence is very critical. During its operation, an IC engine is exposed to different operating loads like 'Assembly' loads (A), 'Peak Cylinder Pressure (PCP) corresponding to rated power condition and maximum 'Thermal' condition (T). During different running conditions, engine is exposed to different possible combination of such loads as given below:

- A: Only assembly loads due to bolt preloads etc. (i.e., resultant residual static loads primarily imposed via threaded fasteners)
- AP: Assembly + PCP (when the engine is running at PCP corresponding to the rated power, in the start of power-stroke. This unusual condition is a worst case situation where a cold engine is being pushed to create full power without a significant warm-up.)
- AT: Assembly + Maximum thermal condition (engine running condition at maximum thermal condition, typically pre and post power stroke of an IC engine)
- APT: Assembly + PCP + Maximum thermal condition (engine running condition at maximum thermal condition with PCP, typically occurs in the start of power-stroke of an IC engine)

In general, fatigue evaluation is carried out over the duty cycle block of different repetitive load cases or between two extremal repetitive load case reversals. Accordingly, load reversals of AP-A and APT-AT correspond to high cycle fatigue, during which alternating load contribution is because of PCP and mean load contribution is due to combined effect of 'Assembly' and 'Maximum temperature condition'. The load cycle reversal of 'APT-AT' occurs when the engine is operating at full power and at maximum temperature condition. Load cycle reversal of 'AP-A' occurs when the engine is at full power, but the engine is cold or not yet warmed up. Alternatively, AT-A and AP-APT are low cycle approximations, during which alternating load contribution is because of thermal loads and mean load contribution is because of 'Assembly' and 'PCP' loads.

The load cycle reversal of 'AP-APT' occurs between two load cases in which engine is running with maximum PCP during the 'cold start condition/initial engine warming condition' and when engine is running at full power with maximum temperature state. Finally, the load cycle reversal of 'AT-A', corresponds to load reversal between engine stop i.e., no running condition and hot engine condition with maximum thermal condition. Generally. the high cycle approximations occur due to PCP reversals and subsequent fatigue cycle accumulation occurs at high frequency (i.e., occurring many times per second) whereas low cycle approximations occur mainly due to thermal load reversals and corresponding fatigue cycles accumulates rather slowly i.e., at low frequency (i.e., once or twice an hour or even slower). Corresponding FEA model details considered for the fretting fatigue analysis of head-gasket, are discussed next.

4.3. FEA Model Details

FEA model consisting of cylinder head, liner, gasket, cylinder block section and all head bolts is prepared in ANSYS Workbench. The head gasket is modeled with 3D continuum-20 noded element i.e., Solid 186 element [163] with non-linear material properties defined in terms of 'Multilinear kinematic hardening' material model (MKIN) [149]. Alternatively, gasket elements i.e., Inter194/195 could also have been considered to represent the gasket in the FEA model. However, due to the capability of continuum elements to capture material non-linearity, in both directions i.e., in-plane as well as out-of-plane directions, continuum element is a better option towards obtaining more realistic fretting fatigue life prediction for the head gasket. Second-order Tetra (Solid 187) [164] and second order Hex (Solid 186) elements [165] are considered for meshing the remaining engine components except the gasket.

Next, both contact interfaces of the head gasket i.e., 'with head' and 'with block and liner' are considered as frictional contacts with 'Augmented Lagrange' formulation with constant coefficient of friction value of 0.4. Fine mesh size of 0.1 mm is kept for the head gasket and at the contact surfaces of head, block and liner. Here, as compared to the earlier considered mesh refinement as 10 μm in 2D Axi-symmetric FEA model, this considered mesh size of 0.1 mm appears to be higher. However, solving 3D FEA model with 10 μm mesh size, would cause significant challenges towards the possible convergence issues and very high computational resources. Typical solution time with the considered FEA model settings is expected to be around 7-8 days. So, if the mesh size is further refined to 10 μm, it would cause huge increase in the required solution time, resources and convergence issues. Also, as the objective is to carry out comparative assessment with respect to the earlier obtained Ruiz's parameter results [31], identical mesh size is considered during the scope of current work also.

Next, instead of default value for the 'Slip Tolerance' i.e., SLTO parameter as of 1% of the average contact length [166], it is reduced to 0.01μm to minimize the elastic slip error at the head-gasket contact-interface where the fretting results are evaluated. SLTO controls the maximum sliding allowed during each iteration in FEA. Corresponding FE modeling details for the considered engine platform#1 are shown in Figure 92. On the similar basis, FEA model is prepared for remaining two engine platforms also. Corresponding details of the considered three engine platforms are given in Figure 93.

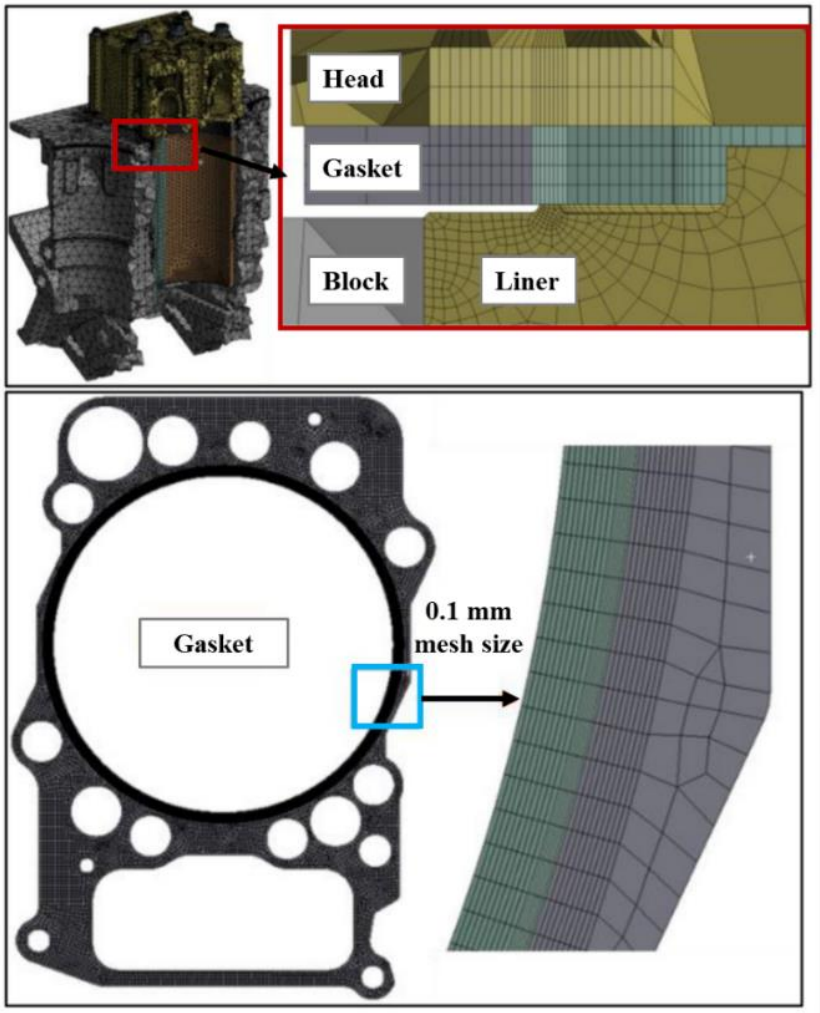

Figure 92: FE modeling details for engine platform#1

The stabilized stress-strain condition at the head's contact surface needs to be considered for realistic fretting damage evaluation of the head gasket. After some initial transient behavior, the material response gradually stabilizes [167]. Hence, to obtain the corresponding stabilized stress-strain state at the head-gasket contact, FEA model is solved for two duty blocks of engine duty cycle. Corresponding loading details are given in Table 27. Stabilized stress-strain results from the last i.e., 2nd duty cycle block are considered for the fretting fatigue life results evaluation [31].

Material details considered for different parts in the FEA model are given in Table 28 and considered nonlinear stress-strain curve for the gasket material is already shown earlier in Figure 86. Different material constants required for the fatigue life evaluation of the head gasket are derived using Seeger's approximation [168], as shown in Table 29 and the resultant fatigue curve i.e., eI-N curve, for the gasket material, is shown in Figure 95.

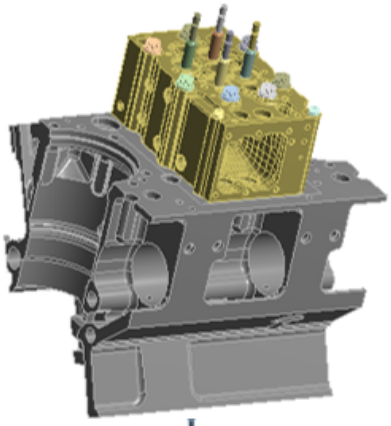

Engine platform#1

Engine type:	Multi-cylinder V engine, Tier 2
Engine capacity per bore:	~ 4.88 liter
Power:	3000-3500 hp

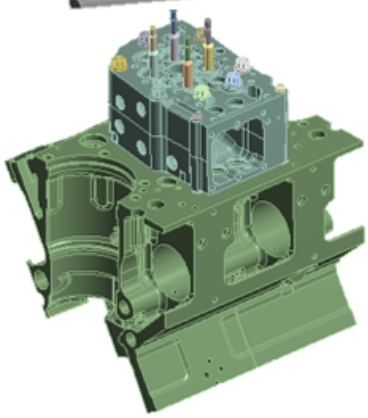

Engine platform#2

Engine type:	Multi-cylinder V engine, Tier 4
Engine capacity per bore:	~ 4.88 liter
Power:	3000-3500 hp

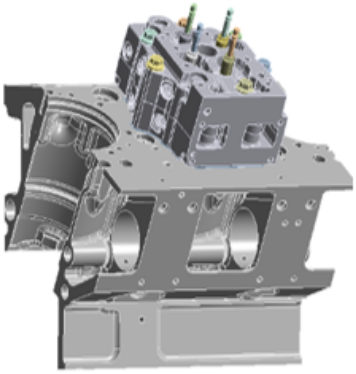

Engine platform#3

Engine type:	Multi-cylinder V engine, Tier 2
Engine capacity per bore:	~ 3.75 liter
Power:	2000-2700 hp

Figure 93: Considered engine platform details (geometry and performance)

4.4. Fretting Fatigue Damage Parameters:

Using the FEA predicted stabilized stress-strain results, fretting damage evaluation is carried out using the eI parameter, corrected for surface wear effect using D_{fret2} parameter (as per the Equation 29). Associated constants towards Ding's parameter, D_{fret2} are given in Table 30 and are considered based on the suitability in terms of corresponding strength values. The results are compared with the traditional approach of Ruiz's parameter *F1* based results. The results are obtained for three different engine

platforms, as mentioned earlier. Resultant correlation between the actual failures and FEA predicted results are presented in next section.

Table 27: Duty cycle considered in FEA

Duty cycle block number	Load step number	Load details	Load case abbreviation
NA	1	Bolt preload adjustment	Adj.
1	2	Assembly i.e., Nominal bolt preload	A
	3	Assembly + PCP	AP
	4	Assembly + PCP+ Maximum thermal state	APT
	5	Assembly + Maximum thermal state	AT
	6	Assembly + PCP	AP
	7	Assembly	A
2	8	Assembly + PCP	AP
	9	Assembly + PCP+ Maximum thermal state	APT
	10	Assembly + Maximum thermal state	AT
	11	Assembly + PCP	AP
	12	Assembly	A

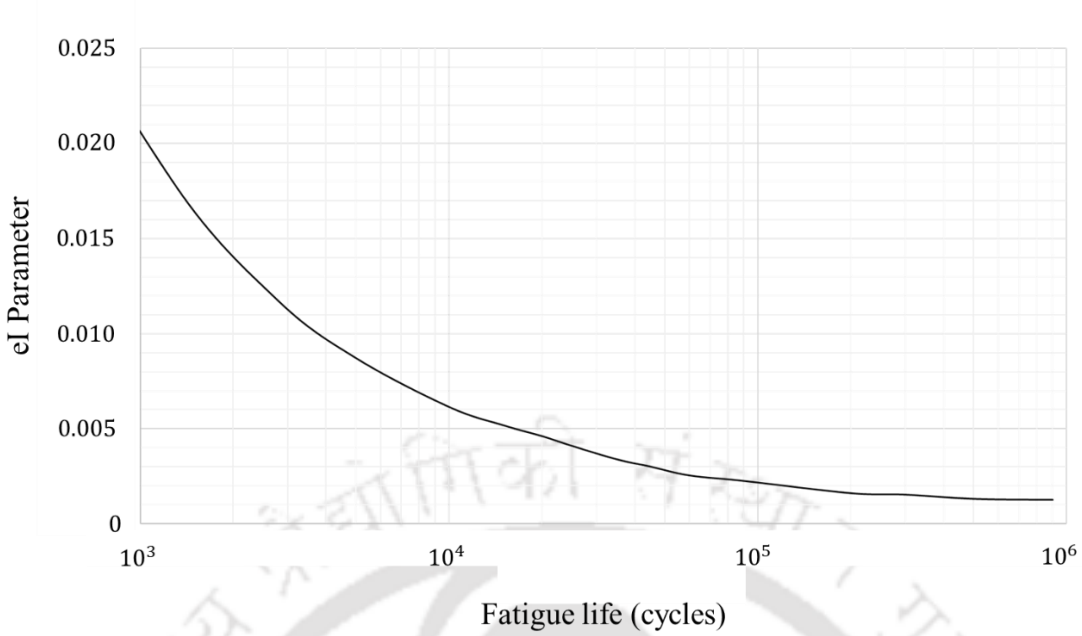

Figure 94: FIP- Fatigue life (eI-N) curve for the gasket material

Table 28: Material properties considered in 3D FEA model of head-gasket assembly

Engine Part	Material	Material properties considered in FEA model
Head gasket	Cold rolled steel	Non-linear material properties as Multi-linear Kinematic (MKIN) hardening material model (Figure 86)
Cylinder head	Grey cast iron	Temperature dependent elastic properties in terms of elastic modulus and Poisson's ratio (Figure 95)
Cylinder block	Grey cast iron	Temperature dependent elastic properties in terms of elastic modulus and Poisson's ratio (Figure 96)
Cylinder liner	Grey cast iron	Elastic modulus (100 GPa) and Poisson's ratio 0.26
Head bolts	Low alloy steel	Non-linear material properties in term of Bi-linear Kinematic (BKIN) hardening material model (Figure 97)

Table 29: Seeger's approximation method [168]

For plain carbon and alloy steel		Reference
σ_f', Fatigue strength coefficient	$1.5\sigma_u$	[168]
ε_f', Fatigue ductility coefficient	$0.59a$	
where, $a = 1.0$ in cases with $\sigma_u/E < 0.003$, otherwise, $a = 1.375 - 1.25\ \sigma_u/E$		
b, Fatigue strength exponent	-0.087	
c, Fatigue ductility exponent	-0.58	
$n^{\wedge}$, Strain hardening exponent	0.15	
K', Strain hardening coefficient	$1.65\sigma_u$	

Table 30: Gasket material constants required for wear correction through Ding's parameter

Material constant	Value	Reference
$(\tau\delta)_{th}$	0.4 MPa mm	[169]
C	0.05 $\text{MPa}^{-1}\text{mm}^{-1}$	
n	-0.085	

4.5. Results

Prior to the fretting fatigue life evaluation, FEA predicted contact pressure results at the contact interface between the cylinder head and gasket, are compared with the actual fuji film results (obtained using high pressure range fuji paper with pressure range capacity as 50-130 MPa [170]). As shown in Figure 98 , good correlation is observed between the two sets of results and thus indicating the correct load split between the liner and block is obtained in FEA model. Since, fretting fatigue results are based on the contact surface stress-strain results, obtaining realistic contact pressure distribution at the head gasket interface is an important step as the initial sanity check. Also, as shown in Figure 99, the resultant equivalent stresses in the head-gasket are observed to be higher than the corresponding tensile yield limit of the gasket material and thus it indicates the necessity to consider the strain-life fatigue initiation method, as considered in this work.

4.5.1. Fretting Results Using Ruiz's parameter *F1*

Ruiz's parameter-based results are evaluated for the head gasket of the three engine platforms. During the scope of current work, fretting fatigue results are calculated between two load steps i.e., LS#8 (AP) and LS#9 (APT) (as shown in Table 27). By considering this load reversal, resultant alternating stress-strain condition due to thermal loads and mean stress-strain condition due to 'Assembly + PCP' loads are getting considered. As mentioned earlier, this load reversal is expected to occur between the two cases in which engine is running cold/not yet completely warmed up and when engine is running hot and operating at full power. Since thermal load reversal generally causes high relative sliding between mating parts like head and gasket, corresponding fretting damage will also be maximum for the thermal load reversal state. Therefore, the load reversal 'AP-APT' is considered here.

Fretting damage results obtained for the head gaskets of three different engine platforms using Ruiz's parameter *F1* are given in Figure 100. Corresponding critical location for each gasket is highlighted in red-dotted rectangle. The maximum fretting damage is observed for the engine platform#1. Further, resultant relative sliding plots for each head gasket are shown in Figure 101 and as observed, maximum relative sliding is also observed for engine platform#1. Hence, for the engine platform#1 and 2, the maximum fretting damage is observed at the highlighted region between the longest bolt-span nearer to the exhaust port. For engine platform#3, relatively very less fretting fatigue damage is observed, as seen in Figure 100. Also, comparatively very less relative sliding distance is also observed for the engine platform#3 (see Figure 101). Further, as shown in Figure 102, the critical location predicted through FEA results correlates well with the actual failure location, as observed on the head-gasket of the engine platform#1.

4.5.2. Fretting Life Results Using Deviatoric Strain Amplitude Based Parameter (eI) Corrected for Surface Wear through Ding's Parameter D_{fret2}

Similar to the Ruiz' parameter evaluation, load steps i.e., LS#8 (AP) and LS#9 (APT) are considered to obtain the corresponding fretting fatigue life results using eI parameter. Different material constants required for fatigue life evaluation of the head gasket are derived using Seeger's approximation [168] and are given in Table 29. These fatigue life results are corrected for surface wear by considering the correction factor applied through

Ding's parameter D_{fret2}. Corresponding constants required to evaluate D_{fret2} parameter are given in Table 30.

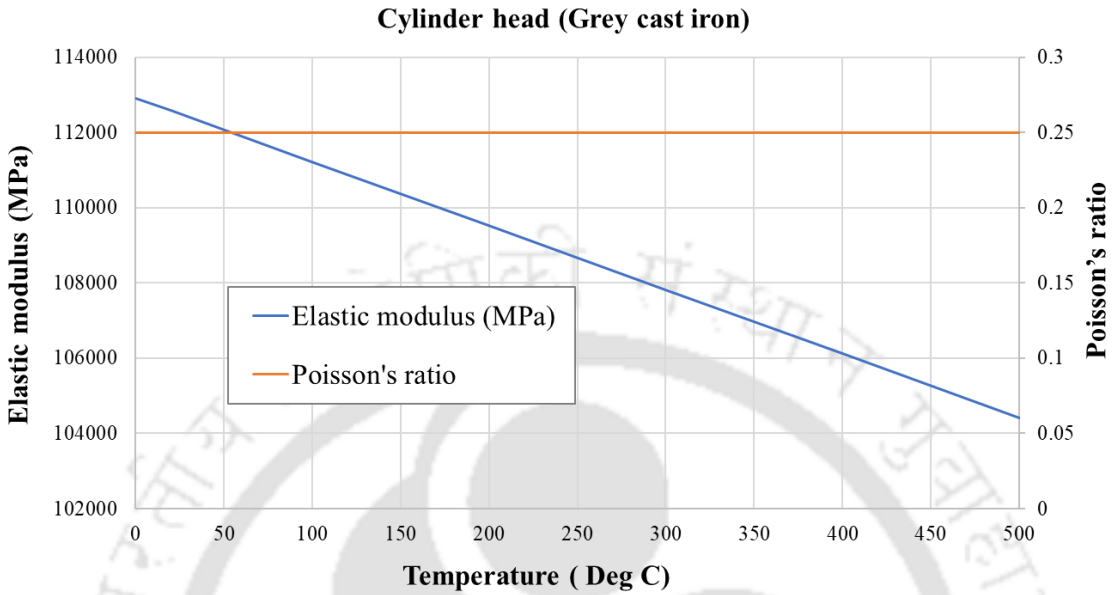

Figure 95: Material properties considered for cylinder head (grey cast iron)

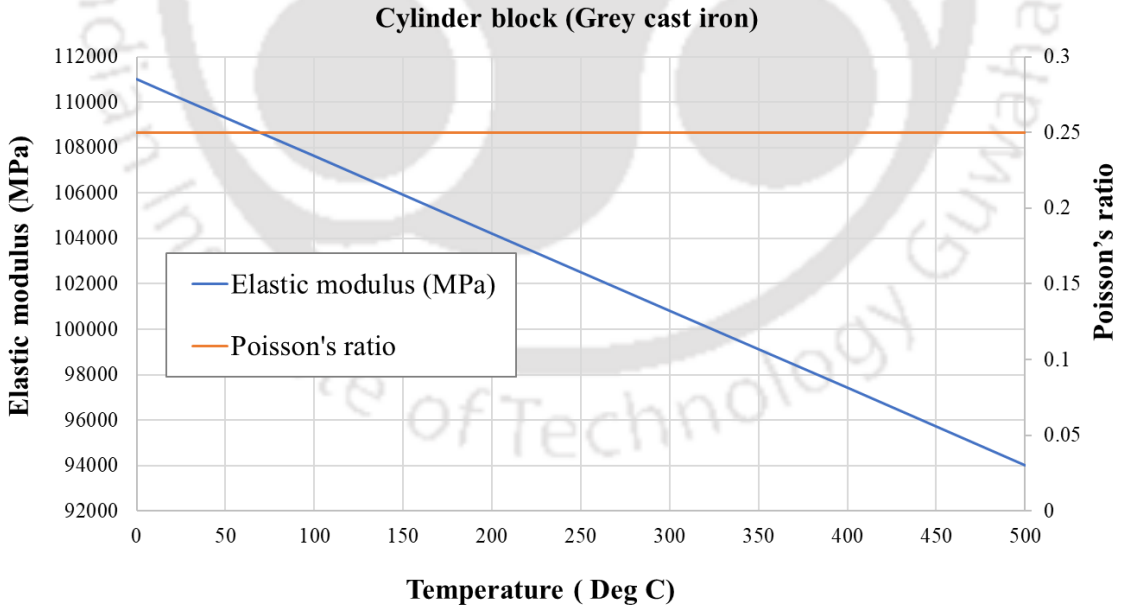

Figure 96: Material properties considered for cylinder block (grey cast iron)

The flow-chart for this new procedure to obtain fretting fatigue life results using deviatoric strain amplitude-based parameter and Ding's parameter D_{fret2} is shown in

Figure 103. The resultant fatigue life results are obtained without any stress-averaging technique applied. At the contact interface susceptible to fretting failure, there always exists a high stress-gradient. To minimize the effect of high stress gradient and subsequent mesh dependency towards the crack initiation predictions, different stress averaging techniques like point, line and area methods are mentioned in different literatures [29, 52].

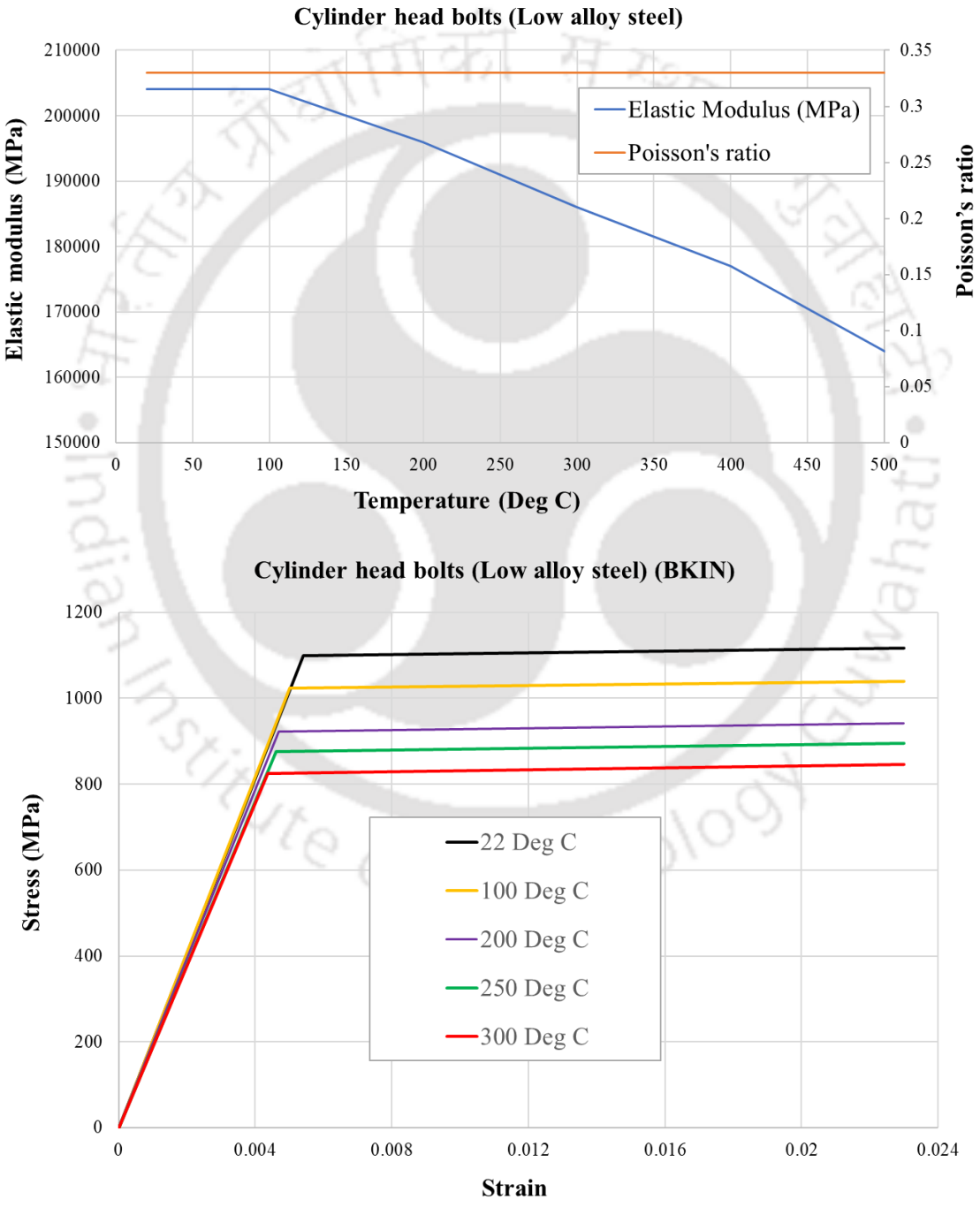

Figure 97: Material properties considered for cylinder head bolts

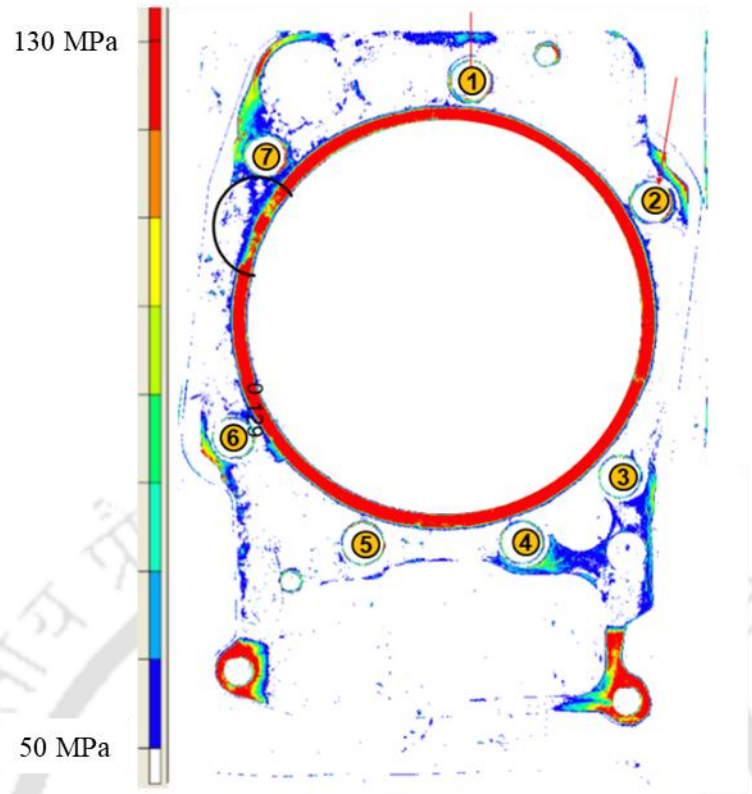

High-grade fuji film results

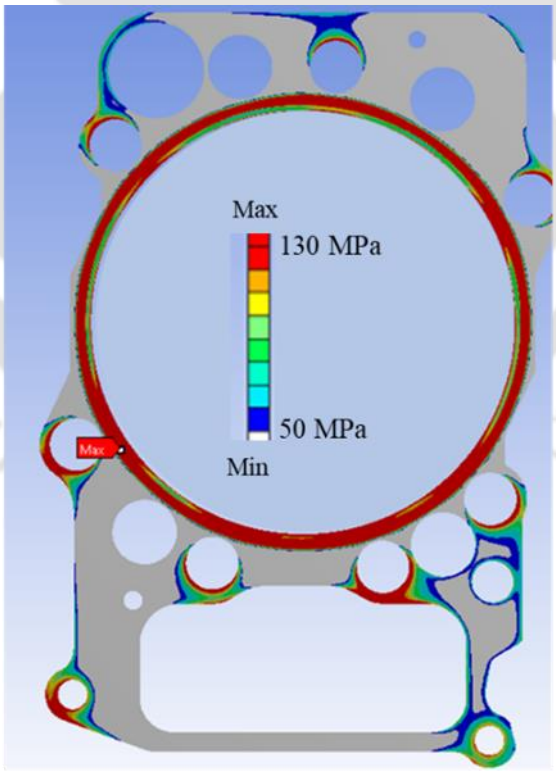

FEA contact pressure results

Figure 98: FEA gasket pressure vs Fuji pressure plot

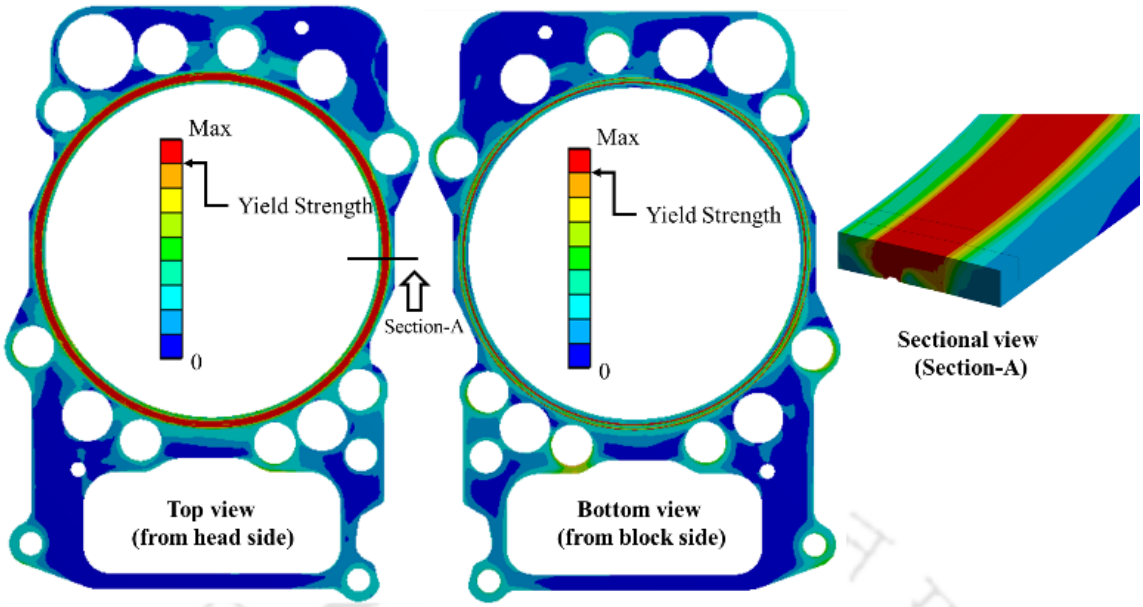

Figure 99: Equivalent stress plot of head gasket

During the scope of current work, area-based stress-strain averaging technique [171] is considered to account for the high stress gradient present below the contact surface. Stress-strain averaging is carried out over the critical dimension, around the identified critical contact surface node. The corresponding critical dimension is akin to a material property and is often comparable to the material grain size [52]. Hence, the Hall-Petch equation [172] is considered to obtain the necessary value required for stress-averaging.

Corresponding relationship between the material yield strength and the grain size is given as

$$\sigma_y = \sigma_0 + \frac{k_y}{\sqrt{d}} \tag{50}$$

where σ_y is the material yield strength, σ_0 is the material constant as the starting stress for dislocation movements (i.e., resistance of lattice to dislocation motion, corresponding value for gasket material is 70 MPa [173]), k_y is the material strengthening coefficient (corresponding value for gasket material is 0.74 [173]) and d is the resultant material grain size.

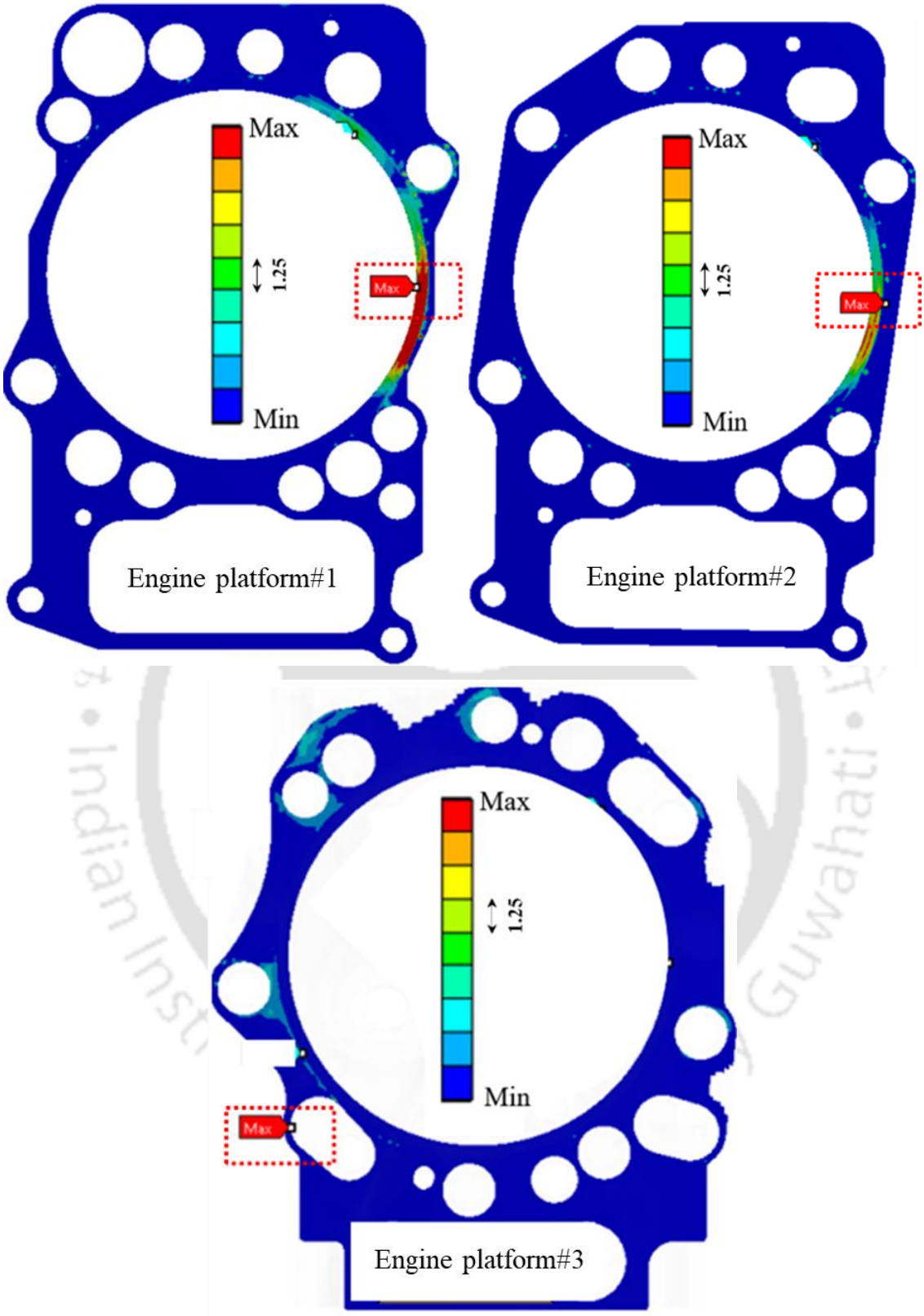

(C)

Figure 100: FEA predicted *F1* parameter results for head gaskets of three engine platforms

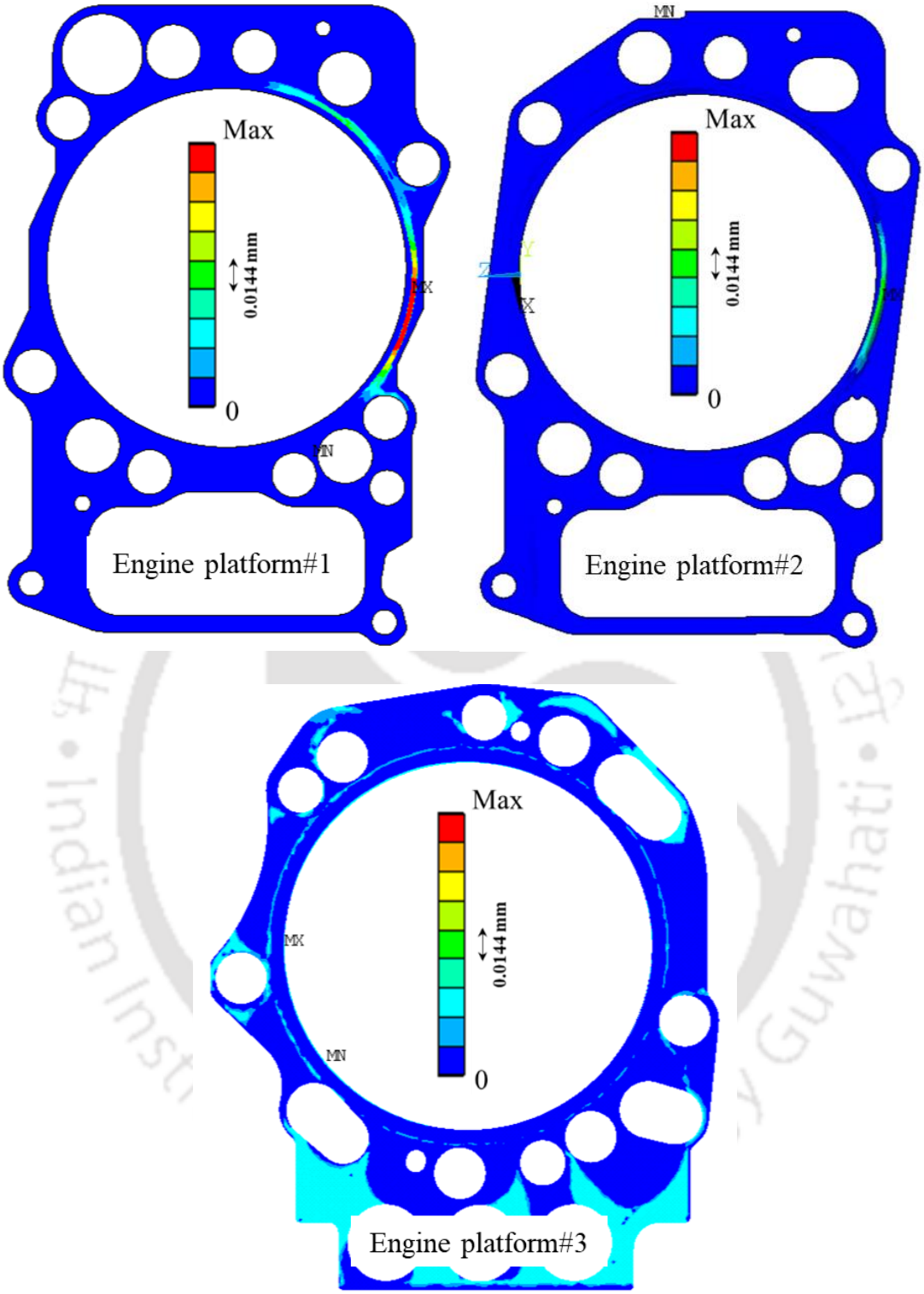

Figure 101: FEA predicted relative sliding distance (RSD) results for head gaskets of three engine platforms

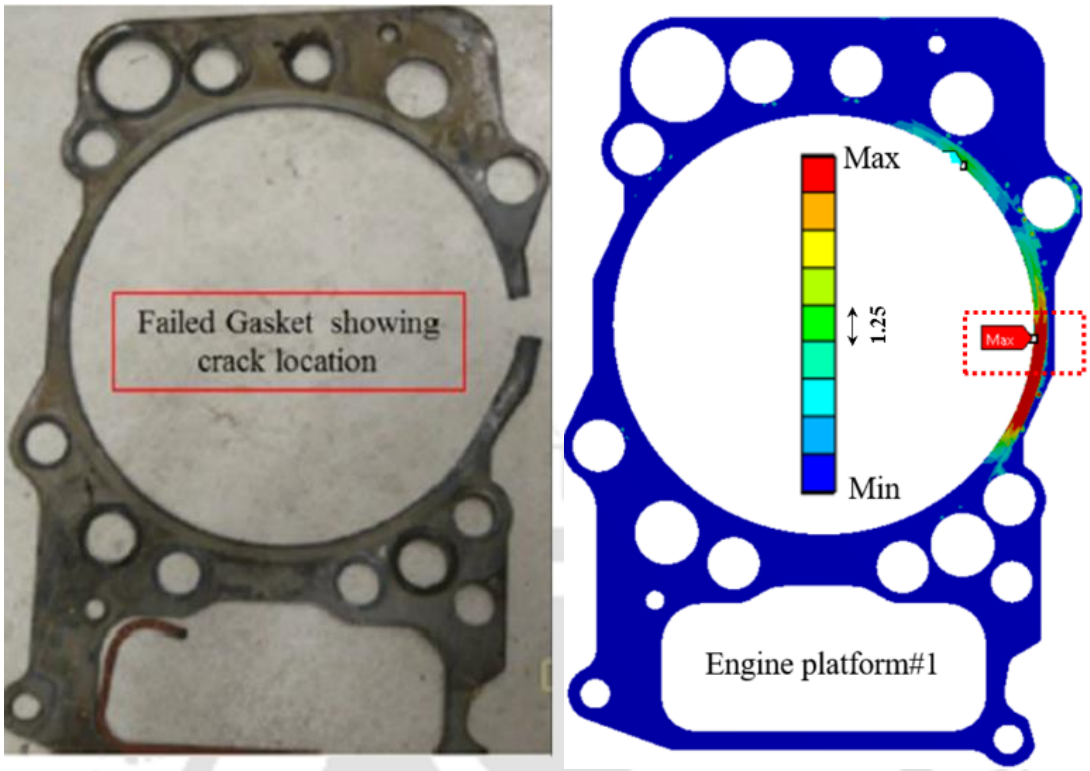

Figure 102: Correlation between FEA predicted *F1* parameter results and actual failures observed on head gasket of engine platform#1

Fretting fatigue life results for the head gaskets are extracted using the eI parameter combined with the Ding's parameter. Further, in order to consider the stress-strain averaging at the critical location, area-based stress-strain averaging technique is considered and corresponding fatigue life is evaluated at the critical location. Corresponding grain size of $17\mu m$, obtained using the Equation 51, is considered here. The averaged stress-strain values are considered to obtain the resultant fatigue life using the eI parameter, combined with the Ding's parameter, similar to the Equation 45. The resultant fretting fatigue life results for the head gaskets of three engine platforms are shown in Figure 104.

Similar to the Ruiz's parameter results, here also a similar trend is observed across the three engine platforms in terms of the minimum fretting fatigue life observed in the head gasket. Also, the predicted critical location closely correlate to the same locations, as observed through Ruiz's parameter-based results and also close to the actual failure location observed on the head gasket of engine platform#1. As shown in the Figure 105, for engine platform#1, in terms of the critical location predicted using the considered two analytical methods, there is difference of just 8 degrees in the circumferential direction.

Hence, there is a good correlation also in terms of critical location prediction. The comparative assessment between Ruiz's parameter results and deviatoric amplitude-based results are given in Figure 106 and a good correlation is observed between the two set of results across the three engine platforms considered. Thus, overall good correlation is observed in both the considered methods in terms of capturing the critical location and also in terms of results trend.

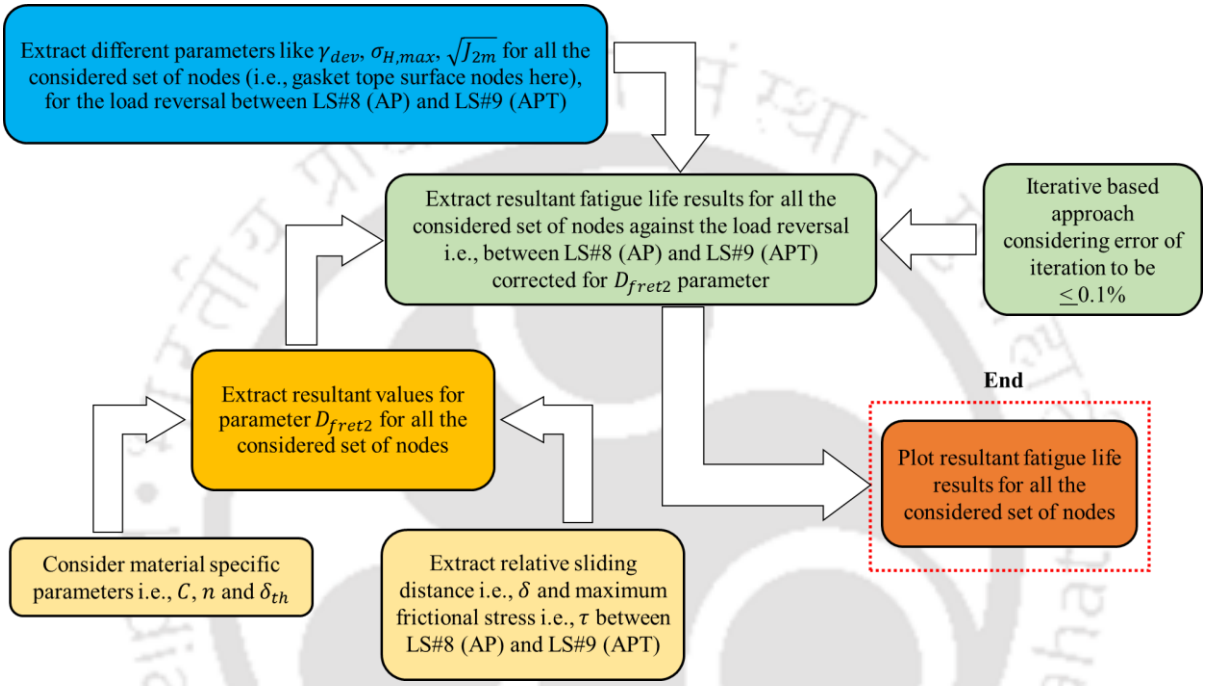

Figure 103: Flow chart of new procedure to obtain gasket's fretting fatigue life results using deviatoric strain amplitude-based parameter corrected for surface wear through Ding's parameter

Like the fretting damage predicted through the fatigue life results, fretting damage results can also be represented graphically, using the alternate 'Fretting limit line' approach. Earlier Sato et al. [15, 19], have evaluated the fretting fatigue damage for main bearing cap by considering the similar approach. On similar basis, during the scope of current work, fretting fatigue damage is evaluated. The key difference is, instead of considering the alternating stress-based limit, deviatoric strain amplitude-based FIP value corresponding to the low cycle fatigue (LCF) limit is considered. Subsequent LCF limit cycles are considered based on the current industry standard. Resultant fatigue life curve for the gasket material is already shown in Figure 95. Resultant fretting fatigue damage

results in terms of ‘Deviatoric strain amplitude-based FIP parameter’ vs ‘Relative slip magnitude’ for the head gaskets of three engine platforms are presented in Figure 107.

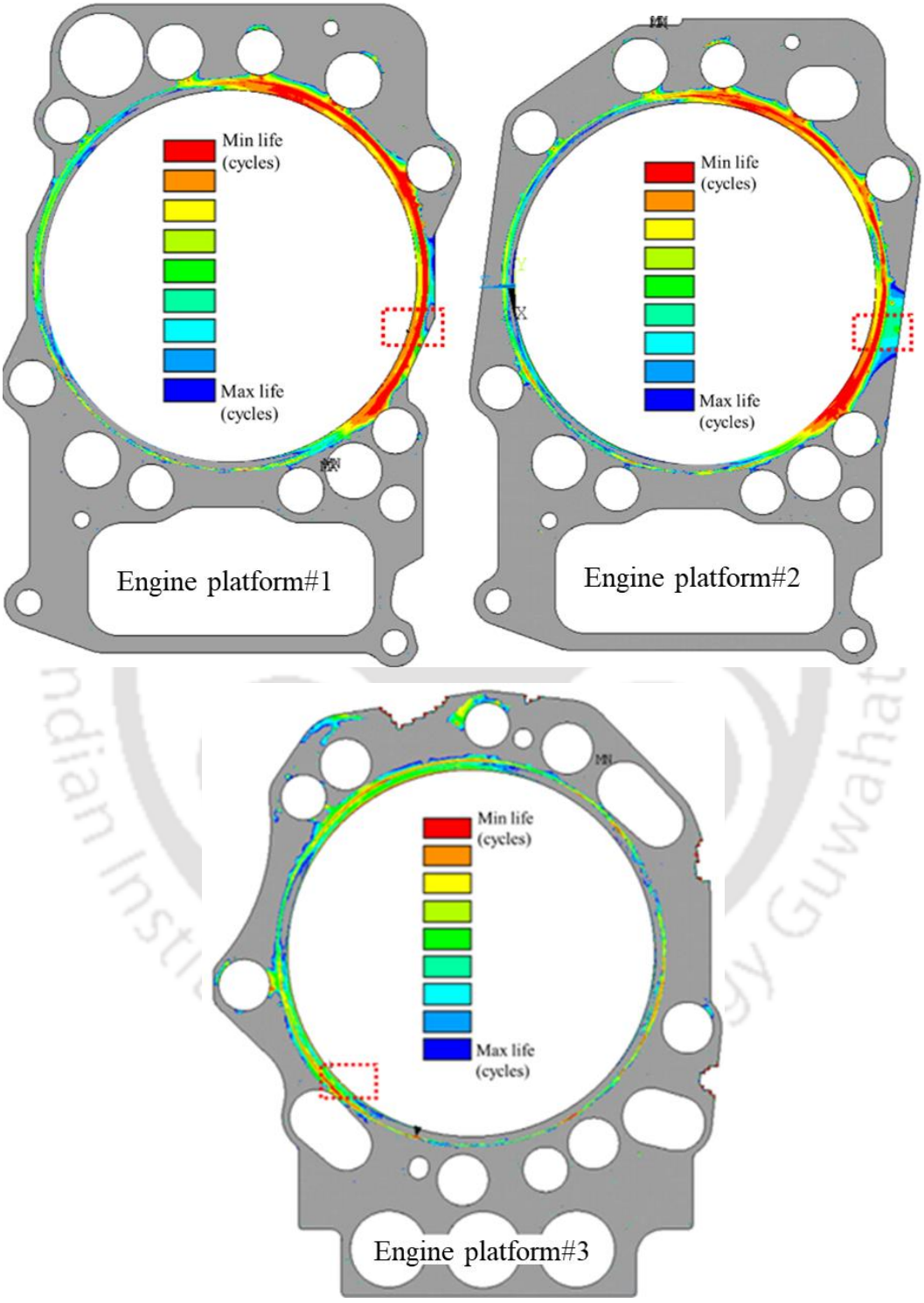

Figure 104: FEA predicted fretting fatigue life results (un-averaged) for head gaskets of three engine platforms, obtained using deviatoric strain amplitude-based parameter with Ding’s parameter

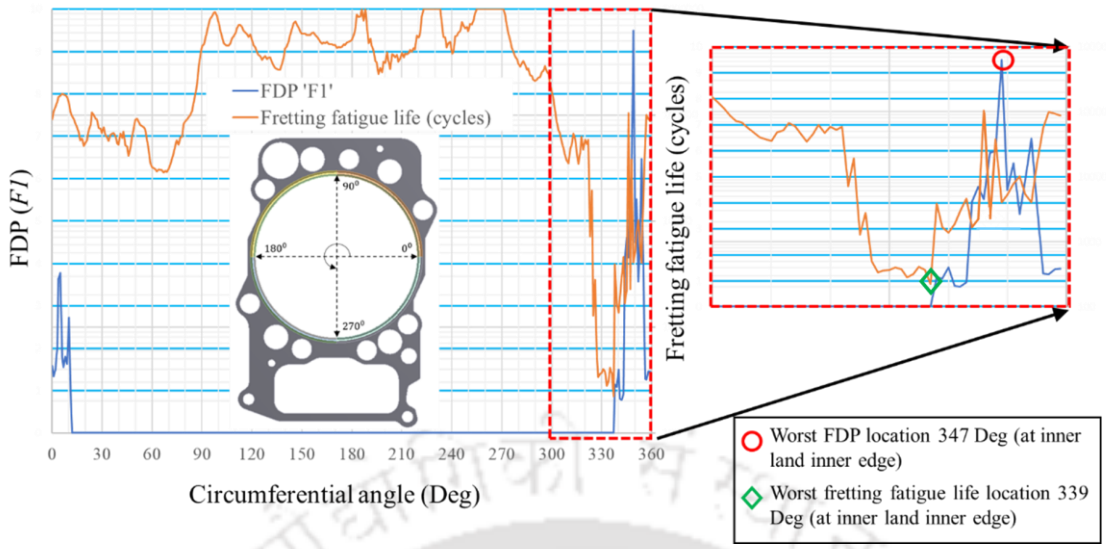

Figure 105: Comparative assessment between of critical location using FDP (*F1*) parameter and deviatoric strain amplitude-based parameter with Ding's parameter for engine platform#1

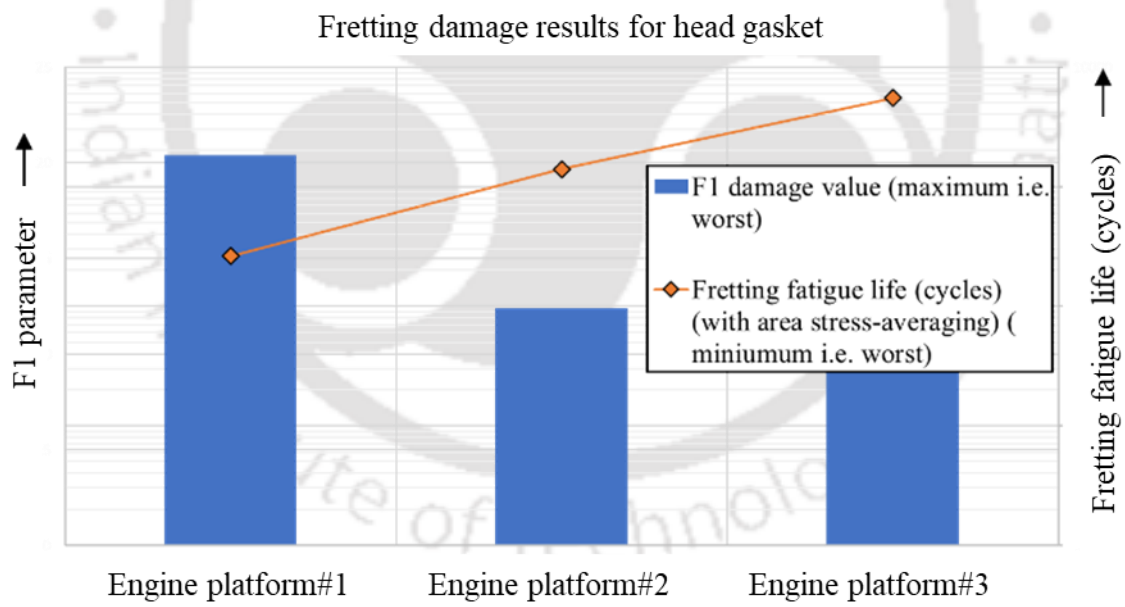

Figure 106: Correlation between *F1* parameter results and fretting fatigue life results obtained considering with deviatoric strain amplitude-based parameter corrected with Ding's parameter for three engine platforms ((with area averaging)

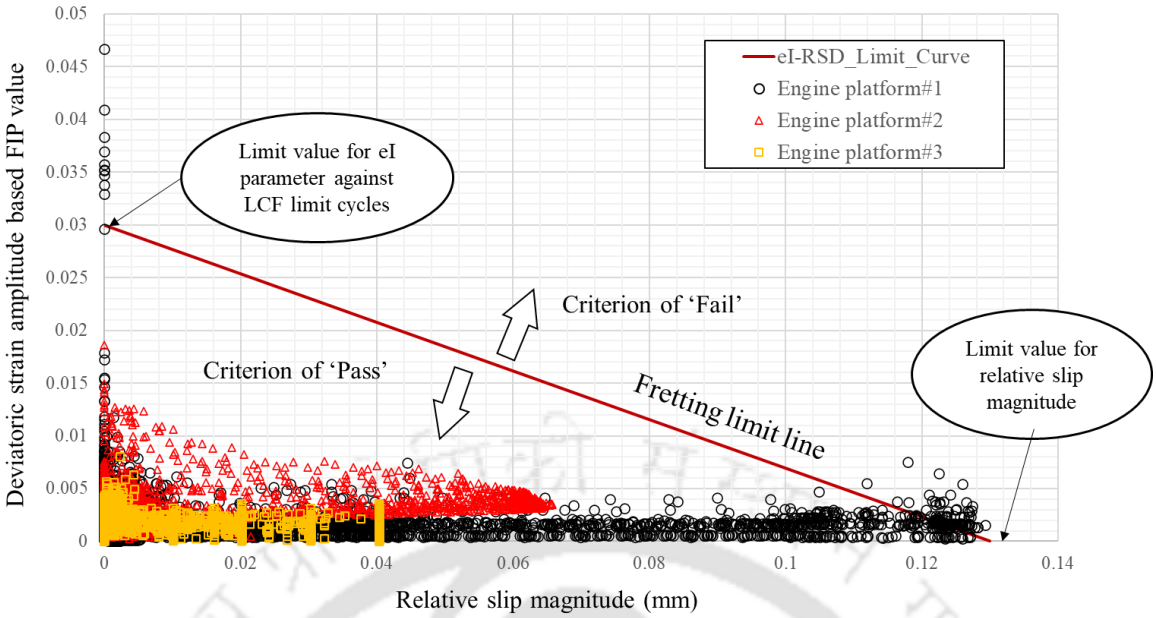

Figure 107: Fretting fatigue damage results in terms of 'Fretting limit line'

Here, the resultant values for 'Deviatoric strain amplitude-based parameter' i.e., eI parameter are without any correction applied through the Ding's parameter D_{fret2}, as the corresponding detrimental effect due to wear is considered through the corresponding relative slip magnitude values. Hence, those are not combined again with the resultant eI parameter values. Here, the fretting limit line connects the 'limit value of eI parameter corresponding to the LCF limit cycles' and 'limit value for the relative slip magnitude'. Resultant results for the gasket's top contact surface nodes are plotted on this graph in terms of Y-parameter as corresponding FIP value i.e., the deviatoric strain amplitude-based parameter and X-parameter as the 'relative sliding distance' (mm). If the corresponding nodal result/s, lie/s below the 'Fretting limit line', then it means that resultant fretting fatigue damage is within the acceptable limit and vice-versa. As observed in the Figure 107, several nodal results for 'engine platform#1' lie above the 'Fretting limit line'. Corresponding location of these nodes closely correlate with the actual critical location as observed earlier for the 'engine platform#1' (as shown earlier in Figure 102). Further the nodal results for 'engine platform#2' and 'engine platform#3' lie well below the 'Fretting limit line' and consequently, those nodal results meet the respective acceptance limit. This observed results trend, is in-line with the earlier observed results so far.

Hence, as observed through these set of results, the approach of graphical representation based on the ‘Fretting limit line’, can also be an effective option towards the absolute as well as the comparative fretting damage assessment between the different designs and should be possibly considered further for similar fretting fatigue damage assessment of different actual engine components.

भारतीय प्रौद्योगिकी संस्थान गुवाहाटी
Indian Institute of Technology Guwahati

5. CONCLUSION

The overall summary of the work is presented in this chapter, followed by the conclusions based on the overall results obtained so far. The scope of future work is discussed towards the end.

5.1. Summary

In this work, fretting fatigue life evaluation of a simple, flat-flat complete contact problem is carried out by considering the deviatoric strain amplitude based crack initiation method. Through this work, this method is considered for the first time towards the fretting fatigue damage and life evaluation. Further, to consider the effect of surface wear, Ding's parameter [102] is considered. Earlier the effectiveness of this parameter was evaluated considering the SWT parameter [102]. Through this work, its effectiveness is also evaluated for parameters like FS [23] and eI [130] FIP's. After the initial evaluation considering a simple, flat-flat complete contact pair, the approach based on combined consideration of deviatoric strain amplitude based parameter and Ding's parameter is applied to the complex case-study of actual head gasket. Fretting fatigue failure of a head gasket is comparatively lesser explored than its other failure modes [28] and therefore, is considered here as an actual case-study. Head gasket is also a flat-flat complete contact pair and hence, equivalent analogy is considered with respect to the considered flat-flat contact problem [58]. Head gasket is a critical joint of any IC engine which is designed to prevent leakage of hot, pressurized combustion gases and coolant/oil out of the designed passages.

Along with the eI parameter, other crack initiation methods like SWT and FS, are also considered during the scope of this work. The deviatoric strain amplitude based method is a non-critical plane based method whereas SWT and FS are critical plane based methods. The critical plane methods are based on the calculation of fatigue damage on different planes passing through each node of the considered FEA domain and the deviatoric strain amplitude based method calculates the fatigue life based on the scalar damage value per node. So, it does not involve the critical plane based calculations.

Therefore, it is computationally more efficient. APDL based macros are developed for the resultant fretting fatigue life evaluation against the each FIP.

The critical evaluation of the fretting damage is also dependent upon many physical and analytical parameters. Consequently, several critical parameters like material non-linearity, varying COF, effect of wear, frictional heat and normal, tangential and axial loads are considered in this work. These parameters are considered primarily based on their relevance to the considered case-study of the head gasket. Based on the initial yielding observed, different material non-linear models like BKIN, MKIN and Chaboche are considered in this work and subsequent predicted fatigue life results are obtained for each material model. Considering the possible path-dependency due to the material and contact non-linearities involved in the FEA model, required number of the duty block repetitions are considered to obtain the stabilized stress-strain conditions.

Surface condition at the contact surface gets considered through the COF. The value of COF keeps on evolving based on the corresponding contact surface condition. Hence, the effect of varying COF is considered through its variation with respect to the relative sliding distance values. The corresponding required data for AL7075-T6 is considered based on the available data for another aluminum material i.e., AL357 [148].

To consider the effect of wear due to the relative sliding between the fretting pad and fretting specimen, two methods i.e., Archard's wear model and Ding's parameter are considered in this work. The Archard's wear model is based on the progressive wear modeling approach whereas the Ding's parameter is based on consideration of fretting specific parameter.

The resultant frictional energy at the contact surface, can possibly cause increase in the surface temperature. Also, a fraction of plastic work can be converted into the thermal energy. The combined effect can further increase the surface temperature. As a result, the possible conversion of frictional energy and plastic work into the thermal energy, is considered through the coupled thermal-structural analysis and considering the 'Taylor-Quinney' coefficient.

Since the effect of normal, tangential and axial loads on the fretting fatigue life results can be geometry specific, 2D axi-symmetric FEA is carried out by considering the actual head-gasket joint. Here these loads correspond to the actual engine operating loads. For example, normal load corresponds to the bolt preload, tangential load corresponds to the

relative thermal sliding of head with respect to the gasket's contact surface and axial load corresponds to the peak cylinder pressure. The subsequent fretting fatigue life results are obtained by considering ± 10% variation in the normal, tangential and axial load values.

Finally, the fretting fatigue evaluation of actual head gasket is carried out. In order to observe the consistency in the predicted results trend, fretting damage evaluation is carried out for three different head gaskets. These three different head gaskets vary with respect to each other in terms of the geometry and resultant loads acting on the head-gasket joint. Hence, it is expected to have different fretting results across these three engine platforms based on the corresponding engine operating loads. The resultant fretting fatigue life results obtained by considering of the 'eI' and Ding's parameters, are compared with the current industry standard approach based on the Ruiz's *F1* parameter. Further, alternative approach based on 'Fretting specific limit' line is also presented towards the end.

5.2. Conclusions

Based on the results obtained in this work, following conclusions are drawn.

5.2.1. Fretting Fatigue Life Evaluation of Flat Contact Pair Using Two-Dimensional FEA

- Based on the mesh convergence study considering the contact pressure results (as shown in Figure 42), a mesh size of 15 μm is considered near the right end of the contact zone.
- After carrying out initial FEA, with the linear material properties, it is observed that the equivalent stresses near the corner are above the material yield limit over the region of radius of ~ 0.2 mm (as shown in Figure 45). The fatigue life results calculated using such stress/strain values can produce erroneous results. Therefore, appropriate material non-linearity needs to be considered to get more realistic results.
- Based on the stress-strain stabilization study, it is observed that FEA needs to be carried for 20 duty cycle blocks to achieve the stabilized stress-strain condition. Here, one duty cycle block corresponds to one complete load reversal cycle. Consequently, 20 duty cycle blocks correspond to 20 such load reversals.

- APDL macros are written to evaluate the corresponding fatigue life against the considered FIP's like SWT, FS and eI parameters. In order to validate the APDL macros, initial verification is carried out by considering the benchmark problem of plain fatigue loadings, 'SAE Keyhole Test Program' [145]. The resultant experimental correlation is observed within $\pm$ 2N scatter band. Hence, the APDL macros are found to be capable for the fretting fatigue life evaluation of the considered fretting fatigue problem [58].

- In the current work, area-based stress-strain averaging method is considered. Resultant value of the critical dimension, r_c is obtained as 55 μm, which is in reasonable agreement with the grain size of 35 μm for AL7075-T6 material [138]. Generally, this critical dimension is of the similar order of the magnitude as the material's grain size [112]. Further, compared to the surface-based method i.e., without considering any stress-strain averaging, better correlation is observed with area-based stress-strain averaging (see Figure 56–59).

- Based on the results obtained with BKIN material model with the area-based stress-strain averaging, experimental correlation is observed with $\pm$ 3N scatter band for most of the cases (see Figure 60). For few cases i.e., Test#1, 4, 7, 10 and 13, corresponding analytical life results are above the + 3N limit line. These tests are with the minimum applied normal load. With minimum normal load applied, relative sliding distance values will be higher and can possibly cause higher damage due to resultant fretting wear. This effect is not considered as the current results are without considering any wear correction/modeling.

5.2.2. Critical Parameters Towards Fretting Fatigue Damage of Flat Contact Pair Through 2D FEA

- Elleuch et al. [148] proposed a load factor and COF based criterion to identify the possible material response to the fretting loads (see Figure 61). Usually fretting specimens which are elasto-plastic in nature, usually responds to the cyclic loadings in three different ways i.e., elastic, elastic shakedown and stabilized plastic dissipation. Based on this criterion, very high load factor results (see Table 15) are predicted for the considered 15 test cases which indicates that the resultant stress-strain condition at the critical location is of the kind of 'stabilized plastic dissipation'. Therefore, in order to evaluate the most suitable material model,

material models of MKIN and Chaboche are considered in addition to the initially considered BKIN material model.

- Further, with three material models, different stabilized stress-strain conditions are observed for the 15 test cases. For certain test-cases, stabilized stress-strain condition do not vary much between three material models whereas for certain test cases, totally different stress-strain stabilization states are observed (see Figure 64). Considering this observation along with the high plastic strain values observed (i.e., around 12-14%), multi non-linear material model of Chaboche, initially appears to be more appropriate than BKIN and MKIN material models.
- After evaluating the resultant fretting fatigue life results, using three material models and considering three different FIP's, it is observed that comparable results are observed between three material models (see Figure 66–68). This can be primarily contributed to the similar alternating strain range and maximum stress values observed for three different material models (see Figure 64). Hence, the fatigue life results are also observed to be comparable between the considered three material non-linear models.
- The COF value is a critical parameter towards the fretting fatigue results. In this work, effect of varying COF with respect to the sliding distance is considered. The fretting fatigue life results obtained with the varying COF are compared with the fretting fatigue life results obtained with constant COF and it is observed that except for Test#1, 4, 7, 10 and 13, for the remaining test cases, there is not significant difference in the two set of results (see Figure 70–72). The above mentioned 5 test cases, correspond to the minimum normal load condition i.e., 2 kN. Consequently, with the increasing axial force, relative sliding distance between the contact specimens will increase and will cause higher fretting damage. The fatigue life results obtained so far, are without considering any possible effect of wear or applying any fretting specific parameter. As seen in Figure 16, as the relative sliding increases, the fretting fatigue life decreases till the threshold limit value of sliding distance and again the fretting fatigue life value starts to increase. Thus, considering these facts and observations, it is important to consider the effect of relative sliding distance while evaluating the fretting fatigue life results.

- In this work, effect of sliding distance on fretting fatigue life results is considered using two approaches, Firstly, by considering the progressive wear modeling technique of Archard's wear and then by considering the fretting specific parameter proposed by Ding et al. [102], i.e., D_{fret2}. In the Archard's model, the contact surface nodes are moved corresponding to the predicted wear depth calculated at each substep and this progressive wear modeling process continues till all the substeps are converged (see Figure 75). This process is computationally more expensive as it involves additional equilibrium iterations for the wear depth calculation. In this work, Archard's wear subroutine available in ANSYS is considered. However, it is observed that the fretting fatigue life results obtained considering Archard's wear model do not vary much as compared to the earlier results obtained without considering any wear correction (see Figure 76). Also, as shown in Figure 77, for test#15, predicted wear depth with Archard's wear model, is very low i.e., 0.0035 μm, indicating no significant loss of material. Hence, there is no change in the fretting fatigue life results also. This observation can be primarily attributed to the earlier discussed limitations in the Archard's model due to which it cannot be effectively considered in the partial slip condition, as seen in this case study.
- Alternatively, to capture the effect of sliding distance, fretting specific parameter, proposed by Ding et al. [102] is considered. This parameter as combined with the FIP's like SWT, FS and eI provide better correlation, within $\pm$ 3N. Also, it does not require progressive wear modeling approach as Archard's model needs and thus, is computationally more efficient and also more accurate. With this parameter, the effect of frictional work ($\tau\delta$) towards the fretting crack initiation gets considered, which otherwise is not considered by considering just plain fatigue initiation methods. Ding's parameter considers the corresponding deteriorating effect towards the fatigue damage value for cases where the relative sliding magnitude δ is higher than the corresponding threshold value, i.e., δ_{th}. For cases in which the relative sliding magnitude, δ is lesser than the threshold value, i.e., δ_{th} , this parameter is not applied in fatigue life calculations. Earlier, Ding et al. [102] have carried out the fretting fatigue life correlation by combining Ding's parameter, D_{fret2}, with the SWT parameter. Further, through this work, fretting fatigue life evaluation is carried out for the first time by combining the Ding's

parameter with the crack initiation methods like FS and eI. Thus, it is observed that this parameter is equally effective with other FIPs also.

- In order to convert the frictional heat and plastic work into the corresponding thermal energy, coupled field analysis is carried out and it is observed that, for all the 15 test cases, frictional dissipated energy leads to the surface temperature increase in the range of 30.87 °C to 45.6 °C for the fretting specimen (see Table 23). This increased temperature is not sufficient to change the material properties of AL7075-T6. Hence, further consideration of frictional energy on fretting fatigue life results is not considered.
- Effect of fretting loads like normal, tangential and axial loads is studied by considering a 2D axi-symmetric FEA model, representing the actual head gasket joint. With the considered $\pm$ 10% variation, it is observed that the axial load which represents the PCP, is the most significant factor in order to cause possible change in the gasket's fretting fatigue life. The next critical parameter is the normal load, which represents the bolt preloads in actual head gasket joint. Comparatively the tangential load is not observed to cause much change in the resultant fretting fatigue life results. The 2D FEA is effective to quickly identify the significant parameters towards the fretting fatigue life results. However, in order to evaluate the actual change in fatigue cycles, 3D FEA should be carried out.

5.2.3. Fretting Fatigue Analysis of Actual Head Gasket Joint Through 3D FEA

- Based on the observations so far, it is observed that deviatoric strain amplitude-based parameter i.e., eI, further combined with the Ding's parameter, D_{fret2} is able to obtain the experimental correlation within $\pm$ 3N, for the considered flat-flat complete contact reference problem [58]. Also, as compared to the other considered FIP's like SWT and FS parameters, it does not need the critical plane based calculations. Further, it is strain based parameter and as a result, it can be considered in both LCF and HCF regime. Hence, it is considered during the fretting fatigue evaluation of the identified case-study of actual head gasket using 3D FEA.
- Overall, very good correlation is observed between the Ruiz's parameter *F1* results and results obtained using the deviatoric strain amplitude-based parameter, corrected for the surface wear through the Ding's parameter, D_{fret2}. Further, the

fretting fatigue results trend also matches very well across the considered three engine platforms. Further, the eI parameter has an advantage over the Ruiz's parameter in terms of its capability to compute the resultant fatigue life results which can be compared with the target design life and being strain-based parameter, it can be considered in cases where material yielding is expected.

- Further, through this study it is observed that for the IC engine components like head gasket, the effect of resultant surface wear damage on the fretting fatigue life results can be considered through the fretting specific parameters like Ding's parameter. It does not require computational expensive progressive wear modeling techniques like Archard's wear. Hence, it is a promising and computationally effective approach for fretting fatigue damage evaluation of complex mechanical systems like head gasket.
- Also, in addition to the approach of calculation of fatigue life results using the eI parameter, combined with the Ding's parameter, alternative approach of 'Fretting limit line' can also be effectively considered for the absolute and comparative fretting fatigue damage assessment across different designs. Similar evaluation using the Ruiz's parameter/s is not possible.

5.3. Scope for Future Work

In this section, the possible scope for future work is discussed.

- In this work, deviatoric strain amplitude-based parameter is considered for the fretting fatigue life evaluation of the head gasket. Similarly, other non-critical plane-based methods like 'Continuum damage mechanics' based methods [89], can be also evaluated for the fretting fatigue damage and life evaluation of actual mechanical system components like IC engine components etc.
- Also, similar to the head gasket, the fretting fatigue damage of other IC engine components can be evaluated using the considered approach.
- To consider the effect of wear due to sliding distance, two approaches i.e., Archard's wear model and Ding's parameter are considered. The results obtained considering the Archard's wear model, do not show any change in the predicted fretting fatigue life results. This can be associated to the earlier discussed

limitations of the Archard's wear model. Similarly, there are other possible wear theories like 'Energy wear' based approach [116], which can be considered to evaluate the individual contribution in the fretting damage cases with the partial slip condition.

- In this work, different fretting loads like normal, tangential and axial loads, corresponding to the engine operating loads are evaluated based on 2D axi-symmetric FEA results. In order to check for the resultant quantitative evaluation in terms of fretting fatigue damage and life results, actual 3D FEA can be carried out in future. Such study can be effective towards the risk assessment and prioritization of critical parameters towards the fretting fatigue damage evaluation of the head gasket.
- Recently 'Machine Learning' (ML) based fretting fatigue damage and life evaluation has been carried out [160, 174–176]. On similar basis, ML based approach can be considered in the fretting fatigue damage and life evaluation of actual engine parts in terms of creation of database which can be used towards new product development as well as towards field failure investigation.

भारतीय प्रौद्योगिकी संस्थान गुवाहाटी
Indian Institute of Technology Guwahati

APPENDIX A

OPTIMIZATION OF DIESEL ENGINE'S LINER GEOMETRY TO REDUCE HEAD GASKET'S FRETTING DAMAGE

To minimize the fretting damage risk to the steel gasket, full factorial 'design of experiment (DOE) based on Ruiz parameter (*F1*) is carried out to identify an optimized liner bite ring geometry. DOE-predicted results based on 2D axisymmetric FEA, are further validated using full 3D FEA, with the boundary conditions consistent with the operating conditions known to accompany the fretting damage.

A.1 Overall Analysis Approach for Liner Bite Ring Optimization

To minimize the gasket's fretting damage and the subsequent increase in the joint's robustness, one of the possible approaches is to carry out the liner bite ring optimization based on the DOE technique. However, for DOE, specific minimum design points need to be solved to correctly capture the design trend, identify the critical design features, and further obtain the optimized solution. During the earlier investigation, it is observed that around six to seven days of computational time is required for the 3D FEA of a single design point. Observing such a long run time, it is believed that if DOE work is carried out in a 2D axisymmetric FEA environment, it will be a much more computationally efficient way. Based on the optimized liner bite ring geometry obtained through the DOE based on 2D FEA results, final validation is carried out in a 3D FEA environment with the actual engine loads. This step of 3D validation of the optimized design point is necessary considering the non-axisymmetric loads like temperature distribution across the entire system and geometry variation in casted parts like head and blocks. The overall analysis approach considered during the scope of liner bite ring optimization study using DOE is shown using the process flow as given in Figure 108.

The contents of present chapter have been published in 'A. P. Ozarde, J. Narayan, D. Yadav, G. McNay and S. S. Gautam, "Optimization of diesel engine's liner geometry to reduce head gasket's fretting damage", SAE International Journal of Engines, vol. 14(1), 2021, doi: 10.4271/03-14-01-0006'.

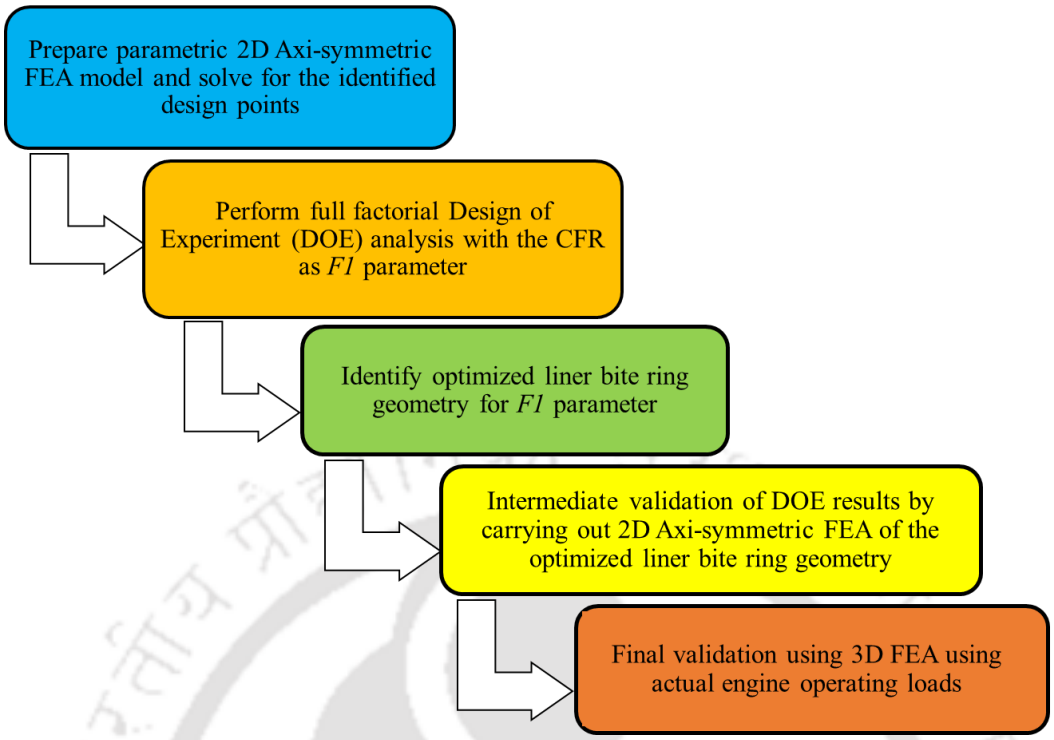

Figure 108: Overall analysis approach's process flow considered in the scope of liner bite ring optimization work

A.2 Full Factorial DOE Analysis and Verification Using 3D FEA

Full factorial DOE analysis is carried out to identify all the significant main factors and interactions for total 2^n experiments, where 'n' is the number of independent variables with two levels [177]. Full factorial DOE analysis is carried out, with two levels against each of the six design parameters. Corresponding details are given in the Table 31. With total of six design parameters and two levels against each parameter; in total 64 FEA runs are solved for carrying out the full factorial DOE analysis. Here, linear behavior is assumed between the two levels of each parameter.

For these 64 design points, the results for Ruiz parameter *F1* are obtained using the APDL postprocessing script. Further, Minitab tool (version Minitab19) is considered for analyzing the obtained data. Considering the p-value limit of 0.05 towards the requirement of the null hypothesis [178], significant main factors and interactions are identified towards the considered "Critical Functional Response" (CFR) of *F1*. A significance level of 0.05 indicates a 5% risk of concluding that an association exists

when there is no actual association [179]. The pareto chart for the considered CFR of *F1* after removing the insignificant terms (both main factors and interaction terms) is shown in Figure 109. Based on the DOE results, it is observed that the inner land width parameter, i.e., "*E*" is observed to be the most significant parameter towards *F1*.

Table 31: Considered DOE parameters and corresponding considered levels

	Parameter	Nominal value (unit)	Lower level (unit)	Higher level (unit)
1	Angle at inner side	A_n (Deg)	$A_n - 0.1$ (Deg)	$A_n + 0.1$ (Deg)
2	Angle at outer side	B_n (Deg)	$B_n - 0.1$ (Deg)	$B_n + 0.1$ (Deg)
3	Bite ring width	C_n (mm)	$C_n - 0.1$ (mm)	$C_n + 0.1$ (mm)
4	Outer land depth	D_n (mm)	$D_n - 0.1$ (mm)	$D_n + 0.1$ (mm)
5	Inner land width	E_n (mm)	$E_n - 0.1$ (mm)	$E_n + 0.1$ (mm)
6	Height difference	F_n (mm)	$F_n - 0.1$ (mm)	$F_n + 0.1$ (mm)

Here, though the interaction term AD falls below the significance line, it cannot be omitted as it is required in another higher-level interaction term of ACD. Hence, as the hierarchical requirement of the DOE model [180], it has to be kept within the DOE scope. Based on the observed value of R-sq of ~83%, it can be interpreted that the model is able to explain approximately 83% of the variation in the response, whereas with the R-sq(pred) value of ~68%, the model is having a predictive ability of approximately 68% for new observations of the response. The DOE predicted regression equation for the CFR of *F1* is

$$\begin{aligned} F1 = {} & 1.20 - 0.0647C - 8.2A - 70.9F + 1.957B + 336E + 0.175AC + 0.926CF - \\ & 2.66CE + 204.6AF - 3.646AB - 724AE - 11.65BF - 3.75BE - 2.344ACF \\ & + 5.94ACE + 22.66ABF \end{aligned} \quad (51)$$

where *A* is value of "Angle at inner side" parameter, *B* is value of "Angle at outer side" parameter, *C* is value of "Bite ring width" parameter, *D* is value of "Outer land depth" parameter, *E* is value of "Inner land width" parameter and *F* is value of "Height difference" parameter.

Further, using the response optimizer feature provided in Minitab, optimized levels of six design parameters are obtained, which are shown in Table 32.

Considering these values in the regression equation i.e., Equation 51, *F1* results are observed to be improved by 23.4% as compared to the baseline. Additionally, 2D FEA is also carried out with the optimized liner bite ring geometry and a 24.4% reduction in fretting damage parameter *F1* is observed, as shown in Figure 111. Hence, the trend matches between the DOE predicted and actual FEA results for *F1*, for the optimized liner geometry.

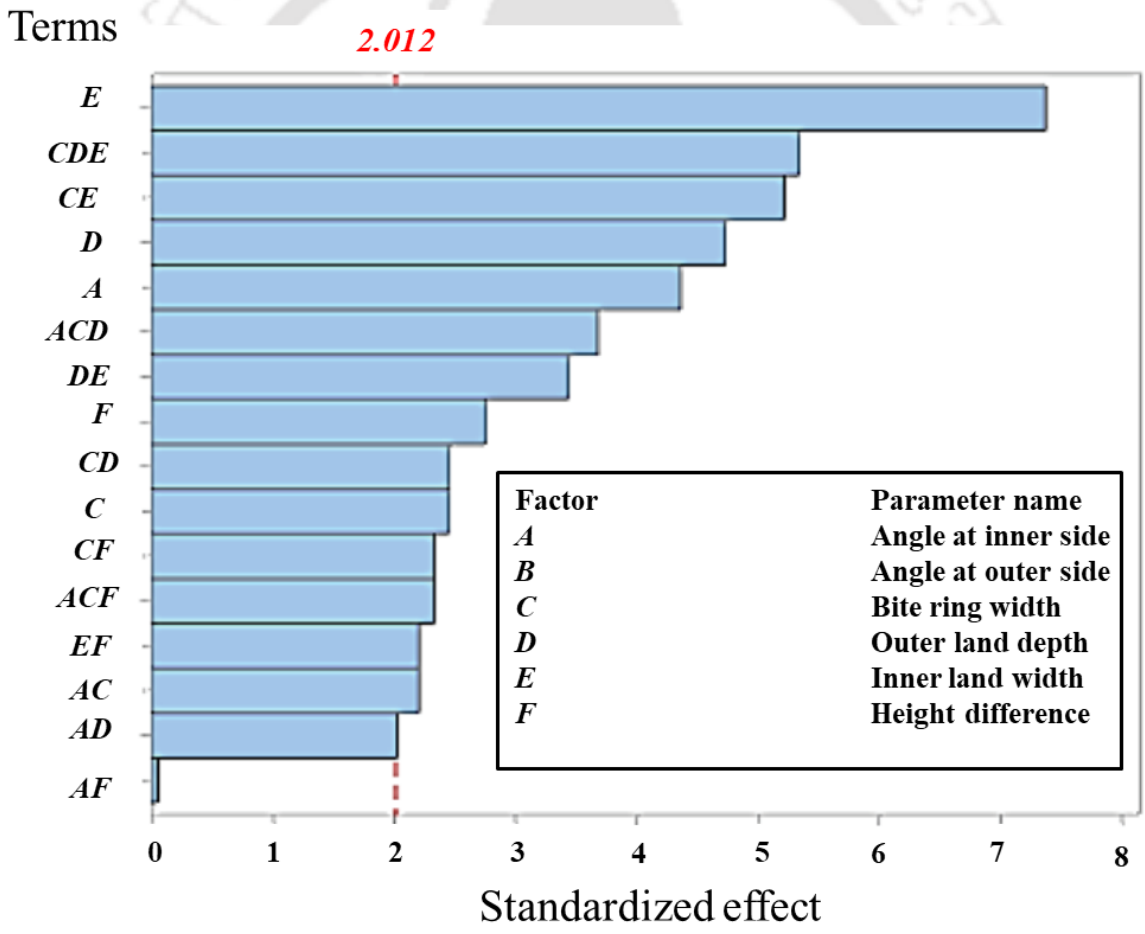

Figure 109: Pareto chart of the standardized effects for *F1* (α= 0.05)

Table 32: Optimized design parameters obtained through DOE

	Parameter	Nominal value (unit)	Optimized level (unit)
1	Angle at inner side	A_n (Deg)	$A_0 = A_n + 0.7$ (Deg)
2	Angle at outer side	B_n (Deg)	$B_0 = B_n - 2.0$ (Deg)
3	Bite ring width	C_n (mm)	$C_0 = C_n - 0.1$ (mm)
4	Outer land depth	D_n (mm)	$D_0 = D_n + 0.04$ (mm)
5	Inner land width	E_n (mm)	$E_0 = E_n + 0.3$ (mm)
6	Height difference	F_n (mm)	$F_0 = F_n + 0.01$ (mm)

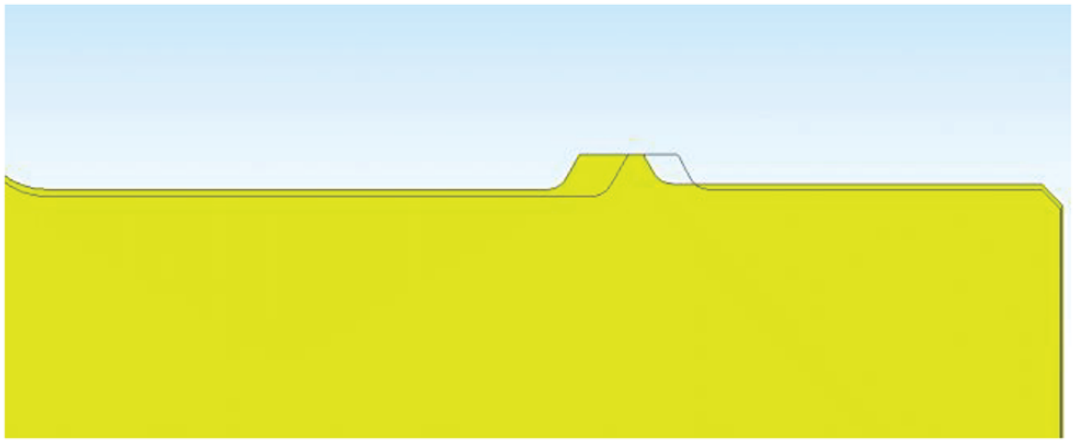

Figure 110: Comparison between baseline liner geometry (highlighted in yellow colour) and optimized liner geometry (transparent wireframe).

In 2D axisymmetric FEA, certain assumptions are considered against some of the actual non-axisymmetric features like actual system-level temperature distributions, corresponding thermal deformation of different engine parts compared to actual variation in 3D FEA. Therefore, to verify the actual improvement in the fretting damage results, 3D FEA analysis is required to be carried out. The cross-sectional view of the baseline versus the modified liner geometry is shown in Figure 110 and the corresponding comparative assessment of the *F1* parameter results, as observed in the 3D FEA models with the baseline and modified liner, is shown in the Figure 111.

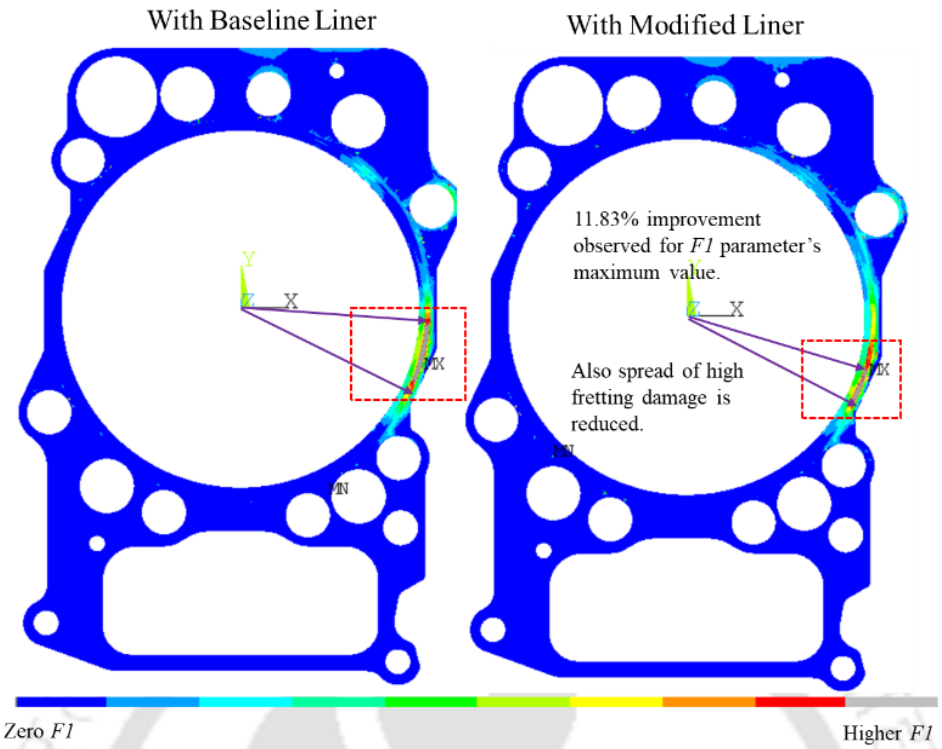

Figure 111: Fretting fatigue results (*F1*) comparison between baseline and optimized liner geometries

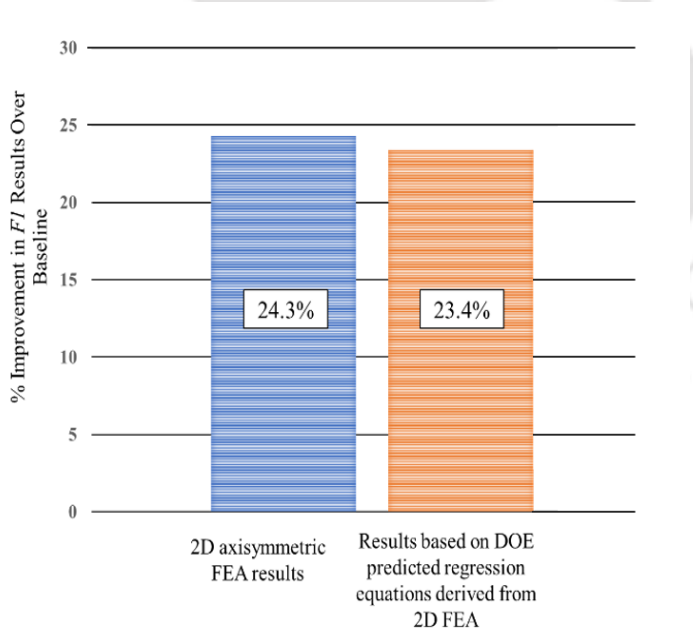

Figure 112: Comparison between *F1* results obtained during 2D evaluation stage

The optimized liner geometry obtained through DOE shows significant improvement in the Ruiz parameter *F1* results. As shown in the Figure 89, the considered approach of carrying out DOE with 2D FEA to obtain the optimized liner geometry has not only

contributed towards the initial aim of reducing the gasket fretting damage results but also provided a significant reduction in computation time otherwise required with 3D FEA.

भारतीय प्रौद्योगिकी संस्थान गुवाहाटी
Indian Institute of Technology Guwahati

REFERENCES

[1] S. Shaffer and W. Glaeser, "Fretting fatigue," in *ASM Handbook on Fatigue and Fracture, Volume 19*, ASM International, 1996, pp. 321-330.

[2] R. B. Waterhouse, "A historical introduction to fretting fatigue," in *Standardization of Fretting Fatigue Test Methods and Equipment*, Philadelphia, USA, ASTM International, 1992, pp. 8-12.

[3] F. L. Bohm, "Surface durability of dry coaxial splines," in *SAE International Off-Highway & Powerplant Congress & Exposition*, Milwaukee, WI, Sept 11-13, 2000.

[4] D. A. Hills and D. Nowell, Mechanics of Fretting Fatigue, Dordrecht, Netherlands: Kluwer Academic Publishers, 1994.

[5] T. Zhang, "Fretting wear-fatigue study of tribologically induced damage in simple and complex geometries," National University of Ireland, Galway, 2012.

[6] P. R. Maia and L. C. R. Lopes, "Analysis of fretting fatigue processes in a sphere-plan contact via FEM, SAE Technical Paper 2013-36-0177," in *22nd SAE Brazil International Congress and Display*, São Paulo, Brazil, 2013.

[7] B. G. Brady, "Fretting wear," *SAE Transactions, Journal of Aerospace, Part 2*, vol. 99, no. 1, pp. 1344-1360, 1990.

[8] K. Masanobu and K. Hirakawa, "The effect of rubber contact on the fretting fatigue strength of railway wheel tire," *Tribology International*, vol. 42, no. 9, pp. 1389-1398, 2009.

[9] M. Dębiński and M. Brezáni, "Fretting wear as an example of destruction of railway vehicles wheelsets," *New Trends in Production Engineering*, vol. 1, no. 1, pp. 371-376, 2018.

[10] R. E. Hobbs and M. Raoof, "Mechanism of fretting fatigue in steel cables," *International Journal of Fatigue*, vol. 16, no. 4, pp. 273-280, 1994.

[11] D. W. Hoeppner and V. Chandrasekaran, "Fretting in orthopaedic implants: A review," *Wear*, vol. 173, no. 1-2, pp. 189-197, 1994.

[12] Riviera Maritime Media Ltd, "Diesel engine fretting fatigue must be understood," 15 Sep 2008. [Online]. Available: ttps://www.rivieramm.com/news-content-hub/diesel-engine-fretting-fatigue-must-be-understood-52764. [Accessed September 2019].

[13] J. H. Son, S. C. Ahn and J. G. Bae, "Fretting damage prediction of connecting rod of marine diesel engine," *Journal of Mechanical Science and Technology*, vol. 25, no. 2, pp. 441-447, 2010.

[14] K. Nice, "How rotary engines work," 9 February 2021. [Online]. Available: https://auto.howstuffworks.com/rotary-engine5.htm. [Accessed 5 August 2021].

[15] K. Sato, T. Hamakawa, T. Yamasaki, Y. Ishihara, H. Hashimoto, C. Shi, H. Haneda and S. Takahashi, "Fretting analysis of an engine bearing cap using computer simulation," *SAE International Journal of Engines,* vol. 9, no. 3, pp. 1847-1853, 2016.

[16] C. Ruiz, P. H. B. Boddington and K. C. Chen, "An investigation of fatigue and fretting in a dovetail joint," *Experimental Mechanics,* vol. 24, pp. 208-17, 1984.

[17] X. Li, Z. Zuo and W. Qin, "Fretting fatigue mechanism of bearing cap bolted joints," *Review of Scientific Instruments,* vol. 85, pp. 1-12, 2014.

[18] *Cummins internal reference document,* Cummins Inc., 2013.

[19] C. Shi, K. Sato, T. Hamakawa, Y. Ishihara and S. Takahashi, "Prediction of fretting fatigue in engine cylinder block SAE Technical Paper 2016-01-0382," in *SAE 2016 World Congress and Exhibition,* Detroit, USA, 2016.

[20] J. Wang, H. Xu, T. Su, Y. Zhang, Z. Guo, H. Mao and Y. Zhang, "Fretting fatigue experiment and analysis of AlSi9Cu2Mg alloy," *Materials,* vol. 9, no. 12, pp. 1-13, 2016.

[21] S. Cha, H. Chang, K.-W. Lee, S.-S. Chao and D.-H. Hwang, "A development of the fretting fatigue analysis techniques for engine aluminum block," *SAE International Journal of Materials and Manufacturing.,* vol. 4, no. 1, pp. 613-619, 2011.

[22] K. Smith, T. Topper and P. Watson, "A stress-strain function for the fatigue of metals," *Journal of Materials,* vol. 5, no. 4, pp. 767-78, 1970.

[23] A. Fatemi and D. Socie, "A critical plane approach to multi-axial fatigue damage including out-of-phase loading," *Fatigue & Fracture of Engineering Materials & Structures,* vol. 11, no. 3, pp. 149-165, 1988.

[24] P. Huo, J. Wang and R. Gao, "Study on the fretting wear failure in the cylinder block of a diesel engine," *Advanced Materials Research,* Vols. 199-200, no. 8, p. 754, 2011.

[25] D. Merritt and G. Zhu, "The prediction of connecting rod fretting and fretting initiated fatigue fracture," *SAE Journal of Engines,* vol. 113, no. 3, pp. 1633-1638, 2004.

[26] M. Rebbert, J. Dohmen and F. Maassen, "Plain bearings in high performance engines - Simulation tools for advanced investigations and layouts, SAE Technical Paper 2006-01-1102," in *SAE 2006 World Congress & Exhibition,* Detroit, USA, 2006.

[27] J. Chao, "Fretting-fatigue induced failure of a connecting rod," *Engineering Failure Analysis,* vol. 96, pp. 186-201, 2019.

[28] T. Brewer and X. Chen, "Cylinder head gasket fretting/scrub mechanism investigation and analysis procedure developments, SAE Technical Paper 2017-01-1091," in *SAE World Congress Experience,* Detroit, 2017.

[29] A. P. Ozarde, G. H. McNay and S. S. Gautam, "Fretting fatigue failures in internal combustion engine components: A review and future scope," *SAE International Journal of Engines,* vol. 14, no. 2, pp. 211- 234, 2021.

[30] M. R. Hirsch and R. Neu, "Friction and fretting study of thin sheet metal," in *SIMULIA Customer Conference*, Providence, RI., 2010.

[31] D. Sangle, A. P. Ozarde and G. H. McNay, "Cylinder head gasket fretting simulation for high horse power engine," *SAE International Journal of Advances and Current Practices in Mobility,* vol. 1, no. 1, pp. 133-136, 2019.

[32] J. F. Archard, "Contact and rubbing of flat surfaces," *Journal of Applied Physics,* vol. 24, no. 8, 1953.

[33] F. Popielas, C. Chen and S. Obermaier, "CAE approach for multi-layer-steel cylinder head gaskets, SAE Technical Paper 2000-01-1348," in *SAE 2000 World Congress*, Detroit, USA, 2000.

[34] A. Mäntylä and C. Lönnqvist, "Fretting simulation for crankshaft-counterweight contact," in *SIMULIA Customer Conference*, London, UK, 2009.

[35] Y. Wang, L. Wu, S. Liu, M. Li and Y. Cui, "Fretting fatigue optimization of piston skirt top surface of marine diesel," *Journal of Mechanical Engineering Science,* vol. 233, no. 4, pp. 1-17, 2018.

[36] T. Christiner, W. Eichlseder, I. Gódor, J. Reiser, F. Trieb and R. Stuehlinger, "Fretting fatigue and wear: Experimental investigations and numerical simulation, SAE Technical Paper 2011-01-0199," in *SAE 2011 World Congress & Exhibition*, Detroit, USA, 2011.

[37] J. Goodman, Mechanics Applied to Engineering, London: Longmans Green, 1899.

[38] J. Draper, Modern Metal Fatigue Analysis, Warrington, UK: EMAS Publications, 2008.

[39] C. R. Soderberg, "Working stresses," *Journal of Applied Mechanics, Transactions of ASME,* vol. 16, pp. 131-144, 1935.

[40] J. Morrow, "Fatigue properties of metals," in *SAE Fatigue Design Handbook,* SAE International, 1968, pp. 21-30.

[41] O. H. Basquin, "The exponential law of endurance tests," *American Society for Testing Materials Proceedings,* vol. 10, pp. 625-630, 1910.

[42] J. A. Bannantine, J. J. Comer and J. L. Handrock, "Strain-Life," in *Fundamentals of Metal Fatigue Analysis,* New Jersey, Prentice Hall, 1989, pp. 40-87.

[43] L. F. Coffin, "A study of the effects of cyclic thermal stresses on a ductile metal," *Transactions of ASME,* vol. 76, no. 6, pp. 931-949, 1954.

[44] S. S. Manson, "Behaviour of materials under conditions of thermal stresses," *Heat Transfer Symposium, University of Michigan Engineering Research Institute,* pp. 9-75, 1953.

[45] FE-SAFE, "Fatigue Theory Reference Manual-Volume 2," Safe Technology Ltd., 2002.

[46] R. Leist and Y. Shi, "Validation of a crack initiation life analysis procedure," *SAE Journal of Aerospace,* vol. 109, no. 1, pp. 10-29, 2000.

[47] G. Chen and Z. Zhou, "Study on transition between fretting and reciprocating sliding wear," *Wear,* vol. 250, no. 1-12, p. 665–672, 2001.

[48] O. Vingsbo and S. Soderberg, "On fretting maps," *Wear,* vol. 126, no. 2, pp. 131-147, 1988.

[49] M. P. Szolwinsk and T. N. Farris, "Mechanics of fretting fatigue crack formation," *Wear,* vol. 198, no. 1-2, pp. 93-107, 1996.

[50] J. Dobromirski, "Variables of fretting process: Are there 50 of them?," in *Standardization of Fretting Fatigue Test,* vol. 1159, Philladelphia, USA, ASTM International, 1992, pp. 60-68.

[51] M. Pujatti, M. Suhadolc and D. Piculin, "Fretting-initiated fatigue in large bore engines connecting rods," *Procedia Engineering, XVII International Colloquium on Mechanical Fatigue of Metals (ICMFM17),* p. 356 – 359, 25-27 July 2014.

[52] N. A. Bhatti and M. A. Wahab, "Fretting fatigue crack nucleation: A review," *Tribology International,* vol. 121, pp. 121-138, 2018.

[53] N. A. Bhatti and M. A. Wahab, "A numerical investigation on critical plane orientation and initiation lifetimes in fretting fatigue under out of phase loading conditions," *Tribology International,* vol. 115, p. 307–318, 2017.

[54] W. Findley, J. Coleman and B. Hanley, "Theory for combined bending and torsion fatigue with data for SAE 4340 steel," Brown University Providence, Engineering Materials Research Lab, 1956.

[55] H. Lee, O. Jin and S. Mall, "Fretting fatigue behavior of Ti–6Al–4V with dissimilar mating materials," *International Journal of Fatigue,* vol. 26, no. 4, pp. 393-402, 2004.

[56] H. Murthy, G. Mseis and T. N. Farris, "Life estimation of Ti–6Al–4V specimens subjected to fretting fatigue and effect of surface treatments," *Tribology International,* vol. 42, no. 9, pp. 1304-1315, 2009.

[57] D. L. McDiarmid, "A general criterion for high cycle multiaxial fatigue failure," *Fatigue & Fracture of Engineering Materials & Structures,* vol. 14, no. 4, pp. 429-453, 1991.

[58] M. Sabsabi, E. Giner and F. J. Fuenmayor, "Experimental fatigue testing of a fretting complete contact and numerical life correlation using X-FEM," *International Journal of Fatigue,* vol. 33, no. 6, pp. 811-822, 2011.

[59] C. Navarro and J. Domı´nguez, "Initiation criteria in fretting fatigue with spherical contact," *International Journal of Fatigue,* vol. 26, no. 12, p. 1253–1262, 2004.

[60] C. Navarro, S. Mun˜oz and J. Domı´nguez, "On the use of multiaxial fatigue criteria for fretting fatigue life assessment," *International Journal of Fatigue,* vol. 30, no. 1, pp. 32-44, 2008.

[61] C. D. Lynkins, S. Mall and V. Jain, "A shear stress-based parameter for fretting fatigue crack initiation," *Fatigue & Fracture Engineering Materials & Structures,* vol. 24, no. 7, pp. 461-473, 2001.

[62] O. Jin and S. Mall, "Effects of slip on fretting behavior: Experiments and analyses," *Wear,* vol. 256, no. 7-8, pp. 671-684, 2004.

[63] T. Matake, "An explaination on fatigue limit under combined stress," *Bulletin of the JSME,* vol. 20, no. 1, pp. 257-263, 1997.

[64] X. Li, Z. Zuo and W. Qin, "A fretting related damage parameter for fretting fatigue life prediction," *International Journal of Fatigue,* vol. 73, pp. 110-118, 2015.

[65] M. W. Brown and K. J. Miller, "A theory for fatigue under multiaxial stress-strain conditions," *Proceedings of the Institute of Mechanical Engineers,* vol. 187, no. 1, pp. 745-756, 1973.

[66] D. Socie, "Critical plane approaches for multiaxial fatigue damage assessment," *Advances in Multiaxial Faituge, ASTM STP 1191*, pp. 7-36, November 1993.

[67] M. P. Szolwinski and T. N. Farris, "Observation, analysis and prediction of fretting fatigue in 2024-T351 aluminum alloy," *Wear,* vol. 221, no. 1, pp. 24-36, 1998.

[68] J. Fash, D. Socie and D. McDowell, "Fatigue life estimates for a simple notched component under biaxial loading," *Multiaxial Fatigue ed. K. Miller and M. Brown (ASTM International),* pp. 497-513, 1 August 1985.

[69] R. D. Lohr and E. G. Ellison, "A simple theory for low cycle multiaxial fatigue," *Fatigue & Fracture of Engineering Materials & Structures,* vol. 3, no. 1, pp. 1-17, 1918.

[70] J. Li, Z.-P. Zhang, Q. Sun, C.-W. Li and Y.-J. Qiao, "A new multiaxial fatigue damage model for various metallic materials under the combination of tension and torsion loadings," *International Journal of Fatigue,* vol. 31, no. 4, p. 776–81, 2009.

[71] D. Socie, "Multiaxial fatigue damage models," *Journal of Engineering Materials and Technology,* vol. 109, no. 4, pp. 293-298, 1987.

[72] B. Alfredsson and A. Cadario, "A study on fretting friction evolution and fretting fatigue crack initiation for a spherical contact," *International Journal of Fatigue,* vol. 26, p. 1037–1052, 2004.

[73] S. A. Namjoshi, S. Mall, V. K. Jain and O. Jin, "Fretting fatigue crack initiation mechanism in Ti-6Al-4V," *Fatigue & Fracture of Engineering Materials & Structures,* vol. 25, no. 10, pp. 955-964, 2002.

[74] C. D. Lykins, S. Mall and V. Jain, "An evaluation of parameters for predicting fretting fatigue crack initiation," *International Journal of Fatigue,* vol. 22, no. 8, p. 703–716, 2000.

[75] S. Naboulsi and S. Mall, "Fretting fatigue crack initiation behavior using process volume approach and finite element analysis," *Tribology International,* vol. 36, no. 2, pp. 121-131, 2003.

[76] H. Proudhon, S. Fouvry and J. Y. Buffiere, "A fretting crack initiation prediction taking into account the surface roughness and the crack nucleation process volume," *International Journal of Fatigue,* vol. 27, no. 5, pp. 569-579, 2005.

[77] W. S. Sum, E. J. Williams and S. B. Leen, "Finite element, critical-plane, fatigue life prediction of simple and complex contact configurations," *International Journal of Fatigue,* vol. 27, no. 4, pp. 403-416, 2005.

[78] K. C. Liu, "A method based on virtual strain-energy parameters for multiaxial fatigue life prediction," *Advances in Multiaxial Fatigue, ASTM STP 1191, American Society for Testing and Materials,* pp. 67-84, 1 January 1993.

[79] R. Rolović and S. M. Tipton, "An energy based critical plane approach to multiaxial fatigue analysis," *Fatigue and Fracture Mechanics ed. T. Panontin and S. Sheppard (ASTM International),* vol. 29, pp. 599-613, 1999.

[80] X. Chen, S. Xu and D. Huang, "A critical plane-strain energy density criterion for multiaxial low-cycle fatigue life under non-proportional loading.," *Fatigue & Fracture of Engineering Materials & Structures,* vol. 22, no. 8, pp. 679-86, 1999.

[81] Boston University Mechanical Engineering, "Mechanics of materials: Stress transformation," [Online]. Available: https://www.bu.edu/moss/mechanics-of-materials-stress-transformation/. [Accessed August 2019].

[82] Engineering.com, "Transformation of strains," 23 October 2006. [Online]. Available: https://www.engineering.com/Library/ArticlesPage/tabid/85/ ArticleID/148/Transformation-of-Strains.aspx. [Accessed August 2019].

[83] J. Marin, "Interpretation of fatigue strength for combined stresses," *Proceedings of International Conference on Fatigue of Metals, Institution of Mechanical Engineers,* pp. 184-194, 1966.

[84] G. Sines, "The prediction of fatigue fracture under combined stresses at stress concentrations," *Bulletin of JSME,* vol. 4, no. 15, p. 443–453, 1961.

[85] I. V. Papadopoulos, P. Davoli, C. Gorla, M. Filippini and A. Bernasconi, "A comparative study of multiaxial high-cycle fatigue criteria for metals," *International Journal of Fatigue,* vol. 19, no. 3, pp. 219-235, 1997.

[86] A. Cristofori, L. Susmel and R. Tovo, "A stress invariant based criterion to estimate fatigue damage under multiaxial loading," *International Journal of Fatigue,* vol. 30, no. 9, pp. 1646-1658, 2008.

[87] M. Nesladek, M. Spaniel, J. Jurenka, J. Ruzicka and J. Kuzelka, "Fretting fatigue - Experimental and numerical approaches," *International Journal of Fatigue,* vol. 44, pp. 61-73, 2012.

[88] B. Crossland, “Effect of large hydrostatic pressures on the torsional fatigue strength of an alloy steel,” *Proceedings of The International Conference on Fatigue of Metals: Institution of Mechanical Engineers*, pp. 138-149, 10-14 September 1956.

[89] L. Kachanov, “Time of the rupture process under creep conditions,” *Izvestiia Akademii Nauk SSSR, Otdelenie Teckhnicheskikh Nauk,* vol. 8, pp. 26-31, 1958.

[90] J. Lemaitre, “Evaluation of dissipation and damage in metals submitted to dynamic loading,” in *International Conference on the Mechanical Behnvior of Materials*, Kyoto, Japan, 1971.

[91] J. L. Chaboche, “Une loi différentielle d'endommagement de fatigue avec cumulation non linéaire,” Office Nationale d'Etudes et de Recherches Aérospatiales, 1974.

[92] J. Lemaitre, “Coupled elasto-plasticity and damage constitutive equations,” *Computer Methods in Applied Mechanics and Engineering,* vol. 51, no. 1-3, pp. 31-49, 1985.

[93] R. Hojjati-Talemi and M. A. Wahab, “Fretting fatigue crack initiation life time predictor tool : Using damage mechanics approach,” *Tribology International,* vol. 60, pp. 176-186, 2013.

[94] R. Hojjati-Talemi and M. A. Wahab, “Numerical estimation of fretting fatigue lifetime using damage and fracture mechanics,” *Tribology Letters,* vol. 52, no. 1, pp. 11-25, 2013.

[95] W. Ramberg and W. R. Osgood, “Description of stress-strain curves by three parameters,” Techncial Note No.902, National Advisory Committee For Aeronautics, Washington DC, 1943.

[96] B. Bhattacharya and B. Ellingwood, “Continuum damage mechanics analysis of fatigue crack initiation,” *International Journal of Fatigue,* vol. 20, no. 9, pp. 631-639, 1998.

[97] S. M. Quraishi, M. M. Khonsari and D. K. Baek, “A thermodynamic approach for predicting fretting fatigue life,” *Tribology Letters,* vol. 19, no. 3, pp. 169-175, 2005.

[98] J. L. Chaboche and P. M. Lesne, “A non-linear continuous fatigue damage model,” *Fatigue & Fracture of Engineering Materials & Structures,* vol. 11, no. 1, pp. 1-17, 1988.

[99] T. Zhang, P. McHugh and S. Leen, “Finite element implementation of multiaxial continuum damage mechanics for plain and fretting fatigue,” *International Journal of Fatigue,* vol. 44, pp. 260-272, 2012.

[100] N. A. Bhatti, K. Pereira and M. A. Wahab, “A continuum damage mechanics approach for fretting fatigue under out of phase loading,” *Tribology International,* vol. 117, pp. 39-51, 2018.

[101] R. Hojjati-Talemi, M. A. Wahab and P. De Baets, “Finite element simulation of phase difference effects on fretting fatigue crack nucleation behaviour,” *Journal of Engineering Tribology,* vol. 228, no. 4, pp. 470-479, 2014.

[102] J. Ding., D. Houghton, E. J. Williams and S. B. Leen, “Simple parameters to predict effect of surface damage on fretting fatigue,” *International Journal of Fatigue,* vol. 33, no. 3, pp. 332-342, 2011.

[103] T. Yue and M. A. Wahab, "A review on fretting wear mechanisms, models and numerical analyses," *CMC, Tech Science Press,* vol. 59, no. 2, pp. 405-432, 2019.

[104] R. Hojjati-Talemi and M. A. Wahab, "Finite element analysis of localized plasticity in AL 2024-T3 subjected to fretting fatigue," *Tribology Transactions,* vol. 55, no. 6, pp. 805-814, 2012.

[105] N. A. Bhatti and M. A. Wahab, "Finite element analysis of fretting fatigue under out of phase loading conditions," *Tribology International,* vol. 109, pp. 552-562, 2017.

[106] C. D. Lynkins, S. Mall and V. K. Jain, "Combined experimental-numerical investigation of fretting fatigue crack initiation," *International Journal of Fatigue,* vol. 23, no. 8, pp. 703-711, 2001.

[107] A. Benhamena, A. Talha, N. Benseddiq, A. Amrouche, G. Mesmacque and M. Benguediab, "Effect of clamping force on fretting fatigue behaviour of bolted assemblies:Case of couple steel–aluminium," *Materials Science and Engineering A,* vol. 527, no. 23, pp. 6413-6421, 2010.

[108] K. Iyer and S. Mall, "Effects of cyclic frequency and contact pressure on fretting fatigue under two-level block loading," *Fatigue & Fracture of Engineering Materials & Structures,* vol. 23, no. 4, pp. 335-346, 2000.

[109] T. Yue and M. A. Wahab, "Finite element analysis of fretting wear under variable coefficient of friction and different contact regimes," *Tribology International,* vol. 107, pp. 274-282, 2017.

[110] S. Fouvry, V. Fridrici, C. Langlade, P. Kapsa and L. Vincent, "Palliatives in fretting: A dynamical approach," *Tribology International,* vol. 39, pp. 1005-1015, 2006.

[111] D. Zhang, S. R. Ge and Y. H. Qiang, "Research on the fatigue and fracture behavior due to the fretting wear of steel wire in hoisting rope," *Wear,* vol. 255, no. 7-12, pp. 1233-1237, 2003.

[112] J. A. Araujo and D. Nowell, "The effect of rapidly varying contact stress fields on fretting fatigue," *International Journal of Fatigue,* vol. 24, pp. 763-775, 2002.

[113] N. P. Suh and H. C. Sin, "The genesis of friction," *Wear,* vol. 69, no. 1, pp. 91-114, 1981.

[114] K. Nishioka and K. Hirakawa, "Fundamental investigations of fretting fatigue, part 3," *Bulletin of JSME,* vol. 12, no. 51, p. 397–407, 1969.

[115] I. Hutchings and P. Shipway, "Chapter 5, Sliding Wear," in *Tribology: Friction and Wear of Engineering Materials*, Butterworth-Heinemann, 2017, p. 117.

[116] S. Fouvry, T. Liskiewicz, P. Kapsa, S. Hannel and E. Sauger, "An energy description of wear mechanisms and its applications to oscillating sliding contacts," *Wear,* vol. 255, no. 1-6, pp. 287-298, 2003.

[117] L. Vincent, Y. Berthier, M. C. Dubourg and M. Godet, "Mechanics and materials in fretting," *Wear,* vol. 153, no. 1, pp. 135-148, 1992.

[118] L. Vincent, Y. Berthier and M. Godet, "Testing methods in fretting fatigue: A critical appraisal," in *Standardization of fretting fatigue test methods and equipment ASTM-STP 1159*, Philadelphia, USA, American Society for Testing and Materials, 1992, pp. 33-48.

[119] R. S. Magaziner, V. K. Jain and S. Mall, "Wear characterization of Ti-6Al-4V under fretting reciprocating sliding conditions," *Wear*, vol. 264, no. 11-12, pp. 1002-1014, 2008.

[120] D. Dini, D. Nowell and I. N. Dyson, "The use of notch and short crack approaches to fretting fatigue threshold prediction: Theory and experimental validation," *Tribology International*, vol. 39, no. 10, p. 1158–1165, 2006.

[121] C. Kouanga, J. Jones, I. Revill, A. Wormald, D. Nowell, R. Dwyer-Joyce, J. Araújo and L. Susmel, "On the estimation of finite lifetime under fretting fatigue loading," *International Journal of Fatigue*, vol. 112, pp. 138-152, 2018.

[122] D. Taylor, The Theory of Critical Distances: A New Perspective in Fracture Mechanics, Amsterdam: Elsevier Science Ltd, 2007.

[123] R. E. Peterson, Stress Concentration Factors, New York, USA: John Wiley & Sons, 1974.

[124] A. Saengsai, Y. Miyashita and Y. Mutoh, "Effects of humidity and contact material on fretting fatigue behavior of an extruded AZ61 magnesium alloy," *Tribology International*, vol. 42, no. 9, p. 1346–1351, 2009.

[125] H. Goto and D. Buckley, "Effect of humidity on fretting wear of several pure metals," NASA Technical Paper 2403, December 1984.

[126] S. Mall, H. K. Kim, W. Porter, J. Ownby and A. Traylor, "High temperature fretting fatigue behavior of IN100," *International Journal of Fatigue*, vol. 32, no. 8, pp. 1289-1298, 2010.

[127] J. Ownby, "The effect of elevated temperature on the fretting fatigue behavior of nickel alloy IN-100," Department of The Air Force, Air Force Institute of Technology, Air University, Dayton, Ohio, USA., 2008.

[128] F. Abbasi and G. Majzoobi, "An investigation into the effect of elevated temperatures on fretting fatigue response under cyclic normal contact loading," *Theoretical and Applied Fracture Mechanics*, vol. 93, pp. 144-154, 2018.

[129] M. Kestly, F. Popielas, D. Grafl and A. Weiss, "Accelerated testing of multi-layer steel cylinder head gaskets, SAE Technical Paper 2000-01-1188," in *SAE 2000 World Congress*, Detroit, Michigan, 2000.

[130] E. N. Mamiya, F. C. Castro, L. Malcher and J. A. Araújo, "Multiaxial fatigue life estimation based on combined deviatoric strain," *International Journal of Fatigue*, vol. 67, pp. 117-122, 2014.

[131] A. T. Bernardo, J. A. Araújo and E. N. Mamiya, "Proposition of a finite element-based approach to compute the size effect in fretting fatigue," *Tribology International*, vol. 39, no. 10, pp. 1123-1130, 2006.

[132] ASM Aerospace Specification Metals Inc., "Aluminum 7075-T6; 7075-T651," [Online]. Available: http://asm.matweb.com/search/SpecificMaterial.asp?bassnum=MA7075T6. [Accessed March 2019].

[133] "ANSYS mechanical APDL 2022 R1, Chapter 7: Element library," ANSYS Inc, 2022.

[134] A. C. Fischer-Cripps, "Elastic Indentation Stress Fields," in *Introduction to Contact Mechanics*, Boston, MA, Springer, 2007, pp. 77-100.

[135] M. A. Wahab, R. Hojjati-Talemi and P. De Baets, "FEA of fretting fatigue: A comparison between ANSYS and ABAQUS," *Key Engineering Materials,* Vols. 488-489, pp. 662-665, 2012.

[136] M. A. Meggiolaro and J. T. P. Castro, "Statistical evaluation of strain-life fatigue crack initiation predictions," *International Journal of Fatigue,* vol. 26, no. 5, pp. 463-476, 2004.

[137] J. Yarishah and F. Mansoub, "Fatigue life prediction of al 7075-T6 notched specimens with circular holes using several multiaxial fatigue criteria," *Indian Journal of Science and Technology,* vol. 8, no. 36, pp. 1-7, 2015.

[138] F. Abbasi and G. Majzoobi, "Effect of out-of-phase loading on fretting fatigue response of Al7075-T6 under cyclic normal loading using a new testing apparatus," *Engineering Fracture Mechanics,* vol. 188, pp. 93-111, 2018.

[139] J. M. Thompson and M. K. Thompson, "A proposal for calculation of wear," in *International ANSYS Users Conference and Exhibition*, Pittsburgh, Pennsylvania, USA, 2006.

[140] O. Kesarkar, "Wear modeling in ANSYS," ANSYS Inc, 2015.

[141] Z. Zhou, S. Fayeulle and L. Vincent, "Cracking behaviour of various aluminium alloys during fretting wear," *Wear,* vol. 155, no. 2, pp. 317-330, 1992.

[142] "Cyclic stress-strain curve," Altair Inc., [Online]. Available: http://www.efatigue.com/glossary/cyclic_stress_strain_curve. [Accessed 14 January 2021].

[143] I. Llavori, J. Esnaola, A. Zabala, M. Larrañaga and X. Gomez, "Fretting: Review on the numerical simulation and modeling of wear, fatigue and fracture," in *Contact and Fracture Mechanics*, London, UK., IntechOpen, 2018, pp. 200-201.

[144] M. A. Meggiolaro, J. T. Pinho de Castro and A. C. d. O. Miranda, "Comparison among fatigue life prediction methods and stress-strain models under multiaxial loading," in *19th International Congress of Mechanical Engineering*, Brasília, 2007.

[145] D. Socie, "efatigue.com," [Online]. Available: https://www.efatigue.com/benchmarks/SAE_keyhole/SAE_keyhole.html. [Accessed 2019].

[146] "ANSYS 2019 R1 Help manual,Section: 4.4.3.2.1,," ANSYS Inc.

[147] E. Giner, M. Sabsabi, J. J. Ródenas and F. J. Fuenmayor, "Direction of crack propagation in a complete contact fretting-fatigue problem," *International Journal of Fatigue,* vol. 58, pp. 172-180, 2014.

[148] K. Elleuch and S. Fouvry, "Experimental and modelling aspects of abrasive wear of a A357 aluminium alloy under gross slip fretting conditions," *Wear,* vol. 258, no. 1-4, pp. 40-49, 2005.

[149] ANSYS Inc, "ANSYS mechanical advanced nonlinear materials, Advanced metal plasticity," 2012.

[150] "ANSYS 2018 help document, Isotropic friction, section 4.15.1,," ANSYS Inc, 2018.

[151] F. P. Bowden and D. Tabor, "The friction and lubrication of solids," *Americal Journal of Physics,* vol. 19, pp. 428-429, 1951.

[152] I. R. McColl, J. Ding and S. B. Leen, "Finite element simulation and experimental validation of fretting wear," *Wear,* vol. 256, no. 11-12, pp. 1114-1127, 2004.

[153] "Contact surface wear, section 13.174.8, ANSYS 2018 help manual," ANSYS Inc, 2018.

[154] L. Chevalier, A. Eddhahak-Ouni and S. Cloupet, "On a simplified model for numerical simulation of wear during dry rolling contacts," *Journal of Tribology,* vol. 131, no. 1, pp. 1-15, 2009.

[155] "ANSYS 18.2 help manual, Modeling heat generation due to friction, section 7.1.7," ANSYS Inc, 2018.

[156] G. I. Taylor and H. Quinney, "The latent energy remaining in a metal after cold working," *Proceedings of the Royal Society A,* vol. 143, no. 849, pp. 307-326, 1934.

[157] T. Zhang, Z.-R. Guo, F.-P. Yuan and Z.-S. Zhang, "Investigation on the plastic work-heat conversion coefficient of 7075-T651 aluminum alloy during an impact process based on infrared temperature measurement technology," *Acta Mechanica Sinica,* vol. 34, pp. 327-333, 2018.

[158] "ANSYS mechanical APDL 2022 R1, Theory reference, section 13.222," ANSYS Inc, 2019.

[159] "Service bulletin no. 15-NA-069 -Information on the reuse of fasteners and the proper reading of torque specifications," November 2015. [Online]. Available: https://static.nhtsa.gov/odi/tsbs/2015/MC-10137258-9999.pdf. [Accessed 25 June 2022].

[160] A. P. Ozarde, J. Narayan, D. Yadav, G. H. McNay and S. S. Gautam, "Optimization of diesel engine's liner geometry to reduce head gasket's fretting damage," *SAE International Journal of Engines,* vol. 14, no. 1, pp. 81-97, 2020, doi:10.4271/03-14-01-0006.

[161] A. P. Ozarde, G. H. McNay and S. S. Gautam, "Comparative fretting fatigue life evaluation between critical plane based and deviatoric strain amplitude based methods corrected for surface wear damage," *SAE International Journal of Materials and Manufacturing,* vol. 15, no. 2, pp. 1-22, 2022.

[162] D. Put, “Liners - top or bottom?,” highpowermedia.com, 13 August 2012. [Online]. Available: https://www.highpowermedia.com/Archive/liners-top-or-bottom. [Accessed 10 November 2021].

[163] ANSYS Inc, “ANSYS Help manual v 18.2, mechanical APDL,” 2018.

[164] “ANSYS 18.2 Help manual, Section 13.187,” ANSYS Inc, 2018.

[165] “ANSYS help manual v. 18.2.0, Real constants,section 3.9.1.,” ANSYS Inc, 15 July 2017.

[166] “ANSYS Help 18.2, section 3.9.4.3-using FKT and SLTO,” ANSYS Inc, 2018.

[167] A. P. Ozarde and G. H. McNay, “Thermo-mechanical fatigue and press-fit loss analysis of valve seat insert, SAE Technical Paper 2021-26-0338,” in *SAE Symposium on International Automotive Technology*, Pune, India, 2021.

[168] A. Baumel, T. Seeger and C. Boller, Materials data for cyclic loading. Supplement 1, Amsterdam: Elsevier Science Publishers, 1990.

[169] S. O'Halloran, P. Shipway, A. Connaire, S. Leen and A. Harte, “A combined wear-fatigue design methodology for fretting in the pressure armour layer of flexible marine risers,” *Tribology International*, vol. 108, pp. 7-15, 2017.

[170] A. B. Liggins, J. C. Stranart, L. B. Finlay and C. H. Rorabeck, “Calibration and manipulation of data from fuji pressure-sensitive film,” in *Experimental mechanics: Technology transfer between high tech engineering and biomechanics*, Limerick, Ireland, Elsevier Science Publishers, 1992, pp. 61-70.

[171] D. Taylor, “Geometrical effects in fatigue: A unifying theoretical model,” *International Journal of Fatigue*, vol. 21, no. 5, pp. 413-420, 1999.

[172] Y. Li, A. Bushby and D. Dunstan, “The Hall–Petch effect as a manifestation of the general size effect,” *Proceedings of The Royal Society A*, vol. 472, no. 2190, pp. 1-17, 01 June 2016.

[173] W. F. Smith and J. Hashemi, Foundations of Materials Science and Engineering, NewYork, USA: McGraw-Hill, 2006.

[174] D. Nowell and P. Nowell, “A machine learning approach to the prediction of fretting fatigue life,” *Tribology International*, vol. 141, pp. 1-8, 2020, https://doi.org/10.1016/j.triboint.2019.105913.

[175] S. K. Vithalbhai and S. S. Gautam, “A machine learning approach to fretting fatigue problem,” in *International Conference on Futuristic Technologies (e-Conference) - Structural Health Monitoring, Energy Harvesting, Green Material and Biomechanics, IIT Delhi*, New Delhi, 2021.

[176] S. S. Gautam and K. M. Khan, “Detection of fretting fatigue using machine learning algorithms,” in *3rd Structural Integrity Conference and Exhibition (SICE 2020) - "Structural Integrity at Multiple Length Scales" (e-Conference), IIT Bombay*, Mumbai, 2020.

[177] J. R. Wagner, E. Mount and H. Giles, “Chapter 25: Design of Experiments,” in *Extrusion, The Definitive Processing Guide and Handbook,* Norwich, NY (USA), Elsevier Science, 2013, pp. 231-245.

[178] J. Berk and S. Berk, “Chapter 11: ANOVA, Taguchi and other design of experiments techniques,” in *Quality Management for the Technology Sector,* Woburn, MA (USA), Butterworth-Heinemann, 2000.

[179] T. Dahiru, “P-Value, a true test of statistical significance? A cautionary note,” *Annals of Ibadan Postgraduate Medicine,* vol. 6, no. 1, pp. 21-26, 2008.

[180] K. Ken, “Design of experiments,” Möbius Wiki, 29 October 2014. [Online]. Available: https://www.mobius.illinois.edu/wiki/index.php/Design_of_Experiments. [Accessed 23 April 2020].

भारतीय प्रौद्योगिकी संस्थान गुवाहाटी
Indian Institute of Technology Guwahati

LIST OF PUBLICATIONS

Journals:

1. A. P. Ozarde, G. H. McNay, S. S. Gautam, "Fretting fatigue damage and life Evaluation of cylinder head gasket using deviotoric strain amplitude-based parameter corrected for surface wear damage", *SAE International Journal of Engines*, vol. 16, no. 4, pp. 1-15, 2023, doi: 10.4271/03-16-04-0024.

2. A. P. Ozarde, G. H. McNay and S. S. Gautam, "Comparative fretting fatigue life evaluation between critical plane based and deviatoric strain amplitude based methods corrected for surface wear damage," *SAE International Journal of Materials and Manufacturing*, vol. 15, no. 2, pp. 1-22, 2022, doi: 10.4271/05-15-02-0009.

3. A. P. Ozarde, G. H. McNay and S. Gautam, "Fretting fatigue failures in internal combustion engine components: A review and future scope," *SAE International Journal of Engines*, vol. 14, no. 2, pp. 211- 234, 2021, doi: 10.4271/03-14-02-0013.

4. A. P. Ozarde, J. Narayan, D. Yadav, G. H. McNay and S. Gautam, "Optimization of diesel engine's liner geometry to reduce head gasket's fretting damage," *SAE International Journal of Engines*, vol. 14, no. 1, pp. 81-97, 2021, doi:10.4271/03-14-01-0006.